Treatment of surface water inoculated with *Aspergillus* species using ultraviolet radiation and photocatalytic membrane reactors

Beatriz Reis Oliveira

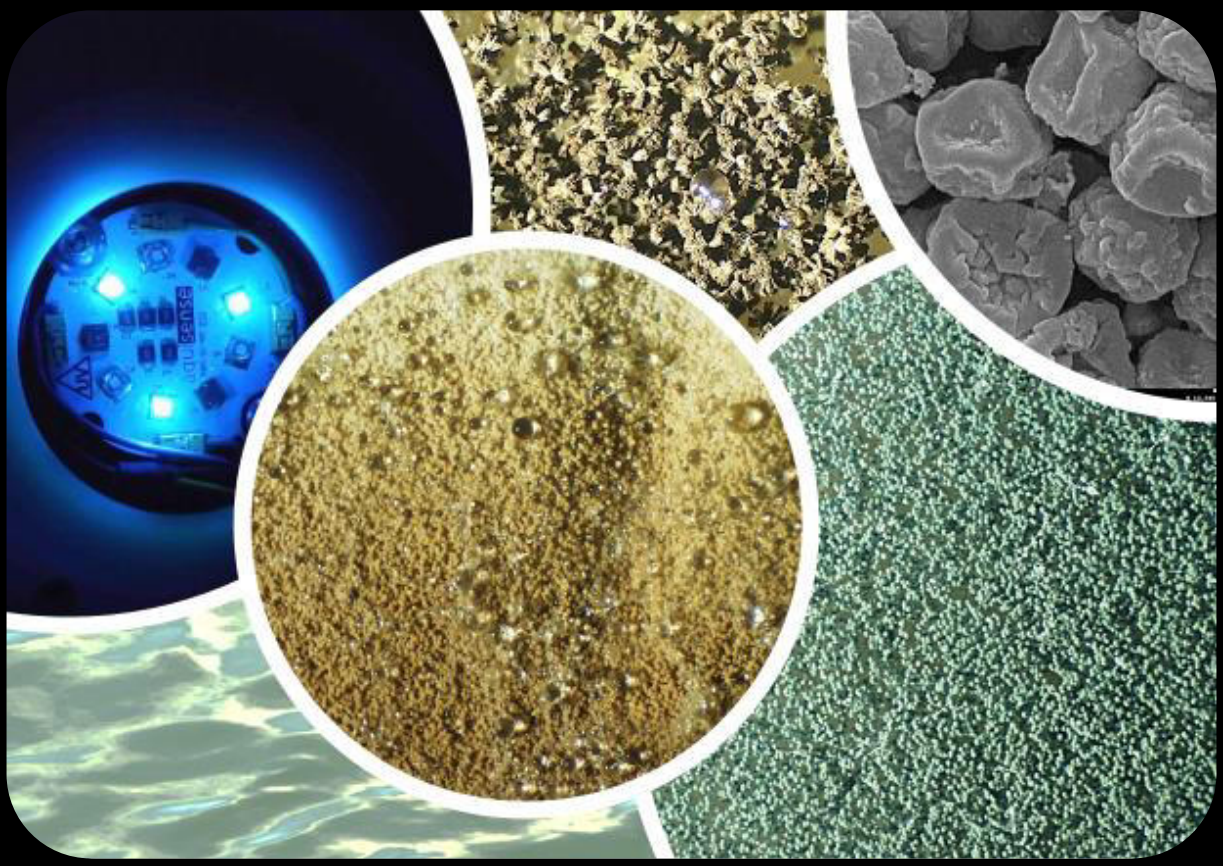

Dissertation presented to obtain the Ph.D degree in Molecular Biosciences

Instituto de Tecnologia Química e Biológica António Xavier | Universidade Nova de Lisboa

Oeiras,
October, 2020

UNIVERSIDADE NOVA DE LISBOA

Treatment of surface water inoculated with *Aspergillus* species using ultraviolet radiation and photocatalytic membrane reactors

Beatriz Reis Oliveira

Dissertation presented to obtain the Ph.D degree in Molecular Biosciences

Instituto de Tecnologia Química e Biológica António Xavier | Universidade Nova de Lisboa

Oeiras, October, 2020

ITQB-UNL and iBET, Microbiology of Man-made Environments Laboratory
Instituto de Tecnologia Química e Biológica António Xavier, Universidade Nova de Lisboa and Instituto de Biologia Experimental e Tecnológica
Apartado 12, 2781-901 Oeiras, Portugal
Fax: +351 21 442 11 61; Phone: +351 21 446 95 52
http://www.itqb.unl.pt
http://www.ibet.pt

SUPERVISORS

Doctor Vanessa Pereira: Principal Scientist at the Laboratory of Membrane Processes, iBET (supervisor).

Doctor Teresa Crespo: Researcher and Head of the Microbiology of Man-Made Environments Laboratory of iBET and ITQB-UNL (co-supervisor).

"If I have seen further,

it is by standing on the shoulders of giants."

Isaac Newton

(1643-1727)

ACKNOWLEDGEMENTS

Porque nada se faz sozinho, gostaria de expressar o meu agradecimento a todas as pessoas que directa ou indirectamente, contribuíram e me ajudaram na realização desta tese.

À minha orientadora, Doutora Vanessa Pereira, que foi a pessoa que me fez ver a luz ao fundo do túnel quando eu estava perdida e confusa, e que, sem ela, este trabalho não estaria concluído. Aprendi muito com a Doutora Vanessa ao longo destes anos, sendo curioso ver na prática o "positive reinforcement", e que me ensinou a ser mais positiva em relação ao trabalho, aos colegas de trabalho, amigos e família! Obrigada por tudo, pelos momentos de descontração como os passeios ao fim de semana e almocinhos na praia; vou ter muitas saudades.

À minha co-orientadora, Doutora Teresa Crespo, por ter confiado no meu trabalho todos estes anos e me ter permitido crescer no laboratório, como pessoa e como profissional. Obrigada pela disponibilidade para me ouvir sempre que precisei e pelo apoio nos momentos de trabalho e familiares mais difíceis.

À Doutora Vitória San Romão, pela paixão que temos pelos fungos, por me ter acolhido tão bem no laboratório e ter permitido que assim iniciasse a minha carreira profissional como investigadora. Obrigada pela amizade ao longo destes anos!

Às pessoas que trabalham na sala das lavagens (Cristina, Cármen, Sónia e Ricardo) e às pessoas que trabalham na manutenção do ITQB (Nuno, Luís, Aníbal, Ninja, Nuno, Tiago e Alexandre) por terem recebido sempre com um sorriso todos os meus pedidos de ajuda e porque sem eles o trabalho não estaria feito.

Ao Doutor Jos Houbraken por sempre responder aos meus e-mails com dúvidas sobre o meu doutoramento.

Aos meus amigos de laboratório, e começando pelos actuais, as companheiras de viagem a Coimbra, Mónica, Micaela, Andreia e Inês, que tornaram aqueles dias muito agradáveis e deu para nos conhecermos melhor. Novamente, a Mónica por estar sempre pronta a ajudar o próximo, pelas suas partidas com gelo seco e pelos docinhos que nos trazia para animar o dia, a Andreia pela troca de bons dias porque eramos sempre as primeiras a chegar, e a Inês pela sua boa disposição e por me ter ajudado no trabalho num momento familiar difícil. O Doudou, pelas infindáveis conversas que tínhamos durante as viagens até Lisboa (e que por vezes deviam ter sido maiores) sobre trabalho, notícias, vida pessoal e pelos momentos extra de diversão que ainda tivemos. A Rosa, pelo gosto pelo trabalho que transmite e pela perseverança em nunca desistir mesmo quando o trabalho parece "dar cabo de nós". Como ela diz sempre "Mañana va a ser más y mejor!". A Beatriz (ou Bia C. ou Bia cappuccino, ou Bia nova), obrigada pela amizade que foi crescendo ao longo destes anos, pelas boleias de e para Lisboa, pelas aventuras a ir buscar água de manhã ao rio e pelos momentos extra de descontração e diversão que bem preciosos foram! O Jorge pela sua boa disposição (ou não), pelas gargalhadas que eram inevitáveis e pelo apoio principalmente no período final do doutoramento. E a mais recente contratação que veio reforçar o nosso laboratório, a Paula Marques, muito obrigada pela ajuda nestes últimos meses, foi muito importante para fechar o trabalho desta tese. Aos amigos de laboratório que já saíram, agradeço à Paula por ter estado sempre presente e pelos almocinhos fora para descontrair; à Filipa por continuar presente mesmo longe e por me ter recebido tão bem em Copenhaga; à Sandra, pela pessoa que és, pela amizade e carinho que temos e por toda a ajuda preciosa durante o doutoramento; à Carmo pelo carinho ao longo dos anos; e à Anabela que, apesar do mau feitio, foi uma pessoa preciosa no laboratório e principalmente fora dele. Obrigada a todas, pela amizade ao longo destes anos!

À Marta pelos almoços que tivemos e encontros em festas do ITQB e iBET que mostram que nada mudou e a amizade mantém-se igual ao longo destes 14 anos. À Maria João, pela força e determinação que tem demonstrado e pela companhia em alguns fins de tarde para dois dedos de conversa.

Porque amizades também nascem de colaborações que existem dentro dos projectos de investigação, queria agradecer à Marisa por me desafiar a sair da zona de conforto e ir à descoberta do mundo!

Aos meus amigos de Solicitadoria, principalmente, ao João e à Carla, que sempre me apoiaram ao longo destes quatro anos para não desistir e arranjar forças para cumprir todos os objectivos propostos. Obrigada também por me ouvirem a desabafar dos problemas de laboratório e de trabalho, mesmo quando não percebiam muito bem do que eu estava a falar.

Aos meus amigos dos Bombeiros, que compreenderam o meu afastamento nestes últimos quatro anos, mas que sempre me receberam de braços abertos!

Aos meus amigos do curso de Biologia, pelo grupo maravilhoso que ainda mantemos, mas principalmente à Andreia e ao João por sempre me aturarem ao falar de trabalho e pelos momentos de descontração.

À Filipa e à Verónica pela amizade desde sempre! Obrigada por tudo!

À minha família toda por sempre mostrar interesse no meu trabalho apesar de no fundo eu saber que eles não fazem ideia do que fazemos no laboratório! Pelos convívios ao fim de semana que são sempre agradáveis e que me mostram o que realmente é importante.

À minha avó que sei que está muito feliz pela minha conquista e que vai estar sempre a olhar por mim.

Ao meu irmão e à Diana pelas conversas rápidas que tivemos e pelo apoio ao longo de toda a minha vida. Pelas sobrinhas lindas que me deram! Adoro-vos! Ao meu irmão novamente, pela ajuda preciosa com o Excel, mesmo fora de horas, sem ti, ainda estava a analisar ficheiros de Excel.

Finalmente, aos meus pais que os amo muito, por todo o apoio em perseguir os meus sonhos, mesmo quando eles divergem. Por nunca duvidarem das minhas capacidades. Por estarem sempre presentes incondicionalmente e por serem o meu porto de abrigo! Obrigada do fundo do coração!

ABSTRACT

Limited attention has been given to the presence of fungi in the aquatic environment when compared to other microorganisms such as bacteria and virus. Our previous research showed that fungi occur widely in drinking water sources and described many fungi species that have not been previously reported in the aquatic environment. Moreover, many filamentous fungi species present in water were found to be able to grow at high temperatures and have conidia measurements lower than 5 µm, being therefore considered as potential pathogenic species to humans and animals.

Chlorine is the most widely used disinfectant in water treatment. However, in our previous studies, *Penicillium* and *Aspergillus* species showed higher resistance to free and combined chlorine disinfection than certain *Cladosporium* and *Phoma* species, so they may resist the conventional treatment. Therefore, further research is needed to address the efficiency of different disinfectants for the inactivation of fungi. The use of ultraviolet (UV) radiation for water treatment has increased along the years since it is extremely effective to achieve inactivation of protozoans, virus, and bacteria. This will decrease the chlorine dose needed as a final disinfectant in the distribution system and consequently, decrease the formation of chlorination disinfection by products.

Low and medium pressure mercury lamps are the most common UV radiation sources used for water treatment. However, light-emitting diodes (LEDs) recently emerged as a promising treatment technology due to their advantages: being mercury free, no stabilization time needed, longer lifetimes, and the ability to build panels with a diversity of LED wavelengths. If proven effective, light emitting diodes can be a good alternative to replace mercury lamps. In this work it is shown that medium pressure mercury lamps can effectively inactivate different *Aspergillus* species (*Aspergillus fumigatus, Aspergillus niger* and *Aspergillus terreus*). Moreover, it

is also shown that three small LEDs that emit at 265 nm can achieve high inactivation of the same species. These results are very promising since they are being achieved with a lower energy consumption and, at full scale, with a higher number of LEDs and intensity, an extremely effective disinfection process is expected.

To further upgrade common water treatment systems, membrane technology is often proposed as an extremely effective treatment process that can achieve high quality effluents. However, there are two drawbacks often associated with these systems, fouling of the membrane as well as the production of a concentrated retentate that will require further treatment. To overcome these drawbacks coupling UV photolysis, stable photoactive titanium dioxide (TiO_2) layers and water filtration in a single photocatalytic membrane reactor can be beneficial to achieve high quality drinking water since the membrane retains microorganisms and chemical pollutants whereas the photocatalytic treatment decreases fouling components and treats the concentrated retentate. In this work this hybrid system was evaluated to treat a real water matrix spiked with the fungal species *A. fumigatus* and an extremely effective treatment of the permeate and retentate was obtained. An increased inactivation of the spores was observed after only 10 minutes of operation when using a ceramic membrane modified with titanium dioxide and silicon dioxide coupled with UV radiation.

The effects of UV radiation on filamentous fungi spores was also addressed by studying their response to the imposed stress in terms of spores' morphology, cell wall/membrane integrity, enzymatic acivity, DNA damage, protein production and their capacity to recover after the imposed stress condition. The most reported inactivation mechanism of microorganisms when subjected to UV radiation is DNA damage. The formation of cyclobutane pyrimidine dimers was detected and quantified in all the species subject to LEDs that emit at 265 nm. The DNA damage induced by the medium pressure lamps used in this study was so intense that did not allow quantification of dimers in *A. fumigatus* and *A. terreus* using this light source.

Depending on the different lamp wavelengths emitted by the light sources other effects can occur in the cells. Changes in the spores' morphology was addressed using scanning electron microscopy. Deformation of the spores was detected in the three tested species using all sources of UV radiation, except for the LEDs that emit at 255 nm. The effect observed was due to the action of UV radiation itself (direct photolysis) and due to the action of hydroxyl radicals ($^{\bullet}OH$) formed by the incidence of UV radiation on titanium dioxide modified membranes (indirect photolysis). Cell wall/membrane integrity and enzymatic activity were also addressed by coupling fluorescent staining dyes with flow cytometry. Results showed that higher loss of cell wall/membrane integrity was observed for *A. terreus*, followed by *A. fumigatus*, and by *A. niger*. The latter was the most resistant species, most of times showing no effect on cell wall/membrane integrity and maintaining all of its enzymatic activity. The proteomic response after radiation exposure was also addressed and it could be verified that *A. niger* produced proteins related with the malate metabolism that, is responsible for the production of citric acid that, has been associated with an increased resistance to oxidative stress. A more diversified proteome response was detected for *A. fumigatus* and *A. terreus* that involved the detection of proteins responsible for the reorganization of the cell wall, an intense synthesis of proteins, and the production of several compounds responsible for enhanced resistance against oxidative stress, like antioxidants.

After UV treatment, some microorganisms have been reported to be able to regrow under light and dark conditions, due to the activation of repair systems. The results obtained showed that *A. fumigatus*, *A. niger* and *A. terreus* were able to photoreactivate to some degree.

This thesis shows for the first time that several sources of UV radiation can be used to achieve an effective inactivation of filamentous fungi, unveils some of the effects of radiation exposure on the spores and evaluates an hybrid UV radiation and filtration system that can be proposed as an effective treatment process to upgrade the

treatment processes of conventional drinking water utilities. This hybrid treatment process will also produce high quality water that protects public health and is able to cope with future more stringent legislations.

RESUMO

Tem sido dada pouca atenção à presença de fungos filamentosos em ambiente aquático comparativamente a outros microrganismos como bactérias e vírus. Estudos anteriores mostraram que os fungos ocorrem amplamente em fontes de água para consumo e descreveram espécies de fungos que nunca tinham sido reportadas no ambiente aquático. Adicionalmente, foram descritas muitas espécies de fungos filamentosos presentes em água com a capacidade de crescer a elevadas temperaturas e com conídeos cujas dimensões são inferiores a 5 µm, sendo por isso, consideradas espécies potencialmente patogénicas para humanos e animais.

O cloro é o desinfectante mais usado no tratamento de água. No entanto, em estudos anteriores, espécies dos géneros *Penicillium* e *Aspergillus* mostraram uma maior resistência à desinfecção utilizando cloro livre e combinado do que algumas espécies dos géneros *Cladosporium* e *Phoma* podendo, por isso, resistir ao tratamento convencional. É assim, necessário estudar a eficiência de diferentes desinfectantes na inactivação de fungos. A utilização de radiação ultravioleta para o tratamento de água tem aumentado ao longo dos anos uma vez que é extremamente eficiente na inactivação de protozoários, virus e bactérias. A utilização de radiação ultravioleta irá diminuir a dose de cloro que é necessária adicionar como desinfectante final nos sistemas de distribuição de água e, consequentemente, diminuir a formação de sub-produtos resultantes da desinfecção por cloro.

Lâmpadas de mercúrio de baixa e média pressão são as fontes de radiação ultravioleta mais usadas no tratamento de água. No entanto, os díodos emissores de luz (light-emitting diodes – LEDs) surgiram recentemente como uma tecnologia potencialmente promissora para o tratamento de água porque têm várias vantagens: não usam mercúrio, não necessitam de tempo de estabilização, têm tempos de vida maiores, e podem ser construídos painéis com uma elevada diversidade de comprimentos de onda. Se for provado que as LEDs são eficazes, estas poderão ser

uma boa alternativa para a substituição das lâmpadas de mercúrio, actualmente usadas para desinfecção. Neste trabalho é mostrado que as lâmpadas de mercúrio de média pressão conseguem inactivar eficientemente diferentes espécies de *Aspergillus* (*Aspergillus fumigatus*, *Aspergillus niger* e *Aspergillus terreus*). Adicionalmente, é também mostrado que três pequenas LEDs que emitem luz a 265 nm conseguem alcançar uma elevada percentagem de inactivação das mesmas espécies. Estes resultados são muito promissores uma vez que, estão a ser obtidos com baixo consumo de energia e, num sistema à escala real, com um maior número de LEDs e intensidade, é expectável um processo de desinfecção extremamente eficaz.

Para melhorar o sistema de tratamento de água comummente utilizado, a tecnologia de filtração por membrana é frequentemente proposta como sendo um processo de tratamento eficaz que pode alcançar elevada qualidade de efluentes. No entanto, existem duas desvantagens normalmente associadas com esta tecnologia, a colmatação da membrana e a produção de um retentado concentrado que requer tratamento adicional. Para ultrapassar estas desvantagens, a combinação de fotólise por radiação ultravioleta, camadas estáveis de dióxido de titânio fotoactivas e a filtração de água num só reactor de membranas fotocatalítico, pode ser benéfica para alcançar água para consumo de elevada qualidade. De facto, a membrana retém os microrganismos e os poluentes químicos enquanto o tratamento fotocatalítico diminui a colmatação da membrana e trata o retentado concentrado. Neste trabalho, um sistema híbrido foi testado para tratar uma matriz de água real inoculada com *A. fumigatus* e foi obtido um tratamento extremamente eficiente do permeado e do retentado. Foi também observado um aumento de inactivação dos esporos após 10 minutos de operação usando membranas de cerâmica modificadas com dióxido de titânio e dióxido de silício acopladas com radiação ultravioleta.

O efeito da radiação ultravioleta nos esporos dos fungos filamentosos foi também avaliado através do estudo da sua resposta ao stress imposto, em termos de morfologia dos esporos, integridade da parede/membrana celular, actividade

enzimática, danos no DNA, produção de proteínas e a possibilidade de reactivação dos esporos depois do stress imposto. O mecanismo de inactivação dos microrganismos mais reportado quando sujeitos a radiação ultravioleta é o aparecimento de danos no DNA. A formação de dímeros de bases de pirimidina foi detectada e quantificada em todas as espécies sujeitas às LEDs que emitem radiação a 265 nm. O dano causado no DNA induzido pelas lâmpadas de mercúrio de média pressão utilizadas neste estudo foi tão elevado que não permitiu a quantificação de dímeros em *A. fumigatus* e *A. terreus* usando essa fonte de luz. Dependendo do comprimento de onda emitido pelas diferentes lâmpadas, outros efeitos podem ocorrer nas células. A morfologia dos esporos foi analisada através de microscopia electrónica de varrimento e foi verificada a deformação dos esporos das três espécies usando todas as fontes de luz testadas, excepto as LEDs que emitem luz a 255 nm. Os efeitos observados ocorreram devido à acção directa da luz (fotólise directa) e devido à acção de radicais hidroxilo (•OH) formados após a incidência da radiação ultravioleta no dióxido de titânio imobilizado nas membranas modificadas (fotólise indirecta). A integridade da parede/membrana celular e a actividade enzimática foi também estudada juntando corantes fluorescentes com citometria de fluxo e, pôde ser visualizada uma maior perda de integridade da parede/membrana celular para o *A. terreus*, seguido do *A. fumigatus*, e do *A. niger*. A última espécie, foi a mais resistente, na maior parte das vezes não mostrando sequer efeitos na integridade da parede/membrana celular e mantendo a sua actividade enzimática. A resposta do proteoma após exposição à radiação foi também estudada e pôde verificar-se que o *A. niger* produziu proteínas relacionadas com o metabolismo do malato, que é responsável pela produção de ácido cítrico que, está associada a um aumento da resistência ao stress oxidativo. Uma resposta mais ampla foi detectada para o *A. fumigatus* e *A. terreus* que envolveu a detecção de proteínas responsáveis pela reorganização da parede celular, uma elevada síntese de proteínas, e a produção de

diversos compostos responsáveis por aumentar a resistência ao stress oxidativo, como os antioxidantes.

Após o tratamento por radiação ultravioleta, alguns microrganismos têm a capacidade para voltar a crescer sob condições de luz e no escuro, devido à activação de sistemas de reparação. Os resultados obtidos neste estudo mostram que *A. fumigatus*, *A. niger* e *A. terreus* possuem até um certo nível de inactivação, capacidade de fotoreactivação.

Esta tese mostra, pela primeira vez, que várias fontes de radiação ultravioleta podem ser usadas para alcançar uma inactivação eficiente de fungos filamentosos e desvenda alguns dos efeitos da exposição à radiação nos esporos. Avalia ainda um sistema híbrido de radiação ultravioleta e filtração que pode ser proposto como um processo de tratamento eficaz para melhorar a capacidade que as estações de tratamento de água para consumo têm para produzir água de elevada qualidade, permitindo-lhes proteger a saúde pública e garantir o cumprimento de legislações futuras mais restringentes.

THESIS PUBLICATIONS

B.R. Oliveira, M.T. Barreto Crespo and V.J. Pereira, 2020. Small but powerful: Light-emitting diodes for inactivation of *Aspergillus* species in real water matrices. Water Research, 168, 115108.

B.R. Oliveira, S. Sanches, R.M. Huertas, M.T. Barreto Crespo, V.J. Pereira. 2020. Treatment of a real water matrix inoculated with *Aspergillus fumigatus* using a photocatalytic membrane reactor. Journal of Membrane Science, 598, 117788.

B.R. Oliveira, A.P. Marques, M. Ressurreição, C.J.S. Moreira, C. Silva Pereira, M.T. Barreto Crespo, V.J. Pereira. Inactivation of *Aspergillus* species in real water matrices using medium pressure mercury lamps. Submitted

B.R. Oliveira, A.P. Marques, M. Asif, M.T. Barreto Crespo, V.J. Pereira. Light-emitting diodes effect on *Aspergillus* species in real water sources: DNA damage, proteome response and potential reactivation. Submitted

LIST OF ABBREVIATIONS

2D DIGE	Two-dimensional difference gel electrophoresis
2DE	Two-dimensional electrophoresis
6-4PP	pyrimidine (6-4) pyrimidone photoproducts
($^{\bullet}$OH)	Hydroxyl radicals
A	Adsorption
A. fumigatus	*Aspergillus fumigatus*
A. niger	*Aspergillus niger*
A. terreus	*Aspergillus terreus*
Al_2O_3	Aluminum oxide
ATR	Attenuated total reflectance
Au	Gold
BP	Biological process
CC	Cellular component
CFU	Colony forming units
COD	Chemical oxygen demand
CPD	Cyclobutane pyrimidine dimer
CUR	Curtain
DHN	Dihydroxynaphthalene
DNA	Deoxyribonucleic acid
DTT	Dithiothreitol
E. coli	*Escherichia coli*
EDS	Energy dispersive spectroscopy
EEM	Excitation-emission matrices
ELISA	Enzyme-linked immunosorbent assay
FDA	Fluorescein diacetate
FDR	False discovery rate
FSC	Forward-scattered light
FTIR	Fourier transform infrared
GO	Gene ontology
GS	Gas source
ICP	Inductively coupled plasma
IDA	Information dependent acquisition
IHT	Interface heater temperature
ILT	International Light Technologies
ISVF	Ion spray voltage floating
kbp	Kilo base pair
LC	Liquid chromatography

LED	Light-emitting diodes
LP	Low pressure
L_p	Membrane permeability
m/z	Mass to charge ratio
MF	Molecular function
MM	Modified membrane
MP	Medium pressure
MS	Mass spectrometry
Na	Sodium
NaCl	Sodium chloride
PARAFAC	Parallel factor analysis
PBS	Phosphate buffered saline
Pd	Palladium
PI	Propidium iodide
PVDF	Polyvinylidene difluoride
PVPP	Polyvinylpolypyrrolidone
R_{app}	Apparent rejection
ROS	Reactive oxygen species
RP	Reversed-phase
RS	Resolubilization buffer
SEM	Scanning electron microscopy
Si	Silicon
SiO_2	Silicon dioxide
SSC	Side-scattered light
SWATH	Sequential window acquisition of all theoretical fragment ion spectra
TCA	Trichloroacetic acid
TEOS	Tetraethyl orthosilicate
TGX	Tris glycine extended
TiO_2	Titanium dioxide
TOC	Total organic carbon
TOF	Time-of-flight
UM	Unmodified membrane
UV	Ultraviolet
Y	Yttrium
ZnSe	Zinc selenide

TABLE OF CONTENTS

LIST OF TABLES

LIST OF FIGURES

CHAPTER 1

Introduction: state-of-the-art and thesis motivation

CONTENTS

This chapter comprises the state-of-the-art on the occurrence of filamentous fungi in drinking water sources with its associated problems and the disinfection treatments commonly used by drinking water facilities. Moreover, it describes the motivation for the thesis, the thesis aims, and the approach followed to attain the objectives proposed.

1.1 FUNGI

Fungi, being eukaryotic, are organisms that contain an individualized nucleus and specialized cell organelles like mitochondria, endoplasmic reticulum and Golgi apparatus. The fungal cell wall is a rigid structure composed of a thick inner layer of chitin or cellulose and a thinner outer layer of glycoproteins. Next to the cell wall there is the cytoplasmic membrane that contains sterols (Reynolds and Pepper, 2000). Fungi range from microscopic yeasts to macroscopic filamentous structures named moulds (Reynolds and Pepper, 2000). Yeasts are unicellular fungi that reproduce asexually through budding where the daughter cell separates from the mature yeast cells. In contrast, moulds contain septate and nonseptate hyphae that are long narrow structures (10 µm to 15 µm in diameter) that entangle together into a mycelium. The nonseptate hyphae contain the cell organelles moving freely and may have several nuclei whereas the septate hyphae are limited into individual compartments by cross-walls or septa. These septa may have small pores enabling the transfer of organelles and nutrients between the compartments or may be closed walls with no transfer of organelles between the compartments (Reynolds and Pepper, 2000). Other septa may be formed to separate old mycelium from new mycelium and vegetative hyphae (responsible for nutrient adsorption) from reproductive hyphae (responsible for the formation of reproductive structures and spores).

Within the fungal kingdom recent high-level taxonomic classification was performed through the application of molecular methods, that have revolutionized the understanding on phylogenetic relationships among Fungi. Following the current International Nucleotide Sequence Databases consortium taxonomy, several changes were performed at the subkingdom, phylum and class level to comprise together reliable ecological and functional features for further ecophysiological and biodiversity analysis (Tedersoo et al., 2018).

1.1.1 The *Aspergillus* genus

The genus *Aspergillus* is one of the most well-known Ascomycete that includes currently at least 446 species (Houbraken et al., 2020). Morphological structures are formed during asexual reproduction, whose main purpose is the production of spores, named conidia, if produced by a conidiogenous cell. The conidiogenesis process in this genus occurs by the differentiation of hypha into a thicker stipe with a swollen apex called conidiophore and vesicle, respectively. At the tip, flask-shaped cells named phialides are the cells responsible for the production of conidia (monoseriate). These phialides, in many species, are placed in short branches (metulae) that are developed from the vesicle (biseriate). The succession production of conidia is basipetal meaning that young conidia are produced at the base of the phialide pushing the older conidia further away. Large numbers of small pigmented, hydrophobic and thick-walled spores are produced for dispersal and for survival under unfavourable conditions. The long-term survival spores are extremely resistant to adverse environmental conditions where solutes like trehalose, mannitol and glycerol ensure dormancy for long periods protecting cellular membrane and proteins.

1.1.2 Selected Species

Three different *Aspergillus* species (*Aspergillus fumigatus*, *Aspergillus niger*, and *Aspergillus terreus*) were selected to perform the experiments conducted in this thesis. These species were selected due to their occurrence in surface water (Oliveira et al., 2013; Pereira et al., 2009), their potential pathogenicity against immunocompromised patients (Oliveira et al., 2013; Parveen et al., 2011) and their different disinfection resistances that might be conferred by different conidial protection mechanisms (Braga et al., 2015). For instance, the cell wall as described above is stronger than bacteria's, enzymes like catalases can be produced to reduce the reactive oxidation compounds produced during disinfection and different pigments like melanin are able to absorb UV light (Braga et al., 2015).

Aspergillus fumigatus (figure 1.1a)) was first described in 1863 by Gerog Fresenius (Schmidt, 1998). Macroscopically, its colonies are dark blue-green formed by a dense felt of conidiophores mixed with conidiophore aerial hyphae attaining a diameter of 4.5 cm - 6.5 cm within 7 days at 27 °C on malt extract agar. Microscopically, conidiophores are short and smooth-walled, often green in the upper part ending in a subclavate vesicle with 20 µm - 30 µm wide. Phialides are present and the formed conidia are globose to subglobose with 2.5 µm - 3.0 µm diameter, green and with a rough to echinulate cell wall (Samson et al., 2004). The bluish-green pigment production by conidia occurs through the dihydroxynaphthalene (DHN)-melanin pathway (Fujii et al., 2004). This species is known to produce toxic metabolites like gliotoxin. It has been reported to occur in food, indoor, soil and water.

Aspergillus niger (figure 1.1b)) was first described in 1867 by Van Tieghem in a manuscript entitled "Physiologie des mucédinées". Macroscopically, its colonies consist of a white or yellow basal felt with a dense layer of dark brown to black

conidiophores attaining 6 cm - 7 cm within 7 days at 27 °C on malt extract agar. Microscopically, conidiophores are smooth-walled, hyaline or pigmented ending in a subspherical vesicle with 50 µm - 100 µm wide. Metulae and phialides are present and the formed conidia are brown globose ornamented with irregular warts, spines and ridges with 3.5 µm - 5.0 µm diameter (Samson et al., 2004). The pigment formation is thought to occur through the 1,8-DHN-melanin pathway since its genes are well conserved among *A. niger* and other aspergilli (Baker, 2008; Jørgensen et al., 2011). This species is known to produce toxic metabolites like ochratoxin A and fumonisins. It has been reported to occur in food, indoor, soil and water.

Aspergillus terreus (figure 1.1c)) was first described in 1918 by Charles Thom and Margaret B. Church (1918). Macroscopically, its colonies are yellowish-brown to cinnamon-brown with a dense felt of conidiophores attaining 3 cm - 5 cm within 7 days at 27 °C on malt extract agar. Microscopically, conidiophores are smooth-walled, hyaline ending in a subspherical vesicle with 10 µm - 20 µm wide. Metulae and phialides are present and the formed conidia are globose and smooth with 1.5 µm - 2.5 µm diameter, hyaline to slightly yellow (Samson et al., 2004). The pigment formation differs from the other two species because *A. terreus* lacks the typical features of DHN-melanin synthesis. *A. terreus* produces Asp-melanin pigment whose biosynthetic pathway was described by Geib *et al.* (2016). This species is known to produce toxic metabolites like citreoviridin. It has been reported to occur in food, indoor, soil and water.

a)

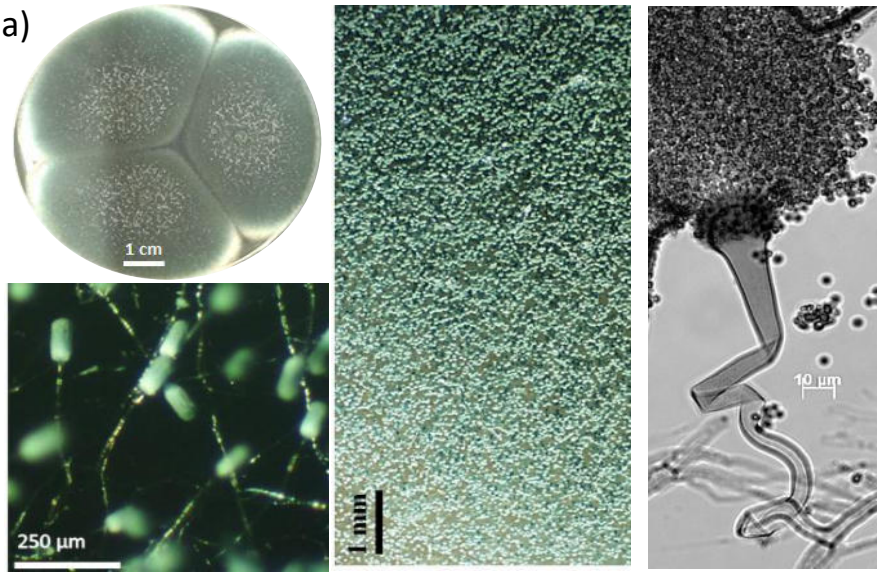

b)

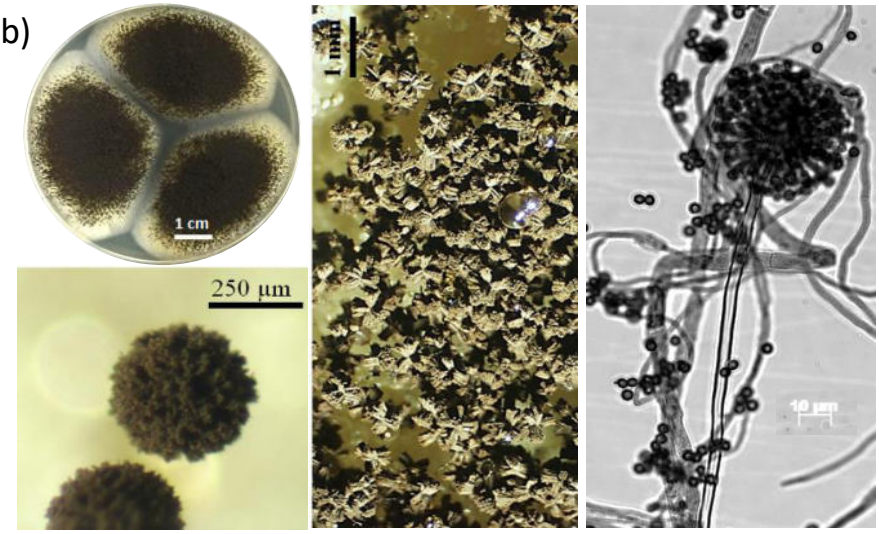

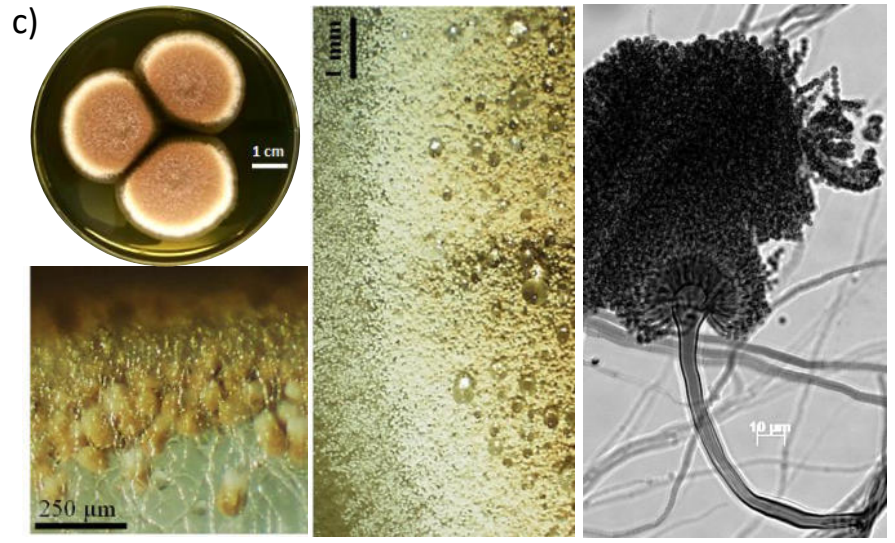

Figure 1.1 – Pictures of the three *Aspergillus* species selected, a) *Aspergillus fumigatus*, b) *Aspergillus niger* and c) *Aspergillus terreus*.

1.2 FILAMENTOUS FUNGI AND THEIR ROLE IN THE ENVIRONMENT

Fungi occur ubiquitously in the environment like air, soil and water. Their main key role in the soil is the decomposition of woody material from forests like lignin and cellulose, that they are able to use as carbon and energy sources. Due to this, fungi are also known as the "Earth's greatest chemists" with almost limitless biogeochemical capabilities (Madigan et al., 2012). Taking advantage of this feature, several bioremediation studies have used fungi for the degradation of complex organic molecules and xenobiotics (e.g. Oliveira et al., 2015). Moreover, fungi can be beneficial to plants due to mycorrhizal symbiotic associations between fungi and plant roots where the first provides mineral salts and water from the soil at long distances whereas the second provides amino acids and carbohydrates. Apart from their natural role, fungi can also be used by pharmaceutical and food industries to produce antibiotics and for fermentation processes, respectively.

On the other hand, the presence of fungi in the environment can be detrimental to plants, food, animals and humans by the contamination of crops (e.g. maize crops) foods and stored commodities such as grains, nuts and spices, the production of mycotoxins in different matrices and their ability to affect human health and welfare.

Safe water for human consumption is defined by the World Health Organization (WHO) as water that does not cause a significant hazard to human health during its consumption. A major concern for the government, water utilities and water consumers is the microbial contamination of water. Among these microbial contaminants, and rarely mentioned as bacteria, virus or protozoa, are filamentous fungi. But, it is the real knowledge on the quality of water that allows the application of better treatments and strategies to obtain water suitable for consumption. This can avoid a great variety of drinking-water related diseases and public health problems (Nichols et al., 2009; Reynolds et al., 2008; Wingender and Flemming, 2011).

Many recent studies have been focusing on describing the occurrence of fungi in the aquatic environment (e.g. Hageskal et al., 2006; Hageskal et al., 2009; Kanzler et al., 2007; Pereira et al., 2010). The most reported genus in European aquatic environment is *Aspergillus*, followed by other widely reported genera like *Cladosporium*, *Fusarium*, *Penicillium*, *Phoma* and *Trichoderma* (Al-gabr et al., 2014; Babič et al., 2017; Bouchiat et al., 2015; Oliveira et al., 2013; Saravanan and Sivakumar, 2013; Schiavano et al., 2014). Pereira et al. (2009) reported the occurrence of filamentous fungi in three different water sources (surface water, spring water and groundwater), at levels ranging from 100 to 1000 CFU/100 mL. Surface water presented the higher diversity of filamentous fungi genera (figure 1.2) (Oliveira et al., 2013).

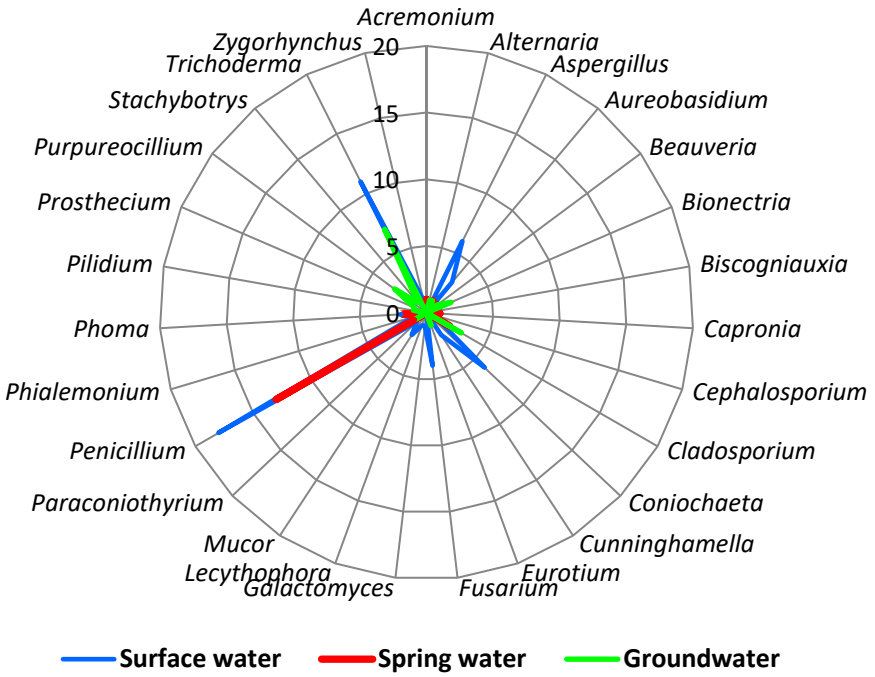

Figure 1.2 – Diagram representing the distribution of the 27 different genera identified in the different drinking water sources analysed (number of filamentous fungi isolates were 252).

These results were not surprising since, as stated above, fungi occur ubiquitously in the environment. However, their presence may be associated with quality and safety problems like unpleasant taste and odour, mycotoxin production, allergies, opportunistic infections and intoxications (Anaissie et al., 2001; Babič et al., 2017; Bucheli et al., 2008; Doggett, 2000). Some potential pathogenic filamentous fungi species were also reported by Oliveira et al (2013) by addressing their ability to grow at high temperatures (37 °C and 42 °C) or to have their spores' size lower than 5 µm which enables the spores to enter the respiratory system and cause pulmonary mycosis (Hoog, 1996). Among the reported species, *A. fumigatus*, *A. niger* and *A.*

terreus have spores' size below 5 µm and the first species was able to grow at 42 °C, being therefore considered potential pathogenic species (Oliveira et al., 2013). Further studies are therefore needed to understand if drinking water treatment process currently applied and novel treatment processes may effectively inactivate these species.

1.3 DRINKING WATER TREATMENT

The main goal of drinking water suppliers is to provide microbiological and chemically clean water to consumers. Although 70 % of the Earth's surface is covered by water, only 2.5 % is freshwater and, from this, only 0.3 % is water from lakes and rivers, which are the most common sources to be treated for drinking water (Oki and Kanae, 2006; Thomas, 1994). The conventional treatment applied for surface water is coagulation, flocculation, sedimentation, filtration, and final disinfection, whereas, for groundwater, disinfection is sometimes enough since the water is cleaner. The final disinfection is often performed by chlorination or chloramination, being the former the most widely applied, ensuring that a residual concentration of chlorine is maintained in the distribution system to protect consumers from drinking water microbial outbreaks. However, these disinfectants can react with natural organic matter from water and form disinfection by-products (Jeong et al., 2012; Pereira and Singer, 2004; Włodyka-Bergier and Bergier, 2011) that have been linked to deleterious health effects like cancer (Costet et al., 2011; Rahman et al., 2010) and adverse reproductive outcomes (James et al., 2010). In addition, inactivation of some microorganisms like viruses, bacteria and protozoa has failed using the conventional treatment (Brunkard et al., 2011). To overcome these drawbacks, water utilities have been testing and applying along the years different treatment processes such as filtration and UV radiation.

1.3.1 UV radiation

The application of UV disinfection for drinking water treatment has increased along the years since it is highly effective for viruses, bacteria and protozoan (oo)cysts inactivation (Hijnen et al., 2006). Another advantage of disinfection by UV radiation is the decrease of the chlorine doses needed to achieve final disinfection, reducing thus the chlorination by-product formation. Regarding chemical compounds, many natural water constituents, inorganic compounds and organic compounds are known to be photodegraded in water by UV direct photolysis and advanced oxidation processes (Marotta et al., 2013; Oppenländer, 2003; Shemer and Linden, 2007; Wu and Linden, 2008).

1.3.1.1 Direct photolysis by mercury lamps and light-emitting diodes

UV direct photolysis occurs by the exposure of contaminants to radiation at the ultraviolet range (200 nm - 380 nm). Medium pressure (MP) mercury lamps and low pressure (LP) mercury lamps are the most common lamps used in drinking water treatment facilities due to their germicidal effect. MP lamps emit polychromatic light ranging within 200 nm - 500 nm while LP lamps emit mainly a monochromatic light at 254 nm. Both lamps are already implemented in some drinking water utilities being LP lamps the ones that lead to less by-products formation, lower energy demand as well as lower operating costs.

Light emitting diodes (LEDs) emerged in the last years as a promising, greener alternative to MP and LP lamps since they are mercury free and therefore no mercury waste is produced, they are compact and robust, have longer lifetimes, do not need stabilization time, lead to a low energy consumption and can be constructed with a diversity of wavelengths (Hamamoto et al., 2007; Song et al., 2016). LEDs that emit within the ultraviolet range of wavelengths (UV-LEDs) still need improvements since

they only operate at 1 % of efficiency when compared to visible LEDs that operate at 75 % of efficiency (Chatterley and Linden, 2010). However, if proven effective, LEDs can be used instead of mercury lamps in the future.

1.3.1.2 Advanced oxidation processes

Advanced oxidation processes occur when UV radiation is combined with hydrogen peroxide or a catalyst and lead to the production of highly reactive and unselective hydroxyl radicals (Ollis et al., 1991). These radicals will likely enhance microorganisms' inactivation (Foster et al., 2011) and degradation of water contaminants (Sanches et al., 2010).

Heterogeneous photocatalysis is a photoreaction process that is accelerated by the presence of a solid semi-conductor. Among the semiconductors applied, titanium dioxide (TiO_2) is the reference material since it is a relatively stable catalyst in water under UV radiation, is non-toxic by ingestion, cheap and can absorb UV photons below 385 nm wavelength (Foster et al., 2011).

Three crystalline polymorphs of TiO_2 (anatase, rutile and brokite), have photocatalytic activity and can be synthesized and applied as pure phases or as mixtures. Combinations of the first two are more common since the last is harder to be synthesized (Addamo et al., 2006). Different commercial formulations with different proportions of anatase and rutile of TiO_2 are available being Degussa® P25 TiO_2 the most widely used photocatalyst. Degussa® P25 TiO_2 contains 70 % anatase and 30 % rutile and an average particle size of 20-30 nm (Alhakimi et al., 2003). TiO_2 photocatalytic process in the presence of water occurs due to the formation of hydroxyl radicals ($^{\bullet}OH$) and superoxide radicals $[O_2]^-$ (Balasubramanian et al., 2004; Konstantinou et al., 2001). The formation of $^{\bullet}OH$ radicals is a surface dependent process therefore TiO_2 has been used several times in suspension to increase the

surface area and consequently the formation of •OH radicals. Sanches *et al.* (2013) conducted heterogenous photocatalysis using TiO_2 in suspension with LP lamps. The authors reported that using TiO_2 in suspension has the disadvantage of its concentration being decreased considerably in the reactors due to TiO_2 adsorption to the flasks and tubing. This problem can be avoided if TiO_2 is used immobilized as a thin film in a surface (e.g. Meng et al., 2005).

1.3.2 Membrane filtration processes

To upgrade conventional water treatment systems, membrane technology may also be a promising solution (e.g. Esfahani et al., 2019). Since the 1990's, membrane filtration has gained particular attention in wastewater and water treatment due to the interest in wastewater reuse and the implementation of more strict regulations to obtain high-quality water. Along the years a big effort has been invested in upgrading the membranes so that they have enhanced chemical, thermal and mechanical properties or better permeability and selectivity, as well as a decrease of operational costs (Fane et al., 2011). Microfiltration, ultrafiltration, nanofiltration and reverse osmosis are pressure-driven membrane processes that function via a size exclusion mechanism. Microfiltration membranes are able to remove particles with size above 0.1 µm, ultrafiltration membranes can remove particles with size above 0.01 µm, nanofiltration membranes can retain particles of 1 nm and reverse osmosis membranes can remove particles of 0.1 nm width (Eriksson, 1988). These pressure-driven membrane processes have already been used for water treatment by removing different size particles (Madaeni, 1999; Peter-Varbanets et al., 2009), chemical contaminants (Sanches et al., 2013) and microorganisms (Madaeni, 1999). However, membrane fouling (inorganic, organic or biological) (Li et al., 2008) and the further

treatment of the highly concentrated retentate obtained (Sanches et al., 2013), are the two main drawbacks of membrane filtration processes.

The most common membranes available in the market are polymeric and ceramic membranes. The former are generally produced from cellulose acetate or polyamide materials and their derivatives. The latter are membranes often composed of a wide variety of materials that include titania, alumina, silica, and zirconia. Ceramic membranes are less prone to fouling, have relatively uniform pore structures and have higher chemical, thermal, and mechanical stability due to their higher hydrophilicity (Kim and Van der Bruggen, 2010).

The modification of membranes can be performed to increase photocatalytic performance, increase the hydrophilicity, decrease fouling and control porosity. Sol-gel is one of the techniques that can be used to perform membrane modifications consisting of using one single reagent that it is dissolved through a chemical reaction creating cross-linkings with itself and forming an inorganic structure. Thus, sols are colloidal particles (diameters 1 nm - 100 nm) dispersed in a liquid and a gel is an interconnected, rigid network with pores lower than 1 μm (Hench and West, 1990). Using the sol-gel technique, Huertas et al. (2017) modified ceramic membranes with TiO_2 and silicon dioxide (SiO_2) that showed a promising photocatalytic effectiveness and reusability potential. This best modification procedure was further improved using aqueous solutions and lower temperatures to produce environmental friendly membranes that also showed efficient and reproducible photocatalytic activity (Huertas et al., 2019). Therefore, the progress on membrane modification processes results in the advantage of using membrane filtration processes, as it does not need chemical additives, presents a reduced plant footprint and can easily be upscaled (Fane et al., 2011).

In this thesis, commercially available flat sheet ceramic substrates composed of a single α-alumina layer (d_{50} =1.8 μm) (Fraunhofer-Gesellschaft, Germany) were used unmodified and as a support for its modification with TiO_2 and SiO_2. TiO_2 ensures the

photocatalytic activity of the modified membrane whereas the combination of TiO_2 with SiO_2 improves the ability of surface adsorption and increases the amount of hydroxyl radicals at the membrane surface (Fateh et al., 2013).

1.3.3 Combination of UV radiation with membrane filtration

There is an increasing interest in the combination of UV disinfection and membrane filtration processes due to their potential to overcome the drawbacks associated with the individual processes. The development of hybrid reactors to perform the two treatments at the same time enables the retention of microorganisms and chemical contaminants by the membrane and decrease of fouling components and treatment of the concentrated retentate by the UV radiation. Chemical retention by the membrane depends on the target chemical and on the membrane used. UV can degrade the chemical compounds, depending on the fluences used, usually higher than those used for disinfection. With this new design comes the challenge to synthesize new membranes or apply new membrane modifications to enhance photocatalytic properties, hydrophilicity and control porosity, like the ones developed by Huertas et al. (2017, 2019).

Some authors have already used hybrid reactors, combining filtration and UV radiation at the same time for water treatment using *Escherichia coli* (Goei and Lim, 2014; Liu et al., 2012; Ma et al., 2009) as a model organism or methyl orange as a model dye (Romanos et al., 2013) and membrane modifications using TiO_2 and silver particles.

In this thesis a newly designed reactor combining UV radiation with filtration using ceramic unmodified and modified membranes (with TiO_2 and SiO_2) was used to treat a real drinking water matrix inoculated with filamentous fungi.

1.4 EFFECT OF TREATMENTS ON MICROORGANISMS

According to the wavelength of UV radiation used, different biological effects are expected to occur in microorganisms. LP lamps that emit a monochromatic wavelength at 254 nm are expected to inactivate microorganisms, by causing DNA damages, since the maximum absorbance of DNA is around 264 nm. These DNA damages occur by the formation of pyrimidine dimers (thymines or cytosines) that can be cyclobutane pyrimidine dimers and/or pyrimidine (6-4) pyrimidone photoproducts (6-4PP) that, when in high number in the DNA blocks DNA replication and inhibits cellular division. MP lamps that emit a wider range of wavelengths (200 nm - 500 nm) are expected to affect not only the DNA but also proteins, by destruction of sulphur bounds.

LEDs reactors, as stated above, can be constructed with different wavelengths depending on the treatment goals. For instance, wavelengths of 254 nm - 255 nm were chosen to be compared with LP mercury lamps (Bowker et al., 2011), wavelengths of 265 nm - 269 nm were chosen due to the absorption spectra of DNA (Oguma et al., 2013) and wavelengths around 280 nm were chosen due to the absorption spectra of proteins (Li et al., 2017; Rattanakul and Oguma, 2018; Song et al., 2019).

Treatments using photocatalysis are expected not only to affect DNA and proteins, depending on the wavelengths used, but are also expected to cause cell wall and membrane damages due to the production of hydroxyl radicals (Foster et al., 2011).

Different methodologies can be applied to verify the effect of treatments on microorganisms. To address morphological changes in the microorganisms, scanning electron microscopy is often used since it enables to acquire magnified images of the sample's surface. Cell wall and membrane damages can also be assessed through microscopic methodologies coupled with fluorescent dyes that bind to the cell wall.

For instance, calcofluor white is a fluorochrome that binds to chitin and allows visualizing under a fluorescent microscope the damages caused in the cell wall of the spores (Rasconi et al., 2009).

Flow cytometry combined with fluorescent-based stains has been widely used for the evaluation of microorganisms' viability as opposed to classic plating techniques that do not consider the physiological state of microorganisms, do not account for non-culturable microorganisms and is time-consuming. Fluorescent stains like SYTO9 and propidium iodide (PI) are often used in kits for live and dead tests, where SYTO9 binds to the entire DNA (free and inside of cells) emitting a green colour whereas PI binds DNA only when the cell wall and membrane are disrupted emitting a red colour (Vanhauteghem et al., 2017). Fluorescein diacetate (FDA), that is converted into a fluorescent product after enzyme activity, combined with PI have also been used for flow cytometry analysis. This allows the detection of four groups of cells: metabolically active (FDA positive), dead (PI positive), quiescent (FDA and PI negative) and damaged cells (FDA and PI positive) (Ehgartner et al., 2016).

To address DNA damages, like the formation of pyrimidine dimers, endonuclease sensitive site assay (Eischeid and Linden, 2007; Oguma et al., 2001) and an enzyme-linked immunosorbent assay (Hull et al., 2017) have been proposed. The former, briefly consists of using the enzyme T4 endonuclease V that cleaves at the pyrimidine dimer site and through alkaline gel electrophoresis the percentage of pyrimidine dimers formed can be determined. The latter method consists of using an enzyme-linked immunosorbent assay to quantify the cyclobutane pyrimidine dimers of the unknown samples based on standard curves.

To address protein profiles before and after treatments two-dimensional electrophoresis (2DE) or fluorescent two-dimensional difference gel electrophoresis (2D DIGE) are widely applied. The 2D DIGE has the advantage of being able to quantify the protein profile right away through the application of fluorescent dyes (Bergh and Arckens, 2004) whereas the 2D only enables quantification after staining. Besides this,

after performing the gels, the obtained bands are analysed through liquid chromatography coupled to tandem mass spectrometry to identify the proteins. Another methodology, consisting in combining liquid chromatography-mass spectrometry (LC-MS) in Data Dependant Acquisition mode, that allows to obtain protein identification and Sequential Window Acquisition of all theoretical fragment ion spectra-MS (SWATH-MS), that allows to quantify thousands of proteins in a single measurement, enables the qualitative and quantitative proteome analysis of a sample using a single LC-MS/MS injection (Gillet et al., 2012).

1.5 THESIS MOTIVATION

Considering the state-of-the-art presented it is clear that there is a gap in research to assess the inactivation of filamentous fungi in drinking water sources. Moreover, taking advantage of the knowledge gained along the years on membrane modification processes and its combination with photocatalytic reactors, more research is needed on the optimization of drinking water treatment utilities to obtain a higher quality of drinking water.

Therefore, filamentous fungi, specifically three *Aspergillus* species (*A. fumigatus*, *A. niger* and *A. terreus*), isolated from surface water, were chosen to conduct the following experiments due to their occurrence in surface water (Oliveira et al., 2013; Pereira et al., 2009), their potential pathogenicity against immunocompromised patients (Oliveira et al., 2013; Parveen et al., 2011) and their different disinfection resistances that might be conferred by different conidial protection mechanisms (Braga et al., 2015). Additionally, a newly design reactor combining filtration with ceramic unmodified and modified membranes with UV radiation was used to evaluate its efficiency for water treatment.

1.6 AIM AND OUTLINE OF THIS THESIS

The aim of the work developed and presented in this thesis is to understand the course of action of different UV radiation sources in three filamentous fungi understudy and the optimization of drinking water treatment processes using the combination of filtration with UV photolysis.

This thesis is divided in 6 chapters. Chapter 1 consists of a revision of the state-of-the-art related with the occurrence of filamentous fungi and the urge necessity to obtain high quality and safe drinking water for consumers. Moreover, an overview of the conventional and emerging drinking water treatments applied by water treatment facilities and the development of new strategies to optimize drinking water treatments was addressed. Ultimately, the possible effect of these treatments on microorganisms was also described.

In Chapter 2, a MP mercury lamp was used to perform the inactivation of *A. fumigatus*, *A. niger* and *A. terreus* isolated from surface water. This study was performed since, to the best of authors' knowledge, no study has been performed addressing the inactivation of filamentous fungi from surface water using a MP mercury lamp. Additionally, effect of this lamp on the filamentous fungi spores was addressed by: i) plating methods to obtain the colony forming units, ii) scanning electron microscopy to visualize the spores' morphology before and after treatment, iii) flow cytometry to verify the membrane integrity and enzymatic activity of the fungal spores, iv) OxiSelect™ UV-induced DNA damage ELISA kit to determine the formation of cyclobutane pyrimidine dimers and v) proteome analysis before and after the treatments.

Chapter 3 presents the inactivation of *A. fumigatus*, *A. niger* and *A. terreus* isolated from surface water using LEDs that emit light at 255 nm and 265 nm. The LEDs that emit at 255 nm wavelength was chosen to conduct this work due to its similarity with the LP wavelength that is widely used in drinking water and wastewater treatment facilities (254 nm) and the LEDs that emit at 265 nm due to the maximum absorbance wavelength of DNA spectra (approximately 264 nm). This was the first study to perform inactivation of filamentous fungi in surface water using LEDs, to the best of authors' knowledge. Additionally, the effect of this LEDs on the filamentous fungi spores was addressed using i) plating methods to obtain the colony forming units, ii) scanning electron microscopy to visualize the spores' morphology before and after treatment and iii) flow cytometry to verify the membrane integrity and enzymatic activity of the fungal spores (Oliveira et al., 2020). As a follow up of Chapter 3, the work of Chapter 4 was performed to verify more effects of the different wavelengths applied (LEDs that emit at 255 nm and 265 nm) on the treatment of the three species of filamentous fungi. To do that the OxiSelect™ UV-induced DNA damage ELISA kit was used to determine the formation of cyclobutane pyrimidine dimers and proteome analysis was performed before and after the treatments.

In Chapter 5 a newly design reactor that combines UV photolysis, stable photoactive TiO_2 layers and water filtration was used to treat surface water spiked with *A. fumigatus*. To the best of authors' knowledge, this is the first study performing this using ceramic substrates modified with TiO_2 and SiO_2. The apparent rejection, adsorption and retentate treatment was addressed through plating methods, membrane integrity and enzymatic activity of the fungal spores was verified by flow cytometry and the spores' morphology before and after treatment was visualized by scanning electron microscopy (Oliveira et al., 2020a).

Finally, Chapter 6 summarizes the main results obtained and described in each chapter and provides an overall discussion of the work presented in this thesis. Future work and perspectives are also presented.

REFERENCES

Addamo, M., Bellardita, M., Di Paola, A. and Palmisano, L. 2006. Preparation and photoactivity of nanostructured anatase, rutile and brookite TiO_2 thin films. Chemical Communications 47, 4943-4945.

Al-gabr, H.M., Zheng, T. and Yu, X. 2014. Occurrence and quantification of fungi and detection of mycotoxigenic fungi in drinking water in Xiamen City, China. Science of The Total Environment 466–467, 1103-1111.

Alhakimi, G., Gebril, S. and Studnicki, L.H. 2003. Comparative photocatalytic degradation using natural and artificial UV-light of 4-chlorophenol as a representative compound in refinery wastewater. Journal of Photochemistry and Photobiology A: Chemistry 157, 103-109.

Allgeier, S. (2005) Membrane Filtration Guidance Manual, US EPA's Office of Water, Malcolm Pimie, Inc, Separation Process, Inc, and The Cadmus Group, Inc.

Anaissie, E.J., Kuchar, R.T., Rex, J.H., Francesconi, A., Kasai, M., Muller, F.-M.C., Lozano-Chiu, M., Summerbell, R.C., Dignani, M.C., Chanock, S.J. and Walsh, T.J. 2001. Fusariosis Associated with Pathogenic *Fusarium* Species Colonization of a Hospital Water System: A New Paradigm for the Epidemiology of Opportunistic Mold Infections. Clinical Infectious Diseases 33(11), 1871-1878.

Babič, M.N., Gunde-Cimerman, N., Vargha, M., Tischner, Z., Magyar, D., Veríssimo, C., Sabino, R., Viegas, C., Meyer, W. and Brandão, J. 2017. Fungal Contaminants in Drinking Water Regulation? A Tale of Ecology, Exposure, Purification and Clinical Relevance. International Journal of Environmental Research and Public Health 14(6), 1-44.

Balasubramanian, G., Dionysiou, D.D., Suidan, M.T., Baudin, I., Audin, B. and Laine, J.M. 2004. Evaluating the activities of immobilised TiO_2 powder films for the photocatalytic degradation of organic contaminants in water. Applied Catalysis B: Environmental 47, 73-84.

Bergh, G.V. and Arckens, L. 2004. Fluorescent Two-dimensional difference gel electrophoresis unveils the potential of gel-based proteomics. Current Opinion in Biotechnology 15(1), 38-43.

Bouchiat, R., Veignie, E., Grizard, D., Soebert, C., Vigier, M. and Rafin, C. 2015. Ability of filamentous fungi to degrade four emergent water priority pollutants. Desalination and Water Treatment, 57:15, 6740-6746.

Bowker, C., Sain, A., Shatalov, M. and Ducoste, J. 2011. Microbial UV fluence-response assessment using a novel UV-LED collimated beam system. Water Research 45(5), 2011-2019.

Braga, G.U.L., Rangel, D.E.N., Fernandes, É.K.K., Flint, S.D. and Roberts, D.W. 2015. Molecular and physiological effects of environmental UV radiation on fungal conidia. Current Genetics 61(3), 405-425.

Brunkard, J.M., Ailes, E., Roberts, V.A., Hill, V., Hilborn, E.D., Craun, G.F., Rajasingham, A., Kahler, A., Garrison, L., Hicks, L., Carpenter, J., Wade, T.J., Beach, M.J. and Yoder, M.J.S. 2011. Surveillance for

waterborne disease outbreaks associated with drinking water - United States, 2007-2008. Morbidity and mortality weekly report. Surveillance summaries 60, 38-68.

Bucheli, T.D., Wettstein, F.E., Hartmann, N., Erbs, M., Vogelgsang, S., Forrer, H.-R. and Schwarzenbach, R.P. 2008. *Fusarium* Mycotoxins: Overlooked Aquatic Micropollutants? Journal of Agricultural and Food Chemistry 56(3), 1029-1034.

Charles, T. and Church, M.B. 1918. *Aspergillus fumigatus*, *A. nidulans*, *A. terreus* N. Sp. and their allies. American Journal of Botany 5(2), 84-104.

Chatterley, C. and Linden, K. 2010. Demonstration and evaluation of germicidal UV-LEDs for point-of-use water disinfection. Journal of Water and Health 8(3), 479-486.

Costet, N., Villanueva, C.M., Jaakkola, J.J.K., Kogevinas, M., Cantor, K.P., King, W.D., Lynch, C.F., Nieuwenhuijsen, M.J. and Cordier, S. 2011. Water disinfection by-products and bladder cancer: is there a European specificity? A pooled and meta-analysis of European case–control studies. Occupational and Environmental Medicine 68(5), 379-385.

Doggett, M.S. 2000. Characterization of Fungal Biofilms within a Municipal Water Distribution System. Applied and Environmental Microbiology 66(3), 1249-1251.

Ehgartner, D., Herwig, C. and Neutsch, L. 2016. At-line determination of spore inoculum quality in *Penicillium chrysogenum* bioprocesses. Applied Microbiology and Biotechnology 100(12), 5363-5373.

Eischeid, A.C. and Linden, K.G. 2007. Efficiency of pyrimidine dimer formation in *Escherichia coli* across UV wavelengths. Journal of Applied Microbiology 103(5), 1650-1656.

Eriksson, P. 1988. Nanofiltration extends the range of membrane filtration. Environmental Progress 7(1), 58-62.

Esfahani, M.R., Aktij, S.A., Dabaghian, Z., Firouzjaei, M.D., Rahimpour, A., Eke, J., Escobar, I.C., Abolhassani, M., Greenlee, L.F., Esfahani, A.R., Sadmani, A. and Koutahzadeh, N. 2019. Nanocomposite membranes for water separation and purification: fabrication, modification, and applications. Separation and Purification Technology 213, 465-499.

Fane, A.G., Wang, R. and Jia, Y. (2011) Membrane and Desalination Technologies. Wang, L.K., Chen, J.P., Hung, Y.-T. and Shammas, N.K. (eds), pp. 1-45, Humana Press, Totowa, NJ.

Fateh, R., Dillert, R. and Bahnemann, D. 2013. Preparation and characterization of transparent hydrophilic photocatalytic TiO_2/SiO_2 thin films on polycarbonate. Langmuir 29(11), 3730-3739.

Foster, H.A., Ditta, I.B., Varghese, S. and Steele, A. 2011. Photocatalytic disinfection using titanium dioxide: spectrum and mechanism of antimicrobial activity. Applied Microbiology and Biotechnology 90(6), 1847-1868.

Fujii, I., Yasuoka, Y., Tsai, H.-F., Chang, Y.C., Kwon-Chung, K.J. and Ebizuka, Y. 2004. Hydrolytic polyketide shortening by Ayg1p, a novel enzyme involved in fungal melanin biosynthesis. The Journal of Biological Chemistry 279, 44613-44620.

Geib, E., Gressler, M., Viediernikova, J., Hillmann, F., Jacobsen, I.D., Nietzsche, S., Hertweck, C. and Brock, M. 2016. A non-canonical melanin biosynthesis pathway protects *Aspergillus terreus* conidia from environmental stress. Cell Chemical Biology 23(5), 587-597.

Gillet, L.C., Navarro, P., Tate, S., Röst, H., Selevsek, N., Reiter, L., Bonner, R. and Aebersold, R. 2012. Targeted Data Extraction of the MS/MS Spectra Generated by Data-independent Acquisition: A New Concept for Consistent and Accurate Proteome Analysis. Molecular & Cellular Proteomics 11(6), O111.016717.

Goei, R. and Lim, T.-T. 2014. Ag-decorated TiO_2 photocatalytic membrane with hierarchical architecture: photocatalytic and anti-bacterial activities. Water Research 59, 207-218.

Hageskal, G., Gaustad, P., Heier, B.T. and Skaar, I. 2006. Occurrence of moulds in drinking water. Journal of Applied Microbiology 102, 774-780.

Hageskal, G., Lima, N. and Skaar, I. 2009. The study of fungi in drinking water. Mycological Research (113), 165-172.

Hamamoto, A., Mori, M., Takahashi, A., Nakano, M., Wakikawa, N., Akutagawa, M., Ikehara, T., Nakaya, Y. and Kinouchi, Y. 2007. New water disinfection system using UVA light-emitting diodes. Journal of Applied Microbiology 103(6), 2291-2298.

Hench, L.L. and West, J.K. 1990. The sol-gel process. Chemical Reviews 90(1), 33-72.

Hijnen, W.A.M., Beerendonk, E.F. and Medema, G.J. 2006. Inactivation credit of UV radiation for viruses, bacteria and protozoan (oo)cysts in water: A review. Water Research 40(1), 3-22.

Hoog, G.S. 1996. Risk assessment of fungi reported from humans and animals. Mycoses 39, 407-417.

Houbraken, J., Kocsubé, S., Visage, C., Yilmaz, N., et al., 2020. Classification of *Aspergillus*, *Penicillium*, *Talaromyces* and related genera (Eurotiales): An overview of families, genera, subgenera, sections, series and species. Studies in Mycology 95, 5-169.

Huertas, R.M., Fraga, M.C., Crespo, J.G. and Pereira, V.J. 2017. Sol-gel membrane modification for enhanced photocatalytic activity. Separation and Purification Technology 180, 69-81.

Huertas, R.M., Fraga, M.C., Crespo, J.G. and Pereira, V.J. 2019. Solvent free process for the development of photocatalytic membranes. Molecules 24, 4481.

Hull, N.M., Isola, M.R., Petri, B., Chan, P.-S. and Linden, K.G. 2017. Algal DNA repair kinetics support culture-based enumeration for validation of ultraviolet disinfection ballast water treatment systems. Environmental Science and Technology Letters 4(5), 192-196.

James, G., Bennett, J., Patelarou, E., Smith, R.B., Toledano, M.B., Rushton, L., Briggs, D.J. and Nieuwenhuijsen, M.J. 2010. Review article: Exposure to disinfection by-products, fetal growth, and prematurity: a systematic review and meta-analysis. Epidemiology 21(3), 300-313.

Jeong, C.H., Wagner, E.D., Siebert, V.R., Anduri, S., Richardson, S.D., Daiber, E.J., McKague, A.B., Kogevinas, M., Villanueva, C.M., Goslan, E.H., Luo, W., Isabelle, L.M., Pankow, J.F., Grazuleviciene, R., Cordier, S., Edwards, S.C., Righi, E., Nieuwenhuijsen, M.J. and Plewa, M.J. 2012. Occurrence and toxicity of disinfection by-products in European drinking waters in relation with the HIWATE epidemiology Study. Environmental Science and Technology 46, 12120-12128.

Jørgensen, T.R., Park, J., Arentshorst, M., Welzen, A.M.v., Lamers, G., vanKuyk, P.A., Damveld, R.A., Hondel, C.A.M.v.d., Nielsen, K.F., Frisvad, J.C. and Ram, A.F.J. 2011. The molecular and genetic basis of conidial pigmentation in *Aspergillus niger*. Fungal Genetics and Biology 48(5), 544-553.

Kanzler, D., Buzina, W., Paulitsch, A., Haas, D., Platzer, S., Marth, E. and Mascher, F. 2007. Occurrence and hygienic relevance of fungi in drinking water. Mycoses (51), 165-169.

Kim, J. and Van der Bruggen, B. 2010. The use of nanoparticles in polymeric and ceramic membrane structures: Review of manufacturing procedures and performance improvement for water treatment. Environmental Pollution 158, 2335-2349.

Konstantinou, I.K., Sakellarides, T.M., Sakkas, V.A., Albanis, T.A. 2001. Photocatalytic degradation of selected s-triazine herbicides and organophosphorus insecticides over aqueous TiO_2 suspensions. Environmental Science and Technology 35, 398-405.

Li, G.-Q., Wang, W.-L., Huo, Z.-Y., Lu, Y. and Hu, H.-Y. 2017. Comparison of UV-LED and low pressure UV for water disinfection: Photoreactivation and dark repair of *Escherichia coli*. Water Research 126, 134-143.

Li, Q., Mahendra, S., Lyon, D.Y., Brunet, L., Liga, M.V., Li, D. and Alvarez, P.J.J. 2008. Antimicrobial nanomaterials for water disinfection and microbial control: potential applications and implications. Water Research 42, 4591-4602.

Liu, L., Liu, Z., Bai, H. and Sun, D.D. 2012. Concurrent filtration and solar photocatalytic disinfection/degradation using high-performance Ag/TiO2 nanofiber membrane. Water Research 46(4), 1101-1112.

Ma, N., Fan, X., Quan, X. and Zhang, Y. 2009. Ag-TiO_2/HAP/Al_2O_3 bioceramic composite membrane: fabrication, characterization and bactericidal activity. Journal of Membrane Science 336(1-2), 109-117.

Madaeni, S.S. 1999. The application of membrane technology for water disinfection. Water Research 33(2), 301-308.

Madigan, M.T., Martinko, J.M., Dunlap, P.V. and Clark, D.P. (2012) Brock Biology of Microorganisms.

Marotta, R., Spasiano, D., Di Somma, I. and Andreozzi, R. 2013. Photodegradation of naproxen and its photoproducts in aqueous solution at 254 nm: a kinetic investigation. Water Research 47, 373-383.

Meng, Y., Huang, X., Yang, Q., Qian, Y., Kubota, N. and Fukunaga, S. 2005. Treatment of polluted river water with photocatalytic slurry reactor using low-pressure mercury lamps coupled with a membrane. Desalination 181, 121-133.

Nichols, G., Lane, C., Asgari, N., Verlander, N.Q. and Charlett, A. 2009. Rainfall and outbreaks of drinking water related disease and in England and Wales. Journal of Water and Health, 7(1), 1-8.

Oguma, K., Katayama, H., Mitani, H., Morita, S., Hirata, T. and Ohgaki, S. 2001. Determination of Pyrimidine Dimers in *Escherichia coli* and *Cryptosporidium parvum* during UV Light Inactivation, Photoreactivation, and Dark Repair. Applied and Environmental Microbiology 67(10), 4630-4637.

Oguma, K., Kita, R., Sakai, H., Murakami, M. and Takizawa, S. 2013. Application of UV light emitting diodes to batch and flow-through water disinfection systems. Desalination 328, 24-30.

Oki, T. and Kanae, S. 2006. Global Hydrological Cycles and World Water Resources. Science 313(5790), 1068-1072.

Oliveira, B.R., Barreto Crespo, M.T. and Pereira, V.J. 2020. Small but powerful: Light-emitting diodes for inactivation of *Aspergillus* species in real water matrices. Water Research 168, 115108.

Oliveira, B.R., Barreto Crespo, M.T., San Romão, M.V., Benoliel, M.J., Samson, R.A. and Pereira, V.J. 2013. New insights concerning the occurrence of fungi in water sources and their potential pathogenicity. Water Research 47(16), 6338-6347.

Oliveira, B.R., Penetra, A., Cardoso, V.V., Benoliel, M.J., Barreto Crespo, M.T., Samson, R.A. and Pereira, V.J. 2015. Biodegradation of pesticides using fungi species found in the aquatic environment. Environmental Science and Pollution Research 22, 11781-11791.

Oliveira, B.R., Sanches, S., Huertas, R.M., Barreto Crespo, M.T., Pereira, V.J. 2020a. Treatment of a real water matrix inoculated with *Aspergillus fumigatus* using a photocatalytic membrane reactor. Journal of Membrane Science 598, 117788.

Ollis, D.F., Pelizzetti, E. and Serpone, N. 1991. Photocatalyzed destruction of water contaminants. Environmental Science and Technology 25(9), 1522-1529.

Oppenländer, T. (2003) Photochemical purification of water and air, Wiley-VCH Verlag.

Parveen, S., Lanjewar, S., Sharma, K. and Kutti, U. 2011. Isolation of fungi from the surface water of river. Journal of Experimental Sciences 2(10), 58-59.

Pereira, V.J., Basílio, M.C., Fernandes, D., Domingues, M., Paiva, J.M., Benoliel, M.J., Crespo, M.T. and Romão, M.V.S. 2009. Occurrence of filamentous fungi and yeasts in three different drinking water sources. Water Research 43(15), 3813-3819.

Pereira, V.J., Fernandes, D., Carvalho, G., Benoliel, M.J., Romão, M.V.S. and Crespo, M.T.B. 2010. Assessment of the presence and dynamics of fungi in drinking water sources using cultural and molecular methods. Water Research 44(17), 4850-4859.

Pereira, V.J.W., Howard S. and Singer, P.C. 2004. Temporal and spatial variability of DBPs in a chloraminated distribution system. American Water Works Association 96(11), 91-102.

Peter-Varbanets, M., Zurbrugg, C., Swartz, C. and Pronk, W. 2009. Decentralized systems for potable water and the potential of membrane technology. Water Research 43, 245-265.

Rahman, M.B., Driscoll, T., Cowie, C. and Armstrong, B.K. 2010. Disinfection by-products in drinking water and colorectal cancer: a meta-analysis. International Journal of Epidemiology 39(3), 733-745.

Rasconi, S., Jobard, M., Jouve, L. and Sime-Ngando, T. 2009. Use of Calcofluor White for Detection, Identification, and Quantification of Phytoplanktonic Fungal Parasites. Applied and Environmental Microbiology 75(8), 2545-2553.

Rattanakul, S. and Oguma, K. 2018. Inactivation kinetics and efficiencies of UV-LEDs against *Pseudomonas aeruginosa*, *Legionella pneumophila*, and surrogate microorganisms. Water Research 130, 31-37.

Reynolds, K.A., Mena, K.D. and Gerba, C.P. 2008. Risk of Waterborne Illness Via Drinking Water in the United States. Reviews of Environmental Contamination and Toxicology 192, 117-158.

Reynolds, K.A. and Pepper, I.L. (2000) Environmental Microbiology. Maier, R.M., Pepper, I.L. and Gerba, C.P. (eds), pp. 31-34, Academic Press.

Romanos, G.E., Athanasekou, C.P., Likodimos, V., Aloupogiannis, P. and Falaras, P. 2013. Hybrid ultrafiltration/photocatalytic membranes for efficient water treatment. Industrial and Engineering Chemistry Research, 13938-13947.

Samson, R.A., Hoekstra, E.S. and Frisvad, J.C. (2004) Introduction to food- and airborne fungi, Centraalbureau voor Schimmelcultures (CBS) - Utrecht.

Samson, R.A., Varga, J. 2007. *Aspergillus* systematics in the genomic era, Studies in Mycology, 59, 1-210.

Sanches, S., Barreto Crespo, M.T. and Pereira, V.J. 2010. Drinking water treatment of priority pesticides using low pressure UV photolysis and advanced oxidation processes. Water Research 44, 1809-1818.

Sanches, S., Penetra, A., Rodrigues, A., Cardoso, V.V., Ferreira, E., Benoliel, M.J., Barreto Crespo, M.T., Crespo, J.G. and Pereira, V.J. 2013. Removal of pesticides from water combining low pressure UV photolysis with nanofiltration. Separation and Purification Technology 115, 73-82.

Saravanan, R. and Sivakumar, T. 2013. Biodiversity and Biodegradation potentials of Fungi isolated from Marine systems of East Coast of Tamil Nadu, India. International Journal of Current Microbiology and Applied Sciences 2(7), 192-201.

Schiavano, G.F., Parlani, L., Sisti, M., Sebastianelli, G. and Brandi, G. 2014. Occurrence of fungi in dialysis water and dialysate from eight haemodialysis units in central Italy. Journal of Hospital Infection 86(3), 194-200.

Schmidt, A. 1998. Georg Fresenius und die Spezies *Aspergillus fumigatus*. Mycoses 41(s2), 89-91.

Shemer, H. and Linden, K.G. 2007. Photolysis, oxidation and subsequent toxicity of a mixture of polycyclic aromatic hydrocarbons in natural waters. Journal of Photochemistry and Photobiology A: Chemistry 187(2-3), 186-195.

Song, K., Mohseni, M. and Taghipour, F. 2016. Application of ultraviolet light-emitting diodes (UV-LEDs) for water disinfection: A review. Water Research 94, 341-349.

Song, K., Taghipour, F. and Mohseni, M. 2019. Microorganisms inactivation by wavelength combinations of ultraviolet light-emitting diodes (UV-LEDs). Science of the Total Environment 665, 1103-1110.

Tedersoo, L., Sánchez-Ramírez, S., Kõljalg, U., et al., 2018. High-level classification of the Fungi and a tool for evolutionary ecological analyses. Fungal Diversity 90, 135-159.

Thomas, C. 1994. Water in crisis: a guide to the world's fresh water resources. International Affairs 70(3), 557-557.

Vanhauteghem, D., Demeyere, K., Callaert, N., Boelaert, A., Haesaert, G., Audenaert, K. and Meyer, E. 2017. Flow Cytometry Is a Powerful Tool for Assessment of the Viability of Fungal Conidia in Metalworking Fluids. Applied and Environmental Microbiology 83(16), e00938-00917.

Wingender, J. and Flemming, H.-C. 2011. Biofilms in drinking water and their role as reservoir for pathogens. International Journal of Hygiene and Environmental Health 214(6), 417-423.

Wu, C. and Linden, K.G. 2008. Degradation and byproduct formation of parathion in aqueous solutions by UV and UV/H_2O_2 treatment. Water Research 42, 4780-4790.

Włodyka-Bergier, A. and Bergier, T. 2011. The occurrence of haloacetic acids in Krakow water distribution system. Archives of Environmental Protection 37, 21-29.

CHAPTER 2

Inactivation of *Aspergillus* species in real water matrices using medium pressure mercury lamps

B.R. Oliveira, A.P. Marques, M. Ressureição, C.J.S. Moreira, C. Silva Pereira, M.T. Barreto Crespo, V.J. Pereira (2020) Inactivation of *Aspergillus* species in real water matrices using medium pressure mercury lamps. Submitted.

Beatriz Oliveira was involved in all the experimental work presented in this chapter. Ana Paula Marques helped performing the experiments to determine the DNA damages. Mariana Ressurreição helped performing the reactivation experiments. Carlos Moreira helped with protein extraction under the supervision of Cristina Silva Pereira. Maria Teresa Barreto Crespo and Vanessa Pereira supervised all the experimental work performed.

CONTENTS

Abstract

The presence of filamentous fungi in the aquatic environment and their potential problems have been reported in recent years. The use of UV radiation for drinking water treatment has increased along the years due to the high efficiency of this process to inactivate resistant microorganisms. The aim of this work is to understand the inactivation efficiency of medium pressure mercury lamps, measured in terms of growth inhibition as well as cell death, damage and response, using three different *Aspergillus* species (*A. fumigatus*, *A. niger* and *A. terreus*) spiked in filtered surface water. A complete characterization of the effect of the treatment on each of the fungal species was assessed considering spores' morphology, cell wall integrity and enzymatic activity, the formation of pyrimidine dimers in the DNA and proteome analysis. Results showed that, when subjected to medium pressure mercury lamps, *A. niger* is the most resistant species to inactivation, that both *A. fumigatus* and *A. niger* suffer more morphological changes and present a higher number of damaged spores and *A. terreus* presented more dead spores. DNA damages detected in *A. niger* were able to be repaired to some extent, under light and dark conditions. Finally, proteome analysis showed that the UV radiation treatment triggered different types of stress response, including cell wall reorganization and DNA repair in *A. fumigatus* and *A. terreus*, and oxidative stress responses like the increase in the production of citric acid and itaconic acid in *A. niger* and *A. terreus*, respectively.

Keywords: Water disinfection; medium pressure mercury lamps; *Aspergillus*; cellular response; reactivation.

2.1 Introduction

Filamentous fungi are known to occur ubiquitously in natural environments such as soil, air and water. In water matrices, these microorganisms have already been reported to occur in groundwater, surface water, spring water, along the water treatment systems, tap water and bottled water (Babič et al., 2017; Hageskal et al., 2011; Nourmoradi et al., 2012; Oliveira et al., 2013; Parveen et al., 2011; Pereira et al., 2009; Pontara et al., 2011). Several genera of fungi have been reported in these studies like *Penicillium*, *Trichoderma*, *Cladosporium*, *Fusarium* and *Aspergillus*. The presence of filamentous fungi in the aquatic environment has been related to several taste, odor and health problems (Doggett, 2000) since some species may cause allergies, opportunistic infections and intoxications (Babič et al., 2017).

In recent years, several disinfection studies have been performed aiming at the elimination of fungi from drinking water sources through the addition of chlorine or chloramines as a final disinfectant (Ma and Bibby, 2017; Pereira et al., 2017; Pereira et al., 2013a; Wen et al., 2017) or through UV inactivation either using low-pressure mercury lamps (Chen et al., 2009; Nourmoradi et al., 2012; Pereira et al., 2013b; Wen et al., 2019b) or UV-light emitting diodes (Oliveira et al., 2020; Wan et al., 2020). The application of UV for drinking water treatment has increased along the years due to its effectiveness to inactivate viruses, bacteria and protozoan (oo)cysts (Hijnen et al., 2006). Since it is chemical free, it reduces the dosage of chlorine to be added as final disinfectant, and thereby reduces the production of chlorination disinfection by products that have been linked to deleterious health effects (Pereira and Singer, 2004). Medium pressure (MP) mercury lamps, although very often used for drinking water treatment, have not been evaluated for the inactivation of filamentous fungi from real water sources. Since MP lamps emit polychromatic light in a wide range of wavelengths, they are expected to affect not only the DNA but also proteins by the destruction of disulfide bonds (Oppenländer, 2003). However, after inactivation, some

spores might be able to reactivate under light exposure (photoreactivation) or in the dark (dark repair).

Three different species from the *Aspergillus* genus were selected to perform these experiments since it is the most common genus reported in drinking water in Europe (Babič et al., 2017). Within its species, *A. fumigatus*, *A. niger*, and *A. terreus* were selected due to their i) different pigmentations that confers them different colors, ii) spores' resistance to conventional drinking water treatments, and iii) potential pathogenicity (Braga et al., 2015; Jørgensen et al., 2011; Oliveira et al., 2013; Youngchim et al., 2004; Zaehle et al., 2014).

The higher resistance of filamentous fungi to UV inactivation compared with other microorganisms has already been reported having two possible explanations: the production of resistant spores that additionally might have pigmentation (Brags et al., 2006; Nascimento et al., 2010) and the production of enzymes that have the ability to neutralize the oxidative species formed (Avalos and Carmen Limón, 2015). Regarding the pigmentation, Brags et al. (2006) stated that different fungi pigmentations confer different resilience to UV inactivation. For instance, the author used fungal conidia with green (wild type), yellow and purple (mutants) pigments and showed that higher germination percentages after UV inactivation were obtained for the green, followed by the yellow and then by the purple strains. According to this, the distinct color pigments of *A. fumigatus* (green), *A. niger* (black) and *A. terreus* (brownish) is expected to influence their response to UV radiation.

The aim of this study was to address the inactivation of three filamentous fungi species (*A. fumigatus*, *A. niger*, and *A. terreus*) spiked into filtered surface water using a medium pressure bench-scale UV collimated beam reactor. Since this is the first study performed using a MP lamp for the inactivation of filamentous fungi, characterization of fungal spores' morphology, membrane permeability and enzymatic activity, DNA damages and proteome response were addressed. To do this, scanning electron microscopy (SEM) was performed to visualize the spores' surface; the combination of

fluorescent dyes like fluorescein diacetate and propidium iodide with flow cytometry was applied to detect dead, live, damage and quiescent spores; an enzyme-linked immunosorbent assay (ELISA) was conducted to quantify the formation of cyclobutane pyrimidine dimers in the DNA; and protein identification was performed to characterize the profile of proteins detected before and after MP UV treatment.

2.2 Methods

2.2.1 Preparation of fungi concentrated suspensions

The tested species were isolated from surface water in previous studies and are preserved in a culture collection under the following references: *A. fumigatus* (T161007_176), *A. niger* (T161007_187) and *A. terreus* (T201107_004).

Most inactivation studies conducted by different authors describe the preparation of the spore suspension without referring if the solution is filtered to retain the mycelia while few other studies refer the separation of mycelia from the spores obtained through filtration. In order to define the fungal inoculum for this study, a preliminary experiment was performed to address the difference in resistance to UV inactivation in solutions spiked with: fungal fresh spores, frozen spores, mycelium as well as spores mixed with mycelium. For this preliminary experiment, *A. fumigatus* was used as a representative of the three *Aspergillus* species understudy. To prepare the fresh spore solution the suspension was filtered using glass wool to retain the mycelium and only the spores were used. For the frozen spores' experiment, a preserved concentrated spores' suspension at -20 °C was used. For the mycelium experiments, the fungi were grown in malt extract broth and the mycelium recovered by centrifugation. Finally, to obtain spores and mycelium, no glass wool filtration was used, and the suspension was used including a mixture of spores and mycelium. Samples were taken at the initial experimental time (0 min) as well as after 0.5 min, 1 min, 5 min, and 30 min of exposure

to the MP lamp. Results presented in figure 2.1 as log (C/C0), where C is the concentration of the fungal spores determined along the experimental time and C0 is the concentration of the spores in the beginning of the experiment (at time 0 min), show that there is an increased resistance to UV disinfection when the mixture (spores and mycelium) is used probably due to scavenging of the UV light by the mycelium. In the samples collected after 30 min of exposure to UV light, growth on plate was only detected in the samples containing mycelium. Moreover, Oliveira et al (2020) showed that the target *Aspergillus* species, *A. fumigatus*, *A. niger* and *A. terreus*, occur in the aquatic environment as a mixture of spores and mycelium. The dry weight measurements of the spores and mycelia collected were measured and are presented in the supplementary information section (table 1 from supplementary information 1). Within the same species, the dry weight measurements obtained in triplicate samples in four different assays are very consistent. However, the dry weight measurements are higher for *A. niger* compared with the dry weight measurements obtained for *A. fumigatus* and *A. terreus*. An increased resistance to UV disinfection can therefore be expected in the solutions of *A. niger* due to scavenging of the UV light by the mycelium. Nevertheless, the concentration of mycelium was not considered in the experiments performed for the different fungi species, since it was decided to have equal concentrations of spores (the most resistant morphological structures).

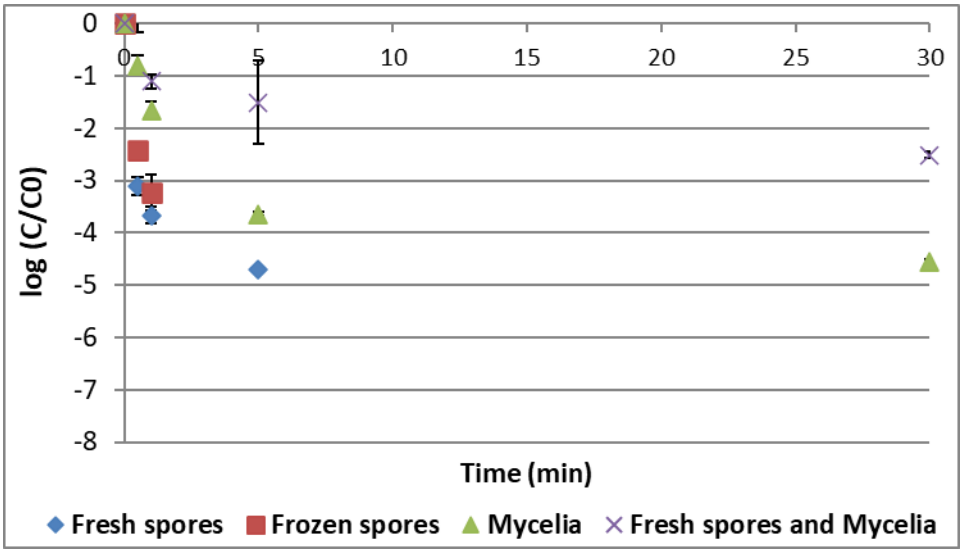

Figure 2.1 – Inactivation of *Aspergillus fumigatus* using a medium pressure mercury lamp. Samples of 1 mL were taken at times 0 min, 0.5 min, 1 min, 5 min, and 30 min of UV exposure. Error bars represent duplicated results obtained in up to 7 dilutions tested.

Considering this, to perform this study, plates containing malt extract agar (Merck, USA) were inoculated with *A. fumigatus*, *A. niger*, and *A. terreus* and incubated for 7 days at 27 °C. After growth, a saline solution (0.9 % w/v) with Tween 80 (0.1 % v/v) was added to the plates and the spores and mycelium recovered. This suspension was washed through centrifugation three times using saline solution (0.9 % w/v) and the final pellet was resuspended in 150 mL of the working matrix (saline solution and filtered surface water described in section 2.2.3). The concentration of this concentrated suspension was determined using the Neubauer chamber. To determine inactivation rate constants, the concentration of spores was determined for each experiment (as detailed in section 2.2.3.1.1).

2.2.2 UV reactor description

The inactivation experiments were performed using a bench-scale UV collimated beam set up coupled with a medium pressure mercury lamp UVH-Lamp Type Z (UV-Technik, UK) that emits polychromatic light (figure 1 from supplementary information 1). The average irradiance of the lamp was measured at 20 cm distance (which is at the same distance used to perform the experiments) after 60 min of stabilization time.

2.2.3 Inactivation experiments

From the concentrated suspension described in section 2.2.1, a working solution was prepared by diluting it in 500 mL of the working matrix to a final concentration of 10^8 spores/mL. Although a high concentration of spores had to be used so that their concentration and influence of light in the spores' (in terms of morphology, cell wall integrity and enzymatic activity, the formation of pyrimidine dimers in the DNA and proteome analysis) could be followed, these high concentrations influence the solution transmittance and thus direct photolysis. For a certain species to be inactivated by direct photolysis, it needs to have the capacity to absorb the emitted light. The transmittance of the working solutions are presented in the supplementary information section (figure 2 from supplementary information 1). The solutions of *A. niger*, *A. fumigatus* and *A. terreus* were black, green and brown, respectively. The solution transmittances, calculated at the wavelengths emitted by the medium pressure lamp were low but similar between the three fungi species tested. Samples of 50 mL from this working solution were maintained, with gentle stirring, in a doubled walled glass Petri dish with cold water circulation inside the walls to maintain temperature at 20 °C. Samples were placed at 20 cm below the medium pressure lamp and collected at time 0 min as well as after 0.5 min, 1 min, 5 min, 10 min, 15 min, 30

min, 45 min, and 60 min of UV exposure. For each sample collected, 1 mL was used to assess colony forming units (CFU)/mL and the rest of the volume centrifuged and resuspended in 10 mL of saline solution and kept at -20 °C until further analysis. A natural light control (samples taken at time 45 min and 60 min) and a dark control (sample taken at time 60 min) were performed to verify the stability of the different fungi throughout the experimental time by being either under natural light conditions or covered with aluminum foil protected from light, respectively. For control samples 1 mL was also taken to assess colony forming units (CFU)/mL.

The matrices used to perform these experiments were i) saline solution (0.9 % w/v) and ii) untreated surface water collected from the river after filtration with 0.2 µm membrane filter to simulate the first steps of conventional drinking water treatment. The untreated surface water used was chemically characterized before and after membrane filtration as detailed in Oliveira et al (2020). Briefly, the filtered surface water used in the experiments had the following characteristics: 20 °C, pH of 7.64, total organic carbon of 2.35 mg/L C, turbidity of 0.22 NTU, chemical oxygen demand of 1172 mg/L O_2, total solids of 38.94 g/L and total suspended solids of 22.60 mg/L.

2.2.3.1 Disinfection efficiency determination

2.2.3.1.1 Plate count

Fungi growth was quantified in the samples collected after different UV exposure times, as well as in the light and dark control samples, in terms of CFU/mL, after performing serial dilutions in buffered peptone water and the pour plate method using malt extract agar (Merck, USA) with plate incubation for 2-3 days at 27 °C.

2.2.3.1.2 Scanning Electron Microscopy

Scanning electron microscopy was conducted to verify effects on fungal spores' morphology before and after exposure to the MP lamp. To do this, the preparation of samples collected before and after 60 min of UV exposure was performed according to Panngom (2014) with some modifications introduced by Oliveira et al (2020). Briefly, the samples were washed with phosphate buffered saline (PBS) solution (pH 7) for 5 min, fixed according to Karnovsky's Fixative (Polysciences Inc., Germany) protocol and then with osmium tetroxide (1 % v/v) for 2 hours in the dark. Between each fixation step, samples were washed three times with PBS and centrifuged at 10 000 rpm (Eppendorf Centrifuge 5415D, Germany) for 5 min. Dehydration of the samples was performed using increasing ethanol concentrated solutions (30, 50, 70, 80, 90, 95 and 100 % v/v). Finally, samples were freeze dried for 30 min and placed on top of carbon conductive tape. The scanning electron microscopy images were acquired using a PC-SEM by JEOL and a FEG-SEM JEOL JSM7001F, with a 15 kV acceleration voltage after being coated with gold and palladium particles using a Quorum Technologies sputter coater, model Q150T ES.

2.2.3.1.3 Flow Cytometry analysis

The flow cytometry technique coupled with fluorescent staining dyes allows the assessment of several morphological, chemical and metabolic changes of the cells understudy. In this study, the Yeast Control Viability Kit (Sysmex Partec, GmbH, Germany) that contains fluorescein diacetate (FDA) and propidium iodide (PI) enabled to separate the filamentous fungi into four groups (Oliveira et al., 2020): 1- metabolically active spores - when there is enzymatic activity the FDA dye is degraded by esterases and transformed into a fluorescent product emitting a positive signal; 2 - dead spores – if the membrane/cell wall is permeable or disrupted the PI dye enters

the cells and intercalates in the DNA emitting a positive signal; 3 - damage spores – if spores have membrane/cell wall permeability (giving a positive signal for PI) but at the same time have enzymatic activity (giving a positive signal for FDA); 4 – quiescent spores – with negative FDA and PI signals, after treatment with the fluorescent staining dyes (as described by the kit's manufacturer).

The samples collected before and after 60 min of UV exposure were diluted in phosphate saline solution buffer (PBS) to a final concentration of 10^6 spores/mL and analyzed using a CyFlow® Cube 6 (Sysmex Partec GmbH, Germany) equipped with a 488 nm excitation blue solid-state laser at 50 mW. The CyViewTM for Cube 6 software (Partec GmbH, Germany) was used to analyze the obtained cytograms. Those cytograms were corrected to eliminate the baseline background signal from the PBS.

2.2.3.1.4 DNA damage

To address the occurrence of DNA damage in the fungal spores, the DNA was extracted from the samples collected before UV exposure, after 30 min of UV exposure and after 60 min of UV exposure using the DNeasy® UltraClean® Microbial Kit (Qiagen, USA) according to the manufacturer's instructions with some modifications. Briefly, cell lysis was performed using a Precellys Evolution tissue homogenizer (Bertin instruments, France) for 2 minutes at 10 000 rpm with 10 seconds break. All centrifugations were performed using twice the time advised in the manufacturer's protocol. DNA samples were quantified by absorbance using the NanoDrop ND-1000 Spectrophotometer (Thermo Fisher Scientific, USA).

The targeted DNA damage was the cyclobutane pyrimidine dimers that were assayed using the OxiSelect™ UV-Induced DNA Damage ELISA Kit (CPD Quantitation) (Cell Biolabs, Inc, USA) according to manufacturer's instructions.

2.2.3.1.5 Proteome analysis

Proteome analysis was performed in samples not subject to UV and those collected after 60 min of UV radiation exposure. Proteins were extracted, quantified and analyzed by Liquid chromatography tandem mass spectrometry (LC-MS/MS). Protein extraction was performed according to Carvalho et al (2013) with some modifications. Briefly, samples were recovered by vacuum filtration using a 0.22 µm of pore size membrane (PALL, USA) and transfer of the retained mycelia and spores into Eppendorf tubes was performed. Samples were then frozen in liquid nitrogen, 0.02 g of polyvinylpolypyrrolidone (Sigma, USA) were added to the tubes and samples were homogenized using a Tissuelyser LT (Qiagen, Germany). Protein precipitation was performed with a cold solution of trichloroacetic acid (TCA – Sigma, USA)/acetone/dithiothreitol (DTT – VWR, USA) (1.5 mL of 10 % (w/v) TCA in acetone and 60 mM DTT) for 1 hour at -20 °C. The pellet was washed 5 times with a cold solution of 60 mM DTT in acetone and air-dried overnight. The cold solutions used were preserved at -20 °C until use and kept on ice during the experiment. A resuspension buffer [7 M urea (GE Healthcare, UK), 2M thiourea (GE Healthcare, UK), 30 mM tris (GE Healthcare, UK), 4 % (w/v) CHAPS (GE Healthcare, UK) and cOmplete ultra-tablets, mini, EDTA-free, EASY pack (Roche, Switzerland)] was used to equilibrate the proteins.

Protein quantification was performed using the 2-D Quant Kit (GE Healthcare, UK) according to the manufacturer's instructions.

Protein extract was loaded onto a NuPAGE™ 4-12% Bis-Tris Protein Gel and electrophoresed for a short time (10 min - 15 min) at 110 V (Anjo et al., 2015) onto 4-20 % pre-casted tris glycine extended (TGX) stain-free gels (Invitrogen, USA). A gel slice containing the entire protein extract was excised, reduced in 10 mM DTT (Sigma, USA) for 40 min at 56 °C, and alkylated in 55 mM iodoacetamide (Sigma, USA) for 30 min in the dark. Excessive iodoacetamide was quenched by further incubation with DTT (10 mM for 10 min in the dark). The resulting sample was digested overnight with trypsin

(Promega, USA) at 37 °C (1:50 protein/trypsin ratio) and cleaned up with octadecylsilane.

Nano-liquid chromatography-tandem mass spectrometry (nanoLC-MS/MS) analysis was performed on an ekspert™ NanoLC 425 cHiPLC® system coupled with a TripleTOF® 6600 with a NanoSpray® III source (Sciex, USA). Peptides were separated through reversed-phase liquid chromatography (RP-LC) in a trap-and-elute mode. Trapping was performed at 2 µL/min on a Nano cHiPLC Trap column (Sciex 200 µm x 0.5 mm, ChromXP C18-CL, 3 µm, 120 Å) with 100% A (10 % of formic acid in LC-MS grade water) for 10 min. The separation was performed at 300 nL/min, on a Nano cHiPLC column (Sciex 75 µm x 15 cm, ChromXP C18-CL, 3 µm, 120 Å). The gradient was as follows: 0-1 min, 5% B (0.1% formic acid in acetonitrile, Fisher Chemicals, Belgium); 1-91 min, 5-30% B; 91-93 min, 30-80% B; 93-108 min, 80% B; 108-110 min, 80-5% B; 110-127 min, 5% B.

Peptides were sprayed into the MS through an uncoated fused-silica PicoTip™ emitter (360 µm O.D., 20 µm I.D., 10 ± 1.0 µm tip I.D., New Objective, France). The source parameters were set as follows: 15 (ion gas source) GS1, 0 GS2, 30 curtain gas (CUR), 2.5 keV ion spray voltage floating (ISVF) and 100 °C interface heater temperature (IHT). An information dependent acquisition (IDA) method was set with a TOF-MS survey scan of 400-2,000 m/z. The 50 most intense precursors were selected for subsequent fragmentation and the MS/MS were acquired in high sensitivity mode for 40 ms. The obtained spectra were processed and analyzed using ProteinPilot™ software, with the Paragon search engine (version 5.0, Sciex). A UniProt database (4686 entries, accessed in 01/09/2019) containing the sequences of the proteins from *Aspergillus* (Taxon ID: 5052) was used. The following search parameters were set: Iodoacetamide, as Cys alkylation; Trypsin, as digestion; TripleTOF 6600, as the Instrument; ID focus as biological modifications and Amino acid substitutions; search effort as thorough; and a false discovery rate (FDR) was used for multiple hypothesis

correction. Only the proteins with Unused Protein Score above 1.3 and 95% confidence were described.

Functional enrichment analysis was performed to find the biological mechanistic representations of the identified proteins. For a given set of genes or proteins, functional enrichment analysis utilizes existing annotation resources to discover the underlying biological mechanisms. In this study, DAVID tool (v6.8) (Huang et al., 2008) was used to employ functional enrichment analysis and Gene Ontology (GO) was selected as an annotation resource. The GO is most commonly used annotation resource which consists of three categories, namely biological process, cellular component and molecular function. GO knowledge is represented in a direct acyclic graph with a clear hierarchical parent to child relationships between biological terms. Frequently, functional enrichment analysis results into highly similar biological terms because of the structure of GO, making it difficult to interpret results. Therefore, REVIGO tool (Supek et al., 2011) was used to cluster highly similar GO terms from functional enrichment analysis. The REVIGO tool uses semantic similarity to group highly similar GO terms. Semantic similarity measures such as SimRel (Schlicker et al., 2006) utilizes the GO hierarchical structure to estimate the similarity between GO terms. The similarity score ranges from 0 to 1 and a score of 1 indicates identical terms. In REVIGO tool, SimRel measures were selected and a semantic similarity score of 0.9 was used to group similar go terms.

2.2.3.2 Photoreactivation and dark repair experiments

Photoreactivation experiments were performed by placing 50 mL of the sample not subject to UV and of the samples collected after 30 min and 60 min of UV exposure into an Environmental Chamber 600 PLH (Aralab, Portugal) at 27 °C for 8 hours under three Osram DULUX L 18W / 21-840 2G11 LUMILUX Cool White lamps (light intensity at 150

mm up to 200 µmol/m2/s, luminous flux of 1200 lm and colour temperature of 4000 K with an average intensity of 102.26 µW/cm^2 = 0.1 mW/cm^2). Dark Repair experiments were equally performed but were placed in the dark and kept at the same temperature (27 °C) for 8 hours. Samples were taken from the incubator after 4 hours and 8 hours of reactivation to be further analyzed in terms of plate counts and DNA damages (as detailed in sections 2.2.3.1.1 and 2.2.3.1.4).

2.3 Results and Discussion

2.3.1 Inactivation results

The inactivation results obtained when *A. fumigatus*, *A. niger* and *A. terreus* were spiked into filtered surface water and subjected to medium pressure UV light are presented in figure 2.2. Samples were collected at the beginning (time 0 min) and along the experimental times (0.5 min, 1 min, 5 min, 10 min, 15 min, 30 min, 45 min and 60 min). The results are presented as log (C/C0). Control samples remained constant throughout the experimental time.

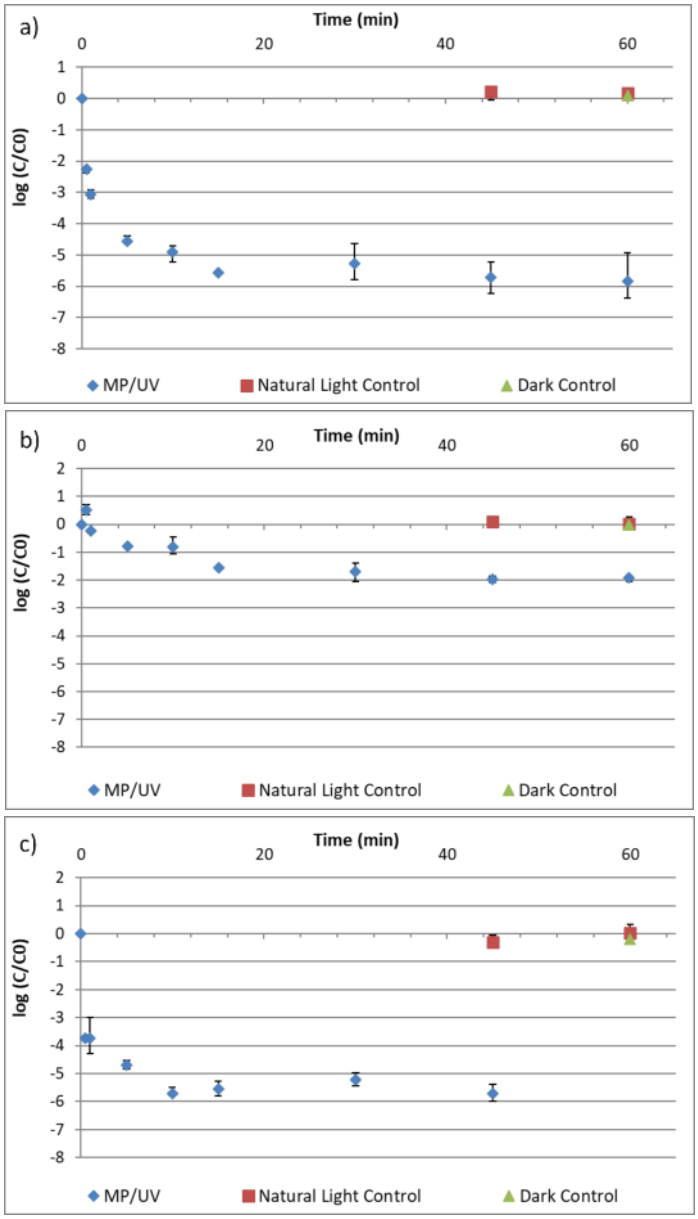

Figure 2.2 – Inactivation results in log (C/C0) of a) *A. fumigatus*, b) *A. niger* and c) *A. terreus* spiked into filtered surface water after UV exposure along the experimental time. Two controls are presented (natural light control and dark control). Error bars represent duplicate results in up to 7 dilutions tested.

Figure 2.2 shows higher inactivation for *A. fumigatus* and *A. terreus* compared to *A. niger* which was very resilient to UV radiation. The log reductions for *A. fumigatus*, *A. niger* and *A. terreus* were 3.05-log, 0.23-log and 3.50-log after 1 min of inactivation and 5.58-log, 1.90-log and 5.63-log after 45 min of inactivation, respectively. Thus, after 45 min of inactivation, *A. niger* shows less log reductions compared to *A. fumigatus* and *A. terreus* right after 1 min of inactivation. Moreover, *A. fumigatus* and *A. terreus* showed higher log reduction differences after 1 min of inactivation than after 45 min of inactivation when similar log reductions were obtained. Similar results were obtained for the inactivation assays conducted using saline solution matrix (figure 3 from supplementary information 1) meaning that there is no matrix interference in the inactivation experiments. The MP/UV results presented in figure 2.2 show that a linear regression can only be used to explain the inactivation obtained for the initial exposure times. For extended exposure times, a polynomial regression can be used to explain the tailing off inactivation curve obtained after inactivation of microorganisms, either due to interfering substances of the matrix or due to the presence of clusters of spores or due to genetic resistance (Gerba, 2000). Since in this case, the matrix components did not interfere with the inactivation (as can be seen by comparing figure 2.2 and figure 3 from supplementary information 1) the presence of clusters of spores or genetic resistance may explain the results obtained. The linear and polynomial regressions with the correspondent coefficients of determination are presented in table 2 from supplementary information 1.

Sisti et al. (2017) tested the efficacy of UV radiation using an UV-C low-pressure mercury lamp to inactivate the spores of 9 *Aspergillus* species in tap water. This study showed that it is possible to remove most of the species tested and achieve a significant reduction in the more resistant species such as *A. flavus* and *A. niger*. This study also showed that *A. terreus* is one of the most sensitive species to UV. The authors claimed that *A. niger* UV resistance is probably due to their particular cellular structure, which includes the presence of pigments as has been observed in melanized fungi.

Nourmoradi et al. 2012, using a continuous flow low pressure UV reactor also showed that *A. fumigatus* is less resistant than *A. niger* to UV light. Oliveira et al. 2020 studied the effectiveness of light emitting diodes to inactivate the same species of *Aspergillus* in water. The inactivation results were consistent with this study showing that *A. niger* is more resistant to UV than *A. terreus* and *A. fumigatus.*

Considering the color of the pigments, *A. niger* (black) was expected to have higher resistance followed by *A. fumigatus* (green) and then by *A. terreus* (brownish) (Brags et al., 2006). However, it can be observed in figure 2.2 that the last two show similar resistances. This study is not sufficient to conclude the existence of a correlation between the presence of a certain pigment and the higher resistance of a species to UV radiation. Therefore, analysis of the pigments by high performance liquid chromatography should be performed to verify if the pigments scavenge the UV light or are being degraded by the UV radiation treatment. Another reason for the different resistance levels observed could be due to spores' size since bigger spores may need more exposure times to be inactivated (Nascimento et al., 2010). *A. niger* has bigger spores (3.5 µm - 4.5 µm) than *A. fumigatus'* (2.5 µm - 3.0 µm) and *A. terreus*' (1.5 µm - 2.5 µm) spores.

2.3.2 Phenotypic effect on fungal spores

To observe morphological changes in the spores of the filamentous fungi used in the inactivation assays, scanning electron microscopy was performed on samples collected before and after 60 min of UV exposure (figure 2.3). The images of the spores before being subjected to UV (figure 2.3 - No Exposure) show that all of them are globose with specific features. *A. fumigatus* spores have rough to echinulate cell wall, *A. niger* spores have irregular warts, spines and ridges and *A. terreus* spores have a smooth cell wall (Samson et al., 2004). After 60 min exposure to a medium pressure lamp, *A. fumigatus* spores seem to keep the globose shape but show increased roughness of the cell wall; *A. niger* spores seem to be the most affected species by the radiation presenting spores more flattened and with cracks and *A. terreus* seem to maintain the same shape and structure showing just few shrank spores.

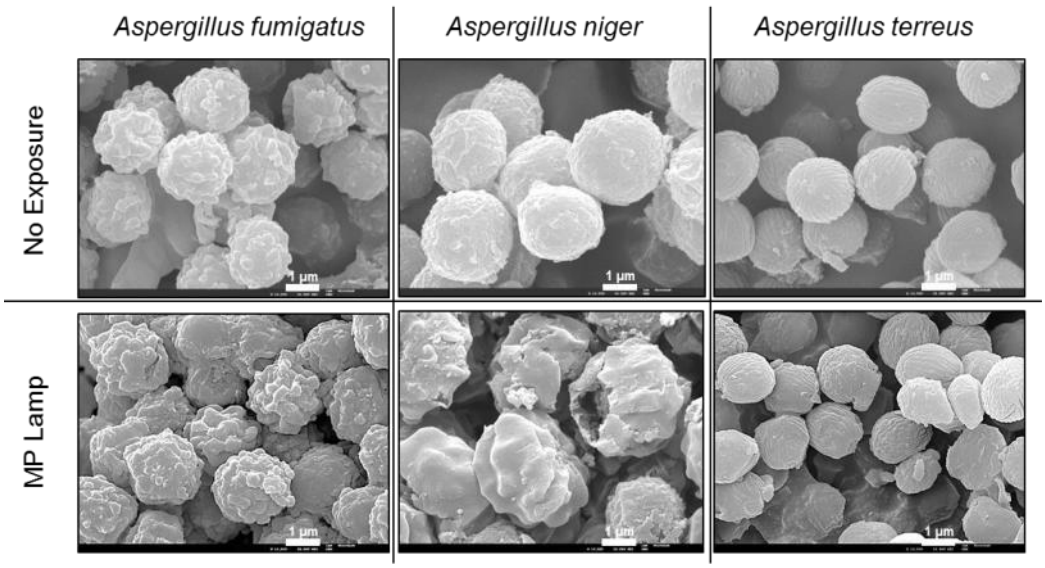

Figure 2.3 – Scanning electron microscopy images acquired from samples collected before (No Exposure) and after 60 min of exposure to a MP lamp of *A. fumigatus*, *A. niger* and *A. terreus*. The total magnification of the images is 13 000 X.

The results obtained showed that two of the less resistant species (*A. terreus* and *A. fumigatus*) did not present a high morphological change after a considerable time of exposure (60min) to medium pressure UV so their inactivation must be explained due to other effects of radiation such as degradation of DNA. For *A. niger*, further studies are needed to evaluate the cell wall morphological changes that occur during UV inactivation considering its components such as chitin, glucans and glycoproteins (Bowman and Free, 2006).

2.3.3 Effect on membrane permeability and enzymatic activity

To address membrane permeability and enzymatic activity of the fungal spores, flow cytometry coupled with fluorescein diacetate (FDA) and propidium iodide (PI) dyes was used. This methodology was already shown to be suitable for fungal spores analysis (Ehgartner et al., 2016; Oliveira et al., 2020) and to be able to discriminate metabolically active (FDA positive), dead (PI positive), quiescent (FDA and PI negative) and damaged (FDA and PI positive) spores (Oliveira et al., 2020).

Samples of filtered surface water spiked with 10^8 spores/mL of the three species before and after 60 min of medium pressure radiation were diluted to a final concentration of $1x10^6$ spores/mL for further analysis. The cytograms obtained were corrected to eliminate the baseline background of PBS. Figure 2.4 shows the results as a percentage bar chart that represents the percentage of fungal spores that are metabolically active, dead, damage and quiescent.

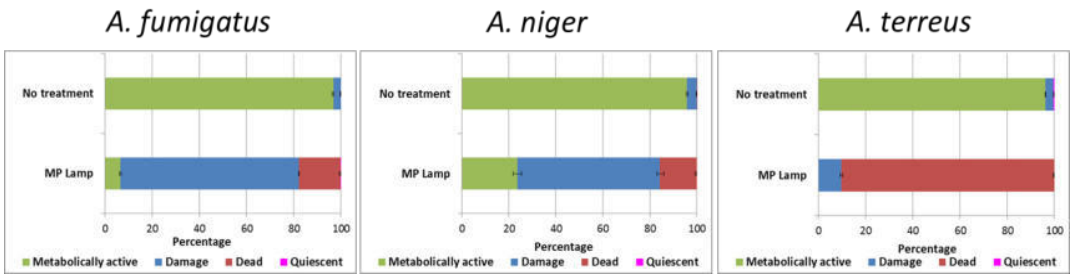

Figure 2.4 – Percentage bar charts representing the cytogram results using FDA/PI fluorescent dyes obtained in the assays conducted with *A. fumigatus*, *A. niger* and *A. terreus* before (No treatment) and after 60 min of UV exposure to a MP lamp. Error bars represent triplicate measurements.

As can be observed in figure 2.4, before treatment the spores of the three fungi species are mainly metabolically active showing a small percentage of damaged spores. After UV inactivation, *A. fumigatus* and *A. niger* show an increase on the percentage of damaged spores and consequently, a decrease in the amount of metabolically active spores. Both species also show a small increase on the percentage of dead spores (around 20%), in contrast to what happens with *A. terreus* (around 90% of dead spores). These results are consistent with the inactivation results shown in figure 2.2, being *A. terreus* the less resistant species followed by *A. fumigatus* and then by *A. niger*, that is the most resistant species in this study. Considering the flow cytometry results presented, that were analyzed after 60 minutes of UV radiation exposure, it can be seen that most of the spores of *A. terreus* are dead (consistent with figure 2.2 since spores were not able to grow on plate) and a few percentage are damaged. Contrastingly, *A. fumigatus* has a low percentage of metabolically active spores and a higher percentage of damaged spores.

The correlation between plate counts and flow cytometry was established by Wen et al. (2020). In this study the correlation between the germinating spores on plate and the metabolically active spores was determined to be 0.99. These results strongly suggest a direct correlation between the two techniques (figure 4 from supplementary

information 1). Nevertheless, it is worth to mention that when exposed to a moderate UV-C radiation, this correlation decreases (Ehgartner et al., 2016; Oliveira et al., 2020). One possible explanation might be that the DNA may be affected while the membrane may remain intact leading to less germination numbers on plate but more metabolically active spores in the flow cytometer (PI cannot enter the cell if the membrane is still intact). The usage of a medium pressure mercury lamp herein means that, due to its high intensity and polychromatic light, other cell components besides DNA are affected. A question that arises is if the differences in correlation may be due to wavelength differences, different UV fluences (resulting from the product of irradiance and exposure times), or both since Bowker et al. (2011) reported that both absorption spectrum and UV fluence affect inactivation.

2.3.4 Determination of DNA damage

Before determining the occurrence of cyclobutane pyrimidine dimers (CPDs), quantification of total DNA present in the samples after exposure to a MP lamp during 30 min and 60 min was performed. Results showed that the MP lamp was able to degrade the DNA of all samples (table 3 from supplementary information 1). Since *A. fumigatus* and *A. terreus* are more sensitive to UV-C radiation, their DNA was highly damaged which did not allow the extraction of the minimum ammount of DNA required (4 ng/µL) to be applied in the enzyme-linked immunosorbent assay (ELISA). Only the DNA samples collected in the assay spiked with *A. niger* could therefore be analyzed. Figure 2.5 shows that, as expected, no CPDs were detected in the sample not exposed to radiation while both samples subject to radiation (collected after 30 min and 60 min of exposure) showed a similar level of CPDs, close to 100 ng/mL. The results are consistent with the tailing off inactivation curve obtained (figure 2.2) that shows similar inactivation results for the samples collected after 30 min and 60 min exposure to radiation.

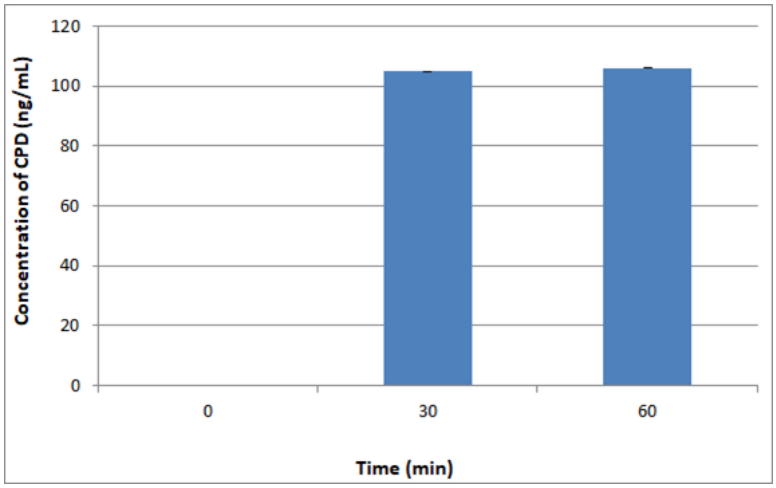

Figure 2.5 – Concentration of *Aspergillus niger* CPDs (ng/mL) formed at the beginning and after 30 min and 60 min exposure to MP/UV radiation. Error bars represent duplicates.

Nascimento et al (2010), using a different UV lamp (peak wavelength at 313 nm) and other CPDs' detection methodology (endonuclease sensitive site assay), determined the concentration of cyclobutane pyrimidine dimers expressed in CPDs/10 kilo base pairs (kbp) for two *Aspergillus* species. The authors verified that *A. fumigatus* was more prone to the formation of CPDs (showed 0.803 CPDs/kbp after 60 min of inactivation time) than *A. nidulans* although being from the same genera. In this study, even though *A. fumigatus* and *A. terreus* were found to be extremelly susceptible to DNA damage, the low DNA concentration from these samples did not allow the dimer quantification.

2.3.5 Proteome response

Several genomes of filamentous fungi species, including *A. fumigatus* (Nierman et al., 2005), *A. niger* (Pel et al., 2007) and *A. terreus* (Askenazi et al., 2003), were sequenced in recent years, which enabled predictions of their proteome by means of bioinformatic tools (Cologna et al., 2018). In the present study, proteome analysis was performed to evaluate major cellular responses after exposure to MP radiation.

Although mycelium has been described as having high metabolic activity in contrast to conidia, it has been reported that the functional classification of the identified proteins from these fungi structures, shows similar abundances of metabolic proteins (Barros et al., 2010 and Leng et al., 2008). Since the purpose of this study was to have data from an overall proteome response of the different *Aspergillus* species to UV radiation, proteins from both mycelia and spores were extracted, quantified, and analyzed by LC-MS/MS. Nevertheless, further studies should be performed to address mycelia and conidia separately, as well as the proteome response to UV radiation of subcellular structures such as cell wall, plasma membrane and cytoplasmic organelles.

The proteome analysis of *A. fumigatus*, *A. niger* and *A. terreus* was thus performed before (non-treated samples) and after 60 min of exposure to MP radiation. The total number of protein accession numbers obtained and the corresponding matches with the background database for DAVID Proteomics and FungiFun2 are presented in table 4 from supplementary information 1. The proteins were clustered according to three gene-ontology (GO) categories (table 2.1 and tables 1, 2 and 3 from supplementary information 2): biological process (BP), that clusters proteins according to their contribution to operations or sets of molecular events essential for the functionality of integrated living units like cells, tissues, organs and organisms; cellular component (CC), that clusters the proteins according to their cell localization; and molecular function (MF), that clusters the proteins according to their activity at the molecular level. The identified proteins from LC-MS by DAVID proteomics, the GO terms from DAVID and

the GO clusters from REVIGO formed for each category and each individual species for the non treated samples and samples collected after 60 min exposure to the MP lamps, are presented in table 2.1.

As can be seen, there are some differences in the number of the identified proteins for each species which may reflect the different protein content obtained for each of the tested species after protein extraction and/or the differences in the number of assigned proteins in their corresponding databases. The lower number of GO terms for *A. niger* compared to the other species is probably due to the lower number of protein' annotations available for *A. niger*. After exposure to 60 min of MP radiation, the proteome response of each individual *Aspergillus* species was addressed in terms of biological process, cellular component and molecular function.

Table 2.1 – Number of proteins identified from LC-MS by DAVID, the GO terms from DAVID and the GO clusters from REVIGO formed for each category (BP, CC and MF) and each individual species (*A. fumigatus*, *A. niger* and *A. terreus*) for non treated samples and samples after 60 min exposure to MP lamps. GO – gene ontology; BP – biological process; CC – cellular component; MF – molecular function.

Species	Identified proteins from LC-MS	Proteins identified by DAVID	GO categories			New GO clusters Total (BP; CC; MF)
			BP terms (clusters)	CC terms (clusters)	MF terms (clusters)	
			A. fumigatus			
Non treated sample	1362	1360	37 (36)	53 (51)	41 (41)	
MP lamp	19	19	2 (2)	5 (5)	1 (1)	2 (1; 1; 0)
			A. niger			
Non treated sample	1574	124	3 (3)	2 (2)	3 (3)	
MP lamp	193	17	2 (2)	1 (1)	1 (1)	2 (1; 0; 1)
			A. terreus			
Non treated sample	424	415	14 (14)	10 (10)	13 (13)	
MP lamp	57	54	4 (4)	3 (3)	4 (4)	5 (2; 0; 3)

2.3.5.1 *Aspergillus fumigatus* response to MP radiation

Regarding the biological process category (table 2.1, figure 2.6 a) and table 1 from supplementary information 2), the detected proteins for *A. fumigatus* were grouped in two GO clusters: cell wall organization (GO:0071555) and translation (GO:0006412). The cell wall organization cluster, that did not appear in the non-treated *A. fumigatus* samples, contains a hydrophobin (P41746) and a glucanase (Q4WG16). Both proteins

are involved in cell wall rearrangements being the former specifically involved in resistance to environmental stress and conidial hydrophobicity. The translation cluster was present in both the non-treated samples and 60 min exposed UV samples, but the number of proteins detected was reduced from 71 to 4 proteins.

Figure 2.6 – Venn diagrams representing the *A. fumigatus* GO clusters formed after 60 min exposure to the MP lamps for a) biological process, b) cellular component and c) molecular function.

For the cellular component category (table 2.1, figure 2.6 b) and table 2 from supplementary information 2), the detected proteins after UV exposure were grouped in 5 GO clusters: anchored component of membrane (GO:0031225), fungal-type cell wall (GO:0009277), intracellular (GO:0005622), nucleosome (GO:0000786) and ribosome (GO:0005840). The first cluster only appeared after exposure to MP radiation and contains two proteins located in the membrane/cell wall (Q4WNS8 and Q4WG16) responsible for cell wall biogenesis. This cellular process consists in the biosynthesis of constituent macromolecules, assembly and arrangement of constituent parts of a cell wall. For the remaining clusters the number of proteins decreased from 9 to 2, 93 to 5, 7 to 3 and 53 to 4, respectively. The GO cluster fungal-type cell wall contains again hydrophobin (P41746) and the protein ecm33 (Q4WNS8) that is involved in cell wall biogenesis. In the intracellular cluster, it is important to mention the presence of the hydroxynaphthalene reductase arp2 protein (E9QUT3) which is involved in the biosynthesis of dihydroxynaphthalene (DHN)- melanin pigment that is deposited on the cell wall and required for the presence of hydrophobins. Additionally, the superoxide

dismutase [Cu-Zn] protein (Q9Y8D9) that destroys radicals toxic to cells, which can be related to an oxidative stress response was also identified. For the nucleosome cluster, the three proteins identified after UV exposure (Q7LKT3, Q4WWC5 and Q4WWC6) are histones involved in several DNA processes like transcription, replication and repair, being the latter, histone H2A, mainly responsible for repairing DNA double strand brakes. In the ribosome cluster the identified proteins are involved in protein biosynthesis.

In the molecular function category (table 2.1, figure 2.6 c) and table 3 from supplementary information 2) only one GO cluster was grouped after MP radiation exposure which was structural constituent of ribosome (GO:0003735). In this cluster 76 proteins were identified in the non-treated samples and 5 proteins in the samples after UV radiation, being all related with protein biosynthesis. This is not surprising since, one of the key cellular events that occurs during cell wall organization is the synthesis of proteins (Free, 2013).

Hence, several cell responses were detected to overcome the effect of the MP radiation on *A. fumigatus* that might explain the phenotypic effect observed by SEM (figure 2.3) and the effects on the membrane permeabiliy and enzymatic activity discussed in section 2.3.3. The adaptation of the cell wall by reorganizing it, the production of DHN-melanin and hydrophobins are responses that seem to be consistent with the higher roughness of the cell wall observed in figure 2.3. Moreover, the identification of proteins related with DNA repair (histone H2A) and oxidative damage (superoxide dismutase) are also consistent with the results of our study (as discussed below in section 2.3.6).

2.3.5.2 *Aspergillus niger* response to MP radiation

Concerning the biological process category (table 2.1, figure 2.7 a) and table 1 from supplementary information 2), the detected proteins for *A. niger* were grouped in two GO clusters: carbohydrate metabolic process (GO:0005975) and malate metabolic process (GO:0006108). These two processes are related with the citric acid cycle which is well studied in *A. niger* (Brandl and Andersen, 2017) due to its industrial importance (Andersen et al., 2011). Aditionally, it has been reported that the production of citric acid may be associated with oxidative stress response (Honda et al., 2012).

Figure 2.7 – Venn diagrams representing the *A. niger* GO clusters formed after 60 min exposure to the MP lamps for a) biological process, b) cellular component and c) molecular function.

In the cellular component category (table 2.1, figure 2.7 b) and table 2 from supplementary information 2) only one GO cluster was grouped which was intracellular (GO:0005622). In this cluster 11 proteins were detected in non-treated samples and only 3 were detected after exposure to radiation, malate dehydrogenase (A2QMH9) that it is related with the citric acid cycle, calcium ion binding (A2QJG6) which might be related with citric acid transportation through vesicle trafficking since it is regulated by voltage dependent calcium channels (Xie et al., 2018) and hydrolases (A2QBX5) that are enzymes with activity for several types of compounds.

For the molecular function category (table 2.1, figure 2.7 c) and table 3 from supplementary information 2), only one GO cluster was grouped, L-malate

dehydrogenase activity (GO:0030060) that appeared after UV inactivation. This cluster contains two proteins (A2QMH9 and A5ABV4) that are related with the malate metabolism.

The response of *Aspergillus niger* to the MP radiation is less diversified compared to the other two *Aspergillus* species, being only related with malate metabolism, possibly linked to oxidative stress response. The different spores' morphology observed in figure 2.3, as well as the increase of damaged and dead spores shown in figure 2.4 are not explained through the proteome analysis, possibly due to the lack of information in the databases that led to the impossibility to cluster several of the proteins identified in this study (table 2.1).

2.3.5.3 *Aspergillus terreus* response to MP radiation

Regarding the biological process category (table 2.1, figure 2.8 a) and table 1 from supplementary information 2), the detected proteins for *A. terreus* were grouped in 4 GO clusters: glycolytic process (GO:0006096), malate metabolic process (GO:0006108), translation (GO:0006412) and translational elongation (GO:0006414). From these, the glicolytic process and translation GO clusters were also detected in the non-treated samples with a higher number of proteins (the first from 6 to 2 and the second from 48 to 5). Considering the new clusters formed, the translational elongation proteins (Q0CTP9 and Q0CPE0) grouped two uncharacterized proteins and, similar to that observed in *A. niger*, there is the malate metabolic process group. In *A. terreus* this group is probably related with the production of itaconic acid which is also very important for the industry (Tevž et al., 2010). Although the metabolic pathway of itaconic acid has been well characterized, little is known about its ecological function in *A. terreus* (Wierckx et al., 2020). There is one study that reported that UV induced *A. terreus* mutants, under 254 nm radiation produced higher quantities of itaconic acid, had color variation and reduced production of conidia compared to wild type (Volz and

Dublin, 1973). This response may suggest a strategy used by *A. terreus* species to protect against oxidative stress.

For the cellular component category (table 2.1, figure 2.8 b) and table 2 from supplementary information 2), the detected proteins are grouped in 3 GO clusters: fungal-type cell wall (GO:0009277), nucleosome (GO:0000786) and ribosome (GO:0005840). The number of proteins grouped in these clusters decreased after UV radiation from 4 to 2, 5 to 4 and 37 to 5, respectively. In the fungal-type cell wall cluster, hydrophobin (Q0CIJ2) remains after UV radiation probably due to adaptation to environmental stress response, together with an uncharacterized protein. In the nucleosome cluster, 4 histones remain (Q0D0E8, Q0D0E7, Q0CBD1 and Q0CBD2) whose function is related with several DNA processes like transcription, replication and repair, being the latter, histone H2A, mainly responsible for repairing DNA double strand brakes. For the ribosome cluster, three of the proteins were uncharacterized and two (Q0D170 and Q0CLK4) responsible for protein biosynthesis.

Figure 2.8 – Venn diagrams representing the *A. terreus* GO clusters formed after 60 min exposure to the MP lamps for a) biological process, b) cellular component and c) molecular function.

In the molecular function category (table 2.1, figure 2.8 c) and table 3 from supplementary information 2), 4 GO clusters were grouped in the samples exposed to radiation: aspartic-type endopeptidase activity (GO:0004190), L-malate dehydrogenase activity (GO:0030060), RNA binding (GO:0003723) and structural constituent of ribosome (GO:0003735). The only cluster that appears in non-treated

samples and after UV radiation samples is the structural constituent of ribosome (with 51 proteins detected in the non-treated samples and 7 proteins detected in the samples exposed to radiation) that contains proteins related with protein biosynthesis. From the new clusters, the first contains two proteins where one is uncharacterized and the other (Q0CNQ8) is a vacuolar protease A which has been predicted to be an extracellular protein (Han et al., 2010). Again, there is the cluster of malate metabolism that might be related with the production of itaconic acid. In the RNA binding cluster, polyadenylate-binding protein, cytoplasmic and nuclear (Q0CR95) is responsible for binding the poly(A) tail of mRNA, ATP-dependent RNA helicase sub2 (Q0CGJ9) is involved in the exportation of mRNA of the nucleus and in transcription elongation and the other two proteins detected (Q0D116 and Q0CPE1) are involved in protein biosynthesis.

Regarding the overall response of *A. terreus* to UV radiation, the adaptation of the cell wall might explain the increased permeability of the membrane observed in figure 2.4 by the increase of damage and mainly dead spores. There is also the presence of proteins related with DNA repair, malate metabolism and consequently, with the itaconic acid biosynthesis that might work as a response to oxidative stress.

2.3.6 Reactivation Experiments

In the reactivation experiments, samples collected at the beginning (time 0 min) as well as after 30 min and 60 min of UV exposure were kept under white lamps (photoreactivation) and in the dark (dark repair) for 4 hours and 8 hours. It is possible to observe in figure 2.9 that the control sample (0 min of UV exposure) presents the same spores' concentration after 4 hours and 8 hours of photoreactivation and dark repair for all the species. Comparing the photoreactivation assays for the three species, a slight increase of the germinating spore concentration was observed after both reactivation times tested (4 hours and 8 hours) for *A. fumigatus* (figure 2.9 a)) and *A.*

terreus (figure 2.9 c)). On the contrary, for *A. niger* (figure 2.9 b)) the spores' concentration remained practically the same. In the dark repair experiments, the concentration of spores for all the tested species remained practically constant, suggesting that no reactivation occurred within the experimental times tested.

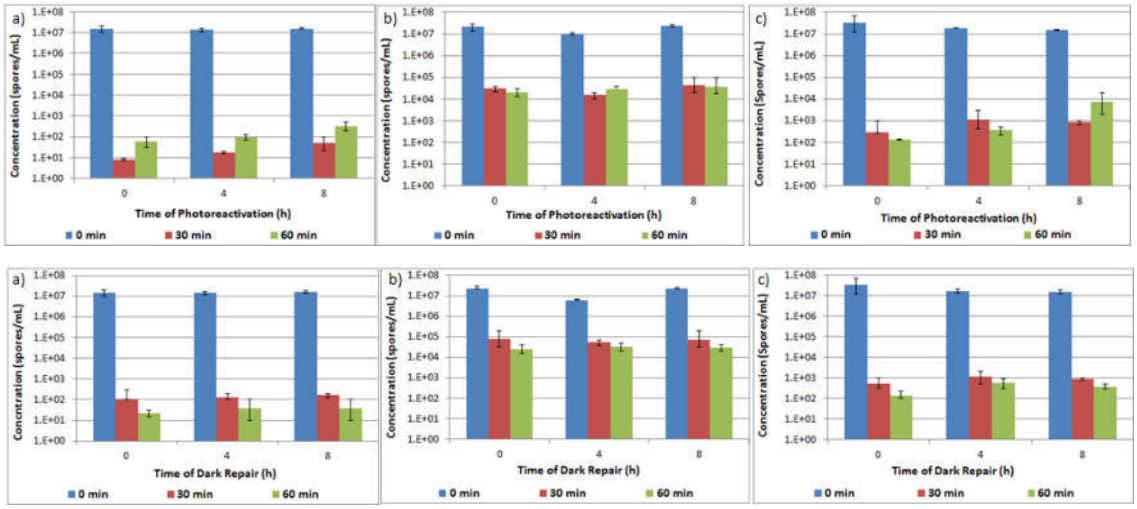

Figure 2.9 – Reactivation results in spores/mL of a) *A. fumigatus*, b) *A. niger* and c) *A. terreus* samples collected at the beginning and after 4 hours and 8 hours of photoreactivation (top pictures) and dark repair (low pictures). Error bars represent duplicates in up to 7 dilutions tested.

The assessment of the potential repair of cyclobutane pyrimidine dimers in the DNA by comparing figure 2.10 with figure 2.5, is only possible for *A. niger*, as explained above. Figure 2.10 shows that there may be a slight DNA repair by photoreactivation and dark repair. The concentration of cyclobutane pyrimidine dimers after exposure to 60 min of UV radiation was 100 ng/mL but decreased to 60 ng/mL after 8 hours of photoreactivation and to 80 ng/mL after 8 hours of dark repair.

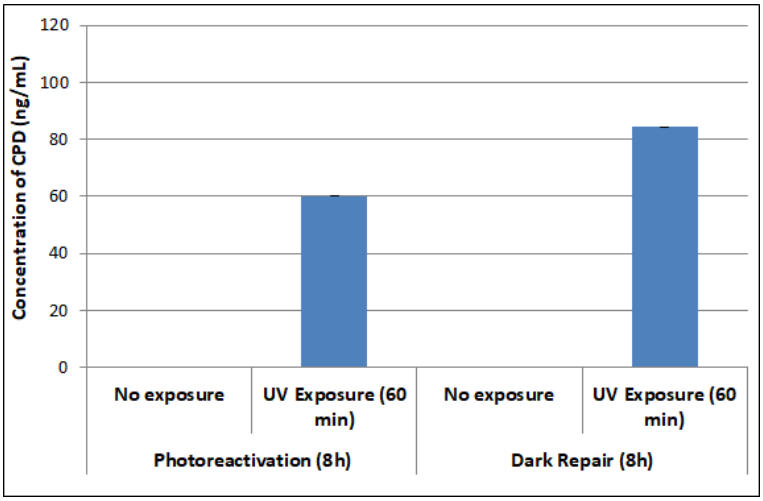

Figure 2.10 - Concentration of *Aspergillus niger* CPDs (ng/mL) after 8 hours of photoreactivation and dark repair at the beginning and after 60 min of MP/UV radiation. Error bars represent duplicates.

Several photoreactivation and dark repair studies were performed using bacteria (Nyangaresi et al., 2018; Oguma et al., 2001; Shafaei et al., 2017) and very few were recently performed using filamentous fungi (Wan et al., 2020; Wen et al., 2019a; Wen et al., 2019b). Oguma et al (2001) verified that *E. coli* after exposure to MP lamps was not able to repair the DNA damages that occurred and consequently did not reactivate. For filamentous fungi, it is stated that they have the ability to repair the DNA damages caused by UV radiation. However, its pathways are still poorly understood. Among the understudy species, *Aspergillus niger* was reported to have the ability to perform photoreactivation but no dark repair has been to date reported using the culturable plates methodology (Wan et al., 2020; Wen et al., 2019a; Wen et al., 2019b). In this study, although a decrease in the cyclobutane pyrimidine dimers concentration under light and dark conditions was observed, the same trend was not observed in plates (figure 2.9), probably because the DNA repair detected was not enough to reactivate spores' and induce germination on plates.

2.4 Conclusions

In this study the effectiveness of medium pressure mercury lamps to achieve inactivation of different filamentous fungi spiked in real surface water matrix was evaluated. The effects of the polychromatic lamp in three *Aspergillus* species with different colors and spore sizes were determined based on cell morphology, membrane permeability and enzymatic activity, DNA damage and proteome response.

The results obtained showed that:

- The filamentous fungi understudy are susceptible to medium pressure UV radiation being *A. niger* the most resistant species, followed by *A. fumigatus* and *A. terreus*.
- After 45 min under UV radiation, 5.58-log, 1.90-log and 5.63-log reductions were observed for *A. fumigatus*, *A. niger* and *A. terreus*, respectively.
- Morphological changes occurred in all the fungal spores being *A. fumigatus* and *A. niger* the most affected.
- An increase in the membrane permeability of spores was detected in the three species. *A. terreus* showed higher percentage of dead spores.
- Degradation of DNA was observed in all species being less intense for *A. niger*. This result enabled the detection and quantification of cyclobutane pyrimidine dimers after UV radiation. Photoreactivation and dark repair was also detected for *A. niger* by the decrease of cyclobutane pyrimidine dimers quantified but, it was not enough to have regrowth on plates.
- Proteome analysis showed cell wall reorganization and DNA repair for *A. fumigatus*, citric acid production as a response to oxidative stress for *A. niger* and cell wall reorganization, DNA repair and itaconic acid production as a response to oxidative stress for *A. terreus*.

In conclusion, UV radiation from these lamps can act through several mechanisms, such as cell wall disruption, DNA damages and metabolism disturbances. Taking these

results into consideration MP mercury lamps are an eligible option for the inactivation of filamentous fungi in drinking water treatment facilities.

Acknowledgements

The authors would like to thank Dr. David Bastien from SYSMEX for helping with the flow cytometry analysis, Inês Luís with protein quantification as well as Bruno Alexandre, Ricardo Gomes and Muhammad Asif for fruitful discussions. Mass spectrometry data were generated by the Mass Spectrometry Unit (UniMS), ITQB/iBET, Oeiras, Portugal. The authors also thank SYSMEX that has kindly provided the flow cytometer used in these experiments.

Financial support from Fundação para a Ciência e a Tecnologia through the fellowship SFRH/BD/111150/2015 and project PTDC/EAM-AMB/30989/2017 is gratefully acknowledged. iNOVA4Health - UID/Multi/04462/2013, a program financially supported by Fundação para a Ciência e Tecnologia/Ministério da Educação e Ciência, through national funds and co-funded by FEDER under the PT2020 Partnership Agreement is gratefully acknowledged. Funding from INTERFACE Programme, through the Innovation, Technology and Circular Economy Fund (FITEC), is gratefully acknowledged.

References

Andersen, M.R., Salazar, M.P., Schaap, P.J. and Baker, S.E. 2011. Comparative genomics of citric-acid-producing *Aspergillus niger* ATCC 1015 versus enzyme-producing CBS 513.88. Genome Research 21, 885-897.

Anjo, S.I., Santa, C. and Manadas, B. 2015. Short GeLC-SWATH: A fast and reliable quantitative approach for proteomic screenings. PROTEOMICS 15(4), 757-762.

Askenazi, M., Driggers, E., Holtzman, D., Norman, T.C. and Madden, K. 2003. Integrating transcriptional and metabolite profiles to direct the engineering of lovastatin-producing fungal strains. Nature Biotechnology 21, 150-156.

Avalos, J. and Carmen Limón, M. 2015. Biological roles of fungal carotenoids. Current Genetics 61(3), 309-324.

Babič, M.N., Gunde-Cimerman, N., Vargha, M., Tischner, Z., Magyar, D., Veríssimo, C., Sabino, R., Viegas, C., Meyer, W. and Brandão, J. 2017. Fungal Contaminants in Drinking Water Regulation? A Tale of Ecology, Exposure, Purification and Clinical Relevance. International Journal of Environmental Research and Public Health 14(6), 1-44.

Barros, B.H.R., Silva, S.H.da, Marques, E.R., Rosa, J.C., Yatsuda, A.P., Roberts, D.W., Braga, G.U.L. 2010. A proteomic approach to identifying proteins differentially expressed in conidia and mycelium of the entomopathogenic fungus *Metarhizium acridum*. Fungal Biology 114, 572-579.

Bowker, C., Sain, A., Shatalov, M. and Ducoste, J. 2011. Microbial UV fluence-response assessment using a novel UV-LED collimated beam system. Water Research 45(5), 2011-2019.

Bowman, S.M. and Free, S.J. 2006. The structure and synthesis of the fungal cell wall. BioEssays 28(8), 799-808.

Braga, G.U.L., Rangel, D.E.N., Fernandes, É.K.K., Flint, S.D. and Roberts, D.W. 2015. Molecular and physiological effects of environmental UV radiation on fungal conidia. Current Genetics 61(3), 405-425.

Brags, G.U.L., Rangel, D.E.N., Flint, S.D., Anderson, A.J. and Roberts, D.W. 2006. Conidial Pigmentation Is Important to Tolerance Against Solar-simulated Radiation in the Entornopathogenic Fungus Metarhizium anisopliae. Photochemistry and Photobiology 82(2), 418-422.

Brandl, J. and Andersen, M.R. 2017. Aspergilli: models for systems biology in filamentous fungi. Current Opinion in Systems Biology 6, 67-73.

Carvalho, M.B., Martins, I., Medeiros, J., Tavares, S., Planchon, S., Renaut, J., Núñez, O., Gallart-Ayala, H., Galceran, M.T., Hursthouse, A. and Silva Pereira, C. 2013. The response of *Mucor plumbeus* to pentachlorophenol: A toxicoproteomics study. Journal of Proteomics 78, 159-171.

Chen, F., Yang, X. and Wu, Q. 2009. Photocatalytic Oxidation of *Escherischia coli*, *Aspergillus niger*, and Formaldehyde under Different Ultraviolet Irradiation Conditions. Environmental Science and Technology 43(12), 4606-4611.

Cologna, N.M., Gómez-Mendoza, D.P., Zanoelo, F.F. and Ricart, C.A.O. 2018. Exploring *Trichoterma* and *Aspergillus* secretomes: proteomics approaches for the identification of enzymes of biotechnological interest. Enzyme and Microbial Technology 109, 1-10.

Doggett, M.S. 2000. Characterization of Fungal Biofilms within a Municipal Water Distribution System. Applied and Environmental Microbiology 66(3), 1249-1251.

Ehgartner, D., Herwig, C. and Neutsch, L. 2016. At-line determination of spore inoculum quality in *Penicillium chrysogenum* bioprocesses. Applied Microbiology and Biotechnology 100(12), 5363-5373.

Free, S.J. 2013. Chapter Two - Fungal cell wall organization and biosynthesis. Advances in Genetics 81, 33-82.

Gerba, C.P. (2000) Environmental Microbiology. Maier, R.M., Pepper, I.L. and Gerba, C.P. (eds), Academic Press.

Hageskal, G., Kristensen, R., Fristad, R.F. and Skaar, I. 2011. Emerging pathogen *Aspergillus calidoustus* colonizes water distribution systems. Medical Mycology 49(6), 588-593.

Han, M.-J., Kim, N.-J., Lee, S.Y. and Chang, H.N. 2010. Extracellular proteome of *Aspergillus terreus* grown on different carbon sources. Current Genetics 56, 369-382.

Hijnen, W.A.M., Beerendonk, E.F. and Medema, G.J. 2006. Inactivation credit of UV radiation for viruses, bacteria and protozoan (oo)cysts in water: A review. Water Research 40(1), 3-22.

Honda, Y., Hattori, T. and Kirimura, K. 2012. Visual expression analysis of the responses of the alternative oxidase gene (aox1) to heat shock, oxidative, and osmotic stresses in conidia of citric acid-producing *Aspergillus niger*. Journal of Bioscience and Bioengineering 113(3), 338-342.

Huang, D.W., Sherman, B.T. and Lempicki, R.A. 2008. Systematic and integrative analysis of large gene lists using DAVID bioinformatics resources. Nature Protocols 4, 44-57.

Jørgensen, T.R., Park, J., Arentshorst, M., Welzen, A.M.v., Lamers, G., vanKuyk, P.A., Damveld, R.A., Hondel, C.A.M.v.d., Nielsen, K.F., Frisvad, J.C. and Ram, A.F.J. 2011. The molecular and genetic basis of conidial pigmentation in *Aspergillus niger*. Fungal Genetics and Biology 48(5), 544-553.

Leng, W., Liu, T., Li, R., Yang, J., Wei, C., Zhang, W., Jin, Q. 2008. Proteomic profile of dormant *Trichophyton rubrum* conidia. BMC Genomics 9(303), 11.

Ma, X. and Bibby, K. 2017. Free chlorine and monochloramine inactivation kinetics of *Aspergillus* and *Penicillium* in drinking water. Water Research 120, 265-271.

Nascimento, É., Da Silva, S.H., Dos Reis Marques, E., Roberts, D.W. and Braga, G.U.L. 2010. Quantification of Cyclobutane Pyrimidine Dimers Induced by UVB Radiation in Conidia of the Fungi

Aspergillus fumigatus, *Aspergillus nidulans*, *Metarhizium acridum* and *Metarhizium robertsii*. Photochemistry and Photobiology 86(6), 1259-1266.

Nierman, W., Pain, A., Anderson, M., Wortman, J., Kim, S., Arroyo, J., Berriman, M., Abe, K., Archer, D., Bermejo, C., Bennet, J., Bowyer, P., Chen, D., Collins, M., Coulsen, R., Davies, R., Dyer, P., Farman, M., Fedorova, N., Fedorova, N., Feldblyum, T., Fischer, R., Fosker, N., Fraser, A., García, J., García, M., Goble, A., Goldman, G., Gomi, K., Griffith-Jones, S., Gwilliam, B., Haas, B., Haas, H., Harris, D., Horiuchi, H., Huang, J. and Denning, D. 2005. Genomic sequence of the pathogenic and allergenic filamentous fungus *Aspergillus fumigatus.* Nature 438, 1151-1156.

Nourmoradi, H., Nikaeen, M., Stensvold, C.R. and Mirhendi, H. 2012. Ultraviolet irradiation: An effective inactivation method of *Aspergillus* spp. in water for the control of waterborne nosocomial aspergillosis. Water Research 46(18), 5935-5940.

Nyangaresi, P.O., Qin, Y., Chen, G., Zhang, B., Lu, Y. and Shen, L. 2018. Effects of single and combined UV-LEDs on inactivation and subsequent reactivation of *E. coli* in water disinfection. Water Research 147, 331-341.

Oguma, K., Katayama, H., Mitani, H., Morita, S., Hirata, T. and Ohgaki, S. 2001. Determination of Pyrimidine Dimers in *Escherichia coli* and *Cryptosporidium parvum* during UV Light Inactivation, Photoreactivation, and Dark Repair. Applied and Environmental Microbiology 67(10), 4630-4637.

Oliveira, B.R., Barreto Crespo, M.T. and Pereira, V.J. 2020. Small but powerful: Light-emitting diodes for inactivation of *Aspergillus* species in real water matrices. Water Research 168, 115108.

Oliveira, B.R., Barreto Crespo, M.T., San Romão, M.V., Benoliel, M.J., Samson, R.A. and Pereira, V.J. 2013. New insights concerning the occurrence of fungi in water sources and their potential pathogenicity. Water Research 47(16), 6338-6347.

Oppenländer, T. (2003) Photochemical purification of water and air, Wiley-VCH Verlag.

Panngom, K., Sang Hark, L., Park, D.H., Sim, G.B., Kim, Y.H., Uhm, H.S., Park, G., Choi, E.H. 2014. Non-Thermal Plasma Treatment Diminishes Fungal Viability and Up-Regulates Resistance Genes in a Plant Host. PLOS One 9(6), e99300.

Parveen, S., Lanjewar, S., Sharma, K. and Kutti, U. 2011. Isolation of fungi from the surface water of river. Journal of Experimental Sciences 2(10), 58-59.

Pel, H.J., Winde, J.H. and Stam, H. 2007. Genome sequencing and analysis of the versatile cell factory *Aspergillus niger* CBS 513.88. Nature Biotechnology 25, 221-231.

Pereira, V.J., Basílio, M.C., Fernandes, D., Domingues, M., Paiva, J.M., Benoliel, M.J., Crespo, M.T. and Romão, M.V.S. 2009. Occurrence of filamentous fungi and yeasts in three different drinking water sources. Water Research 43(15), 3813-3819.

Pereira, V.J., Marques, M., Marques, R., Benoliel, M.J. and Barreto Crespo, M.T. 2017. Inactivation of Fungi in Treated Surface Water by Chloramination. Journal - AWWA 109(1), E19-E23.

Pereira, V.J., Marques, R., Marques, M., Benoliel, M.J. and Barreto Crespo, M.T. 2013a. Free chlorine inactivation of fungi in drinking water sources. Water Research 47(2), 517-523.

Pereira, V.J., Ricardo, J., Galinha, R., Benoliel, M.J., San Romão, M.V. and Barreto Crespo, M.T. 2013b. Low Pressure Ultraviolet Inactivation of Yeasts in Real Water Sources. Photochemical & Photobiological Sciences 12(4), 626 - 630.

Pereira, V.J.W., Howard S. and Singer, P.C. 2004. Temporal and spatial variability of DBPs in a chloraminated distribution system. American Water Works Association 96(11), 91-102.

Pontara, A.V., Oliveira, C.D.D.d., Barbosa, A.H., Santos, R.A.d., Pires, R.H. and Martins, C.H.G. 2011. Microbiological Monitoring of Mineral Water Commercialized in Brazil. Brazilian Journal of Microbiology 42(2), 554-559.

Samson, R.A., Hoekstra, E.S. and Frisvad, J.C. (2004) Introduction to food- and airborne fungi, Centraalbureau voor Schimmelcultures (CBS) - Utrecht.

Shafaei, S., Klamerth, N., Zhang, Y., McPhedran, K., Bolton, J.R. and El-Din, M.G. 2017. Impact of environmental conditions on bacterial photoreactivation in wastewater effluents. Environmental Science: Processes and Impacts 19, 31-37.

Sisti, M., Schiavano, G.F., De Santi, M., Brandi, G. 2017. Ultraviolet germicidal irradiation in tap water contaminated by *Aspergillus* spp. Journal of Preventive Medicine and Hygiene 58, E315-E319.

Supek, F., Bo šnjak, M., Šknunca, N. and Šmuc, T. 2011. REVIGO Summarizes and Visualizes long lists of gene ontology terms. PLoS ONE 6(7), e21800.

Tevž, G., Benčina, M. and Legiša, M. 2010. Enhancing itaconic acid production by *Aspergillus terreus*. Applied Microbiology and Biotechnology 87, 1657-1664.

Volz, P.A. and Dublin, M. 1973. Filamentous fungi exposed to spaceflight stresses including known levels of ultraviolet irradiations. Space Life Sciences 4, 402-414.

Wan, Q., Wen, G., Cao, R., Xu, X., Zhao, H., Li, K., Wang, J. and Huang, T. 2020. Comparison of UV-LEDs and LPUV on inactivation and subsequent reactivation of waterborne fungal spores. Water Research 173, 1-12.

Wen, G., Cao, R., Wan, Q., Tan, L., Xu, X., Wang, J., Huang, T. 2020. Development of fungal spore staining methods for flow cytometric quantification and their application in chlorine-based disifection. Chemosphere, 243, 125453.

Wen, G., Deng, X., Wan, Q., Xu, X. and Huang, T. 2019a. Photoreactivation of fungal spores in water following UV disinfection and their control using UV-based advanced oxidation processes. Water Research 148, 1-9.

Wen, G., Wan, Q., Deng, X., Cao, R., Xu, X., Chen, Z., Wang, J. and Huang, T. 2019b. Reactivation of fungal spores in water following UV disinfection: effect of temperature, dark delay, and real water matrices. Chemosphere 237, 1-9.

Wen, G., Xu, X., Zhu, H., Huang, T. and Ma, J. 2017. Inactivation of four genera of dominant fungal spores in groundwater using UV and UV/PMS: Efficiency and mechanisms. Chemical Engineering Journal 328, 619-628.

Wierckx, N., Agrimi, G., L übeck, P.S., Steiger, M.G., Mira, N.P. and Punt, P.J. 2020. Metabolic specialization in itaconic acid production: a tale of two fungi. Current Opinion in Biotechnology 62, 153-159.

Xie, H., Ma, Q., Wei, D. and Wang, F.-Q. 2018. Transcriptomic analysis of *Aspergillus niger* strains reveals the mechanism underlying high citric acid production. Bioresources and Bioprocessing 5(21), 1-23.

Youngchim, S., Morris-Jones, R., Hay, R.J. and Hamilton, A.J. 2004. Production of melanin by *Aspergillus fumigatus.* Journal of Medical Microbiology 53(3), 175-181.

Zaehle, C., Gressler, M., Shelest, E., Geib, E., Hertweck, C. and Brock, M. 2014. Terrein Biosynthesis in *Aspergillus terreus* and Its Impact on Phytotoxicity. Chemistry & Biology 21(6), 719-731.

CHAPTER 3

Small but powerful: light-emitting diodes for inactivation of *Aspergillus* species in real water matrices

Published in: Water Research

B.R. Oliveira, M.T. Barreto Crespo, V.J. Pereira 2020. Small but powerful: light-emitting diodes for inactivation of *Aspergillus* species in real water matrices. Water Research 168:115108.

Beatriz Oliveira was involved in all the experimental work presented in this chapter. Maria Teresa Barreto Crespo and Vanessa Pereira supervised all the experimental work performed.

CONTENTS

Abstract

This study addressed the effectiveness of light emitting diodes to achieve inactivation of three different *Aspergillus* species (*Aspergillus fumigatus*, *Aspergillus niger* and *Aspergillus terreus*) in a real water matrix. Three single small ultraviolet-C diodes emitting light at two different wavelengths were tested: 255 nm that is similar to the wavelength emitted by low pressure mercury lamps and 265 nm that is closer to the maximum absorbance wavelength of DNA. The ultraviolet-C diodes emitting light at 265 nm were found to be more effective than the 255 nm, achieving 3-log, 1-log and 5-log inactivations of *A. fumigatus*, *A. niger* and *A. terreus* using less than 20 mJ/cm^2 (13,97 mJ/cm^2; 7,28 mJ/cm^2; 19,74 mJ/cm^2). The diodes have also affected the morphology of the fungal spores and increased the percentage of damaged and dead spores.

Keywords: Light emitting diodes; disinfection; *Aspergillus* species; spores morphology; membrane permeability; enzymatic activity

3.1 Introduction

The development of effective disinfection treatment processes will be crucial to help the water industry cope with the inevitable challenges resulting from the increase in human population and climate change. UV treatment using low pressure mercury lamps that emit mainly monochromatic light at 254 nm is widely applied to achieve disinfection of wastewater and drinking water (Hamamoto et al., 2007). The application of UV treatment has increased along the years due to the proven effectiveness of this treatment process against a wide range of waterborne pathogens like viruses, bacteria and protozoan (oo)cysts (Hijnen et al., 2006). In addition to its disinfection effectiveness, UV can also degrade organic compounds by direct photolysis of photolabile compounds as a consequence of light absorption (Pereira et al., 2007).

Although UV-LEDs still need improvements since they only operate at 1 % of efficiency when compared to 75 % of visible LEDs (Chatterley and Linden, 2010), they have several advantages: they are mercury free and therefore don't lead to the production of mercury waste, compact and robust, have longer lifetimes, do not need stabilization time, lead to a low energy consumption and can be constructed with a diversity of wavelengths (Hamamoto et al., 2007; Song et al., 2016). So, if proven effective, they can replace low pressure mercury lamps.

Some studies have already reported the use of different LED wavelengths for the inactivation of different microorganisms in water sources (Beck et al., 2017; Nyangaresi et al., 2018; Song et al., 2016; Song et al., 2018; 2019). The choice of the wavelength in each study differs according to the purpose. Wavelengths in the UV-C range (100-280 nm) such as 254-255 nm, 265-269 nm and around 280 nm are chosen to be compared with the conventional treatment that uses low pressure mercury lamps (Bowker et al., 2011), due to the absorption spectra of DNA (Oguma et al., 2013) and proteins (Li et al., 2017; Rattanakul and Oguma, 2018; Song et al., 2019),

respectively. Most of the experiments using UV-LEDs that have been reported were conducted using bacteria and bacteriophages spiked on laboratory grade water or phosphate-buffered saline solution. To the best of our knowledge, no study has been performed using filamentous fungi in real water sources. Chen et al. (2009) used *Aspergillus niger* inoculated into wood surfaces, while Murdoch et al. (2013) and Vesper et al. (2008) used several fungal species as spore suspensions.

Species from the genus *Aspergillus* are ubiquitous in nature and have been reported in soil, air as well as aquatic environments like marine waters, surface water, groundwater, spring water, water distribution systems, tap water, and processed mineral water (Babič et al., 2017; Hageskal et al., 2011; Nourmoradi et al., 2012; Oliveira et al., 2013; Parveen et al., 2011; Pereira et al., 2009; Pontara et al., 2011). *Aspergillus fumigatus*, *Aspergillus niger* and *Aspergillus terreus* were reported to occur in surface water matrices (Oliveira et al., 2013; Pereira et al., 2009), have been described to be potential pathogenic species (Oliveira et al., 2013; Parveen et al., 2011), and might have different disinfection resistances due to the conidial protection mechanisms against UV radiation (Braga et al., 2015). These defense mechanisms can be due to the existence of pigments such as melanins that absorb the UV light, enzymes like catalases that reduce the reactive oxidation species formed during disinfection (Braga et al., 2015), existence of a thick cell wall containing chitin, mannan, glucan, and various lipids (Donnelly et al., 2008) as well as DNA repair mechanisms.

The aim of this study was to determine the inactivation efficiencies of LEDs that emit light at different wavelengths (255 nm and 265 nm) on three *Aspergillus* species, *A. fumigatus*, *A. niger* and *A. terreus* and the effect of these two wavelengths on the fungal spores, using a real water matrix.

To determine filamentous fungi's susceptibilities to UV disinfection, plate counts were used since it is still a commonly used methodology (Chen et al., 2009; Li et al., 2017; Murdoch et al., 2013; Nourmoradi et al., 2012). However, to complement this

cultivation method, other methodologies can be used to assess several viability indicators. The combination of flow cytometry with fluorescent-based viability stains has been used to access fungi spores' growth, viability, metabolic activity, antifungals' action and spore inoculum quality for bioprocesses (Ehgartner et al., 2016; Mesquita et al., 2013; Ramani et al., 2003). This technique was also used in this study to test the membrane permeability and enzymatic activity of the fungi spores and compared with the plate count results. Additionally, scanning electron microscopy (SEM) was used to evaluate phenotypically the effect of the different wavelengths on the spore's morphology.

3.2 Methods

3.2.1 Inoculum Preparation

To perform this study three different species from the genus *Aspergillus* (*A. fumigatus*, *A. niger*, and *A. terreus*) were chosen due to their reported occurrence in different drinking water sources, potential pathogenicity, different color of their pigments and spores' resistance (Babič et al., 2017; Braga et al., 2015; Oliveira et al., 2013; Parveen et al., 2011; Pereira et al., 2009). *A. fumigatus*, *A. niger*, and *A. terreus* were grown on malt extract agar (Merck, USA) for 7 days at 27 °C. After growth, the mycelium was removed from the plates using a saline solution (0.90 % w/v of NaCl) with Tween 80 (0.10 % v/v). The obtained pellet was washed three times with saline solution (0.90 % w/v of NaCl). The washed pellet was then resuspended in 150 mL of the study matrices (saline solution and surface water characterized in section 3.2.3) and the concentration of the spores was determined using the Neubauer chamber (this solution was designated as concentrated inoculum).

In this work, the experiments were conducted after inoculation with a mixture of mycelium and spores collected from the Petri dishes instead of only spores. The reason for this choice is that the expected living forms of filamentous fungi in the

aquatic environment are as a mixture of spores and mycelium. To understand this, a preliminary experiment was performed. *A. fumigatus*, *A. niger* and *A. terreus*' spores (10^8 spores/mL) were spiked separately into a real water matrix (sterile untreated surface water), with air flow to simulate agitation from surface water, for 3 weeks. SEM images (obtained as detailed in section 3.2.4.2) before and after the experimental time show that in the beginning (as expected) there were only spores but after 3 weeks both mycelium and spores were present in solution (figure 3.1). Based on these observations (figure 3.1), a mixture of mycelium and spores were inoculated in the experiments conducted so that any interference from the mycelium in the inactivation (e.g. scavenging of light) would be taken into consideration. However, only the spores were used to evaluate the inactivation rates.

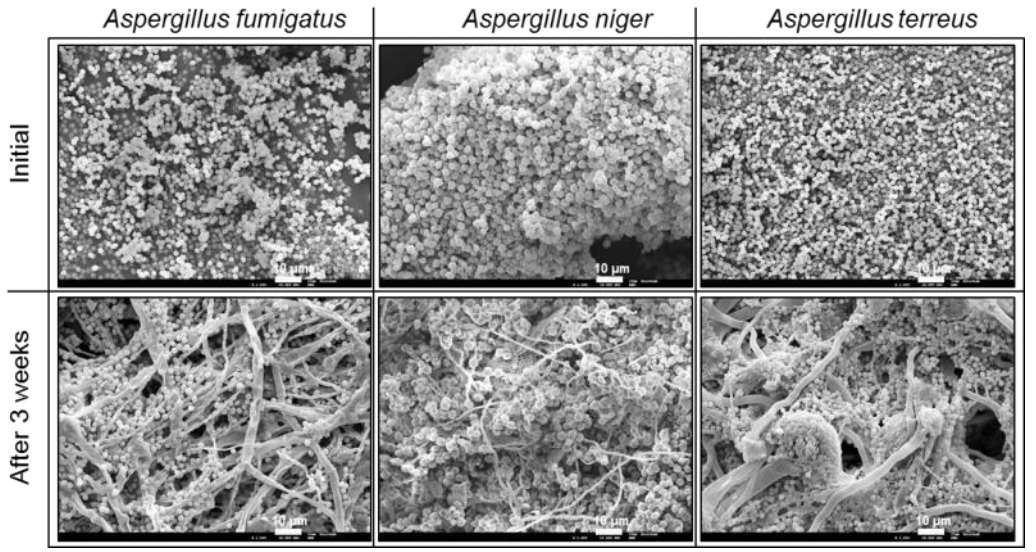

Figure 3.1 – Scanning electron microscopy images of *A. fumigatus*, *A. niger,* and *A. terreus* just after inoculation (Initial) and after 3 weeks of inoculation in sterile untreated surface water. Total magnification is 1 000 x.

3.2.2 LED reactor description

The LED reactor used in this study is a triple wavelength pearl beam reactor (AquiSense Technologies, USA) that contains a triple wavelength UVinaire^{TM}, a control box, a UV homogenizing tube and an AC-DC adapter (12 V 90 W). The selected wavelengths were 255 nm and 265 nm (3 LEDs for each wavelength) with an average intensity measured at 4 cm (the same height used to perform the experiments) of 53.66 µW/cm^2 and 250.30 µW/cm^2 determined using an International Light Technologies (ILT) 950 UV Spectroradiometer (Massachusetts, USA).

3.2.3 Inactivation Assays

To perform the inactivation assays, the concentrated inoculum prepared as described in section 3.2.1 was diluted to prepare fungal working solutions with a final concentration of 10^8 spores/mL. These fungal working solutions of 50 mL were placed in a specially designed Petri dish with a double walled glass that enables the circulation of cold water to maintain the temperature constant at 20 °C. The Petri dish was placed below the LED plate with a distance from the LEDs to the sample top surface of 4 cm.

Inactivation experiments were conducted in saline solution (0.90 % w/v of NaCl) and in filtered surface water. Untreated surface water was collected and used in inactivation experiments after filtration (with a 0.22 µm membrane filter (PALL, NY, USA)) to simulate the treatment processes performed in drinking water treatment facilities. Both waters (before and after filtration) were characterized in terms of temperature, pH (using a MicropH 2002, Crison, Spain), total organic carbon (Standard Method 5310B using a Total Organic Carbon Analyzer, TOC-V, Shimadzu, USA), turbidity (using a Hanna Portable Turbidity Meter HI98703, USA), chemical oxygen demand (Standard Method 5220 using Hach Lange HT200S and Hach Lange

DR2800 equipments with the Hach Lange LCK 514 100-2000mg/L O_2 kits, Germany), total solids (Standard Method 2540B), and total suspended solids (Standard Method 2540D) (Table 3.1).

Table 3.1 – Parameters measured for the surface water matrix before and after filtration.

Parameter	Surface water collected for this study	Surface water collected for this study after filtration
Temperature (°C)	20.00	20.00
pH	7.32	7.64
Total Organic Carbon (mg/L C)	3.97	2.35
Turbidity [NTU]	14.60	0.22
Chemical Oxygen Demand (mg/L O_2)	1670	1172
Total Solids (g/L)	39.62	38.94
Total Suspended Solids (mg/L)	70.50	22.60

Each of the fungal working solutions of 50 mL were analyzed at the beginning (time zero) and after the experimental exposure times of 0.5, 1, 5, 10, 15, 30, 45, and 60 min to each LED wavelength. Two controls were performed to verify if the fungal concentration remained stable along the experimental time under natural light (designated as natural light control) and in the dark (designated as dark control). From the fungal working solutions collected at different exposure times, 1 mL was used to determine colony forming units (CFU)/mL and the rest of the volume was centrifuged, resuspended in 10 mL of saline solution and kept at -20 °C to be further analyzed.

3.2.3.1 Determination of the UV fluence

To enable the comparison of inactivation experiments conducted with other setups, the UV fluence (mJ/cm^2) was determined as the product of the fluence rate (irradiance) and the exposure time in seconds. The average irradiance values in the water was determined after considering different correction factors (reflection, petri dish, water, and divergence) as described by Bolton and Linden (2003). The following correction factors were used: 0.98 for the reflection factor, 0.90 for the petri factor and 0.64 for the divergence factor. The water factor, that takes into account the decrease in irradiance due to sample absorbance at the wavelengths of interest, was also determined for each of the three fungi species tested.

3.2.4 Methods to determine the disinfection efficiency

3.2.4.1 Plate Count

The concentration of fungi present in the samples collected at different contact times was quantified by colony forming units (in CFU/mL) using the pour plate method, through serial dilutions. The medium used was malt extract agar (Merck, USA) and plates were incubated for 48/72 h at 27 °C.

The results are presented as ln(C/C0) where C is the concentration of fungal spores obtained along the experimental time and C0 is the concentration of fungal spores obtained at the initial experimental time.

3.2.4.2 Scan Electron Microscopy

Scanning electron microscopy images were acquired before and after the inactivation assays with the different LED wavelengths to assess the changes in the morphology of the different fungi species tested. The samples were prepared for SEM analysis using 2 mL of the initial and final (collected after 60 min of UV-LED exposure) samples that were kept frozen at -20 °C. Sample preparation was performed according to Panngom (2014) with some modifications. Briefly, the samples were washed with phosphate buffer (pH 7) for 5 min and fixed in Karnovsky's Fixative (Polysciences Inc., Germany) overnight following the protocol's recommendations (2.5 % (v/v) of glutaraldehyde, 2.0 % (v/v) of paraformaldehyde and 0.1 M of phosphate buffered saline (PBS) solution). Samples were then washed three times with PBS for 10 minutes and centrifuged at 10 000 rpm for 5 minutes. Pellet was fixed with osmium tetroxide (1.0 % v/v) for 2 hours protected from light. Samples were then dehydrated using several ethanol solutions with a gradient increase in concentration (30, 50, 70, 80, 90, 95 and 100 %) for 10 minutes being only the last dehydration step (100%) performed twice for 15 minutes. Lastly, the samples were freeze dried for 30 min and mounted in carbon conductive tape. Samples were then covered with a thin film of gold and palladium (Au/Pd) on a Quorum Technologies sputter coater, model Q150T ES. Observations were performed using a FEG-SEM JEOL JSM7001F, with a 15 kV acceleration voltage and a PC-SEM by JEOL used for image acquisition.

3.2.4.3 Flow Cytometry Analysis

Flow cytometry analyses were conducted using the CyFlow® Cube 6 equipment (Sysmex Partec GmbH, Germany) with a 488 nm excitation from a blue solid-state laser at 50 mW. Staining procedure followed the Yeast Control – Viability kit (Sysmex Partec GmbH, Germany) that contains fluorescein diacetate (FDA), which by the action of enzymes (esterases) is converted into a fluorescent product, combined with propidium iodide (PI), which intercalates in the DNA of membrane damaged cells, allowed the determination not only of metabolically active (FDA positive) and dead (PI positive) spores but also quiescent (FDA and PI negative) and damaged (FDA and PI positive) spores.

A preliminary experiment was performed to define particle size (FSC) and spores' granularity (SSC) selectivity gates using an untreated sample. This gate includes the fungal spores and excludes the background (Mesquita et al., 2013). Additionally, using an untreated sample and a sample subjected to medium pressure UV light for 60 min due to its higher radiation intensity and proven effectiveness to achieve inactivation, the Yeast Control – Viability kit was used to define four gates: quiescent - left down quadrant, metabolically active - right down quadrant, dead - left upper quadrant and damaged - right upper quadrant (Figure 3.2). The obtained cytograms were analyzed using a CyViewTM for Cube 6 software (Partec GmbH, Germany).

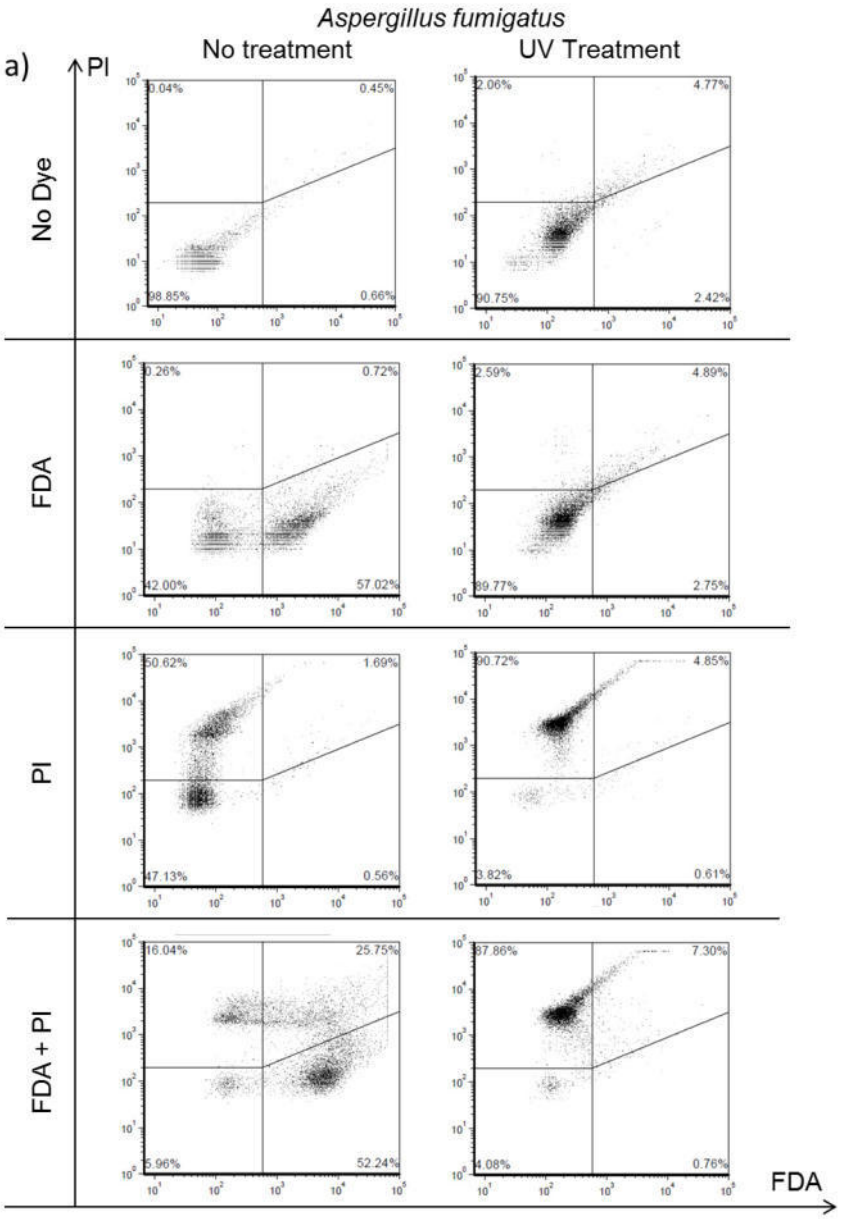
Aspergillus fumigatus
a)
No treatment
UV Treatment
PI
No Dye
FDA
PI
FDA + PI
FDA
99.04%
0.45%
98.85%
0.66%
92.06%
4.77%
90.75%
2.42%
99.26%
0.72%
42.00%
57.02%
92.59%
4.89%
89.77%
2.75%
50.62%
1.69%
47.13%
0.56%
90.72%
4.85%
3.82%
0.61%
16.04%
25.75%
5.96%
52.24%
87.86%
7.30%
4.08%
0.76%

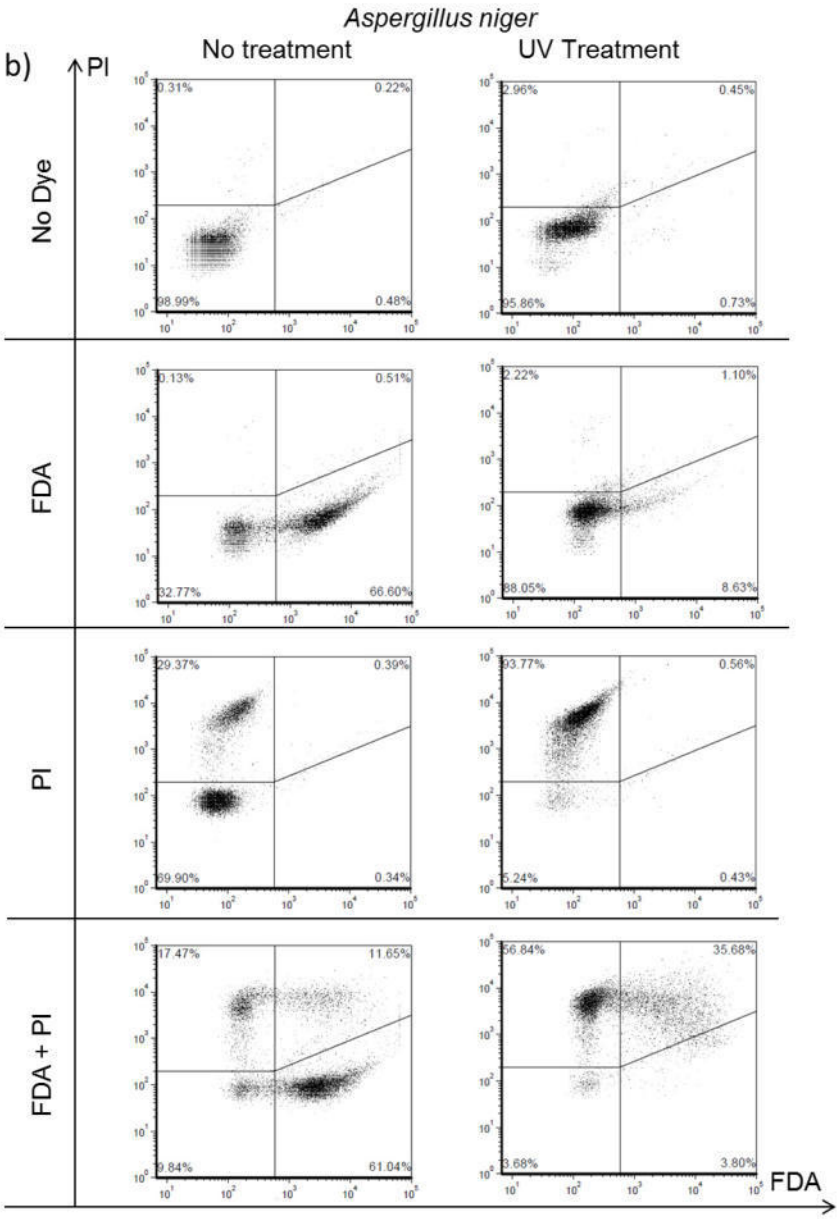
Aspergillus niger
b)
PI
No treatment
UV Treatment
No Dye
FDA
PI
FDA + PI
FDA
0.31%
0.22%
98.99%
0.48%
2.96%
0.45%
95.86%
0.73%
0.13%
0.51%
32.77%
66.60%
2.22%
1.10%
88.05%
8.63%
29.37%
0.39%
69.90%
0.34%
93.77%
0.56%
5.24%
0.43%
17.47%
11.65%
9.84%
61.04%
56.84%
35.68%
3.68%
3.80%

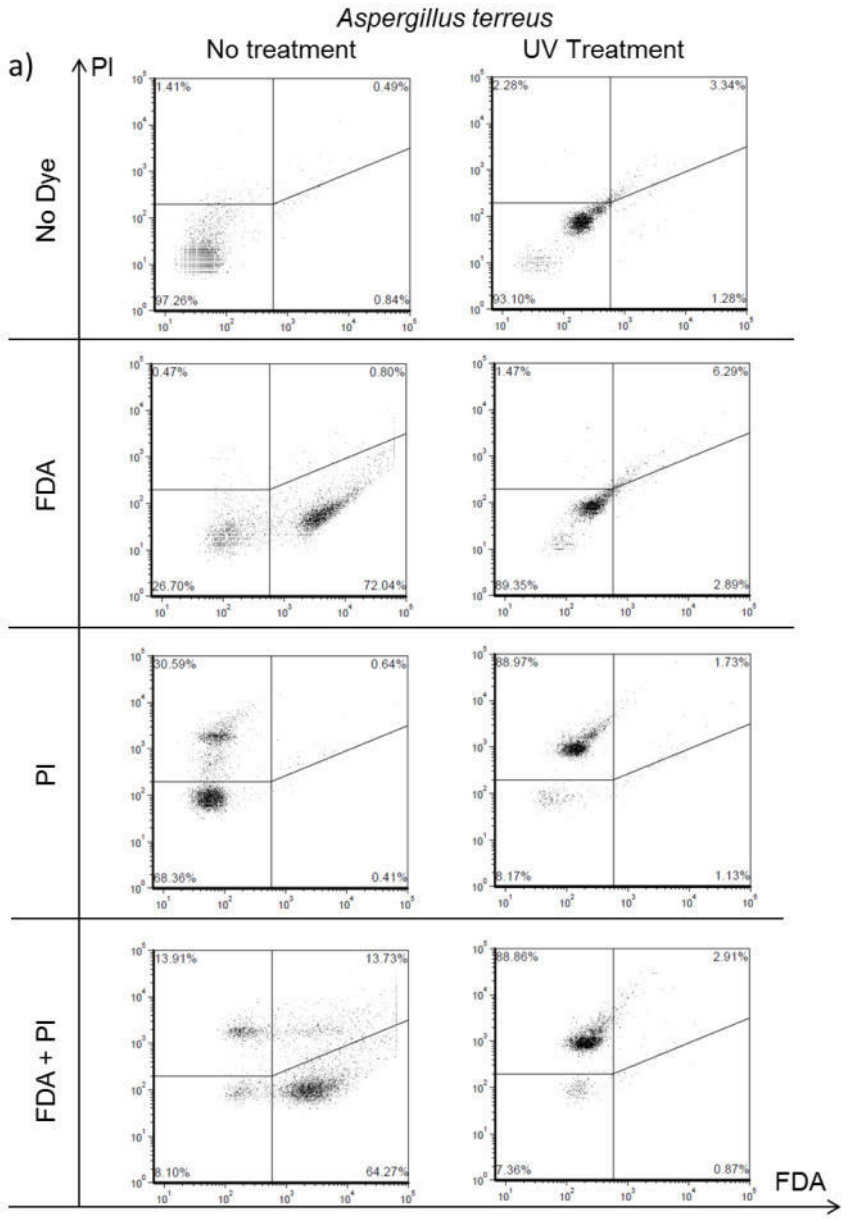

Figure 3.2 – Flow Cytometry dot plots for a) *Aspergillus fumigatus*, b) *Aspergillus niger* and c) *Aspergillus terreus* before and after 60 min of medium pressure UV treatment. The defined gates are: quiescent (left down quadrant), metabolically active (right down quadrant), dead (left upper quadrant) and damaged (right upper quadrant).

3.3 Results and Discussion

3.3.1 LED Inactivation Experiments

Inactivation experiments were conducted using *A. fumigatus*, *A. niger* and *A. terreus* under the pearl beam reactor that was set at 2 different wavelengths: 255 nm and 265 nm (figure 3.3). The action of these different wavelengths was tested separately and samples were analyzed after several exposure times (0, 0.5, 1, 5, 10, 15, 30, 45 and 60 minutes). The correspondent UV fluences were calculated according to 3.2.3.1. Figure 3.4 shows the results presented in UV fluences for the three fungi species using LED 255 nm and 265 nm.

The experiments were conducted using saline solution (Supplementary figure 1) and filtered surface water (figure 3.3). No notorious differences were observed between the two matrices showing that neither negative (scavenging) nor positive (OH production) effects of the matrix composition on photolysis were observed. Figure 3.3 shows that the concentration of the 3 fungi species in the control experiments was stable.

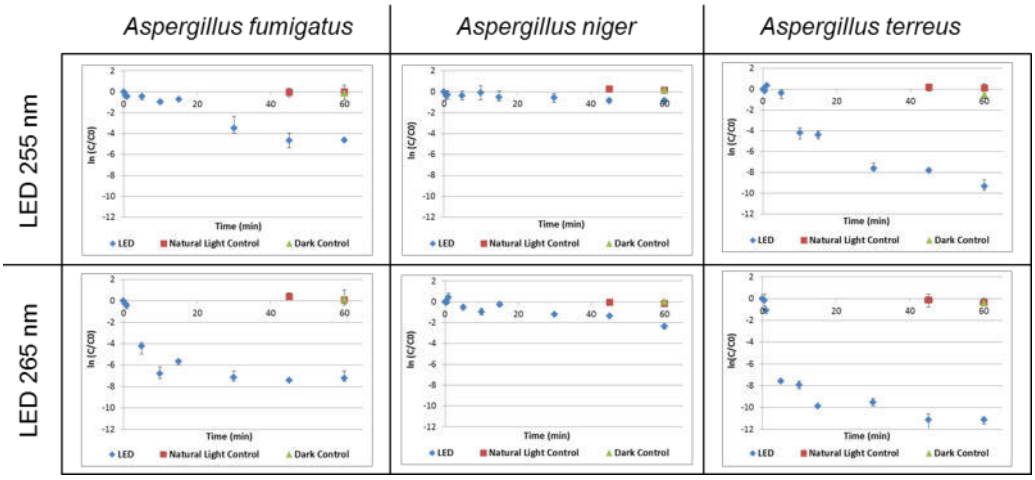

Figure 3.3 – Inactivation results in ln(C/C0) of *A. fumigatus*, *A. niger* and *A. terreus* in filtered surface water after several exposure times (0, 0.5, 1, 5, 10, 15, 30, 45 and 60 min) using two wavelengths, 255

nm and 265 nm. Two controls are presented (natural light control and dark control). Error bars represent duplicate results obtained in up to 7 dilutions tested.

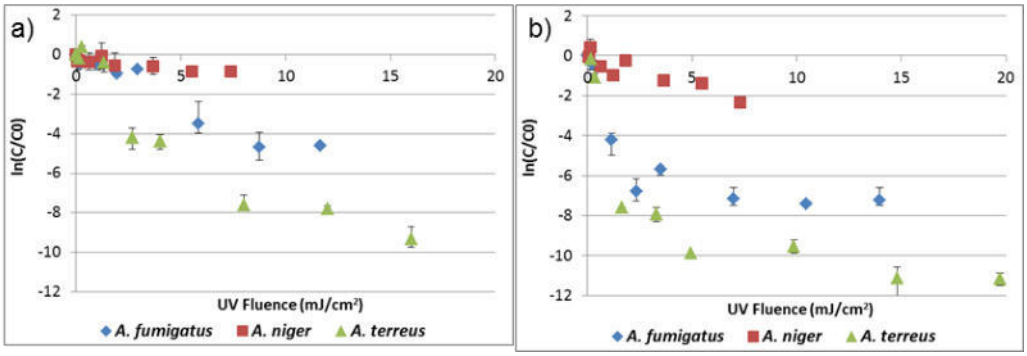

Figure 3.4 – UV inactivations (ln(C/C0)) represented as a function of UV fluence (mJ/cm^2) for the three fungi species using a) LED 255 nm and b) LED 265 nm. Error bars represent duplicate results obtained in up to 7 dilutions tested.

As can be seen in figures 3.3 and 3.4, for both UV-LEDs, the most resistant fungi species is *A. niger*, followed by *A. fumigatus* and *A. terreus*, which is the less resistant. Considering the LEDs, LED 265 nm (figure 3.4 b) shows to be more efficient to inactivate the fungi species when compared to LED 255 nm (figure 3.4 a). For instance, to obtain a 2-log reduction of *A. fumigatus* it is necessary an UV fluence of 2.33 mJ/cm^2 (10 min) using LED 265 nm and 11.66 mJ/cm^2 (60 min) when LED 255 nm is used. For *A. terreus*, to obtain 3-log reduction, it is necessary 1.64 mJ/cm^2 (5 min) and 8.00 mJ/cm^2 (30 min) for LED 265 nm and 255 nm, respectively. For *A. niger*, less than 1-log reduction was obtained even for the highest UV fluence (60 min) using both LEDs.

Comparing with other studies, Nascimento et al. (2010) used *A. fumigatus* among other ascomycetes to perform UV inactivations with a 313 nm peak fluorescent lamp and their results show a higher UV fluence needed to obtain the same inactivations. For *A. niger*, more studies have been performed due to its importance in different

areas such as food, chemical and medical industries (Chen et al., 2009; Murdoch et al., 2013). However, much higher UV fluences were used compared to the ones used in this study. For example, Chen et al. (2009) using a low pressure mercury lamp needs 42.30 J/cm^2 to reach 50 % of *A. niger* inactivation. In this study, using the LED that emits at 255 nm for the same fungi species, 1.23 mJ/cm^2 were needed to inactivate 51.7 % and using the LED that emits at 265 nm, 1.21 mJ/cm^2 were needed to inactivate 60.0 %. To the best of authors' knowledge no inactivation studies using *A. terreus* were performed although, some studies used UV radiation to study morphological and biochemically random mutations formed by its action (Hollaender et al., 1945).

The ideal curve observed for the inactivation of microorganisms is a first order curve. However, sometimes it is obtained a shoulder or a tailing off curve. The latter can be obtained for several reasons such as the presence of clumps of spores, genetic resistance, or matrix interference that is able to protect a survival subpopulation with interfering substances like, suspended organic matter (Gerba, 2000). Figure 3.4 (using real water matrix) and supplementary figure 1 (using saline solution) show a tailing off curve for *A. fumigatus* and *A. terreus* so, there is no matrix interference.

The linear and polynomial regressions and the correspondent coefficients of determination obtained for each species after inactivation with LEDs emitting at 255 nm and 265 nm are presented in supplementary table 1.

3.3.2 Resistance to UV inactivation

Several studies have already reported the higher resistance of filamentous fungi when compared to other microorganisms like bacteria, to UV light which could be explained by the presence of pigmented spores (Braga et al., 2006; Nascimento et al., 2010) or enzymes that can inactivate the free radicals formed by the action of light (Avalos and Carmen Limón, 2015). Within the three target species, the spores' size

can explain the order of resilience because bigger spores absorb more radiation and consequently reduces the radiation that goes to the nucleus (Nascimento et al., 2010). *A. niger* have bigger spores' diameter (3.5-4.5 µm), followed by *A. fumigatus* (2.5-3.0 µm) and then, *A. terreus* (1.5-2.5 µm) (Oliveira et al., 2013; Samson et al., 2004). Regarding the growth rate analysis of spores before and after 60 min of UV inactivation, the different species were grown in malt extract agar for 7 days and the colonies' diameter measured along time. It can be seen that the growth rate of the fungi spores remained the same so the resistance of few spores in the species itself may be due to genetic resistance (supplementary figure 2).

The 2 LED wavelengths (255 nm and 265 nm) were selected due to their similarity with the wavelength that low pressure mercury lamps widely used in drinking water and wastewater treatment facilities emit (254 nm) and the maximum absorbance of DNA (approximately 264 nm). Bowker et al. (2011) compared a UV-LED set at 255 nm with a low pressure mercury lamp and verified that the UV-LED showed lower inactivation effectiveness that started with a 0.25-log difference at 3 mJ/cm^2 and reached 2.25-log difference at 7 mJ/cm^2. The explanation given is that the absorption spectrum is not the only factor affecting inactivation effectiveness and in this case, it might be due to the higher power output emitted by the low pressure lamp. LED 265 nm as it is shown in figure 4 promotes higher inactivation of the target fungi species. Chatterley and Linden (2010) compared a 265 nm UV-LED with a low pressure mercury lamp and verified that the UV-LED is more effective to inactivate *Escherichia coli*. Moreover, UV-LED set at 265 nm also showed higher inactivation results when compared with 280 nm and 310 nm wavelengths to inactivate *Escherichia coli*, *Legionella pneumophila*, *Pseudomonas aeruginosa*, *Bacillus subtilis* spores and bacteriophage Qβ (Li et al., 2017; Rattanakul and Oguma, 2018). The higher inactivation results at 265 nm (higher damages and inhibition of cell division and growth) reported in this study and by other studies can be explained by the UV absorption curve of DNA whose peak is at 264 nm.

3.3.2.1 Phenotypic effect on fungal spores

Scanning electron microscopy was performed to monitor the spores' morphology of the three different fungi species before and after 60 min of UV-LED exposure (figure 3.5). *A. fumigatus* have globose rough-walled to echinulate conidia, *A. niger* have globose ornamented with irregular warts, spines and ridges conidia and *A. terreus* have globose smooth conidia (Samson et al., 2004). When comparing the effect of the UV-LEDs, it can be seen that the LED that emits light at 265 nm is able to cause deformation in all of the fungi spores, regardless the species, although there are differences in the species resistance to UV-LED inactivation (figure 3.4). On the other hand, the LED that emits at 255 nm does not cause morphologically changes in the fungal spores although there is some inactivation of the different species as can be seen in figure 3.4. Further studies should be performed to address deeply the spores' morphology constituents that are being affected by the different UV-LED radiation.

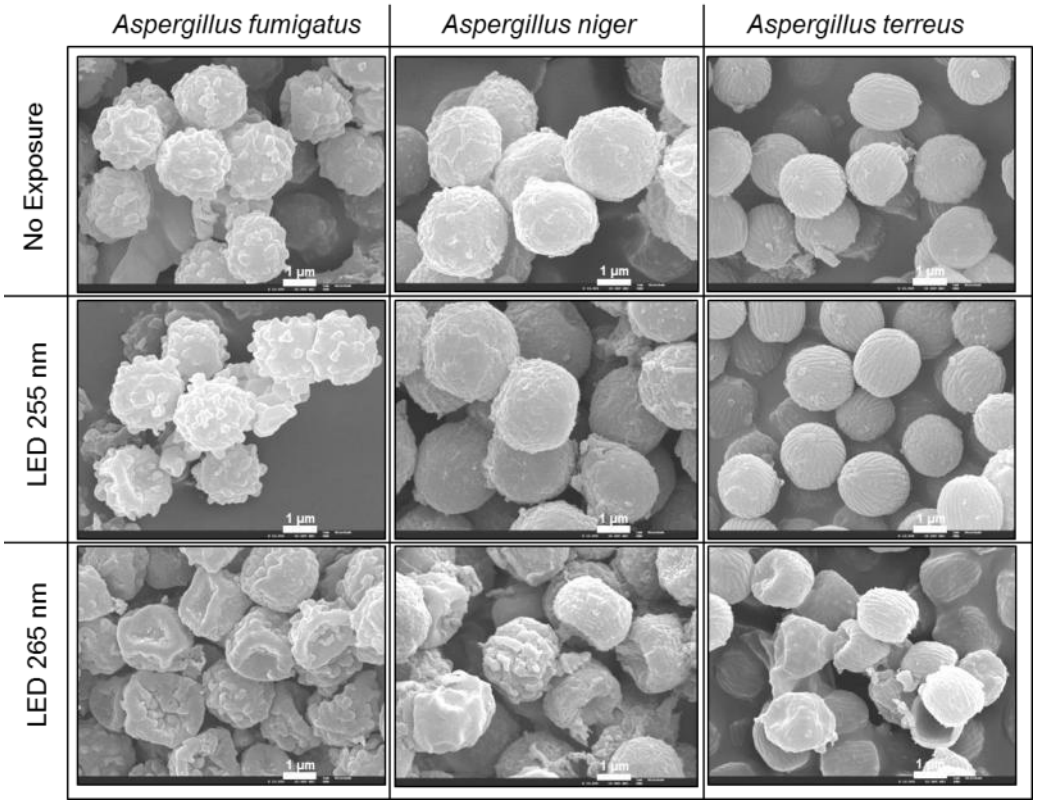

Figure 3.5 – SEM images obtained before (No Exposure) and after 60 min of UV-LED exposure at 255 nm and 265 nm of spores from *A. fumigatus*, *A. niger* and *A. terreus*. Total magnification is 13 000 X.

Although not using the same genera, Wen et al. (2017) have also performed SEM analysis after exposing filamentous fungi' spores (*Cladosporium* sp., *Penicillium* sp., *Acremonium* sp. and *Trichoderma* sp.) to a UV dose of 40 mJ/cm^2 and they showed less morphology damage when compared to the images obtained in this study using a lower UV dose (maximum UV fluence for LED 255 nm was 16 mJ/cm^2 and for LED 265 nm was 20 mJ/cm^2).

3.3.2.2 Effect on membrane permeability and enzymatic activity

Flow cytometry analysis was performed using the three fungi species before and after 60 min of UV-LED exposure. The analyses were performed using a final concentration of $1x10^6$ spores/mL and the results corrected according to the baseline background of the different solutions used (PBS and filtered surface water). Figure 3.6 presents the results in triplicate as percentage bar charts that correspond to the percentages obtained for each quadrant of the cytogram.

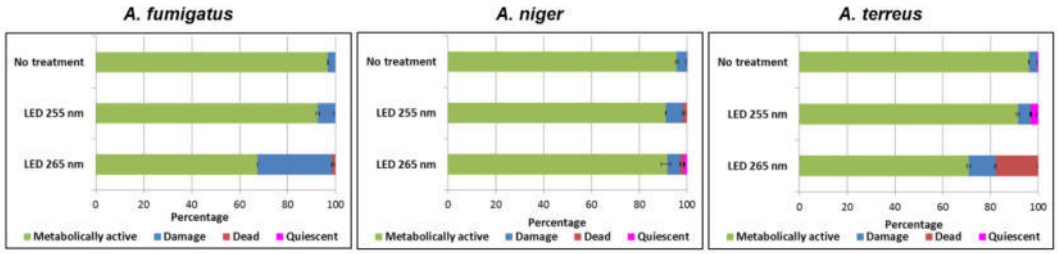

Figure 3.6 – Flow Cytometry results represented as percentage bars charts using the Yeast Control – Viability kit (Sysmex Partec GmbH, Germany) for the three fungi species before and after 60 min of LED 255 nm and 265 nm exposures. Error bars represent triplicates.

In the "no treatment" section it can be seen that most of the spores are metabolically active and that there is a small percentage of spores that are damaged (figure 3.6). This is important to establish the base line from which we can compare the action of the UV-LEDs. In the LED 255 nm section there is a slight increase of damaged spores for the three fungi species and few dead spores appear. Using LED 265 nm, there is an increase of damaged and dead spores. *A. fumigatus* seems quite affected by LED 265 nm showing damaged spores while *A. terreus* having almost the same percentage of affected spores than the former has less damaged spores and more dead spores. For *A. niger* it can be seen that the spores are more resistant to

disinfection although there is also a little increase of damaged and dead spores. The spores that are damaged, having a disrupted membrane but at the same time being still viable are potentially spores that might be able to repair their damages through DNA repair mechanisms.

These results are consistent with figure 3.4, showing that the order of resistance is *A. niger*, followed by *A. fumigatus* and *A. terreus*. Moreover, figure 3.6 also show that LED at 265 nm is more efficient to damage and inactivate (dead) spores which can be related with the SEM images presented in figure 3.5 with morphologically changes in the different fungi spores.

Several studies have been conducted using plate count to analyze general water quality. Flow cytometry is a methodology that provides more information than plate count due to the addition of different lasers to the equipment and the utilization of different dyes in the samples (Nevel et al., 2017). The establishment of correlations between these two techniques has not been defined yet since authors diverge (Ehgartner et al., 2016; Nescerecka et al., 2014). For instance, as it is known and as stated by Nevel et al. (2017) UV-C radiation is able to inactivate microorganisms because it affects the nucleic acids leading to replication and transcription inhibition, whereas the membrane/cell wall may remain intact. So, microorganisms would not grow on plate but will be unstained by propidium iodide, having more live/metabolically active spores in flow cytometry than growing spores on plate. The correlation between grown spores in plate and metabolically active spore counts in flow cytometry was determined to be 0.86 which means that there is a strong uphill correlation and the resulting linear regression represents the stated above (supplementary figure 3). The linear regression and the coefficient of determination obtained in this study are similar to the coefficient of determination 0.80 reported by Ehgartner et al. (2016). The results obtained in this study are consistent since the higher inactivation efficiencies obtained using the UV-LED that emits light at 265 nm

are reflected in the SEM images of the spores that were morphologically damaged and in the flow cytometry results that show an increase in damaged and dead spores.

3.4 Conclusions

This study performed using light-emitting diodes with different wavelengths allowed to conclude that:

- Both LEDs set at 255 nm and at 265 nm were able to inactivate the fungi species understudy, being the LEDs that emit light at 265 nm the most efficient;

- *Aspergillus niger* was the most resistant fungi species, followed by *Aspergillus fumigatus* and by *Aspergillus terrreus*;

- It was possible to verify that the LEDs that emit at 265 nm affected phenotypically all the fungi species tested which reflects biochemical modifications of the spores;

- UV-LED inactivation led to changes in membrane permeability and enzymatic activity that was verified by a combination of flow cytometry with fluorescence-based viability stains; this technique may be useful to evaluate the effectiveness of the disinfectant treatments applied in a drinking water utility;

LEDs that emit light at 265 nm may be an effective and more ecological alternative to current disinfection methods.

Acknowledgements

Financial support from Fundação para a Ciência e a Tecnologia through the fellowship SFRH/BD/111150/2015 and project PTDC/EAM-AMB/30989/2017 is gratefully acknowledged. iNOVA4Health - UID/Multi/04462/2013, a program financially

supported by Fundação para a Ciência e Tecnologia/Ministério da Educação e Ciência, through national funds and co-funded by FEDER under the PT2020 Partnership Agreement is gratefully acknowledged. The authors also thank Dr. David Bastien from SYSMEX for helping with the flow cytometry analysis and SYSMEX that has kindly provided the flow cytometer used in these experiments.

References

Avalos, J. and Carmen Limón, M. 2015. Biological roles of fungal carotenoids. Current Genetics 61(3), 309-324.

Babič, M.N., Gunde-Cimerman, N., Vargha, M., Tischner, Z., Magyar, D., Veríssimo, C., Sabino, R., Viegas, C., Meyer, W. and Brandão, J. 2017. Fungal Contaminants in Drinking Water Regulation? A Tale of Ecology, Exposure, Purification and Clinical Relevance. International Journal of Environmental Research and Public Health 14(6), 1-44.

Beck, S.E., Ryu, H., Boczek, L.A., Cashdollar, J.L., Jeanis, K.M., Rosenblum, J.S., Lawal, O.R. and Linden, K.G. 2017. Evaluating UV-C LED disinfection performance and investigationg potential dual-wavelength synergy. Water Research 109, 207-216.

Bolton, J.R. and Linden, K.G. 2003. Standardization of Methods for Fluence (UV Dose) Determination in Bench-Scale UV Experiments. Journal of Environmental Engineering 129(3), 209-215.

Bowker, C., Sain, A., Shatalov, M. and Ducoste, J. 2011. Microbial UV fluence-response assessment using a novel UV-LED collimated beam system. Water Research 45(5), 2011-2019.

Braga, G.U.L., Rangel, D.E.N., Fernandes, É.K.K., Flint, S.D. and Roberts, D.W. 2015. Molecular and physiological effects of environmental UV radiation on fungal conidia. Current Genetics 61(3), 405-425.

Braga, G.U.L., Rangel, D.E.N., Flint, S.D., Anderson, A.J. and Roberts, D.W. 2006. Conidial pigmentation is important to tolerance against solar-simulated radiation in the entornopathogenic fungus *Metarhizium anisopliae*. Photochemistry and Photobiology 82(2), 418-422.

Chatterley, C. and Linden, K. 2010. Demonstration and evaluation of germicidal UV-LEDs for point-of-use water disinfection. Journal of Water and Health 8(3), 479-486.

Chen, F., Yang, X. and Wu, Q. 2009. Photocatalytic Oxidation of *Escherischia coli*, *Aspergillus niger*, and Formaldehyde under Different Ultraviolet Irradiation Conditions. Environmental Science and Technology 43(12), 4606-4611.

Donnelly, R.F., McCarron, P.A. and Tunney, M.M. 2008. Antifungal photodynamic therapy. Microbiological Research 163(1), 1-12.

Ehgartner, D., Herwig, C. and Neutsch, L. 2016. At-line determination of spore inoculum quality in *Penicillium chrysogenum* bioprocesses. Applied Microbiology and Biotechnology 100(12), 5363-5373.

Gerba, C.P. (2000) Environmental Microbiology. Maier, R.M., Pepper, I.L. and Gerba, C.P. (eds), Academic Press.

Hageskal, G., Kristensen, R., Fristad, R.F. and Skaar, I. 2011. Emerging pathogen *Aspergillus calidoustus* colonizes water distribution systems. Medical Mycology 49(6), 588-593.

Hamamoto, A., Mori, M., Takahashi, A., Nakano, M., Wakikawa, N., Akutagawa, M., Ikehara, T., Nakaya, Y. and Kinouchi, Y. 2007. New water disinfection system using UVA light-emitting diodes. Journal of Applied Microbiology 103(6), 2291-2298.

Hijnen, W.A.M., Beerendonk, E.F. and Medema, G.J. 2006. Inactivation credit of UV radiation for viruses, bacteria and protozoan (oo)cysts in water: A review. Water Research 40(1), 3-22.

Hollaender, A., Raper, K.B. and Coghill, R.D. 1945. The Production and Characterization of ultraviolet-induced mutations in *Aspergillus terreus*. I. Production of the mutations. American Journal of Botany 32(3), 160-165.

Li, G.-Q., Wang, W.-L., Huo, Z.-Y., Lu, Y. and Hu, H.-Y. 2017. Comparison of UV-LED and low pressure UV for water disinfection: Photoreactivation and dark repair of *Escherichia coli*. Water Research 126, 134-143.

Mesquita, N., Portugal, A., Piñar, G., Loureiro, J., Coutinho, A.P., Trovão, J., Nunes, I., Botelho, M.L. and Freitas, H. 2013. Flow cytometry as a tool to assess the effects of gamma radiation on the viability, growth and metabolic activity of fungal spores. International Biodeterioration & Biodegradation 84, 250-257.

Murdoch, L.E., McKenzie, K., Maclean, M., MacGregor, S.J. and Anderson, J.G. 2013. Lethal effects of high-intensity violet 405-nm light on *Saccharomyces cerevisiae*, *Candida albicans*, and on dormant and germinating spores of *Aspergillus niger*. Fungal Biology 117(7-8), 519-527.

Nascimento, É., Da Silva, S.H., Dos Reis Marques, E., Roberts, D.W. and Braga, G.U.L. 2010. Quantification of Cyclobutane Pyrimidine Dimers Induced by UVB Radiation in Conidia of the Fungi *Aspergillus fumigatus*, *Aspergillus nidulans*, *Metarhizium acridum* and *Metarhizium robertsii*. Photochemistry and Photobiology 86(6), 1259-1266.

Nescerecka, A., Rubulis, J., Vital, M., Juhna, T. and Hammes, F. 2014. Biological instability in a Chlorinated Drinking Water Distribution Network. PLOS One 9(5), e96354.

Nevel, S.V., Koetzsch, S., Proctor, C.R., Besmer, M.D., Prest, E.I., Vrouwenvelder, J.S., Knezev, A., Boon, N. and Hammes, F. 2017. Flow cytometric bacterial cell counts challenge conventional heterotrophic plate counts for routine microbiological drinking water monitoring. Water Research 113, 191-206.

Nourmoradi, H., Nikaeen, M., Stensvold, C.R. and Mirhendi, H. 2012. Ultraviolet irradiation: An effective inactivation method of *Aspergillus* spp. in water for the control of waterborne nosocomial aspergillosis. Water Research 46(18), 5935-5940.

Nyangaresi, P.O., Qin, Y., Chen, G., Zhang, B., Lu, Y. and Shen, L. 2018. Effects of single and combined UV-LEDs on inactivation and subsequent reactivation of *E. coli* in water disinfection. Water Research 147, 331-341.

Oguma, K., Kita, R., Sakai, H., Murakami, M. and Takizawa, S. 2013. Application of UV light emitting diodes to batch and flow-through water disinfection systems. Desalination 328, 24-30.

Oliveira, B.R., Barreto Crespo, M.T., San Romão, M.V., Benoliel, M.J., Samson, R.A. and Pereira, V.J. 2013. New insights concerning the occurrence of fungi in water sources and their potential pathogenicity. Water Research 47(16), 6338-6347.

Panngom, K., Sang Hark, L., Park, D.H., Sim, G.B., Kim, Y.H., Uhm, H.S., Park, G., Choi, E.H. 2014. Non-Thermal Plasma Treatment Diminishes Fungal Viability and Up-Regulates Resistance Genes in a Plant Host. PLOS One 9(6), e99300.

Parveen, S., Lanjewar, S., Sharma, K. and Kutti, U. 2011. Isolation of fungi from the surface water of river. Journal of Experimental Sciences 2(10), 58-59.

Pereira, V.J., Basílio, M.C., Fernandes, D., Domingues, M., Paiva, J.M., Benoliel, M.J., Crespo, M.T. and Romão, M.V.S. 2009. Occurrence of filamentous fungi and yeasts in three different drinking water sources. Water Research 43(15), 3813-3819.

Pereira, V.J., Weinberg, H.S., Linden, K.G. and Singer, P.C. 2007. UV degradation kinetics and modeling of pharmaceutical compounds in laboratory grade and surface water via direct and indirect photolysis at 254 nm. Environmental Science and Technology 41(5), 1682-1688.

Pontara, A.V., Oliveira, C.D.D.d., Barbosa, A.H., Santos, R.A.d., Pires, R.H. and Martins, C.H.G. 2011. Microbiological Monitoring of Mineral Water Commercialized in Brazil. Brazilian Journal of Microbiology 42(2), 554-559.

Ramani, R., Gangwar, M. and Chaturvedi, V. 2003. Flow cytometry antifungal susceptibility testing of *Aspergillus fumigatus* and comparison of mode of action of voriconazole vis-à-vis amphotericin B and itraconazole. Antimicrobial Agents and Chemotherapy 47(11), 3627-3629.

Rattanakul, S. and Oguma, K. 2018. Inactivation kinetics and efficiencies of UV-LEDs against *Pseudomonas aeruginosa*, *Legionella pneumophila*, and surrogate microorganisms. Water Research 130, 31-37.

Samson, R.A., Hoekstra, E.S. and Frisvad, J.C. (2004) Introduction to food- and airborne fungi, Centraalbureau voor Schimmelcultures (CBS) - Utrecht.

Song, K., Mohseni, M. and Taghipour, F. 2016. Application of ultraviolet light-emitting diodes (UV-LEDs) for water disinfection: A review. Water Research 94, 341-349.

Song, K., Taghipour, F. and Mohseni, M. 2018. Microorganisms inactivation by continuous and pulsed irradiation of ultraviolet light-emitting diodes (UV-LEDs). Chemical Engineering Journal 343, 362-370.

Song, K., Taghipour, F. and Mohseni, M. 2019. Microorganisms inactivation by wavelength combinations of ultraviolet light.emitting diodes (UV-LEDs). Science of the Total Environment 665, 1103-1110.

Vesper, S., McKinstry, C., Hartmann, C., Neace, M., Yoder, S. and Vesper, A. 2008. Quantifying fungal viability in air and water samples using quantitative PCR after treatment with propidium monoazide (PMA). Journal of Microbiological Methods 72(2), 180-184.

Wen, G., Xu, X., Zhu, H., Huang, T. and Ma, J. 2017. Inactivation of four genera of dominant fungal spores in groundwater using UV and UV/PMS: Efficiency and mechanisms. Chemical Engineering Journal 328, 619-628.

CHAPTER 4

Light-emitting diodes effect on *Aspergillus* species in real water sources: DNA damage, proteome response and potential reactivation

B.R. Oliveira, A.P. Marques, M. Asif, M.T. Barreto Crespo, V.J. Pereira 2020. Light-emitting diodes effect on *Aspergillus* species in real water sources: DNA damage, proteome response and potential reactivation. Submitted

Beatriz Oliveira was involved in all the experimental work presented in this chapter, Ana Paula Marques performed the experiments to detect the presence of DNA damage and Muhammad Asif helped with the proteome bioinformatic analysis. Maria Teresa Barreto Crespo and Vanessa Pereira supervised all the experimental work performed.

CONTENTS

Abstract

Application of UV radiation for drinking water treatment has increased along the years due to its known effective inactivation of several pathogens. The most reported inactivation mechanism is the damage of DNA. However, it is known that depending on the wavelengths emitted by the different UV sources, other effects can occur in the cells. The emerging light-emitting diodes (LEDs) can be acquired with different wavelengths. The aim of this study was to understand the action of different UV-LED wavelengths in the inactivation of fungi. To do that, LEDs that emit at 255 nm and at 265 nm were selected to perform inactivation of *A. fumigatus*, *A. niger* and *A. terreus* spiked into filtered surface water to address the DNA damages and proteome response after inactivation. Additionally, photoreactivation and dark repair were performed to address the potential ability of the spores to recover after exposure to UV-LEDs radiation. Results showed that both LEDs were able to induce the formation of cyclobutane pyrimidine dimers in *A. fumigatus* and *A. terreus* whereas, for *A. niger*, the formation of cyclobutane pyrimidine dimers was only detected when the LEDs that induced more inactivation (that emit at 265 nm) were used. Proteome response showed production of compounds like catalase and threonine by *A. terreus* and *A. fumigatus*, respectively, to protect the spores from oxidative stress, cell wall reorganization for *A. terreus* when exposed to both LEDs and for *A. fumigatus* after exposure to the LEDs that emit at 265 nm. *A. niger* proteome analysis before and after UV exposure did not show any relevant response under the conditions tested. Photoreactivation was detected for all the species except *A. niger* and no dark repair was observed.

Keywords: *Aspergillus* species; LED inactivation; DNA damage; proteome response; reactivation

4.1 Introduction

The application of ultraviolet (UV) irradiation for drinking water treatment has increased along the years since it is highly efficient for the inactivation of several pathogens (Hijnen et al., 2006). The inactivation mechanisms of UV have been intensively reported along the years and according to the UV wavelength used, different biological effects are expected to occur in microorganisms. UV-C wavelengths (100-280 nm) can efficiently inactivate microorganisms causing DNA damages (Oguma et al., 2001; Oguma et al., 2002). These DNA damages occur by the formation of pyrimidine (thymines or cytosines bases) dimers that can be cyclobutane pyrimidine dimers (CPDs) and/or pyrimidine (6-4) pyrimidone photoproducts (6-4PP) that, when in high number in the DNA, will block DNA replication and inhibit cellular division. Light-emitting diodes (LEDs) apart from being mercury free, compact and robust, not needing stabilization time, having longer lifetimes and low energy consumption, can also be assembled and tested with a diversity of wavelengths (Hamamoto et al., 2007; Song et al., 2016). Different studies have been conducted using LEDs with wavelengths set at 255 nm that emit at similar wavelength compared with low pressure (LP) mercury lamps (Bowker et al., 2011; Oliveira et al., 2020), set at 265 nm that have been used due to the maximum absorption peak of DNA (Oguma et al., 2013; Oliveira et al., 2020; Wan et al., 2020) and set at 280 nm due to the absorption spectra of proteins (Li et al., 2017; Rattanakul and Oguma, 2018; Song et al., 2019; Wan et al., 2020).

All the inactivation studies using LEDs mentioned above were conducted using bacteria and bacteriophages except for Oliveira et al (2020) and Wan et al (2020) that focused on the inactivation of filamentous fungi. Filamentous fungi are known to occur in drinking water matrices being their presence associated with many environmental problems like unpleasant taste and odour, mycotoxin production, and health related effects (Anaissie et al., 2001; Bucheli et al., 2008; Doggett, 2000). Moreover, filamentous fungi are known to be able to repair DNA under light (photoreactivation)

and dark conditions (Wan et al., 2020), which enables them to regrow after inactivation.

In a previous study (Oliveira et al., 2020), our group tested the inactivation of *A. fumigatus*, *A. niger* and *A. terreus* after being exposed to LEDs that emit at 255 nm and 265 nm and their effect on spores' morphology, cell wall/membrane permeability and enzymatic activity. Our results showed that LEDs that emit at 265 nm are more effective to achieve the inactivation of the tested fungi species, causing deformations of the spores, increased membrane permeability and decreased enzymatic activity. Further analysis of the effect of these wavelengths on the fungal spores are important to address other inactivation mechanisms caused by the action of UV radiation. Direct analysis of DNA damages, mainly the cyclobutane pyrimidine dimers, caused by UV mercury lamps have already been performed for several microorganisms including filamentous fungi (Nascimento et al., 2010) but, to the best of our knowledge, no studies were performed using LEDs. Apart from DNA damages, UV radiation has other effects on filamentous fungi. For instance, an effect on protein expression can occur thus, proteome analysis should be performed to assess filamentous fungi response to stress conditions, which can be defined as any situation that reduces spores' viability or fitness (de Nadal et al., 2011), like exposure to UV radiation.

The aim of this work is to assess the effect of UV-LEDs that emit at 255 nm and 265 nm on three *Aspergillus* species, *A. fumigatus*, *A. niger* and *A. terreus*, in terms of cyclobutane pyrimidine dimers formation, potential reactivation and proteome response. This study constitutes the first report to identify, at a species-specific level, the critical biological, cellular and molecular processes that are affected by each target wavelength radiation emitted by LEDs.

4.2 Methods

4.2.1 Inoculum preparation

Three species of the *Aspergillus* genus, *A. fumigatus*, *A. niger* and *A. terreus*, were selected to conduct this study due to their occurrence in several drinking water sources being this genus the most reported in Europe (Babič et al., 2017), potential pathogenicity, different color of their pigments and spores' resistance (Braga et al., 2015; Oliveira et al., 2013; Parveen et al., 2011; Pereira et al., 2009). These species were isolated from surface water in previous studies (Oliveira et al., 2013; Pereira et al., 2009) and are preserved in a culture collection with the following references: *A. fumigatus* (T161007_176), *A. niger* (T161007_187) and *A. terreus* (T201107_004).

From the selected species grown separately in malt extract agar (Merk, USA), the mycelium and spores were collected and washed according to Oliveira et al. (2020). The obtained inoculum for each species was resuspended in filtered surface water and its concentration determined using the Neubauer chamber (concentrated inoculum). The filtered surface water used in these assays was characterized in a previous study (Oliveira et al, 2020): 20 °C, pH 7.64, 2.35 mg/L C of total organic carbon, turbidity of 0.22 NTU, 1172 mg/L O_2 of chemical oxygen demand, 38.94 g/L of total solids and 22.60 mg/L of total suspended solids.

4.2.2 Inactivation experiments

The experiments were performed using a triple wavelength pearl beam reactor (AquiSense Technologies, USA) that contains three small light-emitting diodes (LEDs) of each wavelength. The selected wavelengths for this study were 255 nm and 265 nm because the former is closer to the low-pressure mercury lamps' wavelength (254 nm) and the latter is closer to the maximum absorbance peak of DNA (264 nm). The average

intensity of both LEDs was 53.66 µW/cm^2 and 250.30 µW/cm^2, respectively, measured at the same height used in the inactivation experiments (4 cm).

The inactivation of *A. fumigatus*, *A. niger* and *A. terreus* spiked separately into filtered surface water with a final concentration of 10^8 spores/mL was assessed by exposing 50 mL samples to the selected wavelengths (Oliveira et al., 2020). For this study, samples were taken at the beginning and after 30 min and 60 min of UV-LEDs exposure.

4.2.2.1 Plate count to assess inactivation

Samples collected before (at time 0 min) and after exposure to 30 min and 60 min of UV-LEDs radiation were analyzed by plate count to assess the colony forming units per mL (CFU/mL). To do this, buffered peptone water was used to perform serial dilutions that were incorporated by pour plate into malt extract agar media (Merck, USA). Plates were incubated for 2-3 days at 27 °C. Results of plate counting are presented in ln (C/C0) where C is the concentration of the fungal spores along the experimental time and C0 is the concentration of the fungal spores at the beginning of the experiment.

4.2.2.2 Inactivation effect on DNA damage

To assess DNA damage before and after 30 min and 60 min of exposure to UV-LEDs, DNA was extracted from the samples using the DNeasy® UltraClean® Microbial Kit (Qiagen, USA) following the manufacturer's protocol with some changes to optimize the DNA extraction of fungi. For cell lysis, Precellys Evolution tissue homogenizer (Bertin instruments, France) was used for 2 min at 10 000 rpm with 10 seconds break and all centrifugations were performed using twice the time advised in the

manufacturer's protocol. After extraction, DNA was quantified using a NanoDrop ND-1000 Spectrophotometer (Thermo fisher scientific, USA). An enzyme-linked immunosorbent assay (OxiSelectTM UV-Induced DNA Damage ELISA Kit, CPD Quantitation, Cell Biolabs, Inc, USA) was used to quantify the presence of cyclobutane pyrimidine dymers in the samples after DNA extraction.

4.2.2.3 Inactivation effect on proteome response

The collected samples at the beginning and after 60 min of UV-LEDs exposure were vacuum filtered with a membrane filter (0.22 µm pore size, PALL, USA). The mycelium and spores retained were transferred into Eppendorf tubes, frozen in liquid nitrogen and kept at -80 °C. Protein extraction was performed according to Carvalho et al (2013) with some modifications. In brief, samples were homogenized using a TissueLyser LT (Qiagen, Germany) with the addition of 0.02 g of polyvinylpolypyrrolidone (Sigma, USA) to the tubes. Proteins were precipitated with a cold solution of 1.5 mL of trichloroacetic acid (TCA, Sigma, USA) at 10 % (w/v) in acetone with 60 mM of dithiothreitol (DTT) molecular biology grade (VWR, USA), for 1 hour. Supernatant was discarded and the pellet washed 5 times with a cold solution of 60 mM DTT in acetone. The cold solutions used were preserved at -20 °C until use and kept on ice during their use. The tubes were air-dried overnight and equilibrated in the resuspended buffer [7 M urea (GE Healthcare, UK), 2M thiourea (GE Healthcare, UK), 30 mM tris (GE Healthcare, UK), 4 % (w/v) CHAPS (GE Healthcare, UK) and cOmplete ultra-tablets, mini, EDTA-free, EASY pack (Roche, Switzerland)]. Samples were centrifuged and supernatant quantified using the 2-D Quant Kit (GE Healthcare, UK) according to manufacturer's instructions.

Protein extract was loaded onto a NuPAGE™ 4-12% Bis-Tris Protein Gel and electrophoresed for a short time (10 min - 15 min) at low voltage onto 4-20 % pre-casted tris glycine extended (TGX) stain-free gels (Invitrogen, USA) and electrophoresed

for 15 min at 110 V (Anjo et al., 2015). A gel slice containing the entire protein extract was excised, reduced in 10 mM DTT (Sigma, USA) for 40 min at 56 °C, and alkylated in 55 mM iodoacetamide (Sigma, USA) for 30 min in the dark. Excessive iodoacetamide was quenched by further incubation with DTT (10 mM for 10 min in the dark). The resulting sample was digested overnight with trypsin (Promega, USA) at 37 °C (1:50 protein/trypsin ratio) and cleaned up with octadecylsilane.

Nano-liquid chromatography-tandem mass spectrometry (nanoLC-MS/MS) analysis was performed on an ekspert™ NanoLC 425 cHiPLC® system coupled with a TripleTOF® 6600 with a NanoSpray® III source (Sciex, USA). Peptides were separated through reversed-phase liquid chromatography (RP-LC) in a trap-and-elute mode. Trapping was performed at 2 µL/min on a Nano cHiPLC Trap column (Sciex 200 µm x 0.5 mm, ChromXP C18-CL, 3 µm, 120 Å) with 100% A (0.1 % formic acid in LC-MS grade water) for 10 min. The separation was performed at 300 nL/min, on a Nano cHiPLC column (Sciex 75 µm x 15 cm, ChromXP C18-CL, 3 µm, 120 Å). The gradient was as follows: 0-1 min, 5% B (0.1% formic acid in acetonitrile, Fisher Chemicals, Belgium); 1-91 min, 5-30% B; 91-93 min, 30-80% B; 93-108 min, 80% B; 108-110 min, 80-5% B; 110-127 min, 5% B.

Peptides were sprayed into the MS through an uncoated fused-silica PicoTip™ emitter (360 µm O.D., 20 µm I.D., 10 ± 1.0 µm tip I.D., New Objective, France). The source parameters were set as follows: 15 ion gas source (GS) 1, 0 GS2, 30 curtain gas (CUR), 2.5 keV ion spray voltage floating (ISVF) and 100 °C interface heater temperature (IHT). An information dependent acquisition (IDA) method was set with a TOF-MS survey scan of 400-2,000 m/z. The 50 most intense precursors were selected for subsequent fragmentation and the MS/MS were acquired in high sensitivity mode for 40 msec. The obtained spectra were processed and analyzed using ProteinPilot™ software, with the Paragon search engine (version 5.0, Sciex). A UniProt database (4686 entries, accessed in 01/09/2019) containing the sequences of the proteins from *Aspergillus* (Taxon ID: 5052) was used. The following search parameters were set: Iodoacetamide, as Cys alkylation; Trypsin, as digestion; TripleTOF 6600, as the

Instrument; ID focus as biological modifications and Amino acid substitutions; search effort as thorough; and a false discovery rate (FDR) was used for multiple hypothesis correction. Only the proteins with Unused Protein Score above 1.3 and 95% confidence were considered.

Functional enrichment analysis was performed to find the biological mechanistic representations of the identified proteins. For a given set of genes or proteins, functional enrichment analysis utilizes existing annotation resources to discover the underlying biological mechanisms. In this study, DAVID tool (v6.8) (Huang et al., 2008) was used to employ functional enrichment analysis and Gene Ontology (GO) was selected as an annotation resource. The GO is most commonly used annotation resource which consists of three categories, namely biological process, cellular component and molecular function. GO knowledge is represented in a direct acyclic graph with a clear hierarchical parent to child relationships between biological terms. Frequently, functional enrichment analysis results into highly similar biological terms because of the structure of GO, making it difficult to interpret results. Therefore, REVIGO tool (Supek et al., 2011) was used to cluster highly similar GO terms from functional enrichment analysis. The REVIGO tool uses semantic similarity to group highly similar GO terms. Semantic similarity measures such as SimRel (Schlicker et al., 2006) utilizes the GO hierarchical structure to estimate the similarity between GO terms. The similarity score ranges from 0 to 1 and a score of 1 indicates identical terms. In REVIGO tool, SimRel measures were selected and a semantic similarity score of 0.9 was used to group similar go terms.

4.2.3 Photoreactivation and dark repair experiments

After the inactivation experiments, samples of 50 mL taken after 30 min and 60 min of UV-LEDs exposure, of the three different *Aspergillus* species spiked into surface water were immediately assayed in terms of their potential ability to reactivate. To do this, the collected samples were incubated at 27 °C under three lamps of white light (Osram DULUX L 18W / 21-840 2G11 LUMILUX Cool White lamps) to address photoreactivation and kept in the dark at the same temperature to address dark repair. The average intensity of the lamps that emitted at three wavelengths (436 nm, 365 nm and 313 nm), measured using an ILT 950 UV Spectroradiometer (Massachusetts, USA), was 0.1 mW/cm^2. Reactivation samples were taken after 4 hours and 8 hours of incubation to evaluate plate counts, flow cytometry and DNA damage recovery. A control sample, spiked sample not exposed to UV inactivation, was used to verify the spores' concentration and DNA damage during the reactivation assays, under light and dark conditions.

4.2.3.1 Plate count to assess reactivation

All the samples and controls generated in the reactivation experiments were analyzed by plate count to assess the colony forming units per mL at the beginning (at time 0 min) and after the samples were placed for 4 hours and 8 hours under light and dark conditions, as detailed in section 4.2.2.1.

4.2.3.2 Flow Cytometry analysis to assess reactivation

The Yeast Control – Viability Kit (Sysmex Partec, GmbH, Germany) was used to couple fluorescent dyes with flow cytometry and detect effects on membrane permeability and enzymatic activity. This kit contains fluorescein diacetate (FDA) that, becoming fluorescent when degraded by cellular enzymes and allows the detection of metabolically active spores and propidium iodide (PI) that intercalates the DNA when the cell wall is disrupted and therefore allows the detection of dead spores. Additionally, it is also possible to distinguish between damage spores (spores that have positive signal for both dyes) and quiescent spores (spores that have negative signal for both dyes) (Oliveira et al., 2020).

The collected samples before reactivation and after 4 hours and 8 hours of reactivation were diluted in phosphate buffered saline (PBS) solution to a final concentration of 10^6 spores/mL and assayed in a CyFlow® Cube 6 (Sysmex Partec GmbH, Germany) equipped with a blue laser (488 nm at 50 mW). The software used was a CyViewTM for Cube 6 (Partec GmbH, Germany) to analyze the cytograms obtained after eliminating the baseline background (PBS).

4.2.3.3 DNA damage

To assess DNA damage in the samples collected before and after the 4 hours and 8 hours of the reactivation experiments samples the methods described in section 4.2.2.2 were followed.

4.3 Results and Discussion

4.3.1 UV-LEDs inactivation

The defined exposure times for the inactivation of *A. fumigatus*, *A. niger* and *A. terreus* using LEDs that emit at 255 nm and 265 nm were 30 min and 60 min. With these defined exposure times, the log reduction of spores obtained is presented in table 4.1. As it can be seen, the LEDs that emit at 255 nm are less efficient to the inactivation of *A. fumigatus* and *A. terreus*, having no inactivation effect on *A. niger* compared with the LEDs that emit at 265 nm that showed 3-log, 2-log and 4-log reduction for *A. fumigatus*, *A. niger* and *A. terreus*, respectively.

Table 4.1 – Log-reductions of *A. fumigatus*, *A. niger* and *A. terreus* after exposure to different UV fluences (30 min and 60 min) to LEDs that emit at 255 nm and 265 nm.

	A. fumigatus **mJ.cm^{-2}/min**	***A. niger*** **mJ.cm^{-2}/min**	***A. terreus*** **mJ.cm^{-2}/min**
LED 255	5.8/30 – 1-log	3.7/30 – 0-log	8.0/30 – 2-log
	11.7/60 – 2-log	7.4/60 – 0-log	16.0/60 – 3-log
LED 265	9.9/30 – 3-log	3.6/30 – 2-log	9.9/30 – 3-log
	14.0/60 – 3-log	7.3/60 – 2-log	19.7/60 – 4-log

4.3.1.1 DNA damage

The DNA damage was assessed by the quantification of cyclobutane pyrimidine dimers formation in the samples collected at the beginning (T0 min) and after 30 min and 60 min of exposure to the different LEDs. Figure 4.1 shows that, as expected, the samples taken before UV exposure did not contain dimers for all fungi species. For *A. fumigatus*, the dimers formation is very similar for the LEDs that emit at 255 nm and

265 nm with a slight increase in the formation of cyclobutane pyrimidine dimers after 60 min exposure to the LEDs that emit at 265 nm. Nascimento et al. (2010) also assessed the formation of pyrimidine dimers in *A. fumigatus*. The authors verified that with increasing exposure times to lamps with a peak wavelength at 313 nm there was an increase in dimers formation in *A. fumigatus* and the same can be seen in figure 4.1 for LEDs that emit at 265 nm. For *A. niger*, since no inactivation occurred using the LEDs that emit at 255 nm, no DNA damage was expected, as can be seen in figure 4.1 whereas, after exposure to LEDs that emit at 265 nm, dimers formation is observed after both exposure times, being higher after 60 minutes exposure. For *A. terreus*, the formation of pyrimidine dimers was detected with similar concentrations for both LEDs after the two different exposure times.

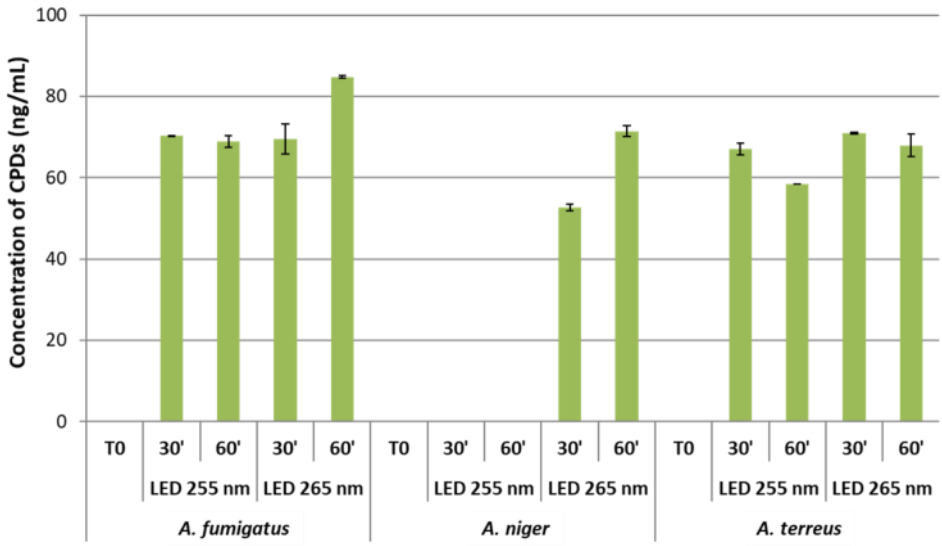

Figure 4.1 – Concentration of CPDs formed in the DNA of *A. fumigatus*, *A. niger* and *A. terreus* before exposure (T0 min) and after 30 min and 60 min of exposure to UV-LEDs that emit light at 255 nm and 265 nm. Error bars represent duplicates.

Comparing the results shown in figure 4.1 with the log-reductions from table 4.1 it can be seen that different log-reductions does not reflect different concentration of cyclobutane pyrimidine dimers detected, for instance, *A. fumigatus* has higher log-reduction after 60 min of exposure to LEDs that emit at 255 nm compared with 30 min and the concentration of cyclobutane pyrimidine dimers is the same for both exposure times. This probably means that the inactivation mechanisms are not only due to the formation of cyclobutane pyrimidine dimers but also due to, other spores' damages.

4.3.1.2 Proteome response

There has been an increased interest on describing the proteome of filamentus fungi due to their industrial importance which resulted in the genome sequencing of several filamentous fungi species, including *A. fumigatus* (Nierman et al., 2005), *A. niger* (Pel et al., 2007) and *A. terreus* (Askenazi et al., 2003). The existance of genome sequences enables the prediction of fungi's proteome through bioinformatic tools (Cologna et al., 2018). However, one disadvantage of these predictions is that it can be misleading with what is actually happening in cells. Conducting proteome analysis before and after a stress condition is therefore important to correctly identify the proteins involved in different cellular processes.

This is the first study to address the response of *A. fumigatus*, *A. niger* and *A. terreus*, at the proteomic level, to UV-LEDs radiation. To do this, proteome analysis were performed in samples collected before and after 60 min of exposure to the LEDs that emit at 255 nm and 265 nm. The identified proteins were clustered according to the three gene-ontology (GO) categories: biological process (BP), that forms protein clusters taking into account their funcionality in cells, tissues, organs and organisms; cellular component (CC), that forms proteins clusters taking into account their locallization in the cell; and molecular function (MF), that forms protein clusters taking

into account their activity at the molecular level. The identified proteins from LC-MS/MS, by DAVID proteomics, the GO terms from DAVID and GO clusters from REVIGO formed for each category and each individual species for the non treated samples and samples after 60 min exposure to the LEDs that emit at 255 nm and 265 nm, are presented in table 4.2.

As can be seen, there was some differences in the number of the identified proteins for each species which could be explained by the different protein concentrations extracted and/or due to difference in the number of reviewed proteins in the database. Adittionaly, the obtained GO terms for *A. niger* were lower when comparing with *A. fumigatus* and *A. terreus* probably due to the lower number of protein annotations that exist in the *A. niger* database. The response of each *Aspergillus* species after exposure to UV-LEDs radiation was assessed at the proteomic level in terms of their biological process, cellular component and molecular function (table 4.2 and tables 1, 2 and 3 for LEDs that emit at 255 nm and tables 4, 5 and 6 for LEDs that emit at 265 nm from supplementary information) as detailed in the next sections.

Table 4.2 – Number of proteins of each individual species (*A. fumigatus*, *A. niger* and *A. terreus*) identified from LC-MS by DAVID, the GO terms from DAVID and the GO clusters from REVIGO formed for each category (BP, CC and MF) for the different samples: non treated samples and samples after 60 min exposure to LEDs that emit at 255 nm and 265 nm. GO – gene ontology; BP – biological process; CC – cellular component; MF – molecular function.

Samples	Identified proteins from LC-MS	Proteins identified by DAVID	GO categories			New GO clusters Total (BP; CC; MF)
			BP terms (clusters)	CC terms (clusters)	MF terms (clusters)	
			A. fumigatus			
Non treated sample	1362	1360	37 (36)	53 (51)	41 (41)	
LED 255 nm	617	614	27 (27)	28 (26)	23 (23)	8 (5; 1; 2)
LED 265 nm	979	976	36 (35)	46 (44)	31 (31)	10 (5;4;1)
			A. niger			
Non treated sample	1574	124	3 (3)	2 (2)	3 (3)	
LED 255 nm	1060	83	2 (2)	2 (2)	2 (2)	0
LED 265 nm	1216	105	3 (3)	2 (2)	2 (2)	0
			A. terreus			
Non treated sample	424	415	14 (14)	10 (10)	13 (13)	
LED 255 nm	228	225	14 (14)	9 (9)	11 (11)	18 (8; 2; 8)
LED 265 nm	282	279	14 (14)	14 (14)	8 (8)	15 (6; 5; 4)

4.3.1.2.1 *Aspergillus fumigatus* response to UV-LEDs that emit at 255 nm and 265 nm

For the biological process category, there are new GO clusters formed (table 4.2, figure 4.2 a), and tables 1 and 4 from supplementary information section) in samples that were subject to LEDs that emit at 255 nm and 265 nm when compared with the initial samples that were not subject to UV-LEDs radiation. Within the common clusters, ATP metabolic process (GO:0046034), cytoplasmic translational initiation (GO:0002183) and secondary metabolite biosynthetic process (GO:0044550) they contain the same proteins, except the latter where the LEDs that emit at 265 nm contains 4 more proteins.

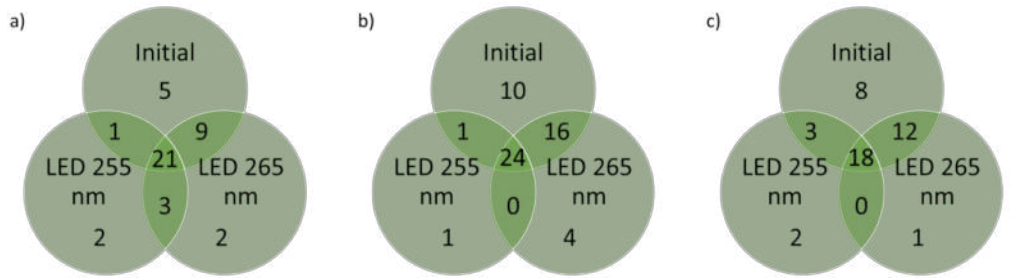

Figure 4.2 – Venn diagrams representing the *A. fumigatus* GO clusters formed before and after 60 min exposure to the LEDs that emit at 255 nm and LEDs 265 nm for a) biological process, b) cellular component and c) molecular function.

The ATP metabolic process cluster contains 3 proteins, adenylate kinase (Q4WJ21) that has an important role in cellular energy homeostasis and two vacuolar proteins (Q4WEB0 and Q4X0J7) that are related with ATP synthesis. In the cytoplasmic translational initiation cluster, there are two translational initiation factors (Q4WG69 and Q4WTH0) that are involved in protein synthesis and ATP-dependent RNA helicase ded1 (Q4WP13) that is involved in initiation of the translation process. In the last

cluster, the LEDs that emit at 255 nm contains 8 proteins whereas the LEDs that emit at 265 nm contains the same 8 proteins and 4 more. From the 8 equal proteins, 6 are involved in the biosynthesis of trypacidin and 2 are involved in the biosynthesis of fumiquinazoline. Trypacidin is a mycotoxin that plays a role in the infection process. Blachowicz et al (2020) tested trypacidin's capacity to protect fungal spores from UV-C due to its aromatic structure but verified that mutants without its biosynthetic pathway were more resistant to UV radiation. Fumiquinazoline is a conidial metabolite that has been shown to protect spores from UV-C radiation (Blachowicz et al., 2020). The remaining four proteins from the LEDs that emit at 265 nm are involved in the biosynthesis of trypacidin (Q4WQZ1, Q4WQY5 and Q4WQZ6) and in the biosynthesis of fumiquinazoline (Q4WLW7). For the LEDs that emit at 255 nm specifically, the cellular amino acid metabolic process cluster contains 5 proteins that seems to be related with the degradation of glutamate to ammonia and alpha-ketoglutarate. The glutamate biosynthetic process cluster contains 3 proteins where two (Q4WMT8 and Q4WJ35) are involved in glutamate biosynthesis and the third (Q4WMU1) is responsible for the first step in the methionine salvage pathway. For the LEDs that emit at 265 nm, the protein refolding cluster contains 4 proteins, heat shock protein Hsp98/Hsp104/ClpA, putative (Q4WRS4), GrpE protein homolog (Q4X0L7) that is part of a complex responsible for translocation of inner membrane proteins into the mitochondrial matrix, antigenic mitochondrial protein HSP60, putative (Q4X1P0) and chaperonin, putative (Q4WM94) that has a role in nucleotide excision repair by maintaining protein repair in their properly folded state (Vermeulen et al., 2018). The pyruvate metabolic process cluster contains three proteins of which two (Q4WW86 and Q4WP18) are involved in the gluconeogenesis pathway and the other (Q4WIE8) is a mitochondrial enzyme involved in reactive oxygen species (ROS) production.

For cellular component category, there are new GO clusters formed (table 4.2, figure 4.2 b), and tables 2 and 5 from supplementary information section) in samples that were subject to LEDs that emit at 255 nm and 265 nm when compared with the

initial samples that were not subject to UV-LEDs radiation. For the new cluster detected after exposure to the LEDs that emit at 255 nm, actin filament bundle (GO:0032432), it contains 3 proteins that are involved in the regulation of actin polymerization. For the LEDs that emit at 265 nm, the mitochondrial inner membrane (GO:0005743) cluster contains 8 proteins of which 7 proteins are involved in the mitochondrial inner membrane like chaperones, respiratory electron transport chain and the maintenance of crista junctions and the last protein, prohibitin (E9R5I4) is a mitochondrial protein required for melanogenin-induced pigmentation. The Swr1 complex (GO:0000812) cluster contains two DNA helicases (Q4WPW8 and Q4WKH9) that are involved in several chromatin remodeling and DNA repair through the INO80 complex and one histone (Q4WE68) that is involved in several DNA processes like transcription, replication and repair. The U6 snRNP (GO:0005688) cluster contains 4 proteins that are involved in the spliceosome. The vacuolar proton-transporting V-type ATPase, V1 domain (GO:0000221) cluster contains 3 proteins that are responsible for the activation of ATPase activity.

For molecular function category, there are new clusters formed (table 4.2, figure 4.2 c), and tables 3 and 6 from supplementary information section) in samples that were subject to LEDs that emit at 255 nm and 265 nm when compared with the initial samples that were not subject to UV-LEDs radiation. For the LEDs that emit at 255 nm, glutathione peroxidase activity (GO:0004602) cluster contains 3 proteins related with trypacidin biosynthesis, and structural constituent of cytoskeleton (GO:0005200) cluster contains 4 proteins that seem to participate in the microtubules formation. For the LEDs that emit at 265 nm, succinate dehydrogenase (ubiquinone) activity (GO:0008177) cluster contains 3 proteins that are involved in the mitochondrial electron transport during the tricarboxylic acid cycle.

As an overall response of *Aspergillus fumigatus* to the LEDs that emit at 255 nm there is the production of a UV-C spores' protective compound (fumiquinazoline), several proteins apparently dissociated (synthesis of glutamate, ammonia and alpha-

ketoglutarate) may have a common role on the methionine salvage pathway maybe for the production of ethylene (Sekowska et al., 2019) and there are proteins related with the reorganization of the cytoskeleton (actin polymerization and microtubules formation). The LEDs that emit light at 265 nm seems to have caused a more intense response in *A. fumigatus*. The production of a UV-C spores' protective compound (fumiquinazoline) was detected and the remaining proteins seem to be related with mitochondria dysfunctions like ROS production, overdeposition of melanin in the cell wall (prohibitin), production of heat shock proteins and DNA repair proteins. These responses were already observed by Li et al. (2014) as being opposite since, the first two may lead to cell apoptosis and the last two are anti-apoptotic factors.

4.3.1.2.2 *Aspergillus niger* response to UV-LEDs that emit at 255 nm and 265 nm

All the clusters detected after inactivation were observed in the samples not exposed to UV-LEDs (table 4.2, figure 4.3, and in supplementary information section). Despite this, after exposure to the LEDs that emit at 265 nm there is a cluster formed between the initial sample and the samples subjected to radiation. This cluster, the malate metabolic process (GO:0006108) in the biological process category (figure 3 a), is related with the citric acid cycle (Brandl and Andersen, 2017) that has been reported to be associated with oxidative stress response (Honda et al., 2012). Additionally, *A. niger* has a consistent cluster in the three categories, translation (GO:0006412) in the biological process, ribosome (GO:0005840) in the cellular component and structural constituent of ribosome (GO:0003735) in the molecular function. These clusters contain mostly the same proteins, all related with protein biosynthesis. The proteasome-mediated ubiquitin-dependent protein catabolic process (GO:0043161) cluster in the biological process and threonine-type endopeptidase activity (GO:0004298) cluster in the molecular function are responsible for cleavage of peptide

bonds. In the cellular component category, the intracellular cluster (GO:0005622) contains a protein named uricase (A2QD69) which is very important for industry in clinical biochemistry (Ali and Ibrahim, 2013).

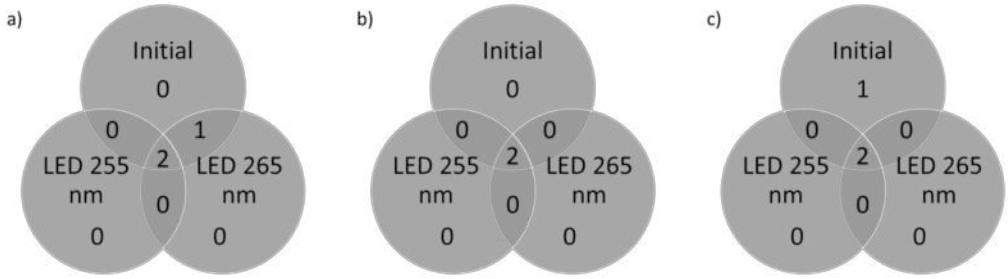

Figure 4.3 – Venn diagrams representing the *A. niger* GO clusters formed before and after 60 min exposure to the LEDs that emit at 255 nm and LEDs 265 nm for a) biological process, b) cellular component and c) molecular function.

Since the LEDs that emit at 255 nm had no effect on *A. niger* inactivation, no proteome response was expected, as could be seen in figure 4.3. It can also be seen that, although no new proteins were detected as a response of *A. niger* to the UV-LEDs radiation, the malate metabolic cluster is maintained after exposure to the LEDs that emit at 265 nm which might mean an increased focus of *A. niger* in the production of citric acid to protect the spores against the oxidative stress.

4.3.1.2.3 *Aspergillus terreus* response to UV-LEDs that emit at 255 nm and 265 nm

For the biological process category, there are new GO clusters formed (table 4.2, figure 4.4 a), and tables 1 and 4 from supplementary information section) in samples that were subject to LEDs that emit at 255 nm and 265 nm when compared with the initial samples that were not subject to UV-LEDs radiation. The common clusters for both LEDs, negative regulation of proteolysis (GO:0045861), positive regulation of translational elongation (GO:0045901), translational elongation (GO:0006414), translational frameshifting (GO:0006452) and protein folding (GO:0006457), contain the same proteins except the last one where the LEDs that emit at 265 nm contain two more proteins. Negative regulation of proteolysis cluster contains 2 proteins (Q0D0I5 and Q0C8W6) named prohibitin that, inferred by homology, are mitochondrial proteins required for melanogenin-induced pigmentation (Snyder et al., 2005). Positive regulation of translational elongation cluster and translational frameshifting cluster contain the same proteins. The eukaryotic translation initiation factor 5A (Q0CR77) protein helps mRNA translation into cell division or cell death (Thompson et al., 2004), and the woronin body major protein (Q0CIA3) is a specific organelle from fungi that plugs the pore in case of cell wall damage (Beck and Ebel, 2013). The translational elongation cluster is composed by two uncharacterized proteins and the protein folding cluster contains 5 proteins, two are prohibitins (Q0D0I5 and Q0C8W6), calnexin (Q0CT18) that is involved in glycosylated protein folding and integrates the control system of the endoplasmic reticulum (Conesa et al., 2002), heat shock protein SSC1, mitochondrial (Q0CPF2) that belongs to the heat shock protein 70 (Hsp70) that is proposed to have a role in the repair or degradation of polypeptides under stress conditions or to stabilize protein folding under no stress conditions (Hartl, 1996) and peptidyl-prolyl cis-trans isomerase (Q0C9W6) that accelerates protein folding. The two additional proteins that appear in samples after being exposed to the LEDs that emit at 265 nm are another heat shock protein (Q0CE88) and thioredoxin domain-containing

protein (Q0CUS6) that has been reported to replace peroxidase-detoxifying peroxiredoxins and cytochrome c peroxidase under long-term oxidative stress (Pusztahelyi et al., 2011). Regarding the clusters specific for the LEDs that emit at 255 nm, the intracellular protein transport cluster contains proteins all related with the transport vesicles from the endoplasmic reticulum (ER) like its formation, its coating and nucleocytoplasmic transport, the replicative cell aging cluster contains two prohibitins (Q0D0I5 and Q0C8W6) and a superoxide dismutase (Q0CQW4) whose role is to destroy radicals that are toxic to the cells which can be related to a stress oxidative response and the phenylalanyl-tRNA aminoacylation cluster contains two proteins that are the same as for the cluster formed in the cellular component category, phenylalanine-tRNA ligase complex (GO:0009328) and for the cluster formed in the molecular function category, phenylalanine-tRNA ligase activity (GO:0004826) named as phenylalanyl-tRNA synthetase alpha chain and beta chain. In the *A. terreus* samples exposed to the LEDs that emit at 265 nm, the protein transport cluster contains 5 proteins where autophagy-related protein 8 (Q0C804) is a protein involved in the formation of autophagosomes that participates in the nucleus or mitochondria degradation to a basal level to avoid excessive ROS production and save cellular energy.

For the cellular component category, there are new GO clusters formed (table 4.2, figure 4.4 b), and tables 2 and 5 from supplementary information section) in samples that were subject to LEDs that emit at 255 nm and 265 nm when compared with the initial samples that were not subject to UV-LEDs radiation. For the LEDs that emit at 255 nm, it was detected the phenylalanine-tRNA ligase complex cluster (already mentioned) and the fatty acid synthase complex cluster (GO:0005835) that contains two proteins, carrier domain-containing protein (Q0CPX5) and fatty acid synthase beta subunit dehydratase (Q0CPX6). For the *A. terreus* samples exposed to the LEDs that emit at 265 nm, the eukaryotic 43S preinitiation complex (GO:0016282) cluster contains three proteins, one uncharacterized and two translational elongation factors (Q0CPV5 and Q0CN46) involved in cell proliferation. The Ino80 complex (GO:0031011)

cluster contains three proteins, actin (Q0CH69), a nuclear envelope protein (Q0CW80) and histone (Q0C919) that is involved in several DNA processes like transcription, replication and repair. The large ribosomal subunit (GO:0015934) cluster contains three proteins all related with ribosomal subunits. The mitochondrial oxoglutarate dehydrogenase complex (GO:0009353) cluster contains two proteins, dihydrolipoyl dehydrogenase (Q0CKS9) that is a mitochondrial enzyme involved in ROS production and 2-oxoglutarate dehydrogenase E1 component, mitochondrial (Q0CQX3) that is probably related with the production of itaconic acid. The proteasome storage granule (GO:0034515) cluster contains 4 proteins where three proteins are related with proteasome subunits and one is a protein C inhibitor (Q0CSM1).

For the molecular function category, there are new GO clusters formed (table 4.2, figure 4.4 c), and tables 3 and 6 from supplementary information section) in samples that were subject to LEDs that emit at 255 nm and 265 nm when compared with the initial samples that were not subject to UV-LEDs radiation.. The common clusters between the LEDs that emit at 255 nm and 265 nm, GTP binding (GO:0005525), GTPase activity (GO:0003924), L-malate dehydrogenase activity (GO:0030060) and structural constituent of cytoskeleton (GO:0005200), possess the same proteins except GTP binding cluster where the samples exposed to the LEDs that emit at 255 nm has one more protein. So, in the GTP binding cluster there are 8 common proteins involved in protein trafficking among different cell compartments and 1 protein specific for the LEDs that emit at 255 nm, protein rho1 (Q0CTR9) that regulates the synthesis of β-1,3-glucan which is a central component of the cell wall. The GTPase activity cluster contains the same proteins as the previous cluster. In the L-malate dehydrogenase activity cluster there is malate dehydrogenase (Q0CIX6) and malate dehydrogenase, mitochondrial (Q0CKY1) that probably are related with the production of itaconic acid. In the last cluster there are two tubulin proteins that are the major component of microtubules (Q0D197 and Q0CN96) and actin (Q0CH69) that together are important in cell trafficking.

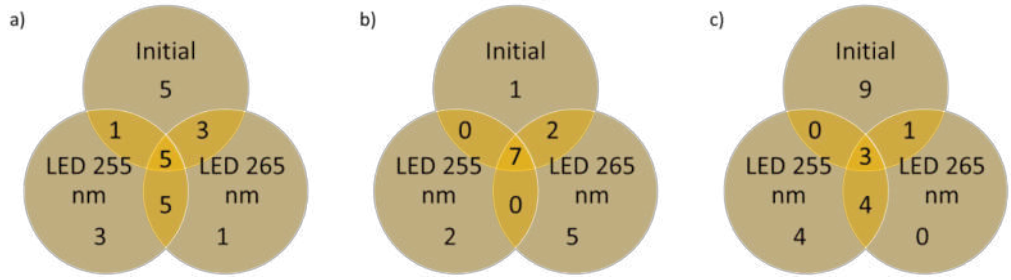

Figure 4.4 – Venn diagrams representing the *A. terreus* GO clusters formed before and after 60 min exposure to the LEDs that emit at 255 nm and LEDs 265 nm for a) biological process, b) cellular component and c) molecular function.

In the remaining clusters specific for the LEDs that emit at 255 nm, the phenylalanine-tRNA ligase activity (GO:0004826) cluster was already discussed above. The glucan endo-1,3-beta-D-glucosidase activity (GO:0042973) cluster contains one uncharacterized protein and another (Q0C7P6) that has a role in cell expansion, cell-cell fusion and spore release during growth, mating and sporulation, respectively. In the structural constituent of cell wall cluster there are two proteins, Zn(2)-C6 fungal-type domain-containing protein (Q0C7L1) that is a transcriptional regulator involved in several biological processes of the fungal cells and hydrophobin (Q0CIJ2) that is involved in cell wall rearrangements probably due to adaptation to environmental stress response. The metal ion binding cluster, contains 14 proteins: one is uncharacterized, 5 proteins (Q0CUL6, Q0CFB9, Q0CPE3, Q0D0B1 and Q0CS25) are involved in the mitochondrial respiratory chain, two catalases (Q0CFQ7 and Q0CZU0) protect cells from hydrogen peroxide toxic effects and two superoxide dismutase (Q0CIE1 and Q0D128) destroy radicals that are toxic to the cells which can be related to a stress oxidative response, one enzyme (Q0CR35) is involved in the metabolism of beta-glucan which is a major component of the cell wall, ATP-grasp domain-containing

protein (Q0C7T0) that has been reported to participate in many metabolic pathways like gluconeogenesis and fatty acid synthesis (Fawaz et al., 2011), vacuolar protein sorting-associated protein 27 (Q0CJV3) that might participate in vacuoles formation and these can be involved in a wide range of processes, like protein turnover, cellular homeostasis, membrane trafficking and pathogenesis (Veses et al., 2008) and a transketolase (Q0D0I2) that might be involved in the pentose phosphate pathway for the production of NADPH.

Thus, comparing with the other two species, *A. terreus* shows a higher proteome response to both UV-LEDs. As a response to exposure to the LEDs that emit at 255 nm, mitochondrial dysfunction was described for *A. fumigatus* and *A. terreus*. In addition, cytoskeleton and cell wall reorganizations (e.g. woronin bodies and hydrophobins) were detected and production of superoxide dismutase and catalase that protects the cells from ROS. Samples exposed to the LEDs that emit at 265 nm also show mitochondrial dysfunction and the cytoskeleton and cell wall reorganization just with woronin bodies production. The production of antioxidants (thioredoxin) was detected that protects cells from oxidative stress (Braga et al., 2015) and an increase of autophagy due to oxidative stress (Li et al., 2014).

4.3.2 Reactivation experiments

Photoreactivation and dark repair experiments were immediately performed after 30 min and 60 min of UV-LEDs exposure incubating the samples at 27 °C under white light and in the dark, respectively. A control sample that was not exposed to any UV-LEDs radiation was also tested for its photoreactivation and dark repair. Figure 4.5 shows the results obtained for the photoreactivation experiment. For time 0 min of photoreactivation it is shown the results before reactivation for the control sample and after 30 min and 60 min of UV-LEDs exposure. It also shows that the LEDs that emit at 265 nm have higher efficiency to inactivate the three fungi species when compared to

the LEDs that emit at 255 nm, which had no effect on *A. niger*. These results are consistent with the log-reduction in plate counting experiments presented in table 4.1.

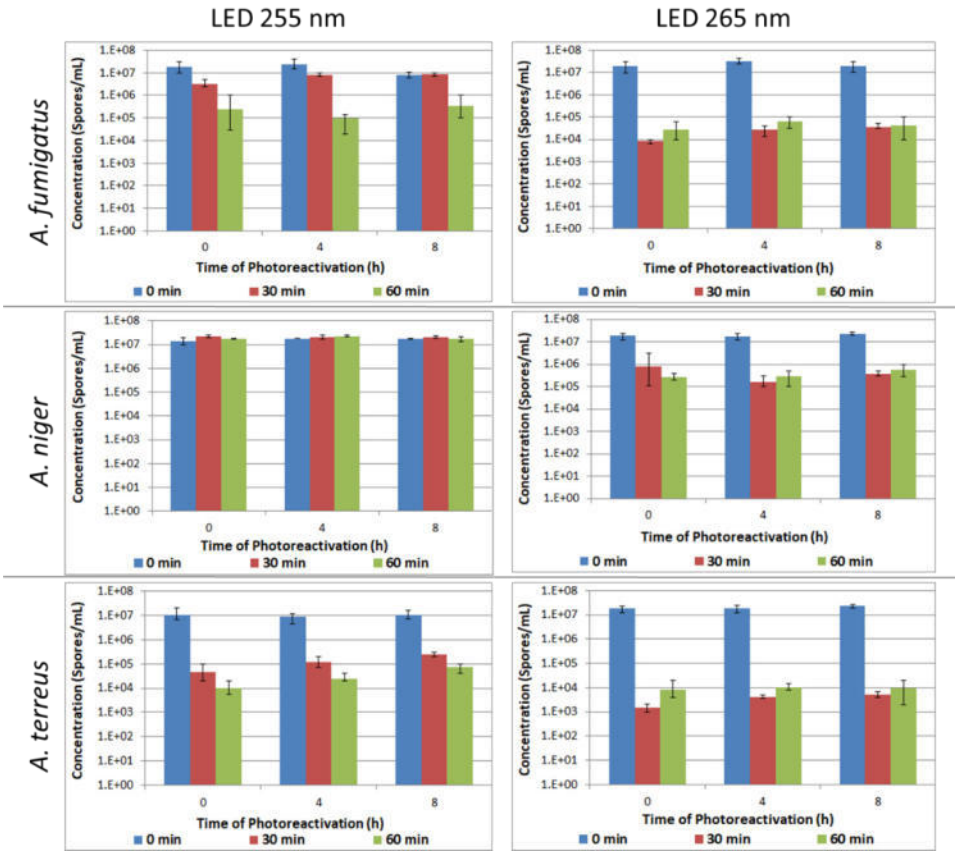

Figure 4.5 – Reactivation results in spores/mL of *A. fumigatus*, *A. niger* and *A. terreus* samples collected before and after 4 hours and 8 hours of photoreactivation. Error bars represent duplicates in up to 7 dilutions tested.

For *A. fumigatus* there is a slight photoreactivation for both LEDs. For *A. terreus* there is a small reactivation occurring after exposure to LEDs that emit at 255 nm after being exposed to 30 min and 60 min whereas, for the LEDs that emit at 265 nm there is only a slight reactivation after being exposed to 30 min. For *A. niger*, no photoreactivation was observed after 30 min and 60 min exposure to the LEDs that emit at 265 nm. Wan et al (2020) performed studies to verify the photoreactivation of different fungi species after being exposed to several LEDs wavelengths, including the 265 nm wavelength. The authors attained the same log-reduction (2-log) for *A. niger* and verified that it was able to photoreactivate up to 65 %, while, in this study no photoreactivation was observed for *A. niger*. The different results obtained in this study compared with Wan et al (2020) might be the different lamps wavelength used in the reactivation assays, mainly 436 nm compared with 365 nm, or due to lamps intensity, 0.1 mW/cm^2 compared with 0.25 mW/cm^2, for this present study and Wan et al (2020), respectively.

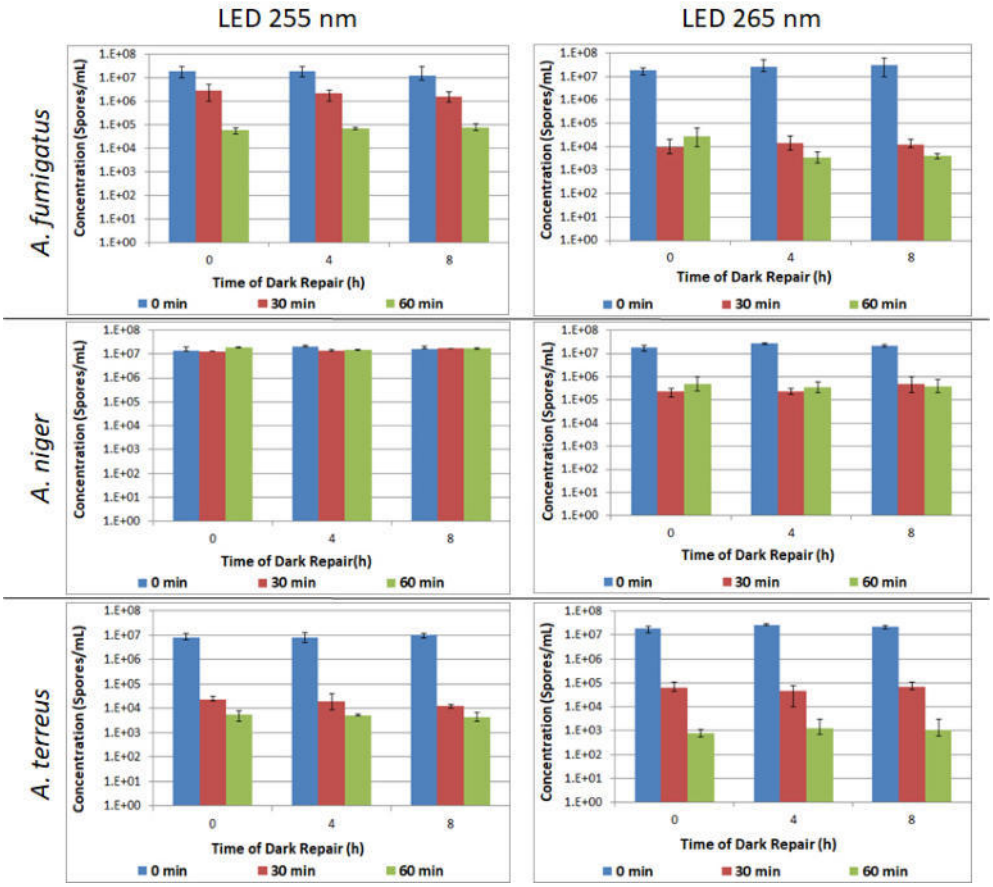

Figure 4.6 – Reactivation results in spores/mL of *A. fumigatus*, *A. niger* and *A. terreus* samples collected before and after 4 hours and 8 hours of dark repair. Error bars represent duplicates in up to 7 dilutions tested.

For dark repair reactivation after 8 hours, figure 4.6 shows that no reactivation was observed for all the fungi species and after exposure to both LED systems. This result is in agreement with the results obtained by Wan et al (2020) that also considered that the dark repair makes no difference in the reactivation process.

4.3.2.1 Effect on membrane permeability and enzymatic activity

Performing flow cytometry coupled with the Yeast Control – Viability kit (Sysmex Partec GmbH, Germany) that contains fluorescein diacetate (FDA) and propidium iodide (PI) enabled the separation of the fungal spores into four groups: metabolically active (spores that have positive signal for FDA and negative signal for PI), damage spores (spores that have positive signal for both dyes), dead (spores that have positive signal for PI and negative signal for FDA) and quiescent (spores that have negative signal for both dyes). When the signal is positive for FDA means that the fungal spores have enzymatic activity whereas when the signal is positive for PI means that the fungal spores have its membrane permeabilized. Figure 4.7 and 4.8 show the cytogram results obtained after the reactivation experiments conducted under white light (photoreactivation) and dark (dark repair) conditions, respectively.

Regarding the photoreactivation (figure 4.7) conducted after exposure to the LEDs that emit at 255 nm no major differences were observed between the initial samples (no exposure and 30 min and 60 min exposure to UV radiation) and the samples after 4 hours and 8 hours of reactivation. A slight increase of the damage spores was observed with the increase of time of exposure to the LEDs that emit at 255 nm being the remaining spores metabolically active, except for *A. niger* that show no effect of the UV-LEDs radiation, which was already expected. This result is consistent with the log-reductions in plate counts presented in table 4.1.

In the photoreactivation assays conducted after exposure to the LEDs that emit at 265 nm, *A. fumigatus* and *A. terreus* show the same photoreactivation capacity in the samples subjected to 30 min to UV-LEDs radiation with an observed increase in the metabolically active spores and a decrease of the damage spores after 4 hours and 8 hours of reactivation. These results are consistent with the ones presented in figure 4.5 where there is a slight increase of spores after the photoreactivation time of samples subject to 30 min of UV-LEDs radiation for *A. fumigatus* and *A. terreus*. For *A. fumigatus*, spores exposed to 60 min of UV-LEDs radiation were not able to recover after 4 hours

and 8 hours of reactivation showing a high percentage of damage and dead spores over time. For *A. terreus* the same result is observed but with a decrease of damage spores and an increase of dead spores. Most probably the damage spores could not recover and passed to the dead group of spores. For *A. niger*, most of the spores remained metabolically active.

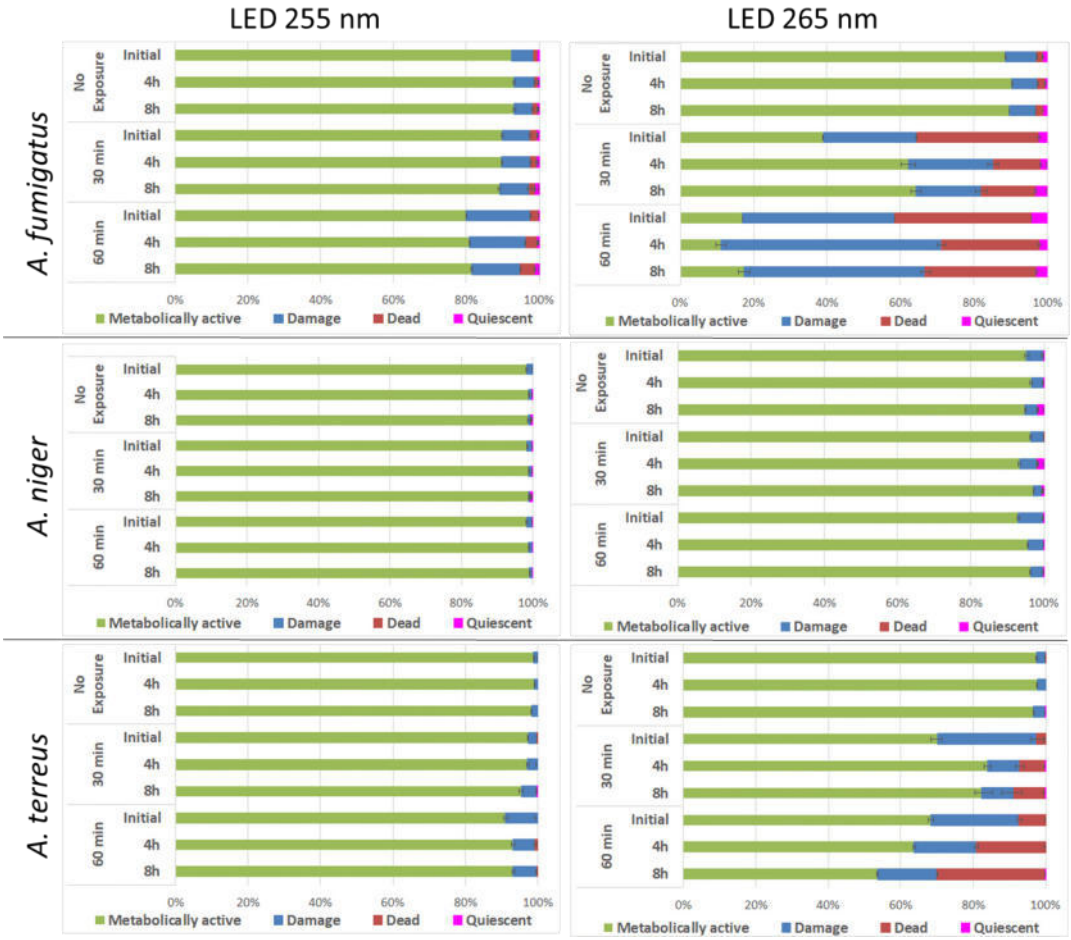

Figure 4.7 – Flow cytometry data represented as percentage bars using the Yeast Control – Viability kit (Sysmex Partec GmbH, Germany) of *A. fumigatus*, *A. niger* and *A. terreus* samples collected at the beginning (no exposure) and after 30 min and 60 min of UV-LEDs exposure at the beginning and after 4 hours and 8 hours of photoreactivation. Error bars represent triplicates.

Regarding the dark repair assays (figure 4.8) conducted after exposure to the LEDs that emit at 255 nm it is observed the same as for the photoreactivation with no major differences between the initial samples (no exposure and 30 min and 60 min exposure to UV radiation) and the samples collected after 4 hours and 8 hours of reactivation and no effect of the radiation on *A. niger* spores, as expected. The same trend observed for photoreactivation in the samples exposed for 30 min to the LEDs that emit at 265 nm was also observed in the dark repair assays conducted with *A. fumigatus* and *A. terreus* but lower percentages of increase in the metabolically active spores were observed showing that in the presence of light the spores have a higher capacity to reactivate. For *A. fumigatus* samples exposed to 60 min of UV-LEDs radiation there is higher percentage of recovery of the damage spores compared to the samples exposed 30 min since the percent of metabolic active spores increased. On the other hand, *A. terreus* samples exposed to 60 min of UV-LEDs radiation were not able to recover after 4 hours and 8 hours of reactivation since, although the damage spores decreased, the metabolically active decreased and the dead spores increased over time. For *A. niger*, most of the spores remained metabolically active.

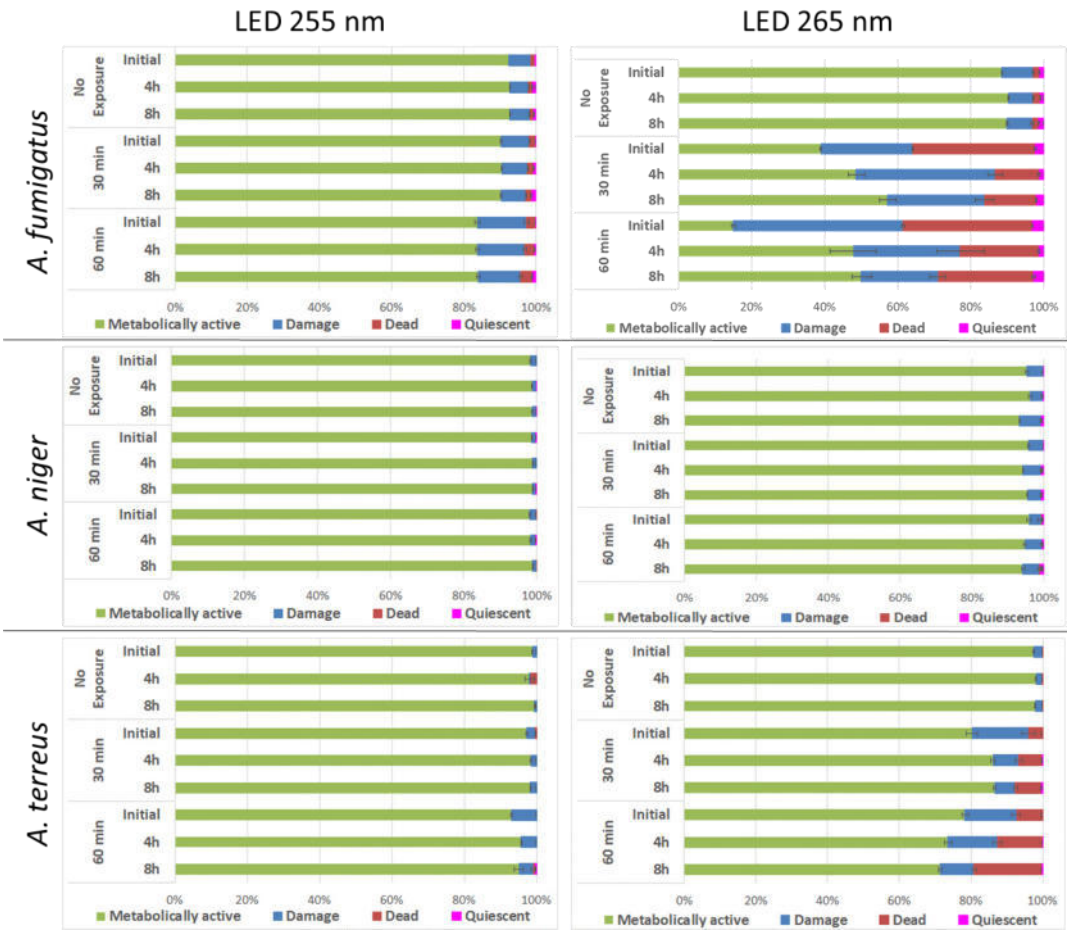

Figure 4.8 – Flow cytometry data represented as percentage bars using the Yeast Control – Viability kit (Sysmex Partec GmbH, Germany) of *A. fumigatus*, *A. niger* and *A. terreus* samples collected at the beginning (no exposure) and after 30 min and 60 min of UV-LEDs exposure at the beginning and after 4 hours and 8 hours of dark repair. Error bars represent triplicates.

The results shown in figure 4.8 are not at all consistent with the results presented in figure 4.6. For instance, it can be seen photoreactivation of *A. fumigatus* spores of samples exposed 60 min to the LEDs that emit at 265 nm in figure 4.8 but not in figure 4.6. Thus, it seems that, although the spores were repaired to some extent (increased of metabolically active spores), they were still not able to grow on plates. This was

already reported by other authors. The correlation between the germinating spores on plate and the metabolically active spores detected by flow cytometry when using a moderate UV-C radiation is low because although the membrane may be intact or repaired, the DNA may still be affected. This results in a lower number of germinating spores and higher number of metabolically active spores (Ehgartner et al., 2016; Oliveira et al., 2020).

4.3.2.2 Determination of DNA damage

Concerning the DNA damage determined by the quantification of cyclobutane pyrimidine dimers after the reactivation experiment, samples collected before and after 60 min exposure to UV-LEDs were subject to 8 hours of photoreactivation and dark repair (figure 4.9). The results for the LEDs that emit at 255 nm show a slight increase of the cyclobutane pyrimidine dimers for *A. fumigatus* and *A. terreus* meaning that no reactivation occurred under light and dark conditions. These results are consistent with figure 4.6 where it can be seen no reactivation on plate after dark repair and with figures 4.7 and 4.8 where no increase of the metabolically active spores was observed after photoreactivation and dark repair for both species. On the other hand, these results are not consistent with figure 4.5 where a slight photoreactivation of the spores of *A. fumigatus* and *A. terreus* was observed. This means that the inactivation mechanisms are not only due to the formation of cyclobutane pyrimidine dimers but, other spores' damages might have occurred.

The results for the LEDs that emit at 265 nm show a decrease in the formation of cyclobutane pyrimidine dimers for *A. fumigatus*, an increase for *A. niger* and similar concentration for *A. terreus*, under light and dark conditions. For *A. niger*, although it is the most resistant species to inactivation, having lower log reductions (table 4.1), lower cell wall/membrane permeability maintaining its enzymatic activity (figure 4.7 and 4.8), it can be seen that its DNA is being affected by the LEDs that emit at 265 nm

meaning that it must be its rigid spores' structure that avoids its inactivation. For *A. fumigatus* there is DNA repair, and this is observed in figure 4.8 that had an increase of metabolically active spores. *A. terreus*, seems to not be able to repair its DNA which is consistent with figure 4.7 and 4.8 that had an increase of damage and dead spores.

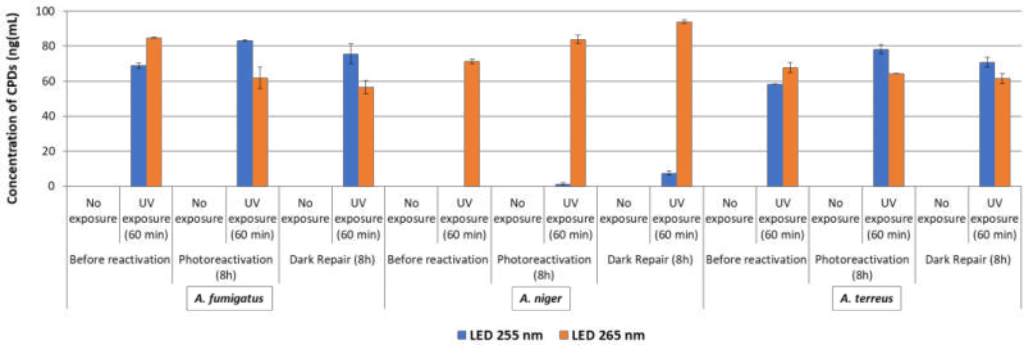

Figure 4.9 – Concentration of CPDs formed in the DNA of *A. fumigatus*, *A. niger* and *A. terreus* collected at the beginning and after 8 hours of photoreactivation and dark repair. Error bars represent duplicates.

4.4 Conclusions

In this study several methodologies were applied to verify the effect of UV-LEDs radiation that emit at 255 nm and 265 nm, for the first time, on the DNA, proteome and potential reactivation of *A. fumigatus*, *A. niger* and *A. terreus* spores. It could be seen that the utilization of plate counts and flow cytometry complement the DNA damage addressed showing that the DNA repair through photoreactivation does not necessarily mean that the spore is able to regrow on plate. Moreover, the proteome response to the imposed stress was also new since most studies that focused on this had only biotechnological interest to obtain higher quantity of a desirable secondary metabolite or were only performed with protein predictions obtained through mRNA sequences and bioinformatic tools.

Thus, this work allowed to conclude that:

- LEDs that emit at 255 nm and 265 nm were able to induce the formation of cyclobutane pyrimidine dimers in the DNA of *A. fumigatus* and *A. terreus*; *A. niger* was only susceptible to the LEDs that emit at 265 nm probably because the LEDs that emit at 255 nm needed more time of exposure or higher intensities to achieve any inactivation.
- When exposed to UV-LEDs radiation, *A. fumigatus* and *A. terreus* produced proteins that are related with their protection against oxidative stress and cell wall reorganization, respectively. *A. niger*, contrarily, did not produce proteins due to the imposed stress, but maintained the focus on the malate metabolism that is responsible for the production of citric acid and this compound, is associated with a response to oxidative stress.
- DNA repair mechanism by photoreactivation occurred for *A. fumigatus* and no dark repair was observed for all species.
- Membrane permeability and enzymatic activity reactivations show that *A. fumigatus* and *A. terreus* were able to recover after 30 min exposure to the LEDs that emit at 265 nm specially, under light conditions.

Considering the application of these UV-LEDs radiation systems for drinking water treatment is thus important since three single small LEDs were able to induce different types of damages on the fungal spores with high inactivation effectiveness. Thus, in a full scale system, with more LEDs and a higher intensity, a higher water quality is expected to be obtained with less energy consumption, than when using mercury lamps.

Acknowledgements

The authors would like to thank Professor Natalie Hull for discussions regarding the best methods to quantify the formation of dimers, Dr. David Bastien from SYSMEX for helping with the flow cytometry analysis, Inês Luís for helping with protein quantification as well as Bruno Alexandre and Ricardo Gomes for discussions about mass spectrometry analysis of proteins. The authors also thank SYSMEX that has kindly provided the flow cytometer used in these experiments. Mass spectrometry data were generated by the Mass Spectrometry Unit (UniMS), ITQB/iBET, Oeiras, Portugal.

Financial support from Fundação para a Ciência e a Tecnologia through the fellowship SFRH/BD/111150/2015 and project PTDC/EAM-AMB/30989/2017 is gratefully acknowledged. Financial support from iBET through the project LightUp is gratefully acknowledged. The authors acknowledge the project "MobFood – Mobilizing scientific and technological knowledge in response to the challenges of the agri-food market" (POCI-01-0247-FEDER-024524) financed by European Regional Development Fund (ERDF), through the Incentive System to Research and Technological development, within the Portugal2020 Competitiveness and Internationalization Operational Program. iNOVA4Health - UID/Multi/04462/2013, a program financially supported by Fundação para a Ciência e Tecnologia/Ministério da Educação e Ciência, through national funds and co-funded by FEDER under the PT2020 Partnership Agreement is gratefully acknowledged. Funding from INTERFACE Programme, through the Innovation, Technology and Circular Economy Fund (FITEC), is gratefully acknowledged.

References

Ali, U.F. and Ibrahim, Z.M. 2013. Effect of irradiation on uricase produced by two strains of *Aspergillus niger*. Life Science Journal 10(1), 962-967.

Anaissie, E.J., Kuchar, R.T., Rex, J.H., Francesconi, A., Kasai, M., Muller, F.-M.C., Lozano-Chiu, M., Summerbell, R.C., Dignani, M.C., Chanock, S.J. and Walsh, T.J. 2001. Fusariosis Associated with Pathogenic *Fusarium* Species Colonization of a Hospital Water System: A New Paradigm for the Epidemiology of Opportunistic Mold Infections. Clinical Infectious Diseases 33(11), 1871-1878.

Askenazi, M., Driggers, E., Holtzman, D., Norman, T.C. and Madden, K. 2003. Integrating transcriptional and metabolite profiles to direct the engineering of lovastatin-producing fungal strains. Nature Biotechnology 21, 150-156.

Babič, M.N., Gunde-Cimerman, N., Vargha, M., Tischner, Z., Magyar, D., Veríssimo, C., Sabino, R., Viegas, C., Meyer, W. and Brandão, J. 2017. Fungal Contaminants in Drinking Water Regulation? A Tale of Ecology, Exposure, Purification and Clinical Relevance. International Journal of Environmental Research and Public Health 14(6), 1-44.

Beck, J. and Ebel, F. 2013. Characterization of the major Woronin body protein HexA of the human pathogenic mold *Aspergillus fumigatus* International Journal of Medical Microbiology 303, 90-97.

Blachowicz, A., Raffa, N., Bok, J.W., Choera, T., Knox, B., Lim, F.Y., Huttenlocher, A., Wang, C.C.C., Venkateswaran, K. and Keller, N.P. 2020. Contributions of Spore Secondary Metabolites to UV-C Protection and Virulence Vary in Different *Aspergillus fumigatus* Strains. mBio 11(1), e03415-03419.

Bowker, C., Sain, A., Shatalov, M. and Ducoste, J. 2011. Microbial UV fluence-response assessment using a novel UV-LED collimated beam system. Water Research 45(5), 2011-2019.

Braga, G.U.L., Rangel, D.E.N., Fernandes, É.K.K., Flint, S.D. and Roberts, D.W. 2015. Molecular and physiological effects of environmental UV radiation on fungal conidia. Current Genetics 61(3), 405-425.

Brandl, J. and Andersen, M.R. 2017. Aspergilli: models for systems biology in filamentous fungi. Current Opinion in Systems Biology 6, 67-73.

Bucheli, T.D., Wettstein, F.E., Hartmann, N., Erbs, M., Vogelgsang, S., Forrer, H.-R. and Schwarzenbach, R.P. 2008. *Fusarium* Mycotoxins: Overlooked Aquatic Micropollutants? Journal of Agricultural and Food Chemistry 56(3), 1029-1034.

Carvalho, M.B., Martins, I., Medeiros, J., Tavares, S., Planchon, S., Renaut, J., Núñez, O., Gallart-Ayala, H., Galceran, M.T., Hursthouse, A. and Silva Pereira, C. 2013. The response of *Mucor plumbeus* to pentachlorophenol: A toxicoproteomics study. Journal of Proteomics 78, 159-171.

Cologna, N.M., Gómez-Mendoza, D.P., Zanoelo, F.F. and Ricart, C.A.O. 2018. Exploring Trichoterma and *Aspergillus* secretomes: proteomics approaches for the identification of enzymes of biotechnological interest. Enzyme and Microbial Technology 109, 1-10.

Conesa, A., Jeenes, D., Archer, D.B., van den Hondel, C.A.M.J.J. and Punt, P.J. 2002. Calnexin Overexpression Increases Manganese Peroxidase Production in *Aspergillus niger.* Applied and Environmental Microbiology 68(2), 846-851.

de Nadal, E., Ammerer, G. and Posas, F. 2011. Controling gene expression in response to stress. Nature Reviews Genetics 12, 833-845.

Doggett, M.S. 2000. Characterization of Fungal Biofilms within a Municipal Water Distribution System. Applied and Environmental Microbiology 66(3), 1249-1251.

Ehgartner, D., Herwig, C. and Neutsch, L. 2016. At-line determination of spore inoculum quality in *Penicillium chrysogenum* bioprocesses. Applied Microbiology and Biotechnology 100(12), 5363-5373.

Fawaz, M.V., Topper, M.E. and Firestine, S.M. 2011. The ATP-grasp enzymes. Bioorganic Chemistry 39(5-6), 185-191.

Hamamoto, A., Mori, M., Takahashi, A., Nakano, M., Wakikawa, N., Akutagawa, M., Ikehara, T., Nakaya, Y. and Kinouchi, Y. 2007. New water disinfection system using UVA light-emitting diodes. Journal of Applied Microbiology 103(6), 2291-2298.

Hartl, F.U. 1996. Molecular chaperones in cellular protein folding. Nature 381, 571-580.

Hijnen, W.A.M., Beerendonk, E.F. and Medema, G.J. 2006. Inactivation credit of UV radiation for viruses, bacteria and protozoan (oo)cysts in water: A review. Water Research 40(1), 3-22.

Honda, Y., Hattori, T. and Kirimura, K. 2012. Visual expression analysis of the responses of the alternative oxidase gene (aox1) to heat shock, oxidative, and osmotic stresses in conidia of citric acid-producing *Aspergillus niger.* Journal of Bioscience and Bioengineering 113(3), 338-342.

Huang, D.W., Sherman, B.T. and Lempicki, R.A. 2008. Bioinformatics enrichment tools: paths toward the comprehensive functional analysis of large gene lists. Nucleic Acids Research 37(1), 1-13.

Huertas, R.M., Fraga, M.C., Crespo, J.G. and Pereira, V.J. 2019. Solvent free process for the development of photocatalytic membranes. Molecules 24(24), 4481.

Li, G.-Q., Wang, W.-L., Huo, Z.-Y., Lu, Y. and Hu, H.-Y. 2017. Comparison of UV-LED and low pressure UV for water disinfection: Photoreactivation and dark repair of *Escherichia coli.* Water Research 126, 134-143.

Li, L., Hu, X., Xia, Y., Xiao, G., Zheng, P. and Wang, C. 2014. Linkage of Oxidative Stress and Mitochondrial Dysfunctions to Spontaneous Culture Degeneration in *Aspergillus nidulans*. Molecular & Cellular Proteomics 13(2), 449-461.

Nascimento, É., Da Silva, S.H., Dos Reis Marques, E., Roberts, D.W. and Braga, G.U.L. 2010. Quantification of Cyclobutane Pyrimidine Dimers Induced by UVB Radiation in Conidia of the Fungi *Aspergillus fumigatus*, *Aspergillus nidulans*, *Metarhizium acridum* and *Metarhizium robertsii.* Photochemistry and Photobiology 86(6), 1259-1266.

Nierman, W., Pain, A., Anderson, M., Wortman, J., Kim, S., Arroyo, J., Berriman, M., Abe, K., Archer, D., Bermejo, C., Bennet, J., Bowyer, P., Chen, D., Collins, M., Coulsen, R., Davies, R., Dyer, P., Farman, M., Fedorova, N., Fedorova, N., Feldblyum, T., Fischer, R., Fosker, N., Fraser, A., García, J., García, M., Goble, A., Goldman, G., Gomi, K., Griffith-Jones, S., Gwilliam, B., Haas, B., Haas, H., Harris, D., Horiuchi, H., Huang, J. and Denning, D. 2005. Genomic sequence of the pathogenic and allergenic filamentous fungus *Aspergillus fumigatus*. Nature 438, 1151-1156.

Oguma, K., Katayama, H., Mitani, H., Morita, S., Hirata, T. and Ohgaki, S. 2001. Determination of Pyrimidine Dimers in *Escherichia coli* and *Cryptosporidium parvum* during UV Light Inactivation, Photoreactivation, and Dark Repair. Applied and Environmental Microbiology 67(10), 4630-4637.

Oguma, K., Katayama, H. and Ohgaki, S. 2002. Photoreactivation of *Escherichia coli* after Low- or Medium-Pressure UV Disinfection determined by an Endonuclease Sensitive Site Assay. Applied and Environmental Microbiology 68(12), 6029-6035.

Oguma, K., Kita, R., Sakai, H., Murakami, M. and Takizawa, S. 2013. Application of UV light emitting diodes to batch and flow-through water disinfection systems. Desalination 328, 24-30.

Oliveira, B.R., Barreto Crespo, M.T. and Pereira, V.J. 2020. Small but powerful: Light-emitting diodes for inactivation of *Aspergillus* species in real water matrices. Water Research 168, 115108.

Oliveira, B.R., Barreto Crespo, M.T., San Romão, M.V., Benoliel, M.J., Samson, R.A. and Pereira, V.J. 2013. New insights concerning the occurrence of fungi in water sources and their potential pathogenicity. Water Research 47(16), 6338-6347.

Parveen, S., Lanjewar, S., Sharma, K. and Kutti, U. 2011. Isolation of fungi from the surface water of river. Journal of Experimental Sciences 2(10), 58-59.

Pel, H.J., Winde, J.H. and Stam, H. 2007. Genome sequencing and analysis of the versatile cell factory *Aspergillus niger* CBS 513.88. Nature Biotechnology 25, 221-231.

Pereira, V.J., Basílio, M.C., Fernandes, D., Domingues, M., Paiva, J.M., Benoliel, M.J., Crespo, M.T. and Romão, M.V.S. 2009. Occurrence of filamentous fungi and yeasts in three different drinking water sources. Water Research 43(15), 3813-3819.

Pusztahelyi, T.ü., Klement, É., Szajli, E., Klem, J. and Pócsi, I. 2011. Comparison of transcriptional and translational changes caused by long-term menadione exposure in *Aspergillus nidulans*. Fungal Genetics and Biology 48, 92-103.

Rattanakul, S. and Oguma, K. 2018. Inactivation kinetics and efficiencies of UV-LEDs against *Pseudomonas aeruginosa*, *Legionella pneumophila*, and surrogate microorganisms. Water Research 130, 31-37.

Schlicker, A., Domingues, F.S. and Rahnenf ührer, J. 2006. A new measure for functional similarity of gene products based on Gene Ontology. BMC Bioinformatics 7(302), 1-16.

Sekowska, A., Ashida, H. and Danchin, A. 2019. Revisiting the methionine salvage pathway and its paralogues. Microbial Biotechnology 12(1), 77-97.

Snyder, J.R., Hall, A., Ni-Komatsu, L., Khersonsky, S.M., Chang, Y.-T. and Orlow, S.J. 2005. Dissection of melanogenesis with small molecules identifies prohibitin as a regulator. Chemistry and Biology 12(4), 477-484.

Song, K., Mohseni, M. and Taghipour, F. 2016. Application of ultraviolet light-emitting diodes (UV-LEDs) for water disinfection: A review. Water Research 94, 341-349.

Song, K., Taghipour, F. and Mohseni, M. 2019. Microorganisms inactivation by wavelength combinations of ultraviolet light-emitting diodes (UV-LEDs). Science of the Total Environment 665, 1103-1110.

Supek, F., Bo šnjak, M., Šknunca, N. and Šmuc, T. 2011. REVIGO Summarizes and Visualizes long lists of gene ontology terms. PLoS ONE 6(7), e21800.

Thompson, J.E., Hopkins, M.T., Taylor, C. and Wang, T.-W. 2004. Regulation of senescence by eukariotic translation initiation factor 5A: implications for plant growth and development. Trends in Plant Science 9(4), 174-179.

Vermeulen, E., Carpentier, S., Kniemeyer, O., Sillen, M., Maertens, J. and Lagrou, K. 2018. Proteomic differences between azole-susceptible and -resistant *Aspergillus fumigatus* strains. Advances in Microbiology 8, 77-99.

Veses, V., Richards, A. and Gow, N.A. 2008. Vacuoles and fungal biology. Current Opinion in Microbiology 11(6), 503-510.

Wan, Q., Wen, G., Cao, R., Xu, X., Zhao, H., Li, K., Wang, J. and Huang, T. 2020. Comparison of UV-LEDs and LPUV on inactivation and subsequent reactivation of waterborne fungal spores. Water Research 173, 1-12.

CHAPTER 5

Treatment of a real water matrix inoculated with *Aspergillus fumigatus* using a photocatalytic membrane reactor

Published in: Journal of Membrane Science

B.R. Oliveira, S. Sanches, R.M. Huertas, M.T. Barreto Crespo, V.J. Pereira 2020. Treatment of a real water matrix inoculated with *Aspergillus fumigatus* using a photocatalytic membrane reactor. Journal of Membrane Science 598:117788.

Beatriz Oliveira was involved in all the experimental work presented in this chapter Sandra Sanches was involved in the conception of the photocatalytic membrane reactor, Rosa Huertas developed the modified membranes used in this work. Maria Teresa Barreto Crespo and Vanessa Pereira supervised all the experimental work performed.

CONTENTS

Abstract

Coupling UV photolysis, stable photoactive TiO_2 layers and water filtration in a single photocatalytic membrane reactor can be beneficial to achieve high quality drinking water since the membrane retains microorganisms and chemical pollutants whereas the photocatalytic treatment decreases fouling components and treats the concentrated retentate.

In this work, a newly designed photocatalytic membrane reactor combining filtration with UV photolysis/photocatalysis under a low pressure mercury lamp (wavelength emission at 254 nm) using ceramic modified membranes was used to treat filtered surface water inoculated with *Aspergillus fumigatus*. The photocatalytic membranes used in this study were produced using an environmental friendly modification process. Results showed high percentages of adsorption and retention of the spores for both the unmodified and modified membranes. The lower pore size of the modified membrane has the advantage of retaining the spores at the surface instead of trapping the spores inside as observed for the unmodified membrane. Direct photolysis achieved retentate treatment percentages up to 99 % after 60 minutes of treatment. The effect of the combined treatment showed that direct photolysis and photocatalysis were able to cause the deformation of spores and led to changes in membrane permeability and enzymatic activity.

Keywords: Photocatalytic membrane reactor; Surface Water; *Aspergillus fumigatus*; Membrane permeability effect; Morphology effect.

5.1 Introduction

The drive to answer to the worldwide population demand for safe drinking water and to protect water sources urges the improvement of conventional water treatment systems (Pendergast and Hoek, 2011).

The final stage of conventional drinking water treatment often consists of adding a final disinfectant that ensures a residual concentration is maintained in the distribution system to protect consumers from drinking water outbreaks. However, disinfectants such as free chlorine and chloramines react with natural organic matter from water and form disinfection by-products that have been linked to deleterious health effects. Adding UV radiation to the treatment will reduce the concentration of final chemical disinfectants and consequently the disinfection by-products formation. Direct and indirect photolysis can be used to achieve disinfection. Inactivation by direct photolysis occurs just as a consequence of exposure to irradiation. Low pressure mercury lamps are the most common lamps used in drinking water treatment facilities for inactivation of microorganisms because, they emit mainly monochromatic light at 254 nm and the maximum absorbance wavelength of DNA is 264 nm, leading to an inhibition of replication. Indirect photolysis occurs when hydrogen peroxide or a catalyst are exposed to the light source and produce the highly reactive and unselective hydroxyl radicals (Ollis et al., 1991) that will likely enhance microorganisms' inactivation (Foster et al., 2011) and degrade water contaminants (Sanches et al., 2010). For instance, titanium dioxide (TiO_2) is a relatively stable catalyst in water under UV radiation, non-toxic by ingestion, cheap and can absorb photons from UV with a wavelength below 385 nm leading to the production of hydroxyl radicals that will have a lethal action on microorganisms by membrane and cell wall damage (Foster et al., 2011).

This catalyst has been used several times in suspension but Sanches et al. (2013) showed that in this form, TiO_2 concentration in the reactors decreases considerably

due to adsorption to the flasks, tubing and membrane. This problem is avoided if TiO_2 is used immobilized as a thin film in a surface (e.g. Meng et al., 2005).

To upgrade the common water treatment systems, membrane technology is a good alternative that can be used (e.g. Esfahani et al., 2019). Microfiltration, ultrafiltration, nanofiltration and reverse osmosis are membrane separation processes able to remove different size particles (Madaeni, 1999; Peter-Varbanets et al., 2009), chemical contaminants (Sanches et al., 2013) and microorganisms (Madaeni, 1999) that may be present in different water sources. As it is known, the two main drawbacks of using membrane treatment systems is fouling of the membrane, either inorganic, organic or biological (Li et al., 2008), as well as the production of a concentrated retentate that will need further treatment (Sanches et al., 2013). To overcome these drawbacks, modification of ceramic membranes can be performed to increase the photocatalytic performance, increase the hydrophilicity and thus decrease fouling, and to control porosity. In previous work, a sol-gel process using ethanol as solvent has been used to coat commercial silicon carbide membranes with silicon dioxide and titanium dioxide to obtain reusable photocatalytic membranes with a lower molecular weight cut-off as well as high hydrophilicity (Huertas et al., 2017). The presence of the titanium dioxide ensures the photocatalytic activity of the modified membranes, whereas the combination of titanium dioxide with silicon dioxide enhances the photocatalytic performance by improving the ability of surface adsorption and increasing the amount of hydroxyl surface groups (Fateh et al., 2013).

These modifications were further improved using a methodology based on the use of aqueous solutions and low temperatures to produce environmental friendly membranes with high photocatalytic activity (Huertas et al., 2019).

Regarding the inactivation of microorganisms, most of the studies using photocatalytic membranes have been performed to demonstrate its efficiency in biofilm control (Ciston et al., 2009). Few studies have been performed coupling in the

same space and at the same time, membrane filtration with UV radiation (Goei and Lim, 2014; Liu et al., 2012; Ma et al., 2009; Romanos et al., 2013) and all of them used *E. coli* in a saline solution suspension as a model microorganism for inactivation purposes except Romanos et al (2013) that tested the reactor for the degradation of the methyl orange dye. Additionally, membrane modifications of these studies focused on the combination of TiO_2 and silver particles.

The presence of filamentous fungi in the aquatic environment was already established by many authors (Hageskal et al., 2009; Oliveira et al., 2013; Parveen et al., 2011; Pereira et al., 2009), being the genus *Aspergillus* the most reported (17 out of 19 countries) (Babič et al., 2017).

The aim of this work was to use a novel photocatalytic membrane reactor combining membrane filtration with UV photolysis and photocatalysis using a low pressure mercury lamp (that emits monochromatic light at 254 nm) in the same space and at the same time, to treat filtered surface water inoculated with filamentous fungi. To the best of the authors' knowledge this is the first study performed using a photocatalytic membrane reactor to treat real water matrix inoculated with *Aspergillus fumigatus* using ceramic membranes modified with TiO_2 and silicon dioxide (SiO_2). Unmodified and modified membranes were characterized using different techniques to evaluate and compare their physico-chemical and morphological features. Additionally, tests were performed to elucidate the treatment effect on the morphology, membrane permeability and enzymatic activity of the filamentous fungi species selected (*Aspergillus fumigatus*).

5.2 Methods

5.2.1 Matrices used and Inoculum Preparation

The matrices used in this study were saline solution (0.9 % w/v) and surface water collected from Tagus river after being subjected to filtration (using a 0.22 µm membrane filter, PALL, NY, USA) to simulate the treatment process performed in drinking water treatment facilities. The real surface water matrix was characterized before and after filtration in terms of temperature, pH, total organic carbon, turbidity, chemical oxygen demand, total solids, and total suspended solids (Oliveira et al., 2020). The uninoculated and inoculated filtered surface water samples were also characterized by 2D fluorescence using a Varian Cary Eclipse Fluorescence Spectrophotometer (Agilent, USA). Data acquisition was carried out for pairs of excitation-emission wavelengths ranging from 200-660 nm (excitation) and 210-650 nm (emission) with increments of 5 nm at a scan rate of 12000 nm/min. Optimum excitation and emission slits of 10 nm were applied. Excitation-emission matrices (EEMs) were obtained using the PARAFAC (parallel factor analysis) function in Octave 5.1.0.0.

Aspergillus fumigatus was selected due to its reported occurrence in different drinking water sources, potential pathogenicity and spores' resistance (Braga et al., 2015; Jørgensen et al., 2011; Oliveira et al., 2013; Parveen et al., 2011; Pereira et al., 2009; Youngchim et al., 2004; Zaehle et al., 2014). *A. fumigatus* was grown on malt extract agar (Merck, USA) for 7 days at 27 °C. The mycelium was removed using saline solution (0.9 % w/v) with Tween 80 (0.1 % v/v) and washed using saline solution (0.9 % w/v). The experiments were performed using spores and mycelia since both forms are expected to be present in water (Oliveira et al., 2020). The spores' concentration inoculated in the different matrices was determined using the Neubauer chamber. Plate counts were used to quantify all the samples before and after treatment.

5.2.2 Membranes

Commercially available flat sheet ceramic substrates composed of a single α-alumina layer (d_{50} =1.8 μm) (Fraunhofer-Gesellschaft, Germany) were tested in this study as unmodified membranes and used as support for the immobilization of a photocatalytically active TiO_2 layer.

5.2.2.1 Membrane Modification

Before membrane modification, alumina substrates were cleaned with a 2 % solution of MicroClean 90 ® (Sigma-Aldrich, USA) and distilled water, followed by an overnight thermal treatment at 80 °C.

The alumina membranes were modified using the solvent-free process with a tetraethyl orthosilicate (TEOS 98 %, Sigma-Aldrich, USA) as silicon dioxide source and titanium dioxide Degussa P25 (30-90 nm of nominal diameter, Evonik Industries, Germany) as titania source based on Huertas et al. (2019). Briefly, a concentrated stock solution of TEOS (1.69 M) was prepared in aqueous acidic conditions (pH=1). The miscibility with water was attained after 20 min due to the addition of acid as catalyst. The hydrolysis was maintained for 2 hours and the transparent stock solution was stable for one month. The hydrolyzed TEOS was diluted with distilled water and added to Degussa nanoparticles, with a final concentration of 0.045 M SiO_2 and 0.050 M TiO_2 that corresponds to 0.9:1 molar ratio of SiO_2:TiO_2.

The sol solution obtained was sonicated for 20 min. The membranes were mounted into a glass support to be modified on one side using the dip-coating method conducted at room temperature. The substrates were coated three times using a dip coater (Nadetech Innovations, Spain) at a speed of 150 mm/s for immersion and withdrawal. The substrates were immersed for 10 seconds in the sol-

solution at the first deposition, and 2 seconds at the second and third ones. After each coating deposition, the membranes were dried at 80 °C for 24 h.

5.2.2.2 Membrane Characterization

Alumina membranes before and after modification were characterized in terms of morphology, chemical constituents, contact angle and permeability.

a) Scanning electron microscopy with energy dispersive spectroscopy (SEM-EDS)

SEM-EDS analysis were performed according to Panngom et al. (2014) with some modifications introduced by (Oliveira et al., 2020). In short, small pieces of membrane were fixed using the Karnovsky's Fixative (Polysciences Inc., Germany) reagent according to the proposed manufacturer procedure (glutaraldehyde at 2.5 % (v/v), paraformaldehyde at 2% (v/v) and phosphate buffered saline (PBS) solution at 0.1 M) after being washed with PBS for 5 min. Membrane pieces were then washed with PBS again three times for 10 min and placed in osmium tetroxide (1.0 % v/v) for 2 hours in the dark. Dehydration steps were performed using increased concentrations of ethanol solutions (30, 50, 70, 80, 90 and 95 % v/v) for 10 min each and 100 % of ethanol for 15 min twice. The membrane pieces were then freeze dried for 30 min. Since samples in this case were small pieces of membrane, instead of centrifugations, a gentle stirring was used after adding the different solutions described in the protocol. After freeze drying for 30 min, the membranes were covered with a thin film of Au/Pd on a Quorum Technologies sputter coater, model Q150T ES. Observations were performed using a FEG-SEM JEOL JSM7001F, with a 15 kV acceleration voltage and a PC-SEM by JEOL used for image acquisition.

The energy dispersive spectroscopy was performed using a detector of light elements (Oxford, model INCA 250) to identify semi-quantitatively the elements present in the membrane using a database.

The SEM images obtained for both the unmodified and modified membranes were analyzed using the ImageJ software to compare the morphology of the membranes (Masselin et al., 2001). The images were spatially scaled, their total membrane surface area was calculated and the images were binarized. The morphology analysis was performed taking into account the area measurements obtained, pore density (number of pores divided by membrane area), porosity (area of pores divided by membrane area), circularity (Equation 4), and Feret's diameter (the longest distance between any two points along the selection boundary).

$$circularity = 4\pi \left(\frac{Area}{Perimeter^2}\right) \quad (4)$$

b) Fourier transform infrared (FTIR) spectroscopy analysis

FTIR spectroscopy with attenuated total reflectance (ATR) was performed to compare the material and microbial compositions of the unmodified and modified membranes before and after treatment. The equipment used was a Bruker Spectrometer IFS 66/S instrument (USA) equipped with a H-ATR and a ZnSe crystal. Spectra were obtained in the range of 4000 to 550 cm^{-1} during 40 scans with 4 cm^{-1} resolution and normalized.

c) Contact Angle

To further characterize the membranes before and after modification the contact angle was measured using a KSV CAM 100 equipment which is a fully computer controlled instrument based on automatic video capture and image analysis to measure the contact angles. A drop was captured along 2000 ms time obtaining consecutive frames of 0.1 ms each that were analyzed by the software retrieving the

left contact angle, the right contact angle and the mean of these values. A total of four measurements were performed.

5.2.3 Photocatalytic membrane reactor

The laboratory scale photocatalytic membrane reactor assembled is composed by a feed vessel, a magnetic drive gear pump (model MK317, Fluid-o-Tech, USA), and a photocatalytic membrane reactor (Figure 5.1). The reactor, comprising a stainless steel cross-flow filtration unit and a low pressure UV lamp, was designed and developed by the authors of this study (Figure 5.1). The filtration unit includes a synthetic quartz polished window (length=182 mm; width=55 mm; thickness=11 mm; round corners with a radius of 14 mm; Robson Scientific, UK) that supports a pressure of 15 bar and transmits radiation in the range of 180-2000 nm. It therefore enables the irradiation of the membrane by the UV lamp (OSRAM HNS G5 6W UVC Germicidal PURITEC lamp, G6T5/OF RG3, Germany) that is placed above the filtration unit and emits primarily monochromatic radiation at 254 nm. The membrane area irradiated by the lamp is 36 cm^2 and the distance between the lamp and the membrane surface was set at 6 cm for this study (the minimum distance allowed in the set-up). Two manometers were placed upstream and downstream the membrane unit for pressure measurements and the pressure was adjusted on the retentate side using a needle valve. Gentle stirring was provided to the feed solution during the experiments to ensure the homogeneity of the solution without creating bubbles that could disturb the fluid dynamics inside the filtration unit. The tubing of the system and the sealing parts of the filtration unit were made of polyvinylidene difluoride (PVDF) to minimize the adsorption of the matrix components.

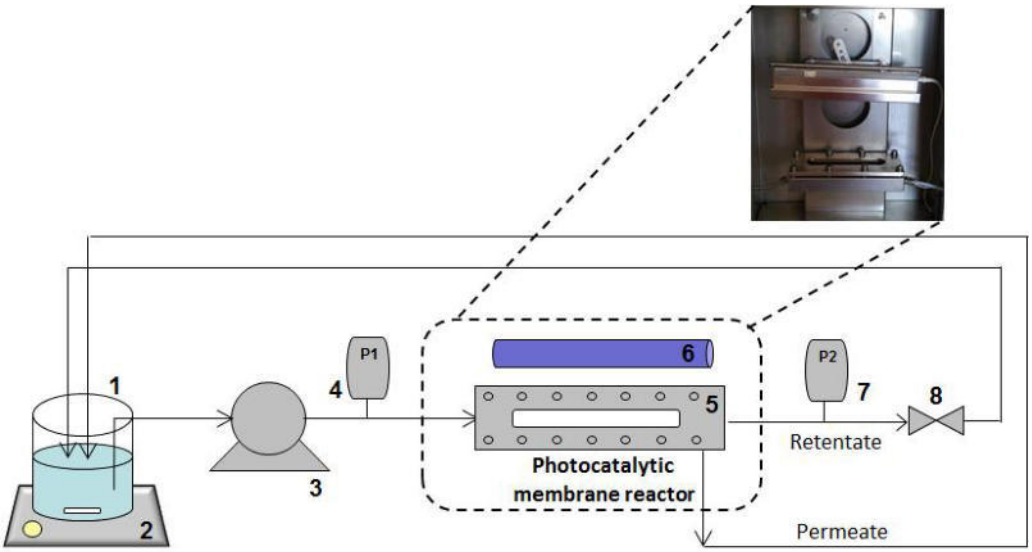

Figure 5.1 – Photocatalytic membrane reactor. 1-feed vessel; 2-magnetic stirrer; 3- magnetic drive gear pump; 4-inlet pressure gauge; 5-cross-flow filtration unit; 6-LP/UV lamp; 7-outlet pressure gauge; 8-needle valve.

5.2.4 Experimental Procedure

One day before the experiments, the photocatalytic membrane reactor was cleaned with a 70 % (v/v) ethanol solution, followed by a rinsing with plenty of distilled water without recirculation to remove traces of ethanol. To verify the baseline contamination of the combined reactor, sterile distilled water was recirculated without membrane for 10 to 20 minutes before the experiments and 10 mL samples were taken from the feed, retentate and permeate streams and analyzed in terms of fungi contamination using the plate count methods described in section 5.2.5.1. All the streams were found to be free from contamination.

The feed vessel was filled with 750 mL of each study matrix tested (saline solution or filtered surface water) containing the fungi with a final concentration of $1x10^8$

spores/mL, which were sampled and allowed to recirculate in the experimental set-up for three hours. All experiments were carried out with total recirculation of both the permeate and the retentate. 10 mL samples of the feed, retentate and permeate were taken at different experimental times (10, 60, 120 and 180 min) to assess the effect of the treatments on the fungal spores using the methods detailed in section 5.2.5. Four experiments were performed to test the efficiency of the filtration process as well as the filtration coupled with LP/UV radiation, using an unmodified membrane and a modified membrane.

Apparent rejection, adsorption and membrane permeability were determined as described below.

The apparent rejection (R_{app}) of fungi was determined using equation (1)

$$R_{app}(\%) = 100 \times \left(1 - \frac{C_p}{C_f}\right) \qquad (1)$$

where C_p and C_f are the concentrations of fungi in the permeate and feed, respectively.

The percentage of rejection due to adsorption and retention of the fungi spores on the membrane (A) was determined for filtration experiments using equation (2)

$$A(\%) = 100 \times \left(1 - \frac{C_{initial,f}\, V_{initial,f} - C_{final,f}\, V_{final,f}}{C_{initial,f} V_{initial,f}}\right) \qquad (2)$$

where $C_{initial,f}$ and $C_{final,f}$ are the concentrations of fungi in the feed at the beginning and at the end of the filtration experiment, respectively, whereas $V_{initial,f}$ and $V_{final,f}$ are the volumes of feed at the beginning and at the end of the filtration experiment, respectively. For experiments carried out by filtration coupled with LP/UV radiation, equation 2 provides the sum of adsorption/retention and inactivation. Even though the effect of inactivation of the fungi retained is not possible to determine, most of the retained spores are expected to be inactive.

Membrane permeability (L_p) was determined as follows (equation 3 and 3.1)

$$Lp = \frac{V_p}{\Delta P \times A \times t} \qquad (3)$$

where V_p is the volume of permeate measured using a sterile graduated cylinder, A is the filtration membrane area, t is the time, and ΔP is the transmembrane pressure determined as

$$\Delta P = \frac{P_f + P_r}{2} - P_p \qquad (3.1)$$

where P_f, P_r, and P_p are the pressures on the feed, retentate, and permeate sides, respectively.

5.2.5 Effect of proposed treatment on *A. fumigatus*

5.2.5.1 Fungi removal and inactivation

From the 10 mL samples collected (see section 5.2.4), 1 mL was used to quantify the concentration of *A. fumigatus* at the beginning and after each experimental time (10, 60, 120 and 180 min). To do that, serial dilutions were performed and placed in malt extract agar through the pour plate technique. After 2 to 3 days of incubation at 27 °C, colony forming units (CFU)/mL were quantified. The rest of the volume was kept at -20 °C for further analyzes.

5.2.5.2 Scanning Electron Microscopy with Energy Dispersive Spectroscopy (SEM-EDS)

SEM-EDS was performed to address differences in fungal spores' morphology after performing the experiments. To do that unmodified and modified ceramic membranes after the filtration and filtration coupled with LP/UV radiation were broken into small pieces and subjected to the sample preparation already described in section 5.2.2.2. a).

5.2.5.3 Flow Cytometry Analysis

A CyFlow® Cube 6 equipment (Sysmex PArtec GmbH, Germany) equipped with a solid state laser at 50 mW (488 nm excitation) was used to analyze the collected samples (feed, retentate and permeate). Using the Viability Yeast Control kit (Sysmex Partec GmbH, Germany) that combines fluorescein diacetate (FDA) with propidium iodide (PI) it is possible to determine enzymatic activity and membrane permeability of the fungal spores since FDA is transformed into a detectable fluorescent product after enzyme activity and PI bounds to the DNA of membrane damaged cells. Therefore, this kit enables the separation of the spores into 4 quadrants (metabolically active - FDA positive; dead - PI positive; quiescent - FDA and PI negative; and damaged - FDA and PI positive). Gates to determine these four quadrants were determined in a previous study (Oliveira et al., 2020). The obtained cytograms were analyzed using a CyView™ for Cube 6 software (Partec GmbH, Germany).

5.3 Results and Discussion

In this study, unmodified and modified ceramic membranes were used in a photocatalytic membrane reactor to treat filtered surface water inoculated with *Aspergillus fumigatus*.

5.3.1 Membrane Characterization

To characterize the ceramic membranes, SEM-EDS analysis of the unmodified and modified membrane was performed. Results presented in figure 5.2 show that, as expected, the unmodified membrane contains aluminum and oxygen because the support material is made of Al_2O_3 (figure 5.2 a). The modified membrane contains, additionally, silicon and titanium, due to the modification (figure 5.2 b). Gold (Au) and palladium (Pd) were detected in all samples because these are the elements used to coat the samples for SEM-EDS analysis. Element mapping (supplementary figure 1) shows a uniform distribution of the chemical elements in the membranes.

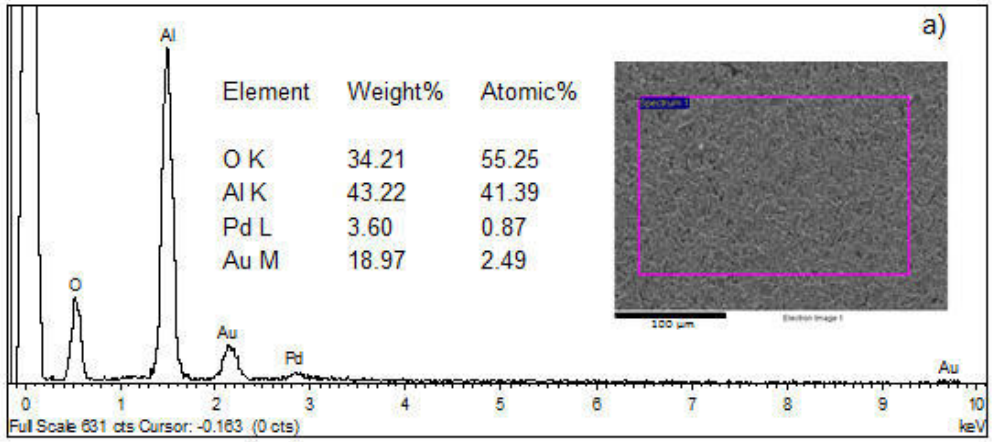

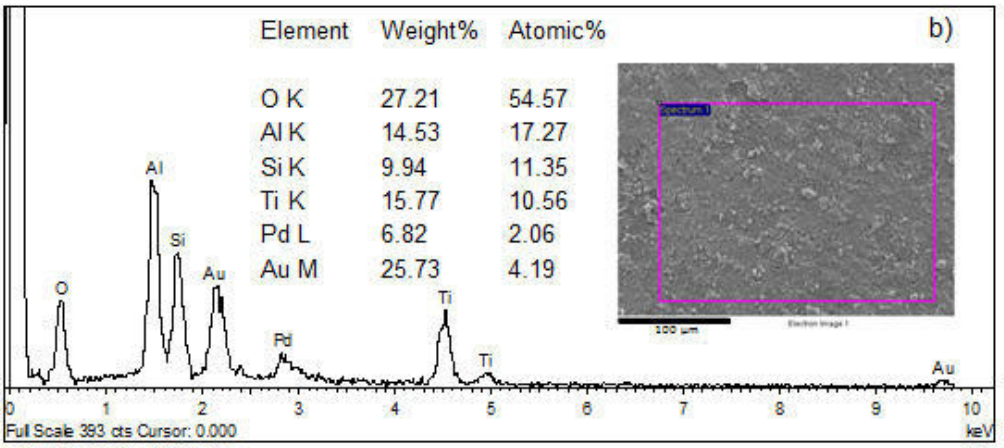

Figure 5.2 – EDS spectra, element contents and SEM image of a) unmodified membrane whose material is Al_2O_3 and b) modified membrane with TiO_2/SiO_2. The Pd and Au peaks are due to coating before the analysis.

The analysis of the SEM images using the ImageJ software (table 5.1) showed that the mean pore area and the Feret's diameter (average of measurements of the longest distance between two points along the selection boundary) of the modified membrane was reduced with the modification from 1.049 μm to 0.002 μm. Therefore, the modification of the membrane resulted in the transformation of a microfiltration support into a nanofiltration membrane. On the other hand, the pore density of the modified membrane increased from 0.111 μm^{-2} to 5534.9 μm^{-2}. Moreover, compared to the unmodified membrane, the modified membrane has higher pore circularity with an average value of 0.919 which is closer to 1 (that corresponds to a perfect circle). This membrane has a higher homogeneity that can be seen by the lower error measurements reported in table 5.1.

The average contact angle measurements were very similar between the two membranes, 16.11 ± 1.50° and 18.08 ± 1.83° for the unmodified and modified membrane, respectively, which means that the modification did not change the

hydrophilicity of the membrane. The decrease in the membrane hydraulic permeability determined from 0.18 ± 0.01 $m^3/(h.m^2.bar)$ for the unmodified membrane to 0.109 ± 0.017 $m^3/(h.m^2.bar)$ for the modified membrane may be explained due to the smaller pore size of the modified membrane.

Table 5.1 - Image J morphology analysis of the unmodified and modified membrane.

Parameters Analyzed	Unmodified	Modified
Pore density (μm^{-2})	0.111	5534.9
Mean Pore Area (μm^2)	0.589± 1.371	0.00001± 0.00021
Minimum Pore Area (μm^2)	0.014	0.000001
Maximum Pore Area (μm^2)	21.741	0.01600
Porosity (%)	6.55	5.28
Average Circularity	0.732 ± 0.280	0.919 ± 0.190
Average Feret's diameter (µm)	1.049 ± 1.318	0.002 ± 0.007
Maximum Feret's diameter (µm)	15.622	0.314
Minimum Feret's diameter (µm)	0.168	0.001

5.3.2 Surface water characterization

The collected surface water (section 5.2.1.) was used in the experiments after filtration using a 0.22 µm membrane filter, to simulate the treatment processes that could be employed by a drinking water treatment facility prior to the membrane filtration process. The characterization of the surface water before and after filtration in terms of temperature, pH, total organic carbon (TOC), turbidity, chemical oxygen demand (COD), total solids, and total suspended solids was performed in a previous study (Oliveira et al, 2020). Briefly, the values were 20 °C for both waters, pH of 7.32 and 7.64, TOC of 3.97 and 2.35 mg/L C, turbidity of 14.60 and 0.22 NTU, COD of 1670

and 1172 mg/L O_2, total solids of 39.62 and 38.94 g/L and total suspended solids of 70.50 and 22.60 mg/L, for surface water before and after filtration, respectively.

The filtered surface water used to conduct the experiments was also characterized before and after the filtration and filtration coupled with LP/UV radiation experiments (detailed in section 5.2.4) by 2D fluorescence and results are presented in figure 5.3 as fluorescence excitation-emission matrices (EEMs). Figure 5.3 a) shows that no fluorescence peaks were detected in the beginning of the experiment. Then, $1x10^8$ spores/mL of *A. fumigatus* were inoculated into the matrix which reveals high fluorescence peaks normally associated with: peak A - fulvic-like ($\lambda_{ex/em}$ = 237-260/400-500 nm), peak C_1 - fulvic-like ($\lambda_{ex/em}$ = 300-325/420-435 nm), peak C_2 – humic-like ($\lambda_{ex/em}$ = 340-355/460-475 nm), peak T_1 – tryptophan-like ($\lambda_{ex/em}$ = 275/340 nm) and peak T_2 - tryptophan-like ($\lambda_{ex/em}$ = 225-237/340-381 nm) (Henderson et al., 2009). After 180 min of filtration or filtration coupled with LP/UV radiation using the unmodified or the modified membrane the EEMs were all very similar (supplementary figure 2). An example of feed (figure 5.3 c) and permeate (figure 5.3 d) after 180 min of filtration coupled with LP/UV radiation using the modified membrane is shown and only peaks T1 and T2 remained which are normally associated with tryptophan-like fluorescence.

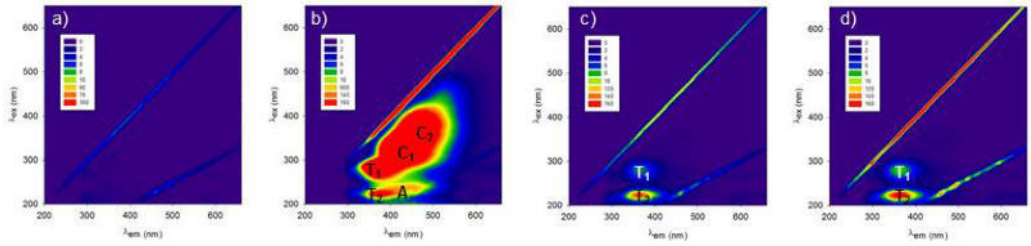

Figure 5.3 – Fluorescence excitation-emission matrices (EEMs) for a) filtered surface water, b) initial feed inoculated with *A. fumigatus*, c) feed after 180 min of filtration coupled with LP/UV radiation using the modified membrane and d) permeate after 180 min of filtration coupled with LP/UV radiation using the modified membrane, where A and C_1 are fulvic like, C_2 are humic-like, T_1 and T_2 are tryptophan-like fluorescence.

The T peak when present is associated with microbial activity since tryptophan normally binds to proteins, peptides or humic structures (Hudson et al., 2008). Strong correlations have been described between tryptophan-like fluorescence and biochemical oxygen demand (Baker and Inverarity, 2004).

5.3.3 Fungi removal and inactivation

To evaluate the treatment efficiency, an unmodified and a modified membrane were used to perform filtration and filtration coupled with LP/UV radiation using *Aspergillus fumigatus*. These experiments were conducted using saline solution (supplementary figure 3) and filtered surface water (figure 5.4) showing neither enhanced nor diminished effects on the removal and inactivation of the spores using the two matrices. Figure 5.4 shows that there are no meaningful apparent rejection differences between the different experiments (unmodified vs modified membrane and filtration vs filtration coupled with LP/UV radiation) meaning that the produced permeate is similar using the two treatment processes. On the other hand, there are

differences between the experiments regarding the adsorption and removal of the spores. Comparing the unmodified membrane (figure 5.4 a) with the modified membrane (figure 5.4 b) in the filtration experiment it can be seen that the rejection is higher in the unmodified membrane (up to 73 %) than when using the modified membrane (up to 66 %). This can be explained due to the Feret's measurements presented in table 5.1. For the unmodified membrane the average Feret's diameter is 1.049 µm ± 1.318 µm being the maximum measured of 15.622 µm so *A. fumigatus* spores' (2.5-3 µm) are being trapped inside the membrane. Using the modified membrane the average Feret's diameter is smaller (0.002 ± 0.007 µm) so the spores may be retained at the surface of the membrane. Coupling LP/UV radiation with filtration (A+inactivation bar from figure 5.4) it can be seen enhanced adsorption+inactivation percentages compared with the filtration experiment because the LP/UV radiation is able to inactivate the circulating spores in the reactor and may also inactivate the adsorbed and retained spores (these spores' numbers cannot be quantified). The apparent rejection results observed in the combined treatment can be explained due to the effect of adsorption and inactivation.

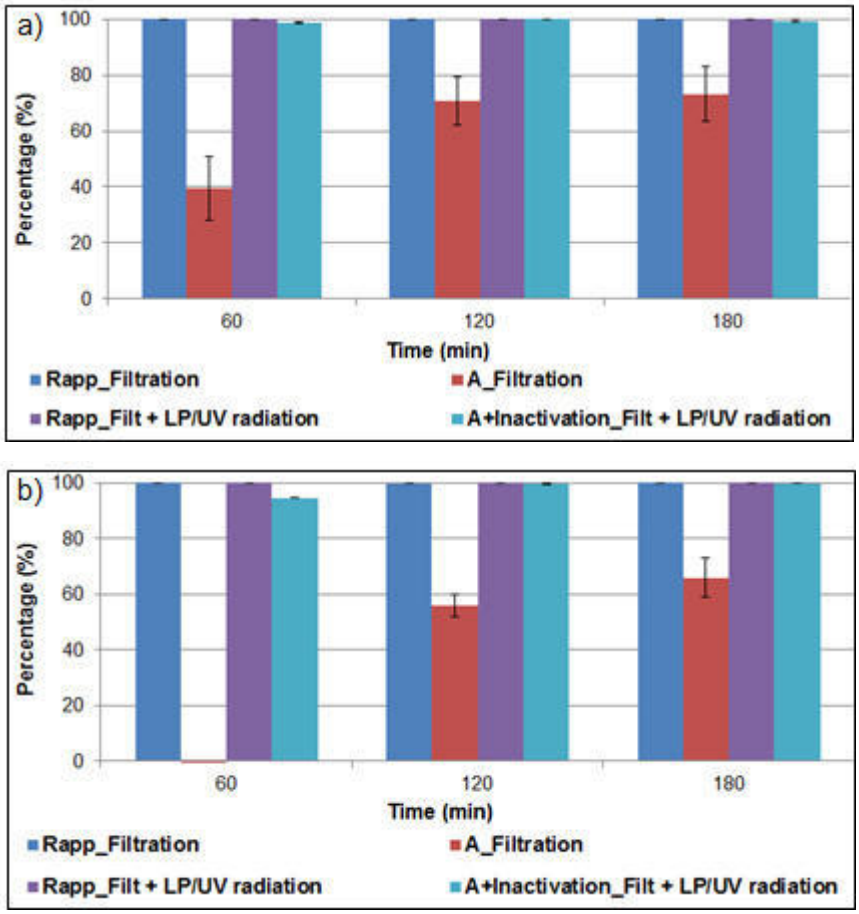

Figure 5.4 – Apparent rejection (R_{app}), adsorption (A) and adsorption+inactivation (A+inactivation) percentages of *Aspergillus fumigatus* ($1x10^8$ spores/mL) after filtration and filtration coupled with LP/UV radiation of filtered surface water along the experimental time using a) unmodified; and b) modified membrane. Error bars represent duplicate results obtained in up to 7 dilutions tested.

In terms of treatment, the modified membrane (with a lower pore size) has the advantage of retaining the spores at the surface instead of trapping the spores inside as observed for the unmodified membrane. Thus, in a long term operation, the unmodified membrane is expected to be more prone to fouling. Cleaning protocols and other flux maintenance strategies (such as backwash and backpulse) are expected

to release the spores from the surface of the modified membrane more easily. Moreover, the spores trapped inside the unmodified membrane will likely be more protected from inactivation and therefore the overall treatment may be less effective.

One major drawback of filtration processes is the production of a retentate more concentrated than the initial water to be treated. Coupling UV photolysis with membrane filtration using an unmodified or a modified membrane could allow the treatment of the retentate through the inactivation of microorganisms. The retentate treatment percentage (figure 5.5) was calculated considering the ratio between the concentration of fungi in the retentate obtained along the experimental times and the initial concentration of fungi in the feed. Figure 5.5 shows that similar retentate treatment results were obtained with the unmodified and modified membrane. Direct photolysis is therefore expected to be the main route to achieve inactivation. Similar results were obtained using saline solution (supplementary figure 4).

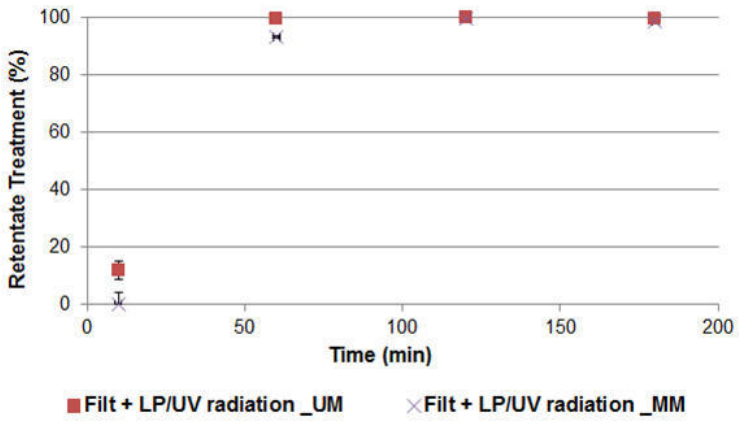

Figure 5.5 – Retentate treatment percentages of *Aspergillus fumigatus* (1x10^8 spores/mL) inoculated into filtered surface water after filtration coupled with LP/UV radiation using an unmodified (UM) and a modified membrane (MM) along the experimental time. Error bars represent duplicate results obtained in up to 7 dilutions tested.

5.3.3.1 Phenotypic effect on fungal spores

To address the effect of the treatment performed on the *Aspergillus fumigatus* spores, SEM with EDS analysis were performed for both unmodified and modified membrane after 180 min of filtration and filtration coupled with LP/UV radiation. When the inactivation results obtained in saline solution and filtered surface water were compared above (section 5.3.3), the latter did not scavenge the light and protect the fungi from inactivation. The SEM images obtained agree with these results since similar effects on the spores' morphology were observed in the experiments conducted in saline solution (supplementary figure 5) and filtered surface water (figure 5.6). Figure 5.6 shows the SEM images of the *Aspergillus fumigatus* spores after 180 min of each treatment using filtered surface water. The results support the discussion on membranes' characterization (section 5.3.1), namely the Feret's diameter, and the discussion on adsorption and inactivation percentages obtained (section 5.3.3). The top surface images show that the modified membrane presents a much tighter pore structure than the unmodified membrane and the cross-section images also show that the spores were trapped in the unmodified membrane driven by the applied pressure while, in the modified membrane, the spores remained at the surface due to size constraints, forming a dense layer in some zones of the membrane.

Concerning the spores morphology, it can be observed that the spores are globose rough-walled to echinulate. In the filtration experiments, for both membranes, the spores maintain their morphology while when LP/UV radiation is coupled some deformation occurs. This might have resulted from the direct action of UV on the fungal spores and from the coupled action of UV and the hydroxyl radicals produced during TiO_2 photocatalysis on the surface of the modified membrane (Goei and Lim, 2014; Liu et al., 2012; Ma et al., 2009).

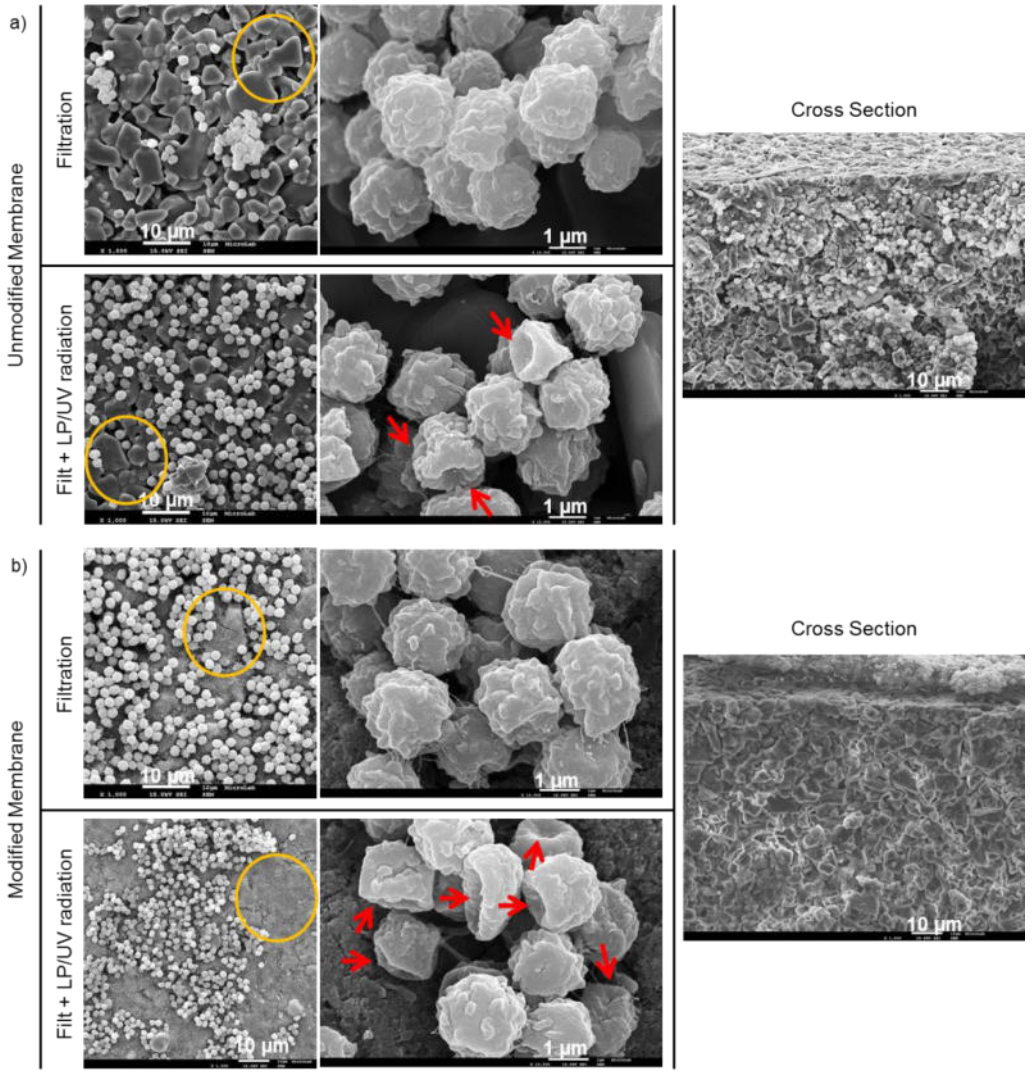

Figure 5.6 – SEM images of *Aspergillus fumigatus*' spores at the surface of the a) unmodified and b) modified membranes after 180 minutes of filtration and filtration coupled with LP/UV radiation (Filt + LP/UV radiation) using filtered surface water. Cross sections are also shown for both membranes. Images of the top surfaces of the membranes have 1 000 x, 3 500 x and 13 000 x of total magnification while cross sections have a total magnification of 1 000 x. Yellow circles illustrate the different morphology of the two membranes used and the red arrows indicate the spores' deformation.

Regarding the EDS analysis, for both membranes after filtration and after filtration coupled with LP/UV radiation, the elements found were aluminum for the unmodified membrane (supplementary figure 5.6 a) and titanium and silicon for the modified membrane (supplementary figure 5.6 b), apart from the elements detected due to the coating process (Au and Pd). However, when analyzing only an area that contained fungi spores, different chemical elements appear like sodium (Na) and yttrium (Y). Figure 5.7 shows an example of the EDS results obtained when analyzing only an area that contained fungi spores for an unmodified membrane after 180 min of filtration coupled with LP/UV radiation.

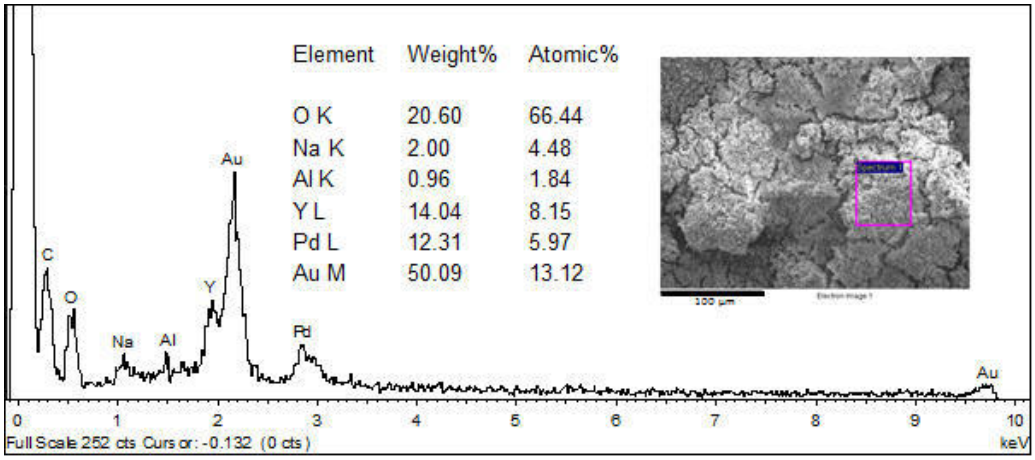

Figure 5.7 - EDS spectra, element contents and SEM image of an unmodified membrane whose material is Al_2O_3 after 180 minutes of filtration coupled with LP/UV radiation of *A. fumigatus*. The Pd and Au peaks are due to coating before the analysis. The Na and Y peaks are due to the presence of fungi.

The presence of sodium may be due the sample preparation to perform the SEM-EDS analysis since it used phosphate buffer saline solution. The presence of yttrium in the samples may be due to the surface water since this element has already been

reported in surface sediments (Brito et al., 2018) and joined with rare earth elements in stream waters and sediments (Leybourne and Johannesson, 2008). The former reports the concentration in mg/kg and the latter as a ratio of Y/Ho_{NASC}. The treated surface water used was therefore characterized by inductively coupled plasma (ICP) and the yttrium concentration was determined to be 37.45 µg/L.

FTIR spectroscopy was also performed to compare the material and microbial compositions of the unmodified and modified membranes before and after the experiments. The FTIR spectra obtained showed that the adsorption of *A. fumigatus* to the membrane surface was not homogenous for both membranes since peaks consistent to the *A. fumigatus* spectrum (supplementary figure 7a) were only obtained when analyzing areas that contained visible fungal pellet at the membrane surface (labeled as b in supplementary figures 7b and c) in contrast with areas that had no visible fungal pellet (labeled as w supplementary figure 7b and 7c). The presence of Si-O bands (1000-1110 cm^{-1}) was detected in the modified membrane when compared to the unmodified membrane whereas in the fungi powder (supplementary figure 7a) and membrane areas where fungi were visible, the presence of chemical groups from lipids and proteins (3200–2800 cm^{-1}), proteins amide I (1695-1625 cm^{-1}), proteins amide II (1560-1525 cm^{-1}), nucleic acids (1300-1200 cm^{-1}) and ribose, glycogen and nucleic acids (1200-900 cm^{-1}) were detected. These peaks are consistent with characteristic infrared absorption frequencies already reported for filamentous fungi given their biomolecular attribution (Lecellier et al., 2014).

5.3.3.2 Effect on membrane permeability and enzymatic activity

To address the effect of the proposed treatment to membrane permeability and enzymatic activity of the *A. fumigatus* spores, flow cytometry analysis were performed to the feed samples after 10 min and 180 min of filtration (filtration 10min and 180min) and filtration coupled with LP/UV radiation (filt+LP/UV radiation 10min and 180min). Only feed was analyzed since permeate at the end of the experiment had very few fungal spores and since the experiment was performed in total recirculation then the final retentate would be similar to the final feed. The results obtained presented in figure 5.8 were corrected by subtracting the baseline background obtained by the different solutions used (PBS solution and filtered surface water matrix used in the experiments).

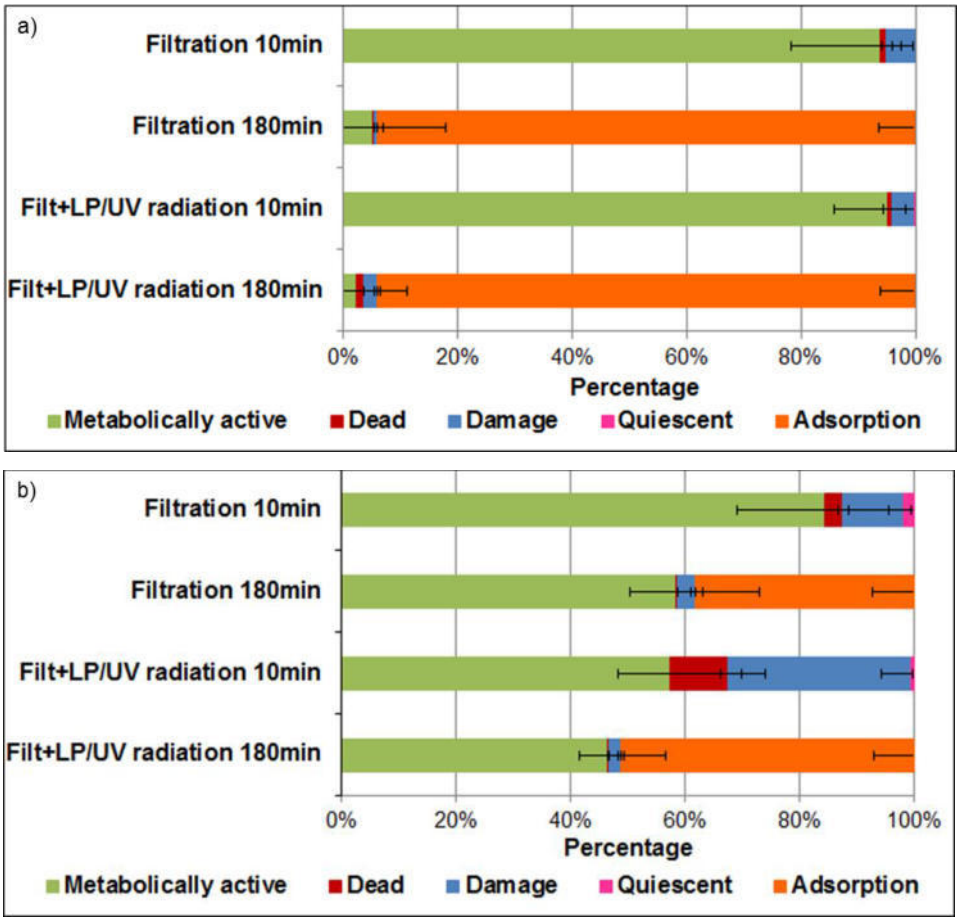

Figure 5.8 - Flow Cytometry results represented as percentage bar charts of *Aspergillus fumigatus* spores from the feed sample after 10 min and 180 min of filtration (filtration 10min and 180min) and filtration coupled with LP/UV radiation (filt+LP/UV radiation 10min and 180min) using an a) unmodified and b) a modified membrane. The Yeast Control – Viability kit (Sysmex Partec GmbH, Germany) used enable to present the metabolically active, dead, quiescent and damage spores and through calculations also the adsorption percentage.

Figure 5.8 shows that when the unmodified membrane is used the samples taken after 10 min of filtration and filtration coupled with LP/UV radiation have high percentage of metabolically active spores and few damaged (metabolically activity spores but have a permeabilized membrane) spores. The same result is observed for the modified membrane for the filtration experiment but coupling it with LP/UV radiation the damaged and dead spores' percentage increased. This means that at initial times (10 min of experiment) there is already an enhanced activity of the OH·radicals produced by the photocatalysis of titanium dioxide on the disruption of spores' membrane.

Bigger differences are observed between the two membranes after 180 min of experimental time since the unmodified membrane has a much higher percentage of adsorption when compared to the modified membrane. This can be explained by the Feret's diameter that, being bigger in the unmodified membrane it adsorbs and retains more spores than the modified membrane (already discussed in sections 5.3.1 and 5.3.3). In the modified membrane there are more metabolically active spores because the fungal spores remain recirculating in the system enabling its quantification and detection by flow cytometry, contrarily in the unmodified membrane that the fungal spores were being trapped within the membrane so less spores were recirculating in the system and consequently less spores were quantified and detected by flow cytometry. Among the two experiments, filtration and filtration coupled with LP/UV radiation, after 180 min, it should be noted that the adsorption percentages obtained when LP/UV radiation is used contains also spores that are metabolically active, damage, dead and quiescent, but that it is not possible to determine the percentages.

Even though the adsorbed spores were not analyzed in terms of membrane permeability and enzymatic activity, it is expected that the spores trapped inside the unmodified membrane will likely be more protected from inactivation and therefore the overall treatment may be less effective when compared to the modified

membrane that retains the spores at the surface. Correlations between the flow cytometry and the plate colony counts obtained for the different experiments (unmodified vs modified membrane and filtration vs filtration coupled with LP/UV radiation) show a strong positive correlation for the unmodified membrane (0.94) and filtration (0.80) experiments and weak for the modified membrane (0.09) and filtration coupled with LP/UV radiation (0.50) (supplementary figure 8). This might be due to the fact that UV-C radiation affects the DNA although the cell wall may remain intact which leads to different results when using flow cytometry and plate count methodology (Nevel et al., 2017).

5.4 Conclusions

In this study it can be concluded that:

- The two membranes tested (unmodified vs modified membrane) obtained high and similar apparent rejection results due to the size of *Aspergillus fumigatus* spores resulting in a permeate of high quality;
- The different pore size of the two membranes led to differences in the retention of the spores; the modified membrane (with a lower pore size) retained the spores at the surface whereas the unmodified membrane trapped the spores within its cross section;
- The combination of filtration with LP/UV radiation effectively removed and inactivated fungi from the water matrix producing not only a treated permeate but also a treated retentate;
- Direct photolysis and photocatalysis were able to affect morphologically the fungal spores;

- Flow cytometry coupled with fluorescent-based viability stains showed that membrane permeability and the enzymatic activity of the spores were more affected by photocatalysis.

Acknowledgements

Financial support from Fundação para a Ciência e a Tecnologia through the fellowship SFRH/BD/111150/2015 and the project PTDC/EAM-AMB/30989/2017 are gratefully acknowledged. iNOVA4Health - UID/Multi/04462/2013, a program financially supported by Fundação para a Ciência e Tecnologia/Ministério da Educação e Ciência, through national funds and co-funded by FEDER under the PT2020 Partnership Agreement is acknowledged. The authors thank the company SYSMEX that has kindly provided the flow cytometer equipment used in these experiments.

References

Babič, M.N., Gunde-Cimerman, N., Vargha, M., Tischner, Z., Magyar, D., Veríssimo, C., Sabino, R., Viegas, C., Meyer, W. and Brandão, J. 2017. Fungal Contaminants in Drinking Water Regulation? A Tale of Ecology, Exposure, Purification and Clinical Relevance. International Journal of Environmental Research and Public Health 14(6), 1-44.

Baker, A. and Inverarity, R. 2004. Protein-like fluorescence intensity as a possible tool for determining river water quality. Hydrological Processes 18(15), 2927-2945.

Braga, G.U.L., Rangel, D.E.N., Fernandes, É.K.K., Flint, S.D. and Roberts, D.W. 2015. Molecular and physiological effects of environmental UV radiation on fungal conidia. Current Genetics 61(3), 405-425.

Brito, P., Prego, R., Mil-Homens, M., Caçador, I. and Caetano, M. 2018. Sources and dintribution of yttrium and rare earth elements in surface sediments from Tagus estuary, Portugal. Science of the Total Environment 621, 317-325.

Ciston, S., Lueptow, R.M. and Gray, K.A. 2009. Controlling biofilm growth using reactive ceramic ultrafiltration membranes. Journal of Membrane Science 342, 263-268.

Esfahani, M.R., Aktij, S.A., Dabaghian, Z., Firouzjaei, M.D., Rahimpour, A., Eke, J., Escobar, I.C., Abolhassani, M., Greenlee, L.F., Esfahani, A.R., Sadmani, A. and Koutahzadeh, N. 2019. Nanocomposite membranes for water separation and purification: fabrication, modification, and applications. Separation and Purification Technology 213, 465-499.

Fateh, R., Dillert, R. and Bahnemann, D. 2013. Preparation and characterization of transparent hydrophilic photocatalytic TiO_2/SiO_2 thin films on polycarbonate. Langmuir 29(11), 3730-3739.

Foster, H.A., Ditta, I.B., Varghese, S. and Steele, A. 2011. Photocatalytic disinfection using titanium dioxide: spectrum and mechanism of antimicrobial activity. Applied Microbiology and Biotechnology 90(6), 1847-1868.

Goei, R. and Lim, T.-T. 2014. Ag-decorated TiO_2 photocatalytic membrane with hierarchical architecture: photocatalytic and anti-bacterial activities. Water Research 59, 207-218.

Hageskal, G., Lima, N. and Skaar, I. 2009. The study of fungi in drinking water. Mycological Research (113), 165-172.

Henderson, R.K., Baker, A., Murphy, K.R., Hambly, A., Stuetz, R.M. and Khan, S.J. 2009. Fluorescence as a potential monitoring tool for recycled water systems: a review. Water Research 43, 863-881.

Hudson, N., Baker, A., Ward, D., Reynolds, D.M., Brunsdon, C., Carliell-Marquet, C. and Browning, S. 2008. Can fluorescence spectrometry be used as a surrogate for the Biochemical Oxygen Demand (BOD)

test in water quality assessment? An example from South West England. Science of the Total Environment 391, 149-158.

Huertas, R.M., Fraga, M.C., Crespo, J.G. and Pereira, V.J. 2017. Sol-gel membrane modification for enhanced photocatalytic activity. Separation and Purification Technology 180, 69-81.

Huertas, R.M., Fraga, M.C., Crespo, J.G. and Pereira, V.J. 2019. Solvent free process for the development of photocatalytic membranes. Molecules 24(24), 4481.

Jørgensen, T.R., Park, J., Arentshorst, M., Welzen, A.M.v., Lamers, G., vanKuyk, P.A., Damveld, R.A., Hondel, C.A.M.v.d., Nielsen, K.F., Frisvad, J.C. and Ram, A.F.J. 2011. The molecular and genetic basis of conidial pigmentation in *Aspergillus niger*. Fungal Genetics and Biology 48(5), 544-553.

Lecellier, A., Mounier, J., Gaydou, V., Castrec, L., Barbier, G., Ablain, W., Manfait, M., Toubas, D. and Sockalingum, G.D. 2014. Differentiation and identification of filamentous fungi by high-throuput FTIR spectroscopic analysis of mycelia. International Journal of Food Microiology 168-169(3), 32-41.

Leybourne, M. and Johannesson, K.H. 2008. Rare earth elements (REE) and yttrium in stream waters, stream sediments, and Fe-Mn oxyhydroxides: fractionation, speciation, and controls over REE + Y patterns in the surface environment. Geochimica et Cosmochimica Acta 72, 5962-5983.

Li, Q., Mahendra, S., Lyon, D.Y., Brunet, L., Liga, M.V., Li, D. and Alvarez, P.J.J. 2008. Antimicrobial nanomaterials for water disinfection and microbial control: potential applications and implications. Water Research 42, 4591-4602.

Liu, L., Liu, Z., Bai, H. and Sun, D.D. 2012. Concurrent filtration and solar photocatalytic disinfection/degradation using high-performance Ag/TiO2 nanofiber membrane. Water Research 46(4), 1101-1112.

Ma, N., Fan, X., Quan, X. and Zhang, Y. 2009. Ag-TiO_2/HAP/Al_2O_3 bioceramic composite membrane: fabrication, characterization and bactericidal activity. Journal of Membrane Science 336(1-2), 109-117.

Madaeni, S.S. 1999. The application of membrane technology for water disinfection. Water Research 33(2), 301-308.

Masselin, I., Durand-Bourlier, L., Laine, J.-M., Sizaret, P.Y., Chasseray, X. and Lemordant, D. 2001. Membrane characterization using microscope image analysis. Journal of Membrane Science 186(1), 85-96.

Meng, Y., Huang, X., Yang, Q., Qian, Y., Kubota, N. and Fukunaga, S. 2005. Treatment of polluted river water with photocatalytic slurry reactor using low-pressure mercury lamps coupled with a membrane. Desalination 181, 121-133.

Nevel, S.V., Koetzsch, S., Proctor, C.R., Besmer, M.D., Prest, E.I., Vrouwenvelder, J.S., Knezev, A., Boon, N. and Hammes, F. 2017. Flow cytometric bacterial cell counts challenge conventional

heterotrophic plate counts for routine microbiological drinking water monitoring. Water Research 113, 191-206.

Oliveira, B.R., Barreto Crespo, M.T. and Pereira, V.J. 2020. Small but powerful: light-emitting diodes for inactivation of *Aspergillus* species in real water matrices. Water Research, 168, 115108.

Oliveira, B.R., Barreto Crespo, M.T., San Romão, M.V., Benoliel, M.J., Samson, R.A. and Pereira, V.J. 2013. New insights concerning the occurrence of fungi in water sources and their potential pathogenicity. Water Research 47(16), 6338-6347.

Ollis, D.F., Pelizzetti, E. and Serpone, N. 1991. Photocatalyzed destruction of water contaminants. Environmental Science and Technology 25(9), 1522-1529.

Panngom, K., Sang Hark, L., Park, D.H., Sim, G.B., Kim, Y.H., Uhm, H.S., Park, G., Choi, E.H. 2014. Non-Thermal Plasma Treatment Diminishes Fungal Viability and Up-Regulates Resistance Genes in a Plant Host. PLOS One 9(6), e99300.

Parveen, S., Lanjewar, S., Sharma, K. and Kutti, U. 2011. Isolation of fungi from the surface water of river. Journal of Experimental Sciences 2(10), 58-59.

Pendergast, M.T.M. and Hoek, E.M.V. 2011. A review of water treatment membrane nanotechnologies. Energy and Environmental Science 4, 1946-1971.

Pereira, V.J., Basílio, M.C., Fernandes, D., Domingues, M., Paiva, J.M., Benoliel, M.J., Crespo, M.T. and Romão, M.V.S. 2009. Occurrence of filamentous fungi and yeasts in three different drinking water sources. Water Research 43(15), 3813-3819.

Peter-Varbanets, M., Zurbrugg, C., Swartz, C. and Pronk, W. 2009. Decentralized systems for potable water and the potential of membrane technology. Water Research 43, 245-265.

Romanos, G.E., Athanasekou, C.P., Likodimos, V., Aloupogiannis, P. and Falaras, P. 2013. Hybrid ultrafiltration/photocatalytic membranes for efficient water treatment. Industrial and Engineering Chemistry Research, 13938-13947.

Sanches, S., Barreto Crespo, M.T. and Pereira, V.J. 2010. Drinking water treatment of priority pesticides using low pressure UV photolysis and advanced oxidation processes. Water Research 44, 1809-1818.

Sanches, S., Penetra, A., Rodrigues, A., Cardoso, V.V., Ferreira, E., Benoliel, M.J., Barreto Crespo, M.T., Crespo, J.G. and Pereira, V.J. 2013. Removal of pesticides from water combining low pressure UV photolysis with nanofiltration. Separation and Purification Technology 115, 73-82.

Youngchim, S., Morris-Jones, R., Hay, R.J. and Hamilton, A.J. 2004. Production of melanin by Aspergillus fumigatus. Journal of Medical Microbiology 53(3), 175-181.

Zaehle, C., Gressler, M., Shelest, E., Geib, E., Hertweck, C. and Brock, M. 2014. Terrein Biosynthesis in *Aspergillus terreus* and Its Impact on Phytotoxicity. Chemistry & Biology 21(6), 719-731.

CHAPTER 6

Discussion and Future work

CONTENTS

The main objectives of the work presented in this thesis was to address the inactivation mechanisms of filamentous fungi using different sources of UV radiation and the optimization of drinking water treatment processes using the combination of filtration with UV photolysis in the same photocatalytic membrane reactor. This study is important to ensure the efficient treatment of *Aspergillus* species that are widely present in drinking water sources even though there is currently no legislation limiting their presence in drinking water. It is also important to demonstrate the effectiveness of new hybrid treatment systems that can be used as an alternative for drinking water treatment. The main achievements are summarized in this section and the proposed future work is discussed.

6.1. UV inactivation effects on filamentous fungi

In this work three different sources of UV radiation were used. Medium and low-pressure mercury lamps (the most common lamps used in drinking water treatment facilities) and light-emitting diodes (LEDs) that emit at 255 nm and 265 nm. The use of medium and low-pressure mercury lamps involve the generation of mercury waste, have shorter lifetimes and require significant amounts of energy consumption. On the other hand, LEDs are mercury free, can be constructed with a specific peak wavelength with a narrow bandwidth and require less energy. However, the UV-LEDs currently tested are only operating at 1 % efficiency when comparing with 75 % efficiency of visible LEDs (Chatterley and Linden, 2010), which requires improvements to increase its operation efficiency.

In laboratory scale experiments, the effectiveness of direct photolysis using the light sources mentioned above were tested on three *Aspergillus* species, *A. fumigatus*, *A. niger* and *A. terreus*. Effects on their morphology, cell wall/membrane permeability, enzymatic activity, DNA damage and proteome response were evaluated. The effects

observed included morphological changes of the spores, increased cell wall/membrane permeability, increased formation of pyrimidine dimers in the DNA and various proteome responses to the radiation stress imposed. With both mercury lamps and light-emitting diodes, these effects were induced on the three species with different intensities, being *A. niger* the most resilient of the species followed by *A. fumigatus* and by *A. terreus*. This study proved that LEDs are a promising new source of UV radiation that can be considered by drinking water treatment facilities to replace mercury lamps.

6.2 Combined Treatment

In this study a first attempt to treat fungi using a combination in the same reactor and at the same time of UV inactivation and membrane filtration processes was addressed. The photocatalytic membrane reactor developed showed to be very promising for drinking water treatment since a clean permeate was obtained. Additionally, one of the major drawbacks associated with membrane filtration systems when operating individually, the production of a concentrated retentate, was reduced since a clean retentate was also obtained due to the inactivation of *A. fumigatus*. The most effective treatment occurred when combining UV radiation with filtration using ceramic membranes modified with titanium dioxide and silicon dioxide. This combination led to an enhanced inactivation of *Aspergillus fumigatus*. Moreover, this system reduces the operational costs associated with treatment/disposal of the retentate.

6.3. Future work

6.3.1 Effect of UV radiation on microorganisms

Regarding the effect of UV radiation on filamentous fungi there is still a lot of work that must be performed to deeply understand what happens inside fungal spores. Considering that the cell wall of the understudy species was highly affected it would be interesting to evaluate by high performance liquid chromatography which components are being affected and degraded (Zhu et al., 2005). Moreover, since different fungal pigmentation confers different resistances to UV radiation, the analysis of the pigments by high performance liquid chromatography could also be performed to verify if they scavenge the UV light or are being degraded by the UV radiation treatment.

Additionally, similar studies should be performed using other water pathogens to understand the mode of action of UV radiation on them and consequently optimize drinking water disinfection.

6.3.2 Proposal of a new photocatalytic membrane reactor

The photocatalytic membrane reactor used in this study, although very promising, has a configuration that is not possible to scale up. Therefore, a new reactor that can be easily scaled up, was designed with submerged UV lamps and flat sheet membranes that filter from the outside to the inside (Fraga et al., 2019; figure 1). In this reactor several UV mercury lamps and LEDs that emit at different wavelengths can be tested in combination with ceramic membranes. Given the results obtained in this work, two panels of LEDs that emit at 265 nm were acquired and tested in the combined system. This combined system in currently being used to evaluate the removal and inactivation potential of fungi and other water microorganisms (total coliforms, *E. coli* and *Enterococcus*). Commercially available high flux flat sheet silicon carbide membranes are being tested unmodified and modified with a combination of titanium dioxide and

silicon dioxide (Huertas et al., 2019) in combination with low pressure mercury lamps and LED panels that emit at 265 nm. Preliminary results show that the combined system is extremely effective to achieve inactivation of the tested bacteria and fungi and that the combined system guarantees an effective retentate treatment.

Figure 6.1 – Newly designed photocatalytic membrane reactor with submerged outside-inside flux membrane filtration system and UV lamps.

6.3.3 Economical evaluation

Considering not only the inactivation of microorganisms but also the degradation of pollutants, the addition of UV radiation will increase the capital and operation costs but conversely, a lower treatment of the retentate will be needed. Additionally, water quality is expected to increase due to the inactivation and removal of microorganisms and pollutants and the reduction of by-products formation due to the decrease of

chlorine doses needed to achieve an effective disinfection. To assess the viability to implement a similar photocatalytic system in a drinking water treatment facility an economical evaluation should be performed. The requirement of an UV radiation system and the development of modified membranes will certainly have costs but, the most important is the trade-off between the costs and benefits in terms of the quality of the water produced and public health protection.

References

Chatterley, C. and Linden, K. 2010. Demonstration and evaluation of germicidal UV-LEDs for point-of-use water disinfection. Journal of Water and Health 8(3), 479-486.

Fraga, M.C., Huertas, R.M., Crespo, J.G. and Pereira, V.J. 2019. Novel submerged photocatalytic membrane reactor for treatment of olive mill wastewaters. Catalysts 9(9), 769.

Huertas, R.M., Fraga, M.C., Crespo, J.G. and Pereira, V.J. 2019. Solvent free process for the development of photocatalytic membranes. Molecules 24(24), 4481.

Zhu, X., Cai, J., Yang, J. and Su, Q. 2005. Determination of glucosamine in impure chitin samples by high-performance liquid chromatography. Carbohydrate Research 340(10), 1732-1738.

APPENDICES

CONTENTS

A.1 SUPPLEMENTARY INFORMATION FROM CHAPTER 2

Supplementary Information 1

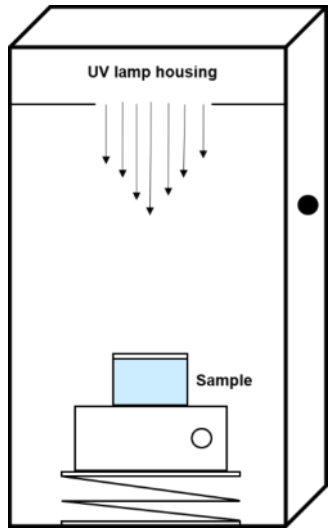

Figure 1 – Experimental configuration of the medium pressure mercury lamp UV reactor.

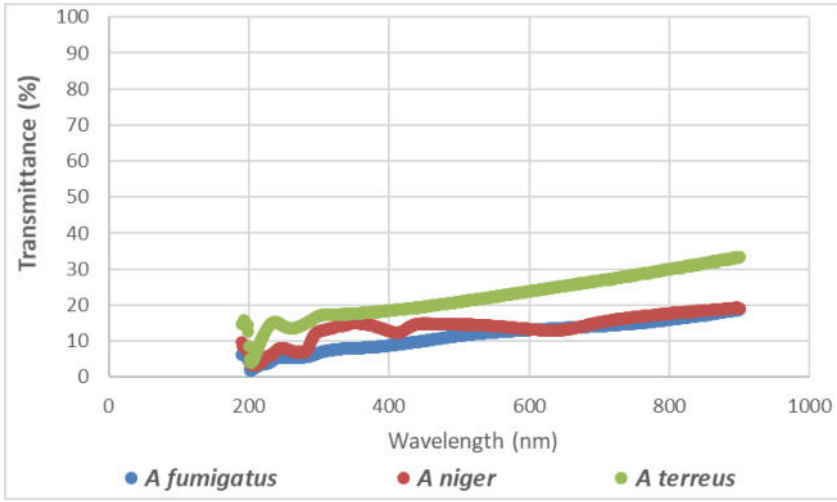

Figure 2 – Transmittance of the working solutions of spores and mycelia of the three different *Aspergillus* species.

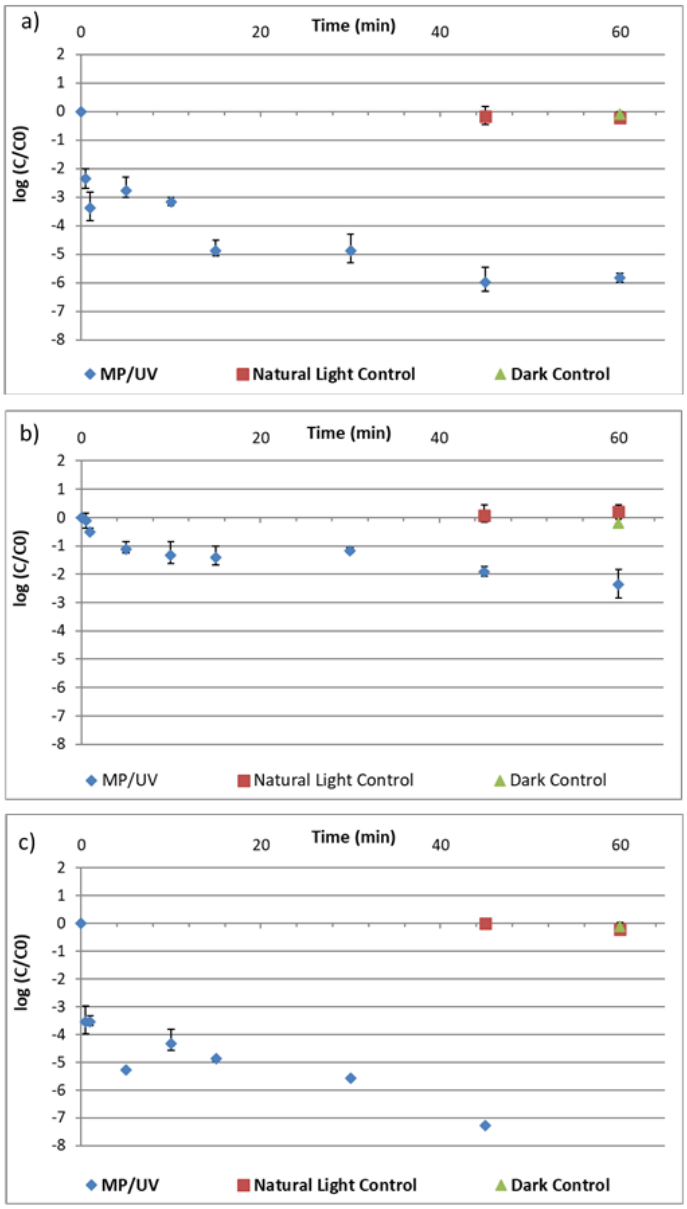

Figure 3 - Inactivation results in log (C/C0) of a) *A. fumigatus*, b) *A. niger* and c) *A. terreus* spiked into saline solution matrix after exposure to a MP lamp along the experimental time. Two controls are presented (natural light control and dark control). Error bars represent duplicate results in up to 7 dilutions tested.

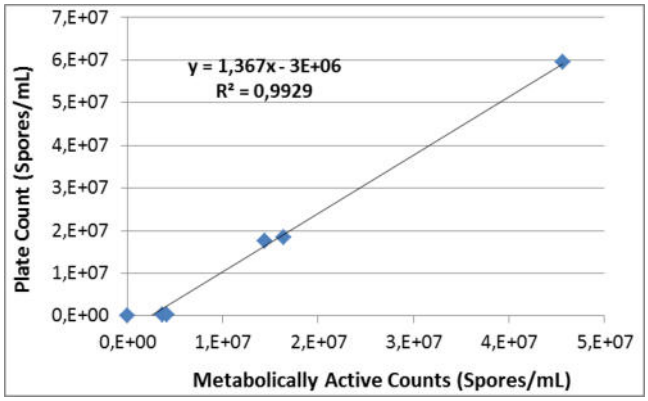

Figure 4 – Correlation between plate count technique and the metabolically active counts measured by flow cytometry.

Table 1 – Dry weight measurements of spores and mycelia from the working solutions.

Filamentous Fungi	Triplicates/Duplicates Assay 1 (mg)	Triplicates/Duplicates Assay 2 (mg)	Triplicates/Duplicates Assay 3 (mg)	Triplicates/Duplicates Assay 4 (mg)
Aspergillus niger	37.6	51.9	37.2	37.9
	37.4	51.3	38.8	35.4
		60	45.1	36
Aspergillus fumigatus	12.1	12.5	15.2	18.9
	13.1	13.2	16.3	17.3
	12.8	13.7		18
Aspergillus terreus	7.1	9.6	8.7	12.3
	6.1	10.6	7.7	14.3
	8.2	9		11.6

Table 2 – Linear and polynomial regressions and the correspondent coefficients of determination obtained for *Aspergillus fumigatus*, *Aspergillus niger* and *Aspergillus terreus* after inactivation with medium pressure mercury lamp. Square brackets indicate the exposure time limits of the linear and polynomial regression used to determine the equations.

	Aspergillus fumigatus	***Aspergillus niger***	***Aspergillus terreus***
MP Lamp	Linear [0;1 minute]: y = -3.0676x – 0.2451 R^2 = 0.9288 Polynomial [0;30 minutes]: y = 0.0114x2 – 0.4603x – 1.6611 R^2 = 0.8005	Linear [0;15 minutes]: y = -0.1088x + 0.0921 R^2 = 0.8318 Polynomial [0;60 minutes]: y = 0.0011x2 – 0.0982x + 0.0119 R^2 = 0.8983	Linear [0;1 minute]: y = -3.7411x – 0.6254 R^2 = 0.7489 Polynomial [0;15 minutes]: y = 0.0346x2 – 0.7448x – 2.0281 R^2 = 0.677

Table 3 – Quantification of DNA (ng/µL) in samples spiked with *A. fumigatus*, *A. niger* and *A. terreus* before and after exposure to a MP lamp during 30 min and 60 min.

MP exposure (min)	***Aspergillus fumigatus*** DNA (ng/µL)	***Aspergillus niger*** DNA (ng/µL)	***Aspergillus terreus*** DNA (ng/µL)
0	92.1	145.2	46.3
30	2.6	40	4.8
60	2.6	11.3	1.3

Table 4 – Total number of protein accession numbers obtained and the corresponding matches with the background database for DAVID Proteomics and FungiFun2.

	A. fumigatus	***A. niger***	***A. terreus***
Proteins Accession numbers	1362	1574	424
DAVID Proteomics	1360	124	415
FungiFun2	1340	202	343

Two different bioinformatic tools (DAVID Proteomics and FungiFun2) were compared in terms of matches between the proteins identified by LC-MS/MS and their databases. The DAVID Proteomics analysis was used for all the analysis because it provided a higher number of matches for *A. fumigatus* and *A. terreus*.

Supplementary Information 2

Table 1 – GO clusters in the biological process category. In green are marked the common GO clusters between samples not exposed to UV radiation (initial) and samples exposed to 60 min of UV radiation. In orange and bold are marked the new GO clusters formed.

	Biological Processes			
	Initial		**After 60 minutes MP/UV**	
***Aspergillus* species**	**GO Term**	**Description**	**GO Term**	**Description**
Aspergillus fumigatus	GO:0000162	tryptophan biosynthetic process	GO:0006412	translation
	GO:0000398	mRNA splicing, via spliceosome	**GO:0071555**	**cell wall organization**
	GO:0001731	formation of translation preinitiation complex		
	GO:0006086	acetyl-CoA biosynthetic process from pyruvate		
	GO:0006094	gluconeogenesis		
	GO:0006096	glycolytic process		
	GO:0006098	pentose-phosphate shunt		
	GO:0006099	tricarboxylic acid cycle		
	GO:0006122	mitochondrial electron transport, ubiquinol to cytochrome c		
	GO:0006334	nucleosome assembly		
	GO:0006337	nucleosome disassembly		
	GO:0006412	translation		
	GO:0006446	regulation of translational initiation		
	GO:0006457	protein folding		
	GO:0006662	glycerol ether metabolic process		
	GO:0006886	intracellular protein transport		
	GO:0006979	response to oxidative stress		
	GO:0008652	cellular amino acid biosynthetic process		
	GO:0009060	aerobic respiration		
	GO:0009082	branched-chain amino acid biosynthetic process		

	GO:0009298	GDP-mannose biosynthetic process		
	GO:0009408	response to heat		
	GO:0010499	proteasomal ubiquitin-independent protein catabolic process		
	GO:0015986	ATP synthesis coupled proton transport		
	GO:0015991	ATP hydrolysis coupled proton transport		
	GO:0034314	Arp2/3 complex-mediated actin nucleation		
	GO:0042438	melanin biosynthetic process		
	GO:0042744	hydrogen peroxide catabolic process		
	GO:0043161	proteasome-mediated ubiquitin-dependent protein catabolic process		
	GO:0043936	asexual sporulation resulting in formation of a cellular spore		
	GO:0045454	cell redox homeostasis		
	GO:0045899	positive regulation of RNA polymerase II transcriptional preinitiation complex assembly		
	GO:0046148	pigment biosynthetic process		
	GO:0051292	nuclear pore complex assembly		
	GO:0070084	protein initiator methionine removal		
	GO:0070682	proteasome regulatory particle assembly		
Aspergillus niger	GO:0006108	malate metabolic process	**GO:0005975**	**carbohydrate metabolic process**
	GO:0006412	translation	GO:0006108	malate metabolic process
	GO:0043161	proteasome-mediated ubiquitin-dependent protein catabolic process		
Aspergillus terreus	GO:0006094	gluconeogenesis	GO:0006096	glycolytic process
	GO:0006096	glycolytic process	**GO:0006108**	**malate metabolic process**

	GO:0006098	pentose-phosphate shunt	GO:0006412	translation
	GO:0006099	tricarboxylic acid cycle	**GO:0006414**	**translational elongation**
	GO:0006122	mitochondrial electron transport, ubiquinol to cytochrome c		
	GO:0006334	nucleosome assembly		
	GO:0006412	translation		
	GO:0006526	arginine biosynthetic process		
	GO:0007017	microtubule-based process		
	GO:0009060	aerobic respiration		
	GO:0009082	branched-chain amino acid biosynthetic process		
	GO:0042026	protein refolding		
	GO:0042744	hydrogen peroxide catabolic process		
	GO:0045454	cell redox homeostasis		

Table 2 – GO clusters in the cellular component category. In green are marked the common GO clusters between samples not exposed to UV radiation (initial) and samples exposed to 60 min of UV radiation. In orange and bold are marked the new GO clusters formed.

	Cellular Components			
	Initial		**After 60 minutes MP/UV**	
***Aspergillus* species**	**GO Term**	**Description**	**GO Term**	**Description**
Aspergillus fumigatus	GO:0000274	mitochondrial proton-transporting ATP synthase, stator stalk	GO:0000786	nucleosome
	GO:0000786	nucleosome	GO:0005622	intracellular
	GO:0000932	P-body	GO:0005840	ribosome
	GO:0005622	intracellular	GO:0009277	fungal-type cell wall
	GO:0005623	cell	**GO:0031225**	**anchored component of membrane**
	GO:0005643	nuclear pore		
	GO:0005665	DNA-directed RNA polymerase II, core complex		
	GO:0005682	U5 snRNP		
	GO:0005685	U1 snRNP		
	GO:0005732	small nucleolar ribonucleoprotein complex		
	GO:0005737	cytoplasm		
	GO:0005739	mitochondrion		
	GO:0005750	mitochondrial respiratory chain complex III		
	GO:0005751	mitochondrial respiratory chain complex IV		
	GO:0005768	endosome		
	GO:0005788	endoplasmic reticulum lumen		
	GO:0005826	actomyosin contractile ring		
	GO:0005829	cytosol		
	GO:0005832	chaperonin-containing T-complex		
	GO:0005840	ribosome		

	GO:0005850	eukaryotic translation initiation factor 2 complex		
	GO:0005852	eukaryotic translation initiation factor 3 complex		
	GO:0005885	Arp2/3 protein complex		
	GO:0005967	mitochondrial pyruvate dehydrogenase complex		
	GO:0008540	proteasome regulatory particle, base subcomplex		
	GO:0008541	proteasome regulatory particle, lid subcomplex		
	GO:0009277	fungal-type cell wall		
	GO:0009986	cell surface		
	GO:0010494	cytoplasmic stress granule		
	GO:0015934	large ribosomal subunit		
	GO:0015935	small ribosomal subunit		
	GO:0016282	eukaryotic 43S preinitiation complex		
	GO:0016586	RSC complex		
	GO:0019013	viral nucleocapsid		
	GO:0019773	proteasome core complex, alpha-subunit complex		
	GO:0019774	proteasome core complex, beta-subunit complex		
	GO:0022625	cytosolic large ribosomal subunit		
	GO:0022627	cytosolic small ribosomal subunit		
	GO:0030126	COPI vesicle coat		
	GO:0030127	COPII vesicle coat		
	GO:0030479	actin cortical patch		
	GO:0031011	Ino80 complex		
	GO:0031428	box C/D snoRNP complex		
	GO:0034515	proteasome storage granule		
	GO:0035838	growing cell tip		
	GO:0042645	mitochondrial nucleoid		
	GO:0043614	multi-eIF complex		
	GO:0046540	U4/U6 x U5 tri-snRNP complex		

	GO:0071540	eukaryotic translation initiation factor 3 complex, eIF3e		
	GO:0071541	eukaryotic translation initiation factor 3 complex, eIF3m		
	GO:1990023	mitotic spindle midzone		
Aspergillus niger	GO:0005622	intracellular	GO:0005622	intracellular
	GO:0005840	ribosome		
Aspergillus terreus	GO:0000786	nucleosome	GO:0000786	nucleosome
	GO:0005623	cell	GO:0005840	ribosome
	GO:0005750	mitochondrial respiratory chain complex III	GO:0009277	fungal-type cell wall
	GO:0005829	cytosol		
	GO:0005840	ribosome		
	GO:0009277	fungal-type cell wall		
	GO:0015935	small ribosomal subunit		
	GO:0022625	cytosolic large ribosomal subunit		
	GO:0022627	cytosolic small ribosomal subunit		
	GO:0042645	mitochondrial nucleoid		

Table 3 – GO clusters in the molecular function category. In green are marked the common GO clusters between samples not exposed to UV radiation (initial) and samples exposed to 60 min of UV radiation. In orange and bold are marked the new GO clusters formed.

	Molecular Function			
	Initial		**After 60 minutes MP/UV**	
***Aspergillus* species**	**GO Term**	**Description**	**GO Term**	**Description**
Aspergillus fumigatus	GO:0000166	nucleotide binding	GO:0003735	structural constituent of ribosome
	GO:0000287	magnesium ion binding		
	GO:0003723	RNA binding		
	GO:0003729	mRNA binding		
	GO:0003735	structural constituent of ribosome		
	GO:0003743	translation initiation factor activity		
	GO:0003746	translation elongation factor activity		
	GO:0003755	peptidyl-prolyl cis-trans isomerase activity		
	GO:0003756	protein disulfide isomerase activity		
	GO:0003924	GTPase activity		
	GO:0003985	acetyl-CoA C-acetyltransferase activity		
	GO:0004022	alcohol dehydrogenase (NAD) activity		
	GO:0004029	aldehyde dehydrogenase (NAD) activity		
	GO:0004049	anthranilate synthase activity		
	GO:0004096	catalase activity		
	GO:0004129	cytochrome-c oxidase activity		
	GO:0004177	aminopeptidase activity		
	GO:0004298	threonine-type endopeptidase activity		
	GO:0004449	isocitrate dehydrogenase (NAD+) activity		
	GO:0004601	peroxidase activity		

	GO:0004775	succinate-CoA ligase (ADP-forming) activity		
	GO:0005198	structural molecule activity		
	GO:0005524	ATP binding		
	GO:0005525	GTP binding		
	GO:0008121	ubiquinol-cytochrome-c reductase activity		
	GO:0008137	NADH dehydrogenase (ubiquinone) activity		
	GO:0008171	O-methyltransferase activity		
	GO:0008237	metallopeptidase activity		
	GO:0008565	protein transporter activity		
	GO:0009055	electron carrier activity		
	GO:0015035	protein disulfide oxidoreductase activity		
	GO:0016597	amino acid binding		
	GO:0019863	IgE binding		
	GO:0030170	pyridoxal phosphate binding		
	GO:0043022	ribosome binding		
	GO:0046872	metal ion binding		
	GO:0046933	proton-transporting ATP synthase activity, rotational mechanism		
	GO:0046961	proton-transporting ATPase activity, rotational mechanism		
	GO:0051287	NAD binding		
	GO:0051920	peroxiredoxin activity		
	GO:0070006	metalloaminopeptidase activity		
Aspergillus niger	GO:0003735	structural constituent of ribosome	**GO:0030060**	**L-malate dehydrogenase activity**
	GO:0004298	threonine-type endopeptidase activity		
	GO:0016853	isomerase activity		
	GO:0000166	nucleotide binding	**GO:0003723**	**RNA binding**

Aspergillus terreus	GO:0003735	structural constituent of ribosome	GO:0003735	structural constituent of ribosome
	GO:0003743	translation initiation factor activity	**GO:0004190**	**aspartic-type endopeptidase activity**
	GO:0003746	translation elongation factor activity	**GO:0030060**	**L-malate dehydrogenase activity**
	GO:0004129	cytochrome-c oxidase activity		
	GO:0004177	aminopeptidase activity		
	GO:0008121	ubiquinol-cytochrome-c reductase activity		
	GO:0008137	NADH dehydrogenase (ubiquinone) activity		
	GO:0015035	protein disulfide oxidoreductase activity		
	GO:0016597	amino acid binding		
	GO:0030145	manganese ion binding		
	GO:0043022	ribosome binding		
	GO:0046933	proton-transporting ATP synthase activity, rotational mechanism		

A.2 SUPPLEMENTARY INFORMATION FROM CHAPTER 3

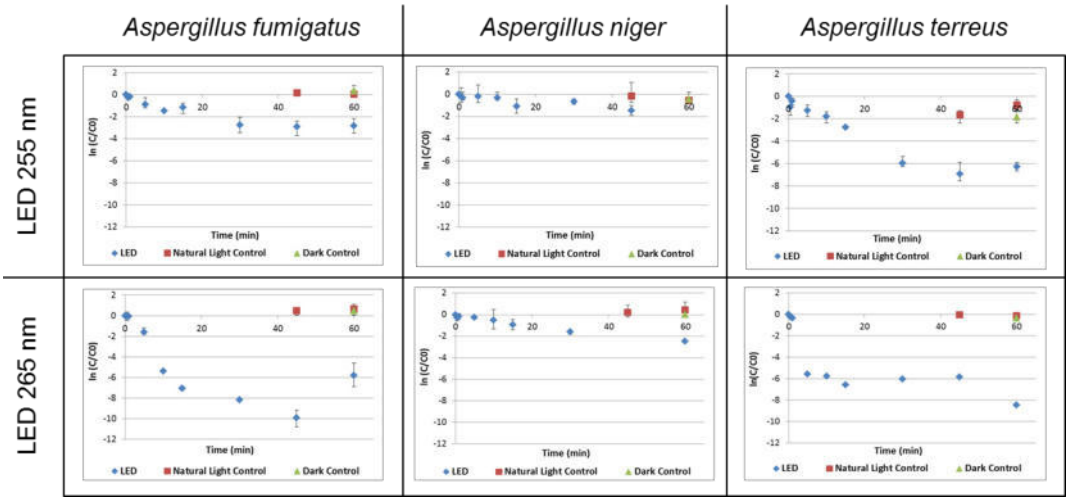

Figure 1 - Inactivation results in ln(C/C0) of *A. fumigatus*, *A. niger* and *A. terreus* in saline solution along the experimental time (60 min) using two wavelengths, 255 nm and 265 nm. Two controls are presented (natural light control and dark control). Error bars represent duplicate results obtained in up to 7 dilutions tested.

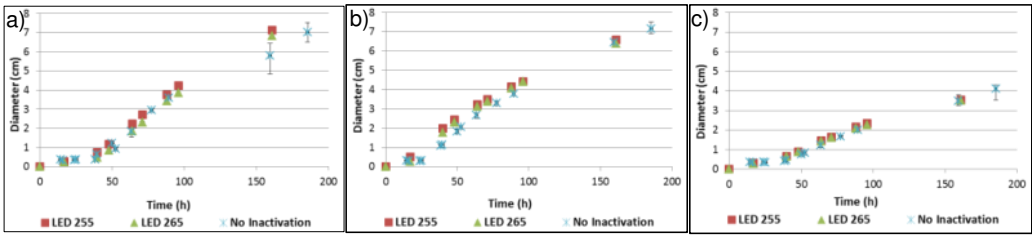

Figure 2 – Growth rates (diameter of colonies measured in petri dish) before (no inactivation) and after 60 min of UV exposure (LED 255 and LED 265 nm) of a) *A. fumigatus*, b) *A. niger* and c) *A. terreus*. Error bars represent triplicates.

Table 1 – Linear and polynomial regressions and the correspondent coefficients of determination obtained for *Aspergillus fumigatus*, *Aspergillus niger* and *Aspergillus terreus* after inactivation with LEDs emitting at 255 nm and 265 nm. Square brackets indicate the UV fluence limits of the linear and polynomial regression used to determine the equations.

	Aspergillus fumigatus	***Aspergillus niger***	***Aspergillus terreus***
LED 255 nm	Linear [0;8.75 mJ/cm²]: y = -0.527x – 0.0268 R^2 = 0.9481	Linear [0;7.36 mJ/cm²]: y = -0.0978x – 0.2121 R^2 = 0,7514	Linear [0;7.99 mJ/cm²]: y = -1.0243x – 0.0527 R^2 = 0.931
	Polynomial [0;11.66 mJ/cm²]: y = 0.0172x² – 0.626x + 0.0048 R^2 = 0.9418	Polynomial [0;7.36 mJ/cm²]: y = 0.006x2 – 0.1389x – 0.188 R^2 = 0.7615	Polynomial [0;15.98 mJ/cm²]: y = 0.0463x2 – 1.3085x + 0.211 R^2 = 0.9627
LED 265 nm	Linear [0;2.33 mJ/cm²]: y = 30.0528x + 0.0009 R^2 = 0.9828	Linear [0;1.21 mJ/cm²]: y = -1.0265x + 0.2327 R^2 = 0,8479	Linear [0;4.93 mJ/cm²]: y = -1.9679x – 1.2513 R^2 = 0.8261
	Polynomial [0;13.97 mJ/cm²]: y = 0.0908x2 – 1.6663x - 0.9395 R^2 = 0.8423	Polynomial [0;7.28 mJ/cm²]: y = 0.0009x2 – 0.3046x – 0.0316 R^2 = 0.8367	Polynomial [0;19.74 mJ/cm²]: y = 0.0543x2 – 1.4742x – 2.2634 R^2 = 0.7848

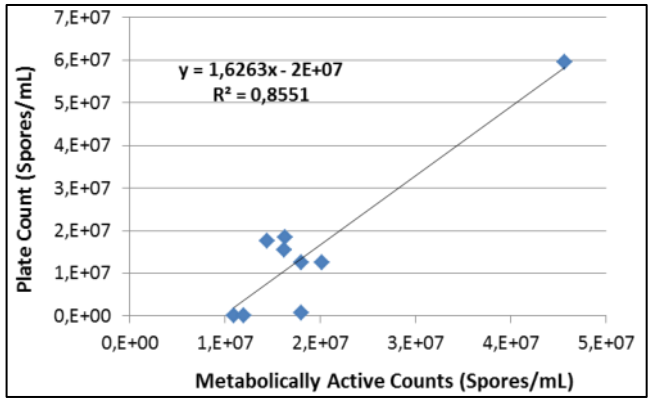

Figure 3 – Correlation of grown spores of plate count and metabolically active spore counts in flow cytometry.

A.3 SUPPLEMENTARY INFORMATION FROM CHAPTER 4

Table 1 – GO clusters in the biological process category for the LEDs that emit at 255 nm. In green are marked the common GO clusters between samples not exposed to UV radiation (initial) and samples exposed to 60 min of UV radiation. In orange and bold are marked the new GO clusters formed.

	Biological Processes			
	Initial		**After 60 minutes UV-LEDs set at 255 nm**	
***Aspergillus* species**	**GO Term**	**Description**	**GO Term**	**Description**
Aspergillus fumigatus	GO:0006086	acetyl-CoA biosynthetic process from pyruvate	GO:0006086	acetyl-CoA biosynthetic process from pyruvate
	GO:0009060	aerobic respiration	GO:0043936	asexual sporulation resulting in formation of a cellular spore
	GO:0034314	Arp2/3 complex-mediated actin nucleation	**GO:0046034**	**ATP metabolic process**
	GO:0043936	asexual sporulation resulting in formation of a cellular spore	GO:0015986	ATP synthesis coupled proton transport
	GO:0015991	ATP hydrolysis coupled proton transport	GO:0045454	cell redox homeostasis
	GO:0015986	ATP synthesis coupled proton transport	**GO:0006520**	**cellular amino acid metabolic process**
	GO:0009082	branched-chain amino acid biosynthetic process	**GO:0002183**	**cytoplasmic translational initiation**
	GO:0045454	cell redox homeostasis	GO:0001731	formation of translation

				preinitiation complex
	GO:0008652	cellular amino acid biosynthetic process	GO:0006094	gluconeogenesis
	GO:0001731	formation of translation preinitiation complex	**GO:0006537**	**glutamate biosynthetic process**
	GO:0009298	GDP-mannose biosynthetic process	GO:0006096	glycolytic process
	GO:0006094	gluconeogenesis	GO:0042744	hydrogen peroxide catabolic process
	GO:0006662	glycerol ether metabolic process	GO:0006886	intracellular protein transport
	GO:0006096	glycolytic process	GO:0042438	melanin biosynthetic process
	GO:0042744	hydrogen peroxide catabolic process	GO:0006122	mitochondrial electron transport, ubiquinol to cytochrome c
	GO:0006886	intracellular protein transport	GO:0006334	nucleosome assembly
	GO:0042438	melanin biosynthetic process	GO:0006098	pentose-phosphate shunt
	GO:0006122	mitochondrial electron transport, ubiquinol to cytochrome c	GO:0046148	pigment biosynthetic process
	GO:0000398	mRNA splicing, via spliceosome	GO:0010499	proteasomal ubiquitin-independent protein catabolic process

	GO:0051292	nuclear pore complex assembly	GO:0043161	proteasome-mediated ubiquitin-dependent protein catabolic process
	GO:0006334	nucleosome assembly	GO:0006457	protein folding
	GO:0006337	nucleosome disassembly	GO:0070084	protein initiator methionine removal
	GO:0006098	pentose-phosphate shunt	GO:0006446	regulation of translational initiation
	GO:0046148	pigment biosynthetic process	GO:0006979	response to oxidative stress
	GO:0045899	positive regulation of RNA polymerase II transcriptional preinitiation complex assembly	**GO:0044550**	**secondary metabolite biosynthetic process**
	GO:0010499	proteasomal ubiquitin-independent protein catabolic process	GO:0006412	translation
	GO:0070682	proteasome regulatory particle assembly	GO:0006099	tricarboxylic acid cycle
	GO:0043161	proteasome-mediated ubiquitin-dependent protein catabolic process		
	GO:0006457	protein folding		
	GO:0070084	protein initiator methionine removal		

	GO:0006446	regulation of translational initiation		
	GO:0009408	response to heat		
	GO:0006979	response to oxidative stress		
	GO:0006412	translation		
	GO:0006099	tricarboxylic acid cycle		
	GO:0000162	tryptophan biosynthetic process		
Aspergillus niger	GO:0006108	malate metabolic process	GO:0043161	proteasome-mediated ubiquitin-dependent protein catabolic process
	GO:0043161	proteasome-mediated ubiquitin-dependent protein catabolic process	GO:0006412	translation
	GO:0006412	translation		
Aspergillus terreus	GO:0009060	aerobic respiration	GO:0009060	aerobic respiration
	GO:0006526	arginine biosynthetic process	GO:0045454	cell redox homeostasis
	GO:0009082	branched-chain amino acid biosynthetic process	GO:0006096	glycolytic process
	GO:0045454	cell redox homeostasis	**GO:0006886**	**intracellular protein transport**

	GO:0006094	gluconeogenesis	GO:0006122	mitochondrial electron transport, ubiquinol to cytochrome c
	GO:0006096	glycolytic process	**GO:0045861**	**negative regulation of proteolysis**
	GO:0042744	hydrogen peroxide catabolic process	**GO:0006432**	**phenylalanyl-tRNA aminoacylation**
	GO:0007017	microtubule-based process	**GO:0045901**	**positive regulation of translational elongation**
	GO:0006122	mitochondrial electron transport, ubiquinol to cytochrome c	**GO:0006457**	**protein folding**
	GO:0006334	nucleosome assembly	**GO:0001302**	**replicative cell aging**
	GO:0006098	pentose-phosphate shunt	GO:0006412	translation
	GO:0042026	protein refolding	**GO:0006414**	**translational elongation**
	GO:0006412	translation	**GO:0006452**	**translational frameshifting**
	GO:0006099	tricarboxylic acid cycle	GO:0006099	tricarboxylic acid cycle

Table 2 – GO clusters in the cellular component category for the LEDs that emit at 255 nm. In green are marked the common GO clusters between samples not exposed to UV radiation (initial) and samples exposed to 60 min of UV radiation. In orange and bold are marked the new GO clusters formed.

	Cellular Components			
	Initial		**After 60 minutes UV-LEDs set at 255 nm**	
Aspergillus species	**GO Term**	**Description**	**GO Term**	**Description**
Aspergillus fumigatus	GO:0030479	actin cortical patch	**GO:0032432**	**actin filament bundle**
	GO:0005826	actomyosin contractile ring	GO:0005623	cell
	GO:0005885	Arp2/3 protein complex	GO:0009986	cell surface
	GO:0031428	box C/D snoRNP complex	GO:0005829	cytosol
	GO:0005623	cell	GO:0022625	cytosolic large ribosomal subunit
	GO:0009986	cell surface	GO:0022627	cytosolic small ribosomal subunit
	GO:0005832	chaperonin-containing T-complex	GO:0005768	endosome
	GO:0030126	COPI vesicle coat	GO:0016282	eukaryotic 43S preinitiation complex
	GO:0030127	COPII vesicle coat	GO:0005852	eukaryotic translation initiation factor 3 complex
	GO:0005737	cytoplasm	GO:0071540	eukaryotic translation initiation factor 3 complex, eIF3e

	GO:0010494	cytoplasmic stress granule	GO:0071541	eukaryotic translation initiation factor 3 complex, eIF3m
	GO:0005829	cytosol	GO:0009277	fungal-type cell wall
	GO:0022625	cytosolic large ribosomal subunit	GO:0005622	intracellular
	GO:0022627	cytosolic small ribosomal subunit	GO:0015934	large ribosomal subunit
	GO:0005665	DNA-directed RNA polymerase II, core complex	GO:0042645	mitochondrial nucleoid
	GO:0005788	endoplasmic reticulum lumen	GO:0000274	mitochondrial proton-transporting ATP synthase, stator stalk
	GO:0005768	endosome	GO:0005967	mitochondrial pyruvate dehydrogenase complex
	GO:0016282	eukaryotic 43S preinitiation complex	GO:0005750	mitochondrial respiratory chain complex III
	GO:0005850	eukaryotic translation initiation factor 2 complex	GO:0005739	mitochondrion
	GO:0005852	eukaryotic translation initiation factor 3 complex	GO:1990023	mitotic spindle midzone

	GO:0071540	eukaryotic translation initiation factor 3 complex, eIF3e	GO:0000786	nucleosome
	GO:0071541	eukaryotic translation initiation factor 3 complex, eIF3m	GO:0019773	proteasome core complex, alpha-subunit complex
	GO:0009277	fungal-type cell wall	GO:0008540	proteasome regulatory particle, base subcomplex
	GO:0035838	growing cell tip	GO:0034515	proteasome storage granule
	GO:0031011	Ino80 complex	GO:0005840	ribosome
	GO:0005622	intracellular	GO:0015935	small ribosomal subunit
	GO:0015934	large ribosomal subunit		
	GO:0042645	mitochondrial nucleoid		
	GO:0000274	mitochondrial proton-transporting ATP synthase, stator stalk		
	GO:0005967	mitochondrial pyruvate dehydrogenase complex		
	GO:0005750	mitochondrial respiratory chain complex III		

	GO:0005751	mitochondrial respiratory chain complex IV		
	GO:0005739	mitochondrion		
	GO:1990023	mitotic spindle midzone		
	GO:0043614	multi-eIF complex		
	GO:0005643	nuclear pore		
	GO:0000786	nucleosome		
	GO:0000932	P-body		
	GO:0019773	proteasome core complex, alpha-subunit complex		
	GO:0019774	proteasome core complex, beta-subunit complex		
	GO:0008540	proteasome regulatory particle, base subcomplex		
	GO:0008541	proteasome regulatory particle, lid subcomplex		
	GO:0034515	proteasome storage granule		

	GO:0005840	ribosome		
	GO:0016586	RSC complex		
	GO:0005732	small nucleolar ribonucleoprotein complex		
	GO:0015935	small ribosomal subunit		
	GO:0005685	U1 snRNP		
	GO:0046540	U4/U6 x U5 tri-snRNP complex		
	GO:0005682	U5 snRNP		
	GO:0019013	viral nucleocapsid		
Aspergillus niger	GO:0005622	intracellular	GO:0005622	intracellular
	GO:0005840	ribosome	GO:0005840	ribosome
Aspergillus terreus	GO:0005623	cell	GO:0005829	cytosol
	GO:0005829	cytosol	**GO:0005835**	**fatty acid synthase complex**
	GO:0022625	cytosolic large ribosomal subunit	GO:0009277	fungal-type cell wall
	GO:0022627	cytosolic small ribosomal subunit	GO:0042645	mitochondrial nucleoid

	GO:0009277	fungal-type cell wall	GO:0005750	mitochondrial respiratory chain complex III
	GO:0042645	mitochondrial nucleoid	GO:0000786	nucleosome
	GO:0005750	mitochondrial respiratory chain complex III	**GO:0009328**	**phenylalanine-tRNA ligase complex**
	GO:0000786	nucleosome	GO:0005840	ribosome
	GO:0005840	ribosome	GO:0015935	small ribosomal subunit
	GO:0015935	small ribosomal subunit		

Table 3 – GO clusters in the molecular function category for the LEDs that emit at 255 nm. In green are marked the common GO clusters between samples not exposed to UV radiation (initial) and samples exposed to 60 min of UV radiation. In orange and bold are marked the new GO clusters formed.

	Molecular Function			
	Initial		**After 60 minutes UV-LEDs set at 255 nm**	
***Aspergillus* species**	**GO Term**	**Description**	**GO Term**	**Description**
Aspergillus fumigatus	GO:0003985	acetyl-CoA C-acetyltransferase activity	GO:0004022	alcohol dehydrogenase (NAD) activity
	GO:0004022	alcohol dehydrogenase (NAD) activity	GO:0004029	aldehyde dehydrogenase (NAD) activity
	GO:0004029	aldehyde dehydrogenase (NAD) activity	GO:0004177	aminopeptidase activity
	GO:0016597	amino acid binding	GO:0004096	catalase activity
	GO:0004177	aminopeptidase activity	**GO:0004602**	**glutathione peroxidase activity**
	GO:0004049	anthranilate synthase activity	GO:0003924	GTPase activity
	GO:0005524	ATP binding	GO:0019863	IgE binding
	GO:0004096	catalase activity	GO:0000287	magnesium ion binding
	GO:0004129	cytochrome-c oxidase activity	GO:0046872	metal ion binding

	GO:0009055	electron carrier activity	GO:0008237	metallopeptidase activity
	GO:0005525	GTP binding	GO:0051287	NAD binding
	GO:0003924	GTPase activity	GO:0000166	nucleotide binding
	GO:0019863	IgE binding	GO:0004601	peroxidase activity
	GO:0004449	isocitrate dehydrogenase (NAD+) activity	GO:0046933	proton-transporting ATP synthase activity, rotational mechanism
	GO:0000287	magnesium ion binding	GO:0046961	proton-transporting ATPase activity, rotational mechanism
	GO:0046872	metal ion binding	GO:0043022	ribosome binding
	GO:0070006	metalloaminopeptidase activity	**GO:0005200**	**structural constituent of cytoskeleton**
	GO:0008237	metallopeptidase activity	GO:0003735	structural constituent of ribosome
	GO:0003729	mRNA binding	GO:0005198	structural molecule activity
	GO:0051287	NAD binding	GO:0004298	threonine-type endopeptidase activity
	GO:0008137	NADH dehydrogenase (ubiquinone) activity	GO:0003746	translation elongation factor activity
	GO:0000166	nucleotide binding	GO:0003743	translation initiation factor activity
	GO:0008171	O-methyltransferase activity	GO:0008121	ubiquinol-cytochrome-c reductase activity

	GO:0003755	peptidyl-prolyl cis-trans isomerase activity		
	GO:0004601	peroxidase activity		
	GO:0051920	peroxiredoxin activity		
	GO:0003756	protein disulfide isomerase activity		
	GO:0015035	protein disulfide oxidoreductase activity		
	GO:0008565	protein transporter activity		
	GO:0046933	proton-transporting ATP synthase activity, rotational mechanism		
	GO:0046961	proton-transporting ATPase activity, rotational mechanism		
	GO:0030170	pyridoxal phosphate binding		
	GO:0043022	ribosome binding		
	GO:0003723	RNA binding		
	GO:0003735	structural constituent of ribosome		
	GO:0005198	structural molecule activity		

	GO:0004775	succinate-CoA ligase (ADP-forming) activity		
	GO:0004298	threonine-type endopeptidase activity		
	GO:0003746	translation elongation factor activity		
	GO:0003743	translation initiation factor activity		
	GO:0008121	ubiquinol-cytochrome-c reductase activity		
Aspergillus niger	GO:0016853	isomerase activity	GO:0003735	structural constituent of ribosome
	GO:0003735	structural constituent of ribosome A2QVJ9 A2RAT8	GO:0004298	threonine-type endopeptidase activity
	GO:0004298	threonine-type endopeptidase activity		
Aspergillus terreus	GO:0016597	amino acid binding	**GO:0042973**	**glucan endo-1,3-beta-D-glucosidase activity**
	GO:0004177	aminopeptidase activity	**GO:0005525**	**GTP binding**
	GO:0004129	cytochrome-c oxidase activity	**GO:0003924**	**GTPase activity**
	GO:0030145	manganese ion binding	**GO:0030060**	**L-malate dehydrogenase activity**
	GO:0008137	NADH dehydrogenase (ubiquinone) activity	**GO:0046872**	**metal ion binding**
	GO:0000166	nucleotide binding	**GO:0004826**	**phenylalanine-tRNA ligase activity**

	GO:0015035	protein disulfide oxidoreductase activity	**GO:0005199**	**structural constituent of cell wall**
	GO:0046933	proton-transporting ATP synthase activity, rotational mechanism	**GO:0005200**	**structural constituent of cytoskeleton**
	GO:0043022	ribosome binding	GO:0003735	structural constituent of ribosome
	GO:0003735	structural constituent of ribosome	GO:0003746	translation elongation factor activity
	GO:0003746	translation elongation factor activity	GO:0008121	ubiquinol-cytochrome-c reductase activity
	GO:0003743	translation initiation factor activity		
	GO:0008121	ubiquinol-cytochrome-c reductase activity		

Table 4 – GO clusters in the biological process category for the LEDs that emit at 265 nm. In green are marked the common GO clusters between samples not exposed to UV radiation (initial) and samples exposed to 60 min of UV radiation. In orange and bold are marked the new GO clusters formed.

	Biological Processes			
	Initial		**After 60 minutes UV-LEDs set at 265 nm**	
***Aspergillus* species**	**GO Term**	**Description**	**GO Term**	**Description**
Aspergillus fumigatus	GO:0006086	acetyl-CoA biosynthetic process from pyruvate	GO:0006086	acetyl-CoA biosynthetic process from pyruvate
	GO:0009060	aerobic respiration	GO:0009060	aerobic respiration
	GO:0034314	Arp2/3 complex-mediated actin nucleation	GO:0034314	Arp2/3 complex-mediated actin nucleation
	GO:0043936	asexual sporulation resulting in formation of a cellular spore	GO:0043936	asexual sporulation resulting in formation of a cellular spore
	GO:0015991	ATP hydrolysis coupled proton transport	GO:0015991	ATP hydrolysis coupled proton transport
	GO:0015986	ATP synthesis coupled proton transport	**GO:0046034**	**ATP metabolic process**
	GO:0009082	branched-chain amino acid biosynthetic process	GO:0015986	ATP synthesis coupled proton transport
	GO:0045454	cell redox homeostasis	GO:0009082	branched-chain amino acid biosynthetic process
	GO:0008652	cellular amino acid biosynthetic process	GO:0045454	cell redox homeostasis
	GO:0001731	formation of translation preinitiation complex	GO:0008652	cellular amino acid biosynthetic process
	GO:0009298	GDP-mannose biosynthetic process	**GO:0002183**	**cytoplasmic translational initiation**
	GO:0006094	gluconeogenesis	GO:0001731	formation of translation preinitiation complex
	GO:0006662	glycerol ether metabolic process	GO:0009298	GDP-mannose biosynthetic process
	GO:0006096	glycolytic process	GO:0006094	gluconeogenesis

	GO:0042744	hydrogen peroxide catabolic process	GO:0006096	glycolytic process
	GO:0006886	intracellular protein transport	GO:0042744	hydrogen peroxide catabolic process
	GO:0042438	melanin biosynthetic process	GO:0006886	intracellular protein transport
	GO:0006122	mitochondrial electron transport, ubiquinol to cytochrome c	GO:0042438	melanin biosynthetic process
	GO:0000398	mRNA splicing, via spliceosome	GO:0006122	mitochondrial electron transport, ubiquinol to cytochrome c
	GO:0051292	nuclear pore complex assembly	GO:0000398	mRNA splicing, via spliceosome
	GO:0006334	nucleosome assembly	GO:0006334	nucleosome assembly
	GO:0006337	nucleosome disassembly	GO:0006098	pentose-phosphate shunt
	GO:0006098	pentose-phosphate shunt	GO:0046148	pigment biosynthetic process
	GO:0046148	pigment biosynthetic process	GO:0045899	positive regulation of RNA polymerase II transcriptional preinitiation complex assembly
	GO:0045899	positive regulation of RNA polymerase II transcriptional preinitiation complex assembly	GO:0010499	proteasomal ubiquitin-independent protein catabolic process
	GO:0010499	proteasomal ubiquitin-independent protein catabolic process	GO:0070682	proteasome regulatory particle assembly
	GO:0070682	proteasome regulatory particle assembly	GO:0043161	proteasome-mediated ubiquitin-dependent protein catabolic process
	GO:0043161	proteasome-mediated ubiquitin-dependent protein catabolic process	GO:0006457	protein folding
	GO:0006457	protein folding	**GO:0042026**	**protein refolding**
	GO:0070084	protein initiator methionine removal	**GO:0006090**	**pyruvate metabolic process**

	GO:0006446	regulation of translational initiation	GO:0006446	regulation of translational initiation
	GO:0009408	response to heat	GO:0006979	response to oxidative stress
	GO:0006979	response to oxidative stress	**GO:0044550**	**secondary metabolite biosynthetic process**
	GO:0006412	translation	GO:0006412	translation
	GO:0006099	tricarboxylic acid cycle	GO:0006099	tricarboxylic acid cycle
	GO:0000162	tryptophan biosynthetic process		
Aspergillus niger	GO:0006108	malate metabolic process	GO:0006108	malate metabolic process
	GO:0043161	proteasome-mediated ubiquitin-dependent protein catabolic process	GO:0043161	proteasome-mediated ubiquitin-dependent protein catabolic process
	GO:0006412	translation	GO:0006412	translation
Aspergillus terreus	GO:0009060	aerobic respiration	GO:0045454	cell redox homeostasis
	GO:0006526	arginine biosynthetic process	GO:0006094	gluconeogenesis
	GO:0009082	branched-chain amino acid biosynthetic process	GO:0006096	glycolytic process
	GO:0045454	cell redox homeostasis	GO:0042744	hydrogen peroxide catabolic process
	GO:0006094	gluconeogenesis	GO:0006122	mitochondrial electron transport, ubiquinol to cytochrome c
	GO:0006096	glycolytic process	**GO:0045861**	**negative regulation of proteolysis**
	GO:0042744	hydrogen peroxide catabolic process	GO:0006098	pentose-phosphate shunt
	GO:0007017	microtubule-based process	**GO:0045901**	**positive regulation of translational elongation**
	GO:0006122	mitochondrial electron transport, ubiquinol to cytochrome c	**GO:0006457**	**protein folding**
	GO:0006334	nucleosome assembly	**GO:0015031**	**protein transport**

	GO:0006098	pentose-phosphate shunt	GO:0006412	translation
	GO:0042026	protein refolding	**GO:0006414**	**translational elongation**
	GO:0006412	translation	**GO:0006452**	**translational frameshifting**
	GO:0006099	tricarboxylic acid cycle	GO:0006099	tricarboxylic acid cycle

Table 5 – GO clusters in the cellular component category for the LEDs that emit at 265 nm. In green are marked the common GO clusters between samples not exposed to UV radiation (initial) and samples exposed to 60 min of UV radiation. In orange and bold are marked the new GO clusters formed.

	Cellular Components			
	Initial		**After 60 minutes UV-LEDs set at 265 nm**	
***Aspergillus* species**	**GO Term**	**Description**	**GO Term**	**Description**
Aspergillus fumigatus	GO:0030479	actin cortical patch	GO:0030479	actin cortical patch
	GO:0005826	actomyosin contractile ring	GO:0005885	Arp2/3 protein complex
	GO:0005885	Arp2/3 protein complex	GO:0031428	box C/D snoRNP complex
	GO:0031428	box C/D snoRNP complex	GO:0005623	cell
	GO:0005623	cell	GO:0009986	cell surface
	GO:0009986	cell surface	GO:0005737	cytoplasm
	GO:0005832	chaperonin-containing T-complex	GO:0010494	cytoplasmic stress granule
	GO:0030126	COPI vesicle coat	GO:0005829	cytosol
	GO:0030127	COPII vesicle coat	GO:0022625	cytosolic large ribosomal subunit
	GO:0005737	cytoplasm	GO:0022627	cytosolic small ribosomal subunit
	GO:0010494	cytoplasmic stress granule	GO:0005768	endosome
	GO:0005829	cytosol	GO:0016282	eukaryotic 43S preinitiation complex
	GO:0022625	cytosolic large ribosomal subunit	GO:0005850	eukaryotic translation initiation factor 2 complex
	GO:0022627	cytosolic small ribosomal subunit	GO:0005852	eukaryotic translation initiation factor 3 complex
	GO:0005665	DNA-directed RNA polymerase II, core complex	GO:0071540	eukaryotic translation initiation factor 3 complex, eIF3e
	GO:0005788	endoplasmic reticulum lumen	GO:0071541	eukaryotic translation initiation factor 3 complex, eIF3m

	GO:0005768	endosome	GO:0009277	fungal-type cell wall
	GO:0016282	eukaryotic 43S preinitiation complex	GO:0031011	Ino80 complex
	GO:0005850	eukaryotic translation initiation factor 2 complex	GO:0005622	intracellular
	GO:0005852	eukaryotic translation initiation factor 3 complex	GO:0015934	large ribosomal subunit
	GO:0071540	eukaryotic translation initiation factor 3 complex, eIF3e	**GO:0005743**	**mitochondrial inner membrane**
	GO:0071541	eukaryotic translation initiation factor 3 complex, eIF3m	GO:0042645	mitochondrial nucleoid
	GO:0009277	fungal-type cell wall	GO:0000274	mitochondrial proton-transporting ATP synthase, stator stalk
	GO:0035838	growing cell tip	GO:0005967	mitochondrial pyruvate dehydrogenase complex
	GO:0031011	Ino80 complex	GO:0005750	mitochondrial respiratory chain complex III
	GO:0005622	intracellular	GO:0005751	mitochondrial respiratory chain complex IV
	GO:0015934	large ribosomal subunit	GO:0005739	mitochondrion
	GO:0042645	mitochondrial nucleoid	GO:0043614	multi-eIF complex
	GO:0000274	mitochondrial proton-transporting ATP synthase, stator stalk	GO:0000786	nucleosome
	GO:0005967	mitochondrial pyruvate dehydrogenase complex	GO:0000932	P-body
	GO:0005750	mitochondrial respiratory chain complex III	GO:0019773	proteasome core complex, alpha-subunit complex

	GO:0005751	mitochondrial respiratory chain complex IV	GO:0008540	proteasome regulatory particle, base subcomplex
	GO:0005739	mitochondrion	GO:0008541	proteasome regulatory particle, lid subcomplex
	GO:1990023	mitotic spindle midzone	GO:0034515	proteasome storage granule
	GO:0043614	multi-eIF complex	GO:0005840	ribosome
	GO:0005643	nuclear pore	GO:0005732	small nucleolar ribonucleoprotein complex
	GO:0000786	nucleosome	GO:0015935	small ribosomal subunit
	GO:0000932	P-body	**GO:0000812**	**Swr1 complex**
	GO:0019773	proteasome core complex, alpha-subunit complex	GO:0005685	U1 snRNP
	GO:0019774	proteasome core complex, beta-subunit complex	GO:0046540	U4/U6 x U5 tri-snRNP complex
	GO:0008540	proteasome regulatory particle, base subcomplex	GO:0005682	U5 snRNP
	GO:0008541	proteasome regulatory particle, lid subcomplex	**GO:0005688**	**U6 snRNP**
	GO:0034515	proteasome storage granule	**GO:0000221**	**vacuolar proton-transporting V-type ATPase, V1 domain**
	GO:0005840	ribosome	GO:0019013	viral nucleocapsid
	GO:0016586	RSC complex		
	GO:0005732	small nucleolar ribonucleoprotein complex		
	GO:0015935	small ribosomal subunit		
	GO:0005685	U1 snRNP		
	GO:0046540	U4/U6 x U5 tri-snRNP complex		

	GO:0005682	U5 snRNP		
	GO:0019013	viral nucleocapsid		
Aspergillus niger	GO:0005622	intracellular	GO:0005622	intracellular
	GO:0005840	ribosome	GO:0005840	ribosome
Aspergillus terreus	GO:0005623	cell	GO:0005829	cytosol
	GO:0005829	cytosol	GO:0022625	cytosolic large ribosomal subunit
	GO:0022625	cytosolic large ribosomal subunit	GO:0022627	cytosolic small ribosomal subunit
	GO:0022627	cytosolic small ribosomal subunit	**GO:0016282**	**eukaryotic 43S preinitiation complex**
	GO:0009277	fungal-type cell wall	GO:0009277	fungal-type cell wall
	GO:0042645	mitochondrial nucleoid	**GO:0031011**	**Ino80 complex**
	GO:0005750	mitochondrial respiratory chain complex III	**GO:0015934**	**large ribosomal subunit**
	GO:0000786	nucleosome	GO:0042645	mitochondrial nucleoid
	GO:0005840	ribosome	**GO:0009353**	**mitochondrial oxoglutarate dehydrogenase complex**
	GO:0015935	small ribosomal subunit	GO:0005750	mitochondrial respiratory chain complex III
			GO:0000786	nucleosome
			GO:0034515	**proteasome storage granule**
			GO:0005840	ribosome
			GO:0015935	small ribosomal subunit

Table 6 – GO clusters in the molecular function category for the LEDs that emit at 265 nm. In green are marked the common GO clusters between samples not exposed to UV radiation (initial) and samples exposed to 60 min of UV radiation. In orange and bold are marked the new GO clusters formed.

	Molecular Function			
	Initial		**After 60 minutes UV-LEDs set at 265 nm**	
Aspergillus species	**GO Term**	**Description**	**GO Term**	**Description**
Aspergillus fumigatus	GO:0003985	acetyl-CoA C-acetyltransferase activity	GO:0004022	alcohol dehydrogenase (NAD) activity
	GO:0004022	alcohol dehydrogenase (NAD) activity	GO:0016597	amino acid binding
	GO:0004029	aldehyde dehydrogenase (NAD) activity	GO:0004177	aminopeptidase activity
	GO:0016597	amino acid binding	GO:0005524	ATP binding
	GO:0004177	aminopeptidase activity	GO:0004096	catalase activity
	GO:0004049	anthranilate synthase activity	GO:0004129	cytochrome-c oxidase activity
	GO:0005524	ATP binding	GO:0009055	electron carrier activity
	GO:0004096	catalase activity	GO:0005525	GTP binding
	GO:0004129	cytochrome-c oxidase activity	GO:0003924	GTPase activity
	GO:0009055	electron carrier activity	GO:0019863	IgE binding

	GO:0005525	GTP binding	GO:0004449	isocitrate dehydrogenase (NAD+) activity
	GO:0003924	GTPase activity	GO:0000287	magnesium ion binding
	GO:0019863	IgE binding	GO:0046872	metal ion binding
	GO:0004449	isocitrate dehydrogenase (NAD+) activity	GO:0003729	mRNA binding
	GO:0000287	magnesium ion binding	GO:0051287	NAD binding
	GO:0046872	metal ion binding	GO:0008137	NADH dehydrogenase (ubiquinone) activity
	GO:0070006	metalloaminopeptidase activity	GO:0004601	peroxidase activity
	GO:0008237	metallopeptidase activity	GO:0003756	protein disulfide isomerase activity
	GO:0003729	mRNA binding	GO:0008565	protein transporter activity
	GO:0051287	NAD binding	GO:0046933	proton-transporting ATP synthase activity, rotational mechanism
	GO:0008137	NADH dehydrogenase (ubiquinone) activity	GO:0046961	proton-transporting ATPase activity, rotational mechanism
	GO:0000166	nucleotide binding	GO:0043022	ribosome binding
	GO:0008171	O-methyltransferase activity	GO:0003723	RNA binding

	GO:0003755	peptidyl-prolyl cis-trans isomerase activity	GO:0003735	structural constituent of ribosome
	GO:0004601	peroxidase activity	GO:0005198	structural molecule activity
	GO:0051920	peroxiredoxin activity	**GO:0008177**	**succinate dehydrogenase (ubiquinone) activity**
	GO:0003756	protein disulfide isomerase activity	GO:0004775	succinate-CoA ligase (ADP-forming) activity
	GO:0015035	protein disulfide oxidoreductase activity	GO:0004298	threonine-type endopeptidase activity
	GO:0008565	protein transporter activity	GO:0003746	translation elongation factor activity
	GO:0046933	proton-transporting ATP synthase activity, rotational mechanism	GO:0003743	translation initiation factor activity
	GO:0046961	proton-transporting ATPase activity, rotational mechanism	GO:0008121	ubiquinol-cytochrome-c reductase activity
	GO:0030170	pyridoxal phosphate binding		
	GO:0043022	ribosome binding		
	GO:0003723	RNA binding		
	GO:0003735	structural constituent of ribosome		
	GO:0005198	structural molecule activity		

	GO:0004775	succinate-CoA ligase (ADP-forming) activity		
	GO:0004298	threonine-type endopeptidase activity		
	GO:0003746	translation elongation factor activity		
	GO:0003743	translation initiation factor activity		
	GO:0008121	ubiquinol-cytochrome-c reductase activity		
Aspergillus niger	GO:0016853	isomerase activity	GO:0003735	structural constituent of ribosome
	GO:0003735	structural constituent of ribosome	GO:0004298	threonine-type endopeptidase activity
	GO:0004298	threonine-type endopeptidase activity		
Aspergillus terreus	GO:0016597	amino acid binding	**GO:0005525**	**GTP binding**
	GO:0004177	aminopeptidase activity	**GO:0003924**	**GTPase activity**
	GO:0004129	cytochrome-c oxidase activity	**GO:0030060**	**L-malate dehydrogenase activity**
	GO:0030145	manganese ion binding	**GO:0005200**	**structural constituent of cytoskeleton**
	GO:0008137	NADH dehydrogenase (ubiquinone) activity	GO:0003735	structural constituent of ribosome
	GO:0000166	nucleotide binding	GO:0003746	translation elongation factor activity

	GO:0015035	protein disulfide oxidoreductase activity	GO:0003743	translation initiation factor activity
	GO:0046933	proton-transporting ATP synthase activity, rotational mechanism	GO:0008121	ubiquinol-cytochrome-c reductase activity
	GO:0043022	ribosome binding		
	GO:0003735	structural constituent of ribosome		
	GO:0003746	translation elongation factor activity		
	GO:0003743	translation initiation factor activity		
	GO:0008121	ubiquinol-cytochrome-c reductase activity		

A.4 SUPPLEMENTARY INFORMATION FROM CHAPTER 5

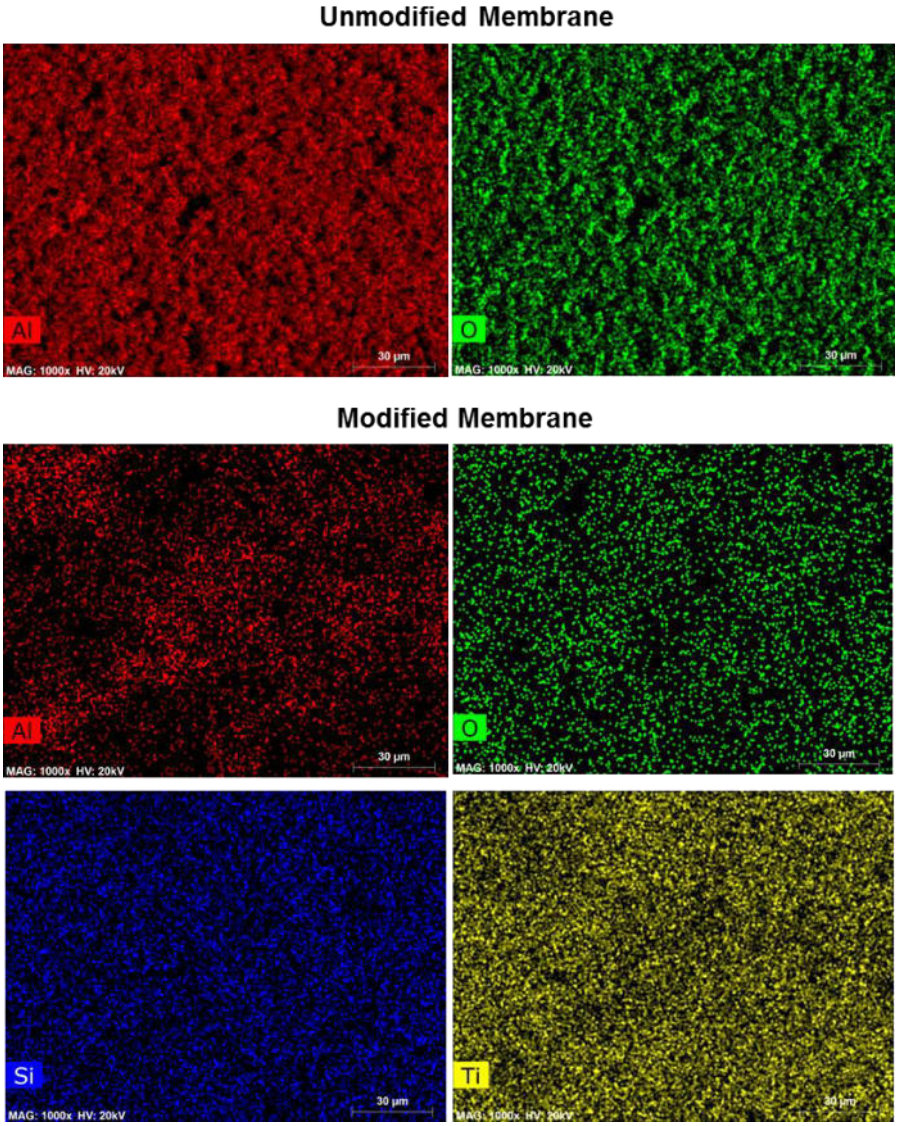

Figure 1 - Element mapping showing the distribution of the chemical elements Al – aluminum, O – oxygen, Si – silicon and Ti – titanium, at the surface of the unmodified and modified membrane.

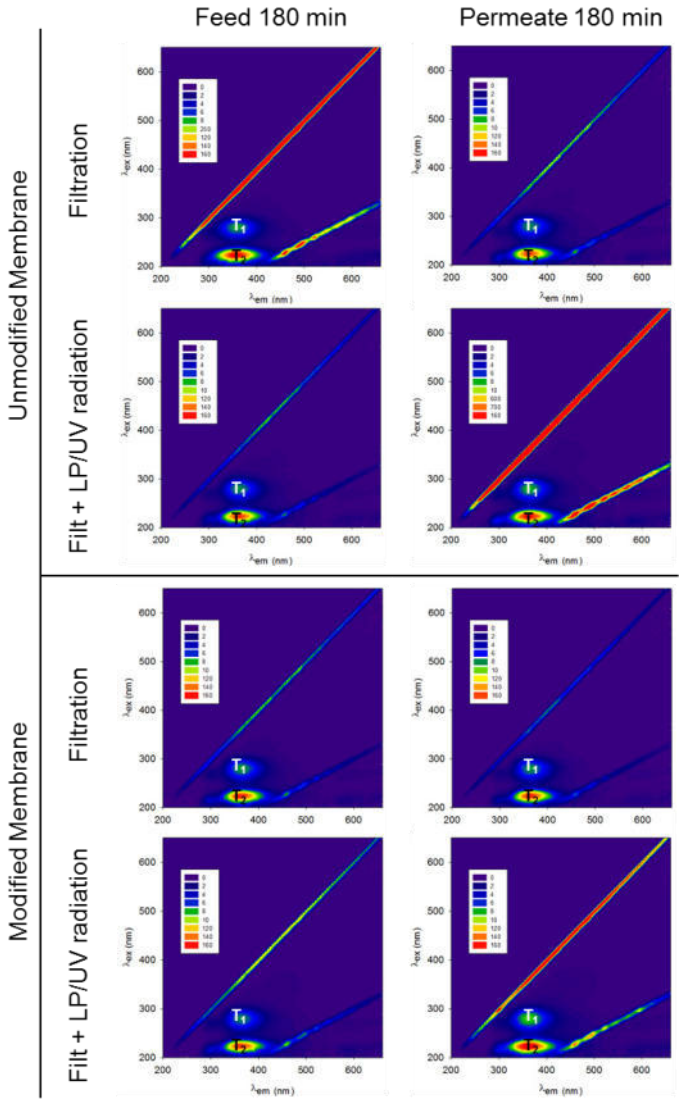

Figure 2 - Fluorescence excitation-emission matrices (EEMs) where T_1 and T_2 are tryptophan-like fluorescence.

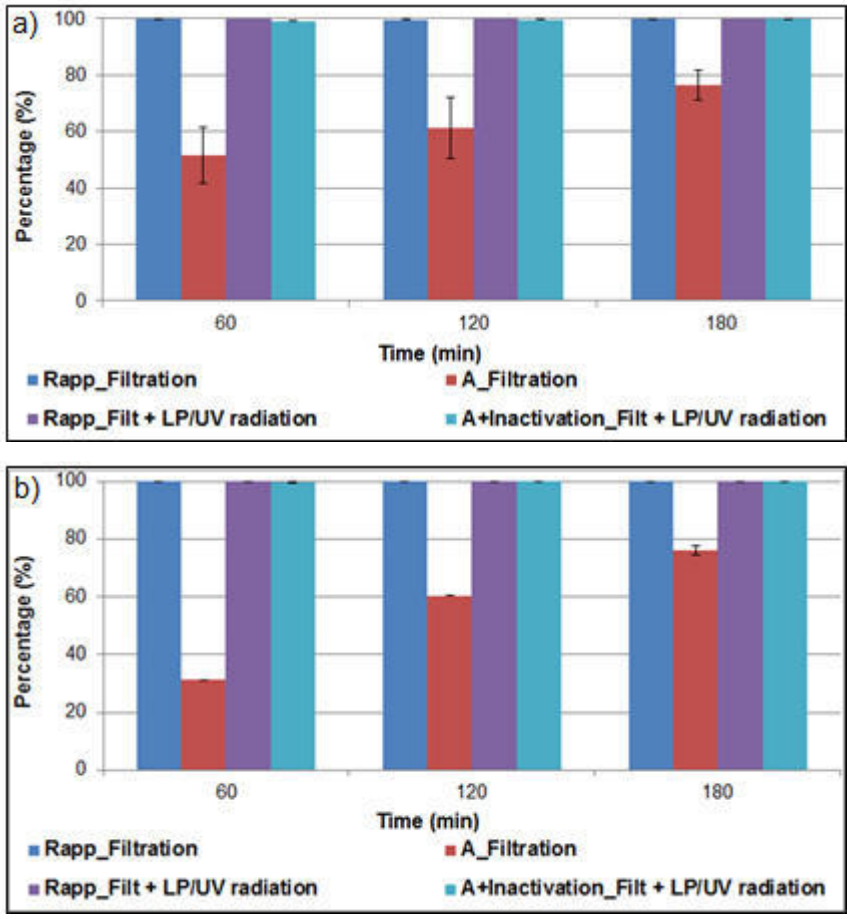

Figure 3 –Apparent rejection (R_{app}), adsorption (A) and inactivation percentages of *Aspergillus fumigatus* ($1x10^8$ spores/mL) after filtration and filtration coupled with LP/UV radiation of saline solution along the experimental time using a) unmodified; and b) modified membrane. Error bars represent duplicate results obtained in up to 7 dilutions tested.

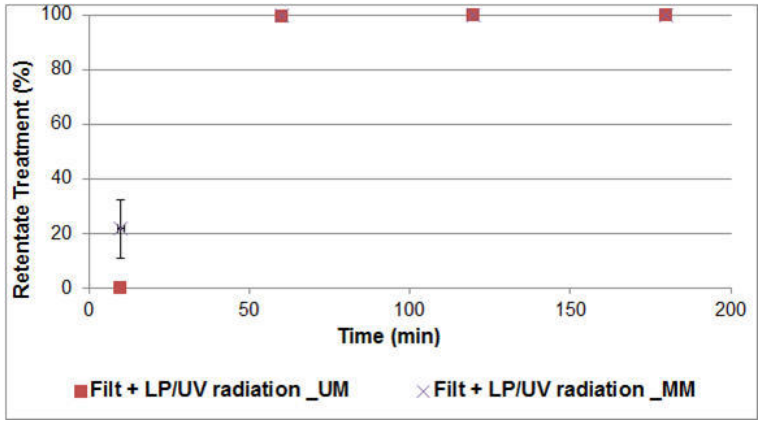

Figure 4 - Retentate treatment percentages of *Aspergillus fumigatus* ($1x10^8$ spores/mL) spiked into saline solution after filtration and filtration coupled with LP/UV radiation (Filtration + UV) using an unmodified (UM) and a modified membrane (MM) along the experimental time. Error bars represent duplicate results obtained in up to 7 dilutions tested.

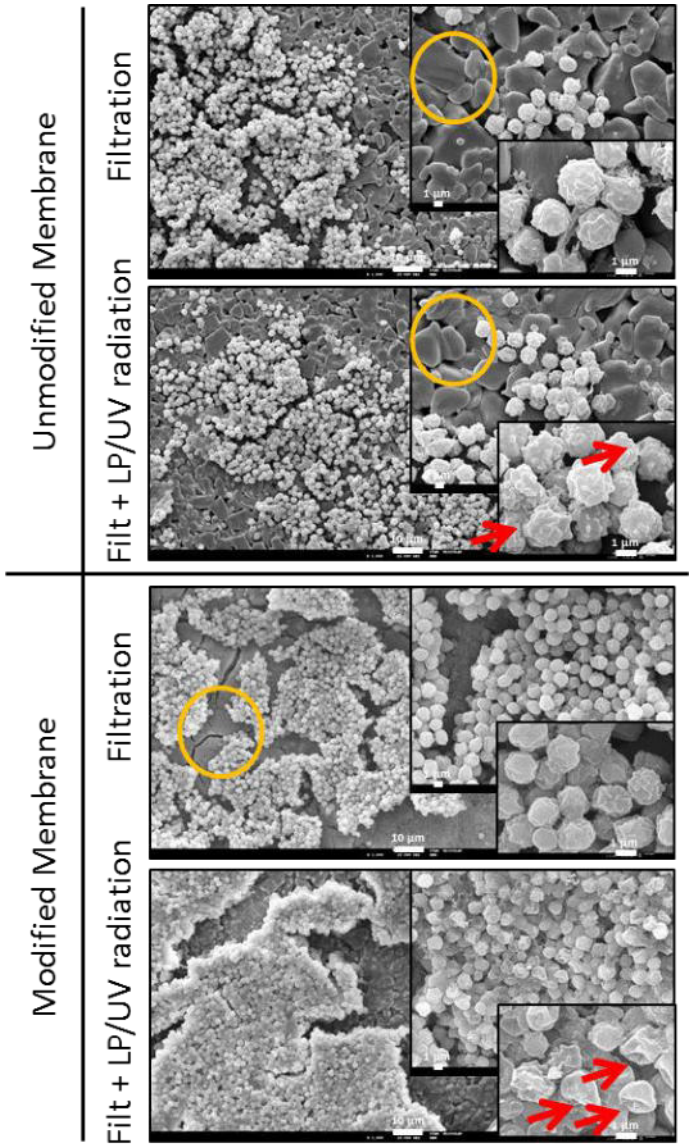

Figure 5 – SEM images of *Aspergillus fumigatus*' spores at the surface of the unmodified and modified membranes after 180 min of filtration and filtration coupled with LP/UV radiation (Filt + LP/UV radiation) using saline solution. Images of the top surfaces of the membranes have 1 000 x, 3 500 x and 13 000 x of total magnification. Yellow circles indicate the different pore size between the two membranes and the red arrows indicate the spores' morphology modifications.

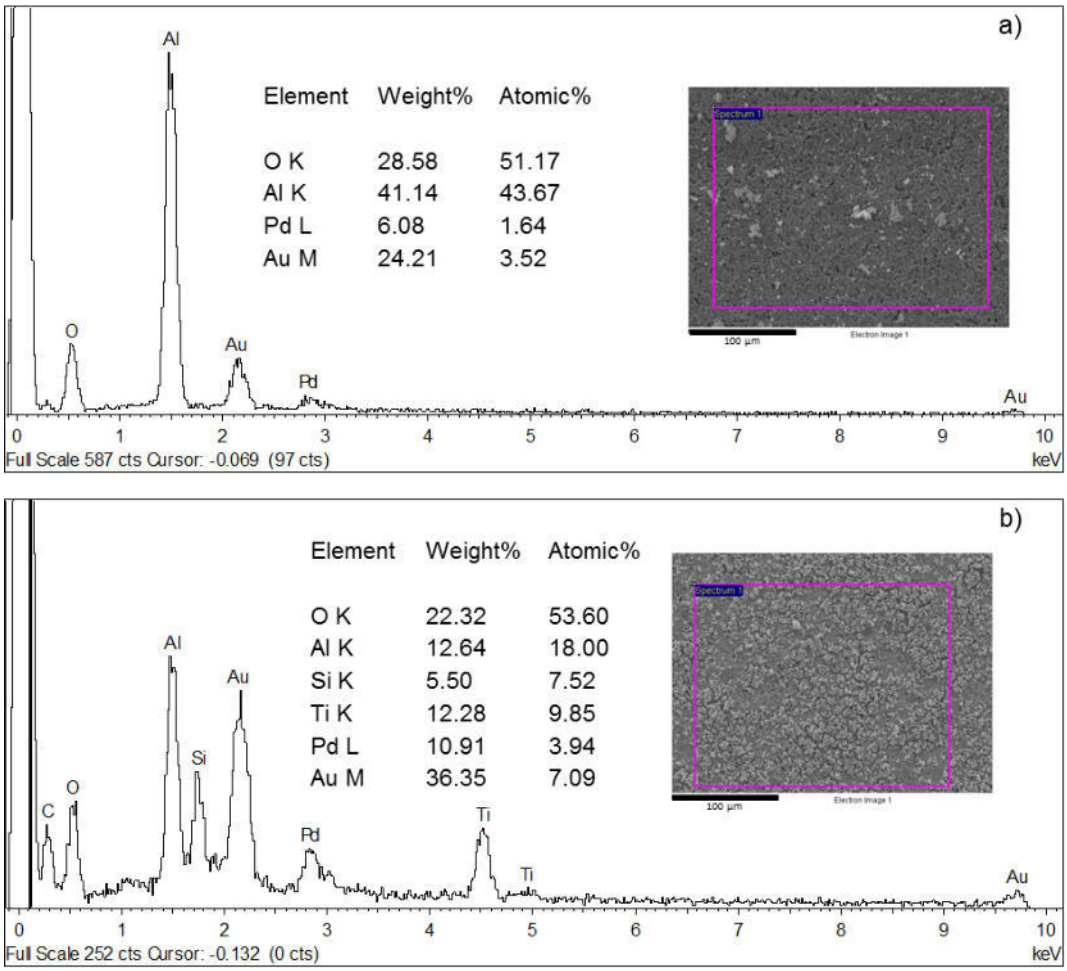

Figure 6 - EDS spectra, element contents and SEM image of the a) unmodified membrane whose material is Al_2O_3 and b) modified membrane with TiO_2/SiO_2 after 180 min of filtration of *A. fumigatus*. The Pd and Au peaks are due to coating before the analysis.

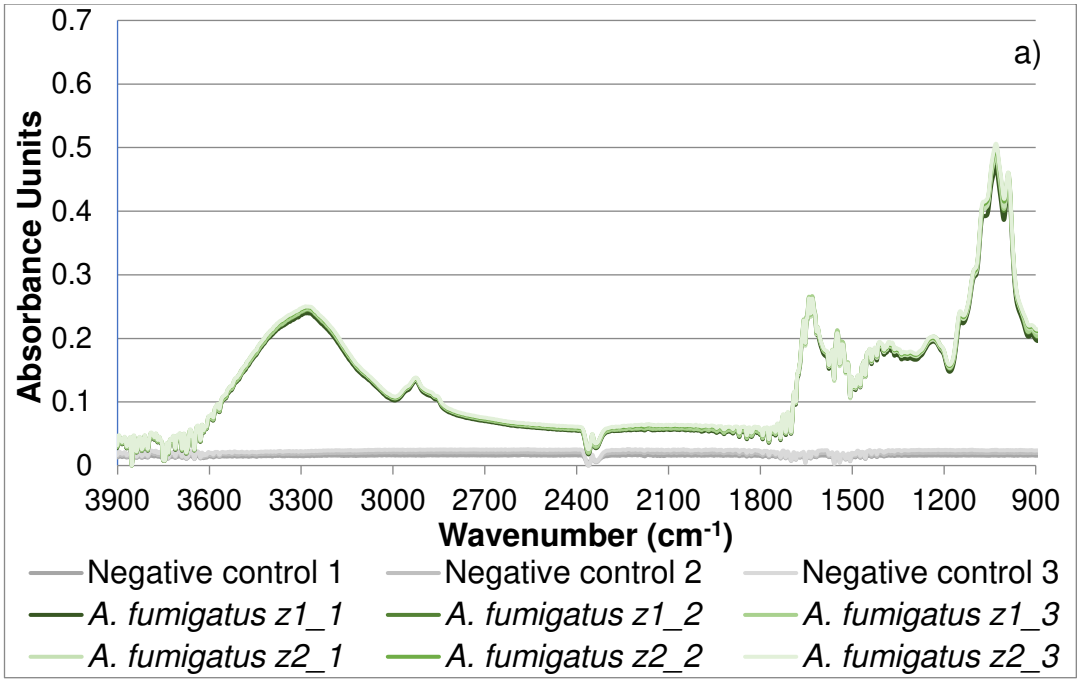
a)
Absorbance Uunits
0.7
0.6
0.5
0.4
0.3
0.2
0.1
0
3900 3600 3300 3000 2700 2400 2100 1800 1500 1200 900
Wavenumber (cm-1)
Negative control 1
Negative control 2
Negative control 3
A. fumigatus z1_1
A. fumigatus z1_2
A. fumigatus z1_3
A. fumigatus z2_1
A. fumigatus z2_2
A. fumigatus z2_3

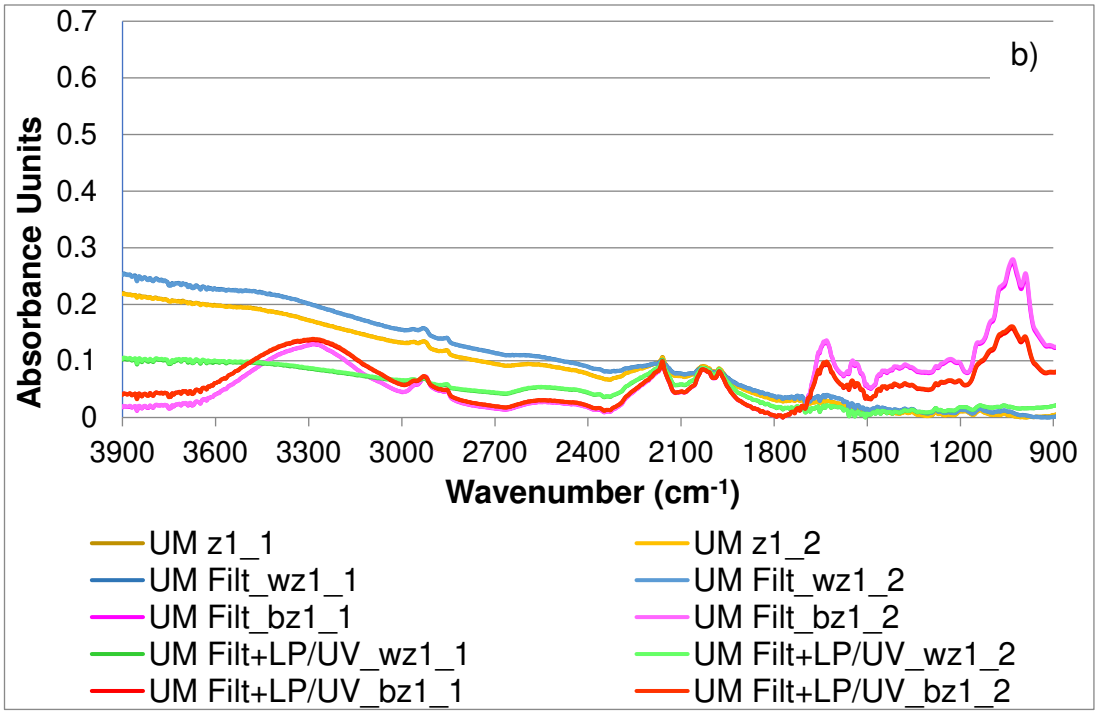
b)
Absorbance Uunits
0.7
0.6
0.5
0.4
0.3
0.2
0.1
0
3900 3600 3300 3000 2700 2400 2100 1800 1500 1200 900
Wavenumber (cm-1)
UM z1_1
UM z1_2
UM Filt_wz1_1
UM Filt_wz1_2
UM Filt_bz1_1
UM Filt_bz1_2
UM Filt+LP/UV_wz1_1
UM Filt+LP/UV_wz1_2
UM Filt+LP/UV_bz1_1
UM Filt+LP/UV_bz1_2

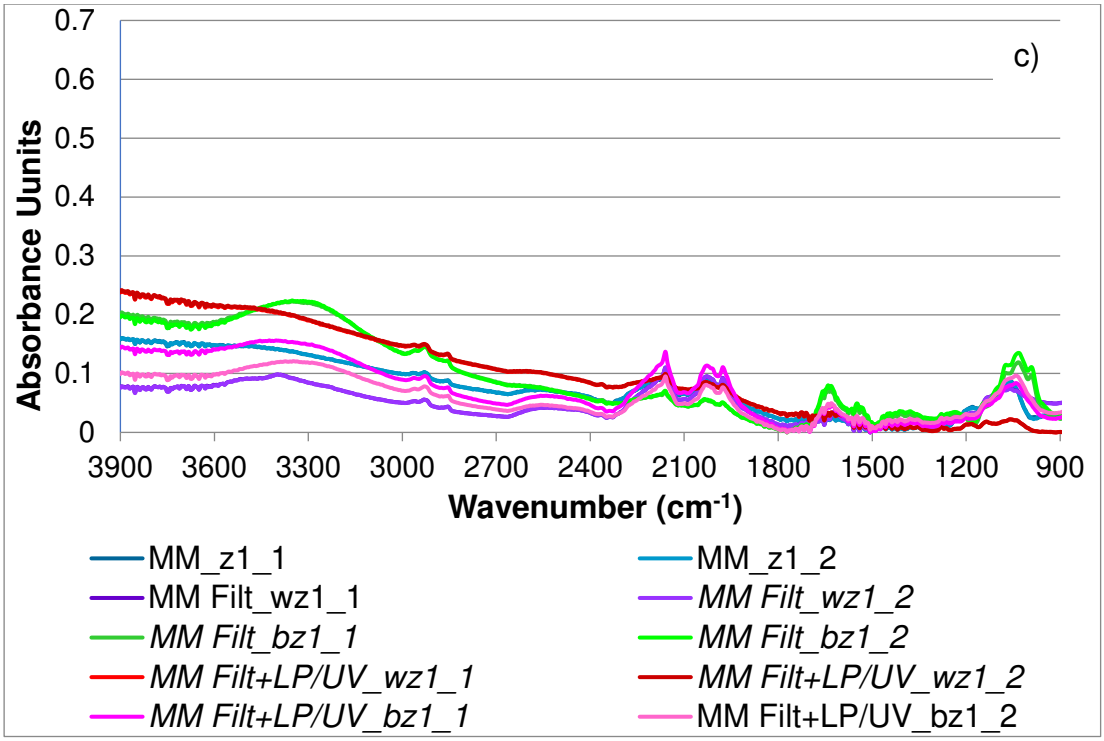

Figure 7 – FTIR spectra of a) *Aspergillus fumigatus* powder, b) unmodified membrane (UM) and c) modified membrane (MM) before and after filtration and filtration coupled with LP/UV radiation. Negative control corresponds to the background signal. z1 and z2 corresponds to different areas of the membranes analyzed. 1, 2 and 3 corresponds to replicates performed in each area analyzed. Filt corresponds to filtration and Filt+LP/UV corresponds to filtration coupled with LP/UV radiation. B corresponds to an area with visible fungal pellet and W to an area where no fungal pellet was visible.

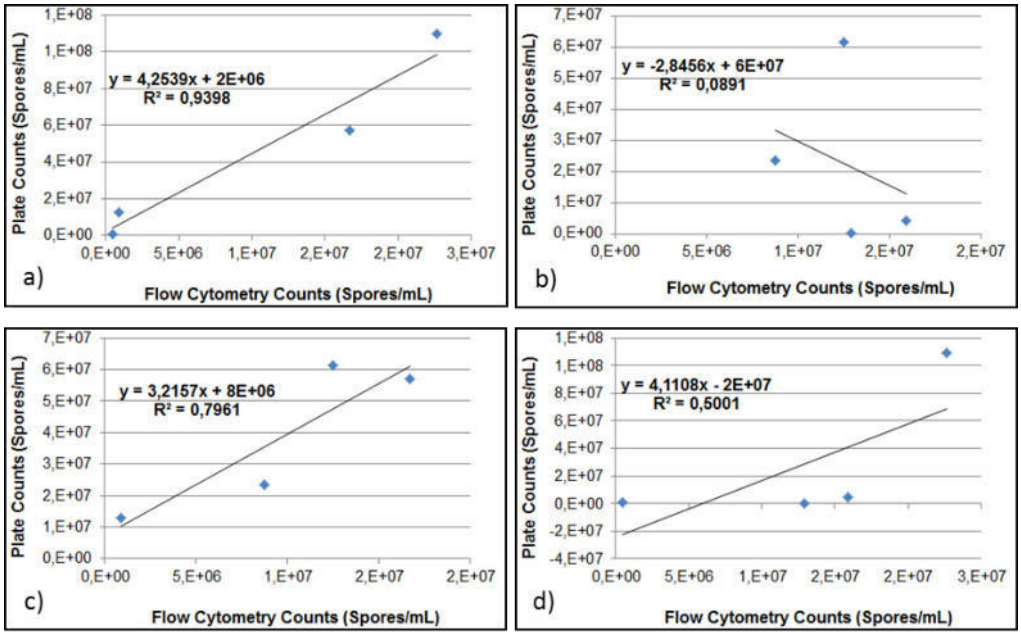

Figure 8 - Correlation of plate count and flow cytometry spore counts of a) unmodified membrane, b) modified membrane, c) filtration and d) filtration coupled with LP/UV radiation.

A.5 PROTOCOLS

A.5.1 Inoculum preparation

1- From the filamentous fungi preserved in cryovials inoculate plates containing malt extract agar (Merck, USA) and incubate for 7 days at 27 °C.
2- With a spreader remove the mycelium from the plates using a saline solution (0.90 % w/v of NaCl) with tween 80 (0.10 % v/v).
3- Collect the solution into a sterile centrifuge tube and centrifuge at 13 500 rpm for 20 minutes at 4 °C.
4- Wash the pellet three times with saline solution (0.90 % w/v of NaCl).
5- Resuspend the pellet into 150 mL of the understudy matrix (this solution is designated as concentrated inoculum).
6- Determine the fungal spores' concentration using the Neubauer chamber.

A.5.2 Inactivation assays using MP Lamps

1- From the concentrated inoculum perform dilutions to obtain working solutions with a final concentration of 10^8 spores/mL.
2- Place 50 mL of the working solutions inside a double walled glass that is connected to a refrigerated bath set at 20 °C and placed on top of a stirrer with a sterile magnetic stirrer inside.
3- Turn on the lamp and let it stabilize for 60 min.
4- Place the samples at 20 cm from the lamp.
5- Take 50 mL samples before the experiment and after 0.5, 1, 5, 10, 15, 30, 45 and 60 minutes of UV radiation exposure.
6- Perform two controls - place 50 mL of the working solution into two sterile glasses and leave one plate at normal light and the other in the dark.
7- Take 50 mL samples from the control glasses after the total experimental time.

8- Use 1 mL of each sample to determine the colony forming units.
9- Centrifuge the remaining volume and resuspend the pellet in 10 mL of saline solution to save it at -20 °C to be further analyzed.

A.5.3 Inactivation assays using LEDs

1- From the concentrated inoculum perform dilutions to obtain working solutions with a final concentration of 10^8 spores/mL.
2- Place 50 mL of the working solutions inside a double walled glass that is connected to a refrigerated bath set at 20 °C and placed on top of a stirrer with a sterile magnetic stirrer inside.
3- Place the LED set up on top of the glass at a 4 cm distance and turn on the wavelength desired.
4- Take 50 mL samples before the experiment and after 0.5, 1, 5, 10, 15, 30, 45 and 60 minutes of UV radiation exposure.
5- Perform two controls - place 50 mL of the working solution into two sterile glasses and leave one plate at normal light and the other in the dark.
6- Take 50 mL samples from the control glasses after the total experimental time.
7- Use 1 mL of each sample to determine the colony forming units.
8- Centrifuge the remaining volume and resuspend the pellet in 10 mL of saline solution to save it at -20 °C to be further analyzed.

A.5.4 Sample preparation for scan electron microscopy

1- Use 1 or 2 mL from the preserved samples and centrifuge at 10 000 rpm for 5 minutes at 4 °C).
2- Wash the pellet with phosphate buffer (pH 7) and centrifuge (10 000 rpm at 4 °C for 5 minutes).

3- Fixate the cells with Karnovsky's fixative overnight at 4 °C. (Glutaraldehyde is used at a concentration of 2.5 %; paraformaldehyde is used at a concentration of 2 %; and PBS at 0.1 M).
4- Wash the samples with phosphate buffer (pH 7) 10 minutes, three times and centrifuge (10 000 rpm at 4 °C for 5 minutes).
5- Post-fixation of the cells with 1 % osmium tetroxide in phosphate buffer (pH 7) for 2 hours at 4 °C.
6- Wash the samples with phosphate buffer (pH 7) 10 minutes, three times and centrifuge (10 000 rpm at 4 °C for 5 minutes).
7- Dehydrate with grade series of ethanol at 4 °C for 10 minutes: 30 %, 50 %, 70 %, 80 %, 90 %, 95 % and 100 % twice for 15 minutes each.
8- Freeze dry the samples for 30 minutes.
9- Put the samples on carbon tape and analyze them.

A.5.5 DNA extraction

1- Centrifuge the collected samples in 2 mL Eppendorf tubes.
2- Resuspend the cell pellet in 300 µL of PowerBead Solution and gently vortex to mix.
3- Transfer resuspended cells to PowerBead Tube.
4- Add 50 µL of Solution SL to the PowerBead Tube.
5- Lyse the cells in a Precellys Evolution tissue homogenizer for 2 min at 10 000 rpm with 10 s break.
6- Centrifuge the tubes at 10 000 g for 120 s at room temperature.
7- Transfer the supernatant to a clean 2 mL collection tube.
8- Add 100 µL of Solution IRS to que supernatant and vortex for 5 s. Incubate at 4 °C for 5 min.

9- Centrifuge the tubes at 10 000 g for 2 min at room temperature.

10- Avoiding the pellet, transfer the entire volume to a clean 2 mL collection tube.

11- Add 900 µL of Solution SB to the supernatant and vortex for 5 s.

12- Load about 650 µL into a MB Spin Column and centrifuge at 10 000 g for 60 s at room temperature. Discard the flow-through, add the remaining supernatant to the MB Spin Column, and centrifuge again at 10 000 g for 60 s at room temperature. Discard the flow-through.

13- Add 300 µL of Solution CB and centrifuge at 10 000 g for 60 s at room temperature (repeat this process until the flow-through is colorless).

14- Discard the flow-through. Centrifuge at 10 000 g for 2 min at room temperature.

15- Place the MB Spin Column in a new 2 mL collection tube.

16- Add 25 µL of Solution EB to the center of the white filter membrane and wait 5 min.

17- Centrifuge at 10 000 g for 60 s at room temperature.

18- Discard the MB Spin Column. Store the DNA at -20 °C.

A.5.6 Sample preparation for flow cytometry

1- From the preserved samples (that were preserved with a final concentration of 10^8 spores/mL) prepare 1 mL of a spore solution with a final concentration of 10^6 spores/mL in phosphate buffered saline solution (PBS).

2- Use the Yeast Control – Viability kit (Sysmex Partec GmbH, Germany) that contains fluorescein diacetate (FDA) and propidium iodide (PI) according to manufacturer's instructions (10 µL of FDA; wait 10 minutes at room temperature in the dark; 10 µL of PI).

3- Perform controls running the PBS and the sterilized matrix dyed with the fluorophores.

A.5.7 Experiments using the photocatalytic membrane reactor – just filtration

On the day before the experiment (cleaning procedure)

1- Clean the reactor with recirculating ethanol at 70 % (v/v).
2- Remove the ethanol by recirculating sterile distilled water and wait a few minutes.
3- Then, without recirculation rinse the reactor with 2 L to 4 L of sterile distilled water.

On the day of the experiment

4- Determine the initial contamination of the reactor by recirculating sterile distilled water for 10 to 20 minutes and take 10 mL samples of feed, retentate and permeate.
5- Analyze the samples in malt extract agar through the pour plate technique with no dilutions.
6- Prepare the concentrated inoculum as described in section A.5.1.
7- From the concentrated inoculum perform a dilution to obtain 10^8 spores/mL in 750 mL of water matrix.
8- Place the feed vessel on top of a magnetic stirrer and the tubes of feed, retentate and permeate inside and turn on the reactor.
9- Take 10 mL samples after 10 minutes, 1, 2 and 3 hours and measure the permeability at each time point.
10- Perform the cleaning procedure.

A.5.8 Experiments using the photocatalytic membrane reactor – filtration coupled with UV radiation

On the day before the experiment (cleaning procedure)

1- Clean the reactor with recirculating ethanol at 70 % (v/v).
2- Remove the ethanol by recirculating sterile distilled water and wait a few minutes.
3- Then, without recirculation rinse the reactor with 2 L to 4 L of sterile distilled water.

On the day of the experiment

4- Determine the initial contamination of the reactor by recirculating sterile distilled water for 10 to 20 minutes and take 10 mL samples of feed, retentate and permeate.
5- Analyze the samples in malt extract agar through the pour plate technique with no dilutions.
6- Prepare the concentrated inoculum as described in section A.5.1.
7- From the concentrated inoculum perform a dilution to obtain 10^8 spores/mL in 750 mL of water matrix.
8- Turn on the low pressure UV lamp a let it stabilize for 60 minutes with the shuttle closed.
9- Place the feed vessel on top of a magnetic stirrer and the tubes of feed, retentate and permeate inside, turn on the reactor to start the filtration process and open the shuttle to let the UV light reach the sample.
10- Take 10 mL samples after 10 minutes, 1, 2 and 3 hours and measure the permeability at each time point.
11- Perform the cleaning procedure.

A.5.9 Membrane samples' preparation for scan electron microscopy

1- Use 1 or 2 small broken pieces of the membranes (unmodified and modified) used for the experiments.
2- Wash the membrane pieces with phosphate buffer (pH 7) for 10 minutes and agitate smoothly.
3- Fixate the cells with Karnovsky's fixative overnight at 4 °C. (Glutaraldehyde is used at a concentration of 2.5 %; paraformaldehyde is used at a concentration of 2 %; and PBS at 0.1 M).
4- Wash the membrane pieces with phosphate buffer (pH 7) for 10 minutes, three times and agitate smoothly between washes.
5- Post-fixate with 1 % osmium tetroxide in phosphate buffer (pH 7) for 2 hours at 4 °C.
6- Wash the membrane pieces with phosphate buffer (pH 7) for 10 minutes, three times and agitate smoothly between washes.
7- Dehydrate with grade series of ethanol at 4 °C for 10 minutes: 30 %, 50 %, 70 %, 80 %, 90 %, 95 % and 100 % twice for 15 minutes each. Agitate smoothly between increasing series of ethanol.
8- Freeze dry the membrane pieces for 30 minutes.
9- Put the membrane pieces on adhesive tape and analyze them.

A.5.10 Protein Extraction

1- Homogenize the mycelia using the Tissuelyser at 50 for 2 minutes (or using a molar and pestle with liquid nitrogen). Weigh approximately 0.05g (50 mg) of mycelia and add it to 0.02 g PVPP in an Eppendorf tube with a metallic bead.
2- Precipitate with 1.5 mL TCA 10 % in acetone with DTT 60 mM.
3- Vortex the tubes and place them at -20 °C for 1 hour.

4- Centrifuge at 4 °C, 13 500 rpm for 15 minutes. Discard supernatant.
5- Wash 5 times with 1 mL DTT 60 mM in acetone (30 mL acetone + 1.8 mL 1M DTT [1.54 g/10 mL]), (keep it cold).
6- Dry the pellet in the hotte (30 minutes to overnight).
7- Resuspend in RS buffer (250 uL) and leave it at 27 °C with agitation 500 rpm (2 h to overnight in the Thermomixer).
8- Freeze at -20 °C (if not quantifying on the same day).
9- Thaw, centrifuge at room temperature, 13 000 rpm for 15 min at -20 °C (if no supernatant is present, add more RS buffer, vortex and centrifuge again).
10- Protein quantification with supernatant.

TCA/acetone (keep at -20 °C)

Reagent	Final Conc	Amount
TCA	10 %	3 g
DTT (1 M)	60 mM	1800 µL (227 mg)
Acetone		up to 30 mL
Volume		30 mL

Acetone Washing (keep at -20 °C)

Reagent	Final Conc	Amount
DTT (1 M)	60 mM	1800 µL (227 mg)
Acetone		up to 30 mL
Volume		30 mL

RS – Resolubilization buffer

Reagent	Final Conc	Amount
Thiurea (FW 76.12)	2 M	3.8 g (T4)
Tris	30 mM	100 µL (sol. 100 %)
Urea (FW 60.06)	7 M	10.5 g
CHAPS	4 % (m/v)	1 g
Complete ultra-tablets, mini, EDTA-free		
Water bidistilled		up to 25 mL

DTT 1 M (keep at -20 °C)

Reagent	Final Conc	Amount
DTT	1 M	1.54 g
Volume		10 mL

ITQB-UNL | Av. da República, 2780-157 Oeiras, Portugal
Tel (+351) 214 469 100 | Fax (+351) 214 411 277

www.itqb.unl.pt